Distribution Agreement

In presenting this thesis or dissertation as a partial fulfillment of the requirements for an advanced degree from Emory University, I hereby grant to Emory University and its agents the non-exclusive license to archive, make accessible, and display my thesis or dissertation in whole or in part in all forms of media, now or hereafter known, including display on the world wide web. I understand that I may select some access restrictions as part of the online submission of this thesis or dissertation. I retain all ownership rights to the copyright of the thesis or dissertation. I also retain the right to use in future works (such as articles or books) all or part of this thesis or dissertation.

Signature:

_____ _____

Jessica R. Petree Date

Deoxyribozyme Nanoparticle Nanozymes: from Splicing to Mechanism

By

Jessica R. Petree

Doctor of Philosophy

Chemistry

Khalid Salaita

Advisor

Stefan Lutz

Committee Member

David Lynn

Committee Member

Accepted:

Lisa A. Tedesco, Ph.D.

Dean of the James T. Laney School of Graduate Studies

Date

Deoxyribozyme Nanoparticle Nanozymes: from Splicing to Mechanism

By

Jessica R. Petree

A.S. Oxford College of Emory, 2009

B.S. University of Georgia, 2011

Advisor: Khalid Salaita, Ph.D.

An abstract of

A dissertation submitted to the Faculty of the

James T. Laney School of Graduate Studies of Emory University

in partial fulfillment of the requirements for the degree of

Doctor of Philosophy

in Chemistry

2019

Abstract

Deoxyribozyme Nanoparticle Nanozymes: from Splicing to Mechanism

By Jessica R. Petree

Nanozymes – created by attaching enzymes to a nanoscale scaffold – are just now coming into their full potential as tools for RNA knockdown and splicing. In Chapters 1-2 of this thesis, we review both gene knockdown technologies and gold nanoparticle-based nanozymes, with emphasis on deoxyribozyme (DNAzyme) nanoparticle (DzNPs) constructs. DzNPs are a subclass of nanozymes that have potential applications ranging from RNA gene regulation to analyte sensing. In Chapter 3, we focus on discovering the mechanism of action of DzNPs inside cells. To address this goal, we report the construction of core-attached DzNPs that are inactive until the DNAzymes are released from their scaffold, leading to a 51-fold increase in DNAzyme activity. Our preliminary data suggests there is gene knockdown by core-attached DzNPs in cells. Since this activity must come from the released DNAzymes, this experiment gives us a window into the mechanism of action of these constructs. In Chapter 4, we characterize DzNPs targeting GATA-3 mRNA, measuring their activity, longevity and stability. We found that these DzNPs can last for up to 9 months when stored in excess salt and DNAzyme; and they are most active when synthesized via the freezing method, rather than the salt aging method. Subsequently in Chapter 5, we discuss the building of a new type of nanozyme comprised of DNAzyme and RtcB ligase subunits attached to a gold nanoparticle core that can splice virtually any RNA stem-loop. The nanozyme cleaves and then ligates RNA targets, performing a splicing reaction that is akin to the function of the spliceosome. Our results show that the three-enzyme reaction can remove a 19 nt segment from a 67 nt RNA loop with up to 66% efficiency. The complete nanozyme can perform the same splice reaction at 10% efficiency. We conclude our studies in Chapter 6 with work exploring methods to show

RNA splicing inside cells, as a future step. These splicing nanozymes, as well as DzNPs for gene knockdown, represent a new promising approach for gene manipulation that has potential for *in vivo* applications.

KEYWORDS: RtcB, deoxyribozyme, DNAzyme, nanozyme, gold nanoparticle, synthetic biology

Deoxyribozyme Nanoparticle Nanozymes: from Splicing to Mechanism

By

Jessica R. Petree

A.S. Oxford College of Emory, 2009

B.S. University of Georgia, 2011

Advisor: Khalid Salaita, Ph.D.

A dissertation submitted to the Faculty of the

James T. Laney School of Graduate Studies of Emory University

in partial fulfillment of the requirements for the degree of

Doctor of Philosophy

in Chemistry

2019

Dedication

This dissertation is dedicated to my husband John Petree, who gave up his career so that I could pursue mine.

“And this is life eternal, that they might know thee the only true God, and Jesus Christ, whom thou hast sent.” —John 17:3

"Never give up on a dream just because of the time it will take to accomplish it. The time will pass anyway." —Earl Nightingale

Acknowledgements

Coming to Emory and being chosen by Khalid Salaita to join his lab was the fulfillment of my wildest dreams since I was small. It began in 8th grade, competing in the Georgia Science and Engineering Fair, and dreaming about one day being a scientist judge myself who was on the cusp of knowledge and pushing those boundaries. I wanted to be an explorer in that last frontier, the world of science! For thanking people on this journey, I must begin at the beginning. Firstly, I must thank my God, Jesus, the Author of my faith. I prayed so many prayers about the future, graduate school, who my advisor would be, and He guided me through it all and answered every hope I had. Without the Lord, and my strong faith in Him, I also couldn't have finished this degree. It took everything I had and then some to stay the course and push through to the end. In graduate school, I came to the end of myself and experienced my God's love in a real, visceral way I had never imagined experiencing.

I would also like to thank my parents, especially my mom, for instilling in me a love of asking questions and the scientific method. Having type I diabetes, I remember many fun afternoons over lunch we would talk and theorize about the possible causes of the disease and potential cures. It whetted my appetite for research and asking those big questions in the lab one day. My mom went back to work to help pay for my college education and I could never have done it without her. Thanks to her, I went to Oxford College for my first two years. At Oxford, I met professors who would forever change my understanding of science and be instrumental in guiding me down my path. Chief among those is my dear friend Brenda Harmon, the then organic lab teacher at Oxford, now the Professor of Pedagogy in Chemistry, who became my close friend and confidant. She taught me, for the first time, how to truly think like a scientist from first principles and instilled in me a passion for chemistry. It is chemistry that informs biology, she showed me: changes in the chemical realm spark changes in biomolecules. Having been trained in her class, I decided to major in biochemistry as my undergraduate degree, moving to the University of Georgia for my junior and senior years. There I met Dr. Bijoy

Mohanty, who would become my mentor as an undergraduate researcher in the Kushner Lab. From him, I learned efficiency and independence, even as a junior scientist, because he expected no less. I learned how to listen and take notes, so I could repeat an experiment that he showed me the first time. Dr. Mohanty amazed me with his sheer efficiency in doing large scale experiments, and I look up to him as a role model of what a research scientist could achieve.

In graduate school, I had the supreme pleasure to be taken under the wing of Khalid Salaita as a graduate student. Khalid embodied everything I wanted in an advisor: someone with passion for science, someone who would speak with me on a regular basis in meetings to discuss data, someone who was approachable and not intimidating to talk to and someone who treated me like an equal rather than a minion. Khalid met all these criteria and more, and it was only a few weeks after coming to Emory that I had made the decision to join his lab. I want to thank Khalid for his advice, his encouragement and his patience with me. I cannot count the times I cried in his office, as I tend to be a highly emotional person. But Khalid never got upset with me. He was someone I felt comfortable talking with, whether I was happy, or overwhelmed, and I always left his office feeling lighter and better than when I entered. Khalid has been a science role model for me in so many ways, and I have idealized him from the beginning. After six years, not much has changed. My high opinion of him remains untouched and I look forward to seeing where the lab goes in future years.

I have so many labmates to whom I am grateful and that have helped me during my PhD career. I'd like to thank Yoshie Narui, for teaching me how to express protein and modeling for me the perfect graduate student. I thank Daniel Stabley for his career advice, his support and encouragement and introducing me to Adobe Illustrator. I'd like to thank Weiwei Zheng for his support and fun lunch conversations. I'd like to thank my mentor Kevin Yehl for always making me laugh, for helping me with data analysis and being like a second PI I could talk to about science. His advice was always spot on. I'd like to thank Carol Schumacher for discussions about experiments and showing me how to order reagents. I'd like to thank Yun Zhang for her

sincere friendship, introducing me to and making me eat Chinese food, and teaching me how to master giving presentations. She helped me with my poise and my slides on so many occasions. I'd like to thank Yuan Chang for her unstinting support, friendship and help when I got sick at school. I'd like to thank Kornelia Galior for making us all laugh, her jokes and fun spirit, and helping express protein for one of my experiments. I'd like to thank Brendan Deal for teaching me how to do flow cytometry. I'd like to thank Alli Ramey for all the fun coffee breaks we had together and fun chats. I'd like to thank Aaron Blanchard for editing my first Physics World articles and introducing me to science writing. I'd like to thank Roxanne Glazier for encouraging me to cook, try new foods, eat healthily and, for her discussions about experiments and help performing FLIM for my paper. I'd like to thank Victor Ma, my classmate, for modeling for me the highest achievements a graduate student can earn and showing me what the top of the mountain looks like. And finally, I'd also like to thank Yang Liu, Zheng Liu, Yixiao Dong, Rong Ma, Kevin Fish, Dale Combs, Alisina Bazrafshan, Anna Kellner, Nusaiba Baker, Han Su and Josh Brockman, for their constant support, jokes and laughs, encouragement and help when I was down, and for giving me their chocolate.

I'd like to thank professor Emily Weinert for encouraging me during difficult days that I had with experiments. She provided perspective on how to deal with and manage stress that I have taken with me to this day. I'd like to thank my committee, David Lynn and Stefan Lutz for their support of me during the many years of my PhD and their ready and willing advice when I dropped by their offices to chat.

And lastly and most importantly of all, I'd like to thank my husband John. He's been with me from the beginning of my college career and chose to give up his career so that I could pursue mine. Through countless stress in college, he'd comfort me, while I cried in his arms about how I thought I was a failure and would never make it. He supported me unstintingly through every trial. He took care of me when I became ill and had my mental health breakdowns. He stood by my side, no matter what, when there wasn't anyone else. To say I couldn't have done this

without him is an understatement. John has been my rock and I love him with everything I have. And thank you to the readers, for choosing to read this dissertation. May it help inspire new avenues of research and thought for future students.

List of Abbreviations

Abbreviation	Full Name
DNAzyme, Dz	deoxyribonucleic acid enzyme
siRNA	short interfering RNA
RNAi	RNA interference
CRISPR	clustered regularly interspaced short palindromic repeats
PS	phosphorothioate
2’-O-Me	2’-O-methyl
PMO	phosporodiamidate morpholino oligomer
PNA	peptide nucleic acids
LNA	locked nucleic acids
CMV	cytomegalovirus
OH	hydroxyl
mRNA	messenger RNA
tRNA	transfer RNA
rRNA	ribosomal RNA
UTR	untranslated regions
nt	nucleotide
nts	nucleotides
miRNA	micro RNA
pre-miRNA	precursor miRNAs
RISC	RNA-induced silencing complex
IFN	interferon
Cas	CRISPR-associated

PAM	protospacer adjacent motif
tracrRNA	trans-encoded crRNA
sgRNA	single-guide RNA
dCas9	dead Cas9
gRNA	guide RNA
PFS	protospacer flanking sequence
PCR	polymerase chain reaction
AuNPs	gold nanoparticles
Fe_3O_4NPs	iron oxide nanoparticles
CeO_2NPs	nanoceria nanoparticles
SOD	superoxide dismutase
CTAB	cetyltrimethylammonium bromide
DIC	differential interference contrast
TEM	transmission electron microscopy
IDT	Integrated DNA Technologies
His	histidine
NTA	nitrilotriacetic acid
HPNP	p-nitrophenyl phosphate
BSA	bovine serum albumin
SNAs	spherical nucleic acids
PEG	polyethylene glycol
HCV	hepatitis C virus
DzNP	DNAzyme-AuNP
T_{10}	10-nucleotide thymidine
GDF15	TGF-β related growth differentiation factor 15

MUA	mercaptoundeconic acid
ICP-OES	inductively coupled plasma atomic emission spectroscopy
MRFs	myogenic regulatory factors
MGMT	O^6-methylguanine-DNA methyltransferase
FBS	fetal bovine serum
TMZ	chemotemozolomide
GBM	glioblastoma multiforme
HDR	homologous recombination
BFP	blue fluorescent protein
GFP	green fluorescent protein
TMC	transition metal catalyst
dsDNA	double-stranded DNA
ssDNA	single-stranded DNA
dsRNA	double-stranded RNA
SR-A	scavenger receptor class A
SR-B1	scavenger receptor class B1
ICP-MS	inductively coupled plasma mass spectrometry
SR	scavenger receptor
FCD	fucoidan
Poly I	polyinosinic acid
A549	human lung adenocarcinoma epithelium
3T3	mouse fibroblast
HaCaT	human keratinocyte

qRT-PCR	quantitative real-time polymerase chain reaction
HPV	human papillomavirus
TEAA	triethylammonium acetate
SDS	sodium dodecyl sulfate
FAM	fluorescein
BHQ™	black hole quencher™
DTT	dithiothreitol
Dz	deoxyribozyme
DzNP	deoxyribozyme gold nanoparticle
RNase A	ribonuclease A
BME	beta-mercaptoethanol
BAL	bronchoalveolar lavage
OVA	ovalbumin
TLR-9	toll-like receptor 9
LAR	late asthmatic response
EAR	early asthmatic response
2’-MOE	2’-O-methoxyethyl
MJ-EndA	*Methanococcus jannaschii* tRNA endonuclease
ADAR	Adenosine deaminases that act on RNA
CFTR	cystic fibrosis transmembrane conductance regulator
BHB	bulge-helix-bulge
PAGE	polyacrylamide gel electrophoresis

NSET	nanometal surface energy transfer
FLIM	fluorescence lifetime imaging microscopy
DLS	dynamic light scattering
PIC	protease inhibitor cocktail
KCN	potassium cyanide
DOL	degree of labeling
PNK	polynucleotide kinase
XBP1	X-box binding protein 1
IRE1α	inositol-requiring protein-1 α
UPR	unfolded protein response
DBD	DNA-binding domain
AD	activation domain

Table of Contents

List of Figures and Schemes

List of Tables

Chapter 1: Introduction on Gene Knockdown

1.1. INTRODUCTION

My research has focused on building and characterizing nucleic acid – nanoparticle therapeutics that can be used both for gene knockdown and RNA splicing. This work increases the toolkit for basic research as well as creates a repertoire from which we can explore useful drugs against a variety of disease targets. These therapeutics consist of nanozymes created by the attachment of RNA-cleaving deoxyribonucleic acid enzymes (DNAzymes) to gold nanoparticles, in addition to other enzymes, forming one enzymatic unit. During the course of this work, the synthesis, catalytic rates, and activity of these therapeutic particles have been characterized *in vitro*. Work continues to characterize these drugs in cells as well as *in vivo*. In order to understand how they operate, chapters 1-2 of this thesis will go over the basics of the field of gene knockdown and relevant nanozymes, respectively, to provide context. Afterward, a discussion of the various therapeutics and their characterization follows, finally projecting what the future may hold for this work.

1.2. Importance of Gene Knockdown

Our ability as science researchers to modulate gene expression – from the nematode *C. elegans* to insects like *Drosphila melanogaster*, *E.coli* and mammalian cells – has experienced explosive growth in the past fifty years. Gene expression, the realization of the genetic information encoded into DNA, is the heart of all life. From the infancy of its discovery, scientists have attempted to artificially regulate DNA, both for basic research and to cure disease states. Being able to modulate gene expression at will, in the cases where it is not functioning correctly, has great possibilities for being beneficial to human kind. The birth of artificial gene regulation really began with the discovery of its natural counterpart, found in the lac operon by François Jacob and Jacques Monod in 1961. Observing that cells could control gene expression convinced scientists that it was then possible to alter these pathways in disease states. The basic research that can be conducted by such manipulation is also many-

fold. For instance, by performing gene knockdown, the lowering of a genetic transcript of a particular gene in the cell, scientists can reverse engineer the properties of newly discovered genes by observing a change in cellular phenotype. Gene knockdown thus became an integral tool not only for basic science research, but also for therapy. Gene knockdown, especially in mammalian cells, is usually transient. Therefore, if used as a treatment to knockdown disease-causing genes, it is not a permanent cure. However, such a method avoids tampering with an organism's DNA which can have side-effects and long-term consequences. It is thus usually looked upon as a safer alternative to DNA editing. Gene knockdown should not be confused with gene knockout, which is the complete removal of a gene from an organism's DNA.

1.3. Methods of Gene Knockdown

There are five signature methods that have been developed to knockdown genes in an organism: antisense oligonucleotides, ribozymes, DNAzymes, RNA interference (RNAi) and clustered regularly interspaced short palindromic repeats (CRISPR). However, the field really began with antisense oligonucleotides and the discovery of ribozymes (Fig. 1.1.).

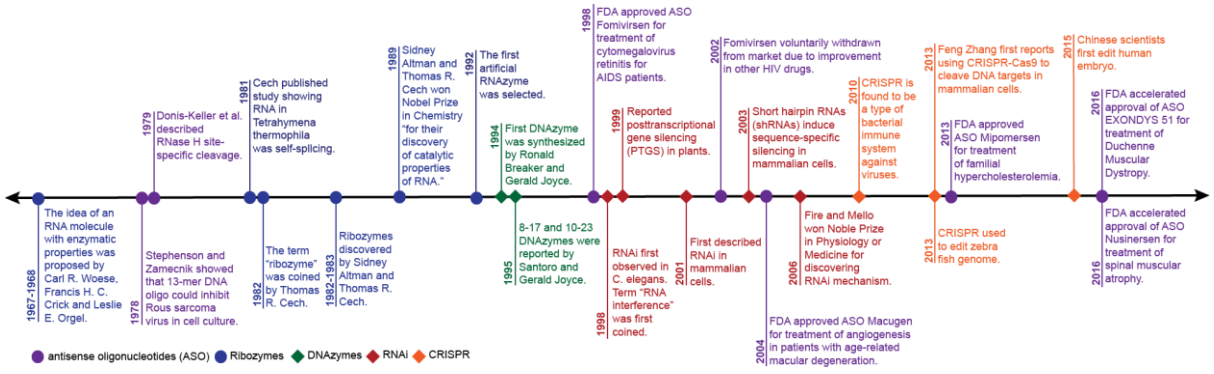

Figure 1.1. Timeline of important discoveries related to gene modulation.

1.3.1. Antisense Oligonucleotides

Several developments in synthetic chemistry and molecular biology paved the way for the eventual rise of antisense oligonucleotides as a therapy. Among them, were the creation of 2'-fluoro (2'-F) modification and development of phosphorothioate (PS) chemistry.[1] PS linkages

replace the phosphodiester bond in a nucleic acid, making it much more stable toward nucleases. This modification is also better able to bind serum proteins *in vivo*, allowing increased biodistribution and circulation time.[2-4] Additionally, the 2'-*O*-methyl (2'-*O*-Me) modification, a commonly used motif to prevent nucleases degradation, was first synthetized in the 1960s.[5] These initial developments laid the ground work for the synthetic oligonucleotide field.[1]

However, the birth of antisense oligonucleotide therapy truly came in the 1970s, when several key papers were published illustrating its utility. In 1977, Paterson and colleagues were the first to block RNA translation in a cell-free system with a DNA oligonucleotide, showing that gene expression could be modified.[6-7] This work was shortly followed by a *PNAS* paper in 1978 by Paul Zamecnik and Mary Stephenson that demonstrated that Rous sarcoma virus was inhibited by a 13-mer oligonucleotide.[8] Next, in 1979, it was shown that RNase H cleaves the RNA in an RNA-DNA heteroduplex, thus revealing two mechanisms behind antisense technology: both steric blocking and also enzyme-mediated cleavage.[9] These results, as well as others, could be said to be the falling dominoes demonstrating that antisense oligonucleotides could block gene expression in a sequence specific manner, laying ground work for potential therapies.[6]

In spite of these important discoveries, further developments in antisense technology faltered for a time due to the lack of information on the gene sequences of organisms and the difficulty of synthetic oligonucleotide synthesis.[6] However, in the mid-to-late 1980s, automated oligonucleotide synthesis was finally developed, bolstering the field. Additionally, in 1987, another key idea, the gapmer concept was first patented by Joseph Walder et al.[1] The idea of the gapmer is to have a central portion of unmodified DNA flanked by 6-8 nts of modified oligos that protect the strand from degradation by nucleases. Other developments that progressed the field in the 1980s and 1990s include phosporodiamidate morpholino oligomer (PMO) chemistry, also known as "morpholinos," developed in 1989, and peptide nucleic acids (PNA) in 1990.[1, 10]

PNAs are a type of modified synthetic oligonucleotide that replaces the phosphate backbone of a nucleic acid with amide bonds, similar to that of a peptide. This type of backbone is neutral and binding shows high affinity.[2] PMOs are also an uncharged DNA analogue, but their binding affinity is not quite as high as PNAs.[2] The 1990s also saw the invention of locked nucleic acid acid (LNA) chemistry, which was developed in Japan[11] and Denmark[12] at the same time and the 2'-*O*-methoxyethyl (2'-MOE) modification in 1995.[2, 13] Not only did these modifications protect against nucleases, they could also increase the potency of the antisense oligonucleotide by increasing its binding affinity to the target. This improvement in potency allows less oligonucleotide to be dosed while achieving the same effect, lowering the likelihood of off-target effects.[2]

The first antisense oligonucleotide entered clinical trials in the early 1990s to treat acute myelogenous leukemia.[14] However, the first to finish phase 3 clinical trials and get FDA approval was Fomivirsen, for the treatment of cytomegalovirus (CMV) in HIV patients.[15] After HIV treatment improved to the point that CMV retinitis was no longer a threat to patients, the drug was voluntarily withdrawn from the market. It should be noted that many other types of oligonucleotide therapeutics exist besides antisense oligonucleotides. These alternate technologies include splice switching antisense oligonucleotides, aptamers, ribozymes, DNAzymes, RNAi, antagomirs and miR mimics. Aptamers, antagomirs and miR mimics fall outside the discussion of this review, but the others will be discussed in more detail later.

1.3.2. Ribozymes

Ribozymes, short for "ribonucleic acid enzymes," are short RNA oligonucleotides with catalytic activity. The first one was discovered in 1982 by Thomas Cech in the organism *Tetrahymena thermophila*.[16] Its ribosomal pre-cursor RNA contained an intron, an intervening segment of RNA between the coded fragments or exons, that was capable of self-splicing. Importantly, no proteins or outside energy sources besides the intron itself appeared to be involved.[16] Shortly

after this work, Altman's lab demonstrated that the M1 RNA, composing part of the RNase P enzyme in *E.coli*, was able to process precursor tRNA without help from proteins or other outside components.[17] Due to this ground-breaking discovery, both Cech and Altman shared the Nobel Prize in Chemistry in 1989.[18] Soon, ribozymes were found in many types of organisms including viruses, bacteria, plants and lower eukaryotes, including one in humans. Many different distinct ribozymes have been found to exist in nature and more are being created synthetically by artificial selection in the lab.[18]

Ribozymes are generally divided into categories based upon their size and catalytic mechanism and can be broken down into groups based on size. The large ribozymes consist of RNase P's M1 RNA, group I and group II ribozymes. These range in size from approximately 100-3,000 nts. As far as activity, they generate reaction intermediates with 3'-hydroxyl (OH) groups and 5'-phosphates. The small ribozymes include the hammerhead ribozyme, the hairpin ribozyme, hepatitis delta and VS RNA ribozyme, ranging in size from ~35 to ~155 nts. These react differently, using the 2'-OH of ribose as a nucleophile and creating 2'-3'cyclic phosphates and 5'-OHs (Fig. 1.2.). In nature, all ribozymes, except M1 RNA from RNase P, modify themselves rather than other nucleic acids, and cannot be considered true enzymes. However, they can easily be modified to shift their catalytic activity from themselves to effect other RNAs *in trans*.[18]

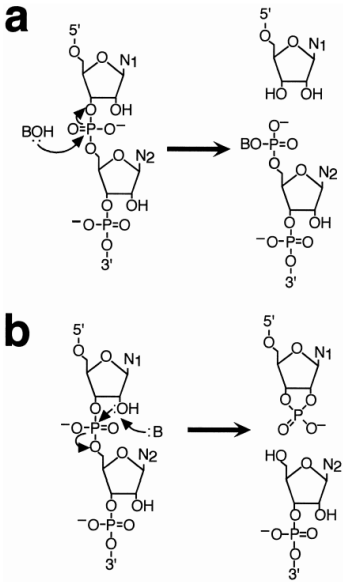

Figure 1.2. The types of catalysis performed by (a) large and (b) small ribozymes. Reprinted by permission from Oxford University Press: FEMS Microbiology Reviews from reference 18, Copyright (1999).[18]

The catalytic efficiency of ribozymes k_{cat} / K_M is 10^8 M^{-1} min^{-1} with reaction rates increased up to 10^{11}-fold, which is close to diffusion-controlled formation of an oligonucleotide duplex.[19] However, even so, the k_{cat} is ~10^3-fold less than the k_{cat} that

can be produced by protein enzymes doing similar chemistry.[20] Additionally, protein enzymes have the advantage of being far more multi-turnover than the average ribozyme, as product release from the ribozyme is slow and its active site is saturated quickly.[18] For their catalytic activity, a ribozyme absolutely requires a divalent metal ion, usually Mg^{2+}. Therefore, ribozymes are classified as metalloenzymes. Large ribozymes generally also need metal cations for structural support and to fold properly. It is not as obvious how metal cations are involved in the catalysis of smaller ribozymes, but they are thought to be important for their activity.[18]

The group I and group II ribozymes are part of five classes of introns that contain different splicing mechanisms. Some of the sequences found in group I and group II are ribozymes – able to catalytically splice themselves out of transcripts *in vitro*. Yet, *in vivo*, most of these RNAs still require a protein cofactor. Group I introns can be found between 100-3,000 nts long and are more prominent in fungi and plants; however, they can be found anywhere except in the higher eukaryotes.[19, 21-22] There is a high amount of sequence diversity and dissimilarity between members of the group I ribozymes; nevertheless, most all contain four conserved elements known as P, Q, R and S. Additionally, the secondary structures of group I introns are relatively conserved, forming ten categorized segments.[18]

Group II introns range in size from 100-2,500 nts. Interestingly, they are not as widely distributed as group I introns, being found in the mitochondria of fungi and plants, chloroplasts, algae and eubacteria.[19, 21, 23-24] Most are found in messenger RNA (mRNA), although some few are also found in transfer RNA (tRNA) and ribosomal RNA (rRNA) genes.[18] This class of intron is much less studied because few of them produce viable ribozymes that can catalyze an *in vitro* reaction, generally requiring catalytic conditions not found in a biological setting. Both group I and group II introns can catalyze splicing, doing so with slightly different steps (Fig. 1.3.). Both perform *trans*-esterification reactions to cleave and ligate the RNA segments. However, group I introns use a guanine cofactor to initiate the reaction, while group II introns use an internal adenosine. Of note, nuclear pre-mRNAs are spliced with the same reaction mechanism as group II introns, except it occurs not through self-splicing but as part of a large ribonucleoprotein complex.[18]

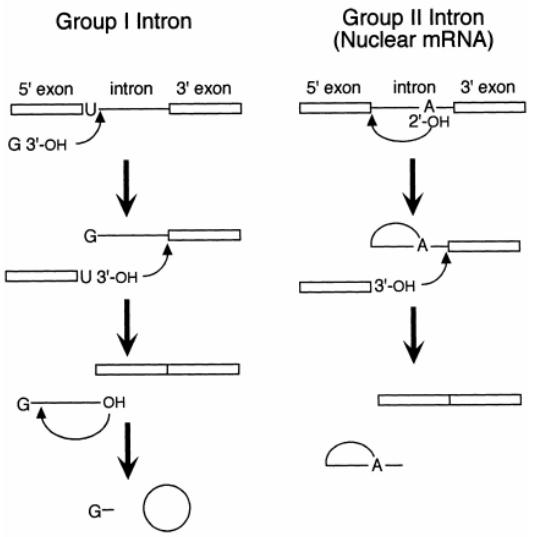

Figure 1.3. Splicing pathways of the group I and group II intron. Reprinted by permission from Oxford University Press: FEMS Microbiology Reviews from reference 18, Copyright (1999).[18]

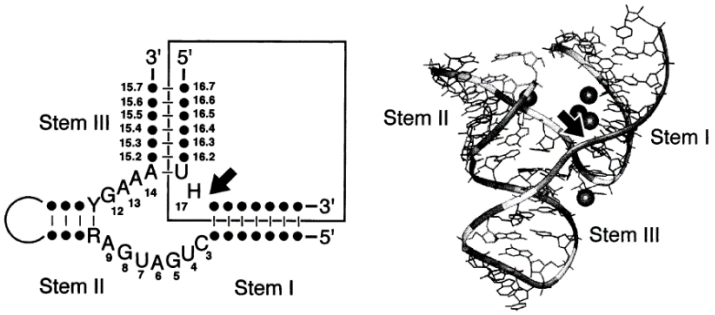

Figure 1.4. Structure of the hammerhead ribozyme. The dots indicate any nucleotide, Y indicates a pyrimidine, R indicates a purine and H indicates any nucleotide besides guanosine. The arrow indicates where cleavage occurs. Reprinted by permission from Oxford University Press: FEMS Microbiology Reviews from reference 18, Copyright (1999).[18]

The small ribozymes, ranging in size from ~220 to ~460 nucleotides are well-understood and more often used in therapeutic applications.[18] Similar to the large ribozymes, they require Mg^{2+} for catalysis and are most often found in viral RNA plant pathogens such as viroids, virusoids and linear satellite viruses.[25-26] However, they can also be found in satellite RNA of salamanders. As stated above, ribozymes naturally function by cleaving themselves. To turn them into an enzyme that cleaves in *trans* one merely must separate the ribozyme from its substrate, putting them on separate sequences.[18] After separation, the substrate still fits into the structure of the ribozyme. This may be one reason why release is so poor. A few of the common small ribozymes will be examined below, with their advantages and disadvantages.

1.3.2.1. Highlight: Hammerhead Ribozyme

The third catalytic RNA to be discovered,[27] the hammerhead ribozyme, is found most often in satellite RNAs and viroids.[18, 25] It is one of the most studied and well-understood, as well as the smallest naturally occurring ribozyme, at 40 – 50 nts long.[18] The ribozyme got its name from the fact that its secondary structure reminded its Australian discoverers of a hammerhead shark. At least sixteen hammerhead motifs exist among plant viruses and another three more are found in the genes of three different species of salamanders. The hammerhead ribozyme consists of three single-stranded regions and three helical regions of variable length and sequence (Fig. 1.4). Most of the conserved residues can be found in the single-stranded regions. These conserved nucleotides are necessary for catalysis, with mutations significantly reducing activity. This ribozyme was the first that had its crystal structure solved,[18] by McKay and coworkers in 1994.[28] As discussed above for other ribozymes, in its natural setting, the hammerhead ribozyme is not a true enzyme in that it cleaves itself, not another substrate. However, it can be modified to cleave *in trans* by separating the enzyme from its substrate loop. Interestingly, the RNA in the hammerhead ribozyme, as well as the hairpin and VS RNA ribozyme, takes an active role in catalysis, making these ribozymes not strictly metalloenzymes, dependent on a

cation alone. It was found that these ribozymes could catalyze a cleavage reaction even without Mg^{2+}, as long as a source of positive charged exists in the reaction (such as Na^{+}). This contradicted the originally held hypothesis that the RNA acted merely as a scaffold for the metal ion that did all the catalysis of the cleavage reaction.[27, 29] The RNA is not passive, but an active participant in the reaction. Under typical reaction conditions of pH 7.0 and 10 mM $MgCl_2$, the hammerhead ribozyme has a catalytic rate of 1 min^{-1}.[30] In plants viruses, the hammerhead ribozyme assists in the processing of the viral genome during rolling-circle amplification.[18] However, more recently, hammerhead ribozymes have also been discovered in mammalian species within the 3' untranslated regions (UTRs) of C-type lectin type II genes (CLEC2), suggesting that they may also have cellular functions.[31]

1.3.2.2. Highlight: Hairpin Ribozyme

The hairpin ribozyme, originally known as "paperclip," can be found in three satellite viruses of plant origin. The one contained in the tobacco ring spot virus is the most well-studied. Its structure consists of four stems whose secondary structure looks like a hairpin or paperclip formation (Fig. 1.5.). Unlike the hammerhead ribozyme, the hairpin ribozyme is effective at both cleaving and ligating its RNA target,[18] making it a tool for clinical applications. Interestingly, the hairpin ribozyme is more efficient at ligation (rate of 3 min^{-1}) than cleavage (rate of 0.2 min^{-1}).[32]

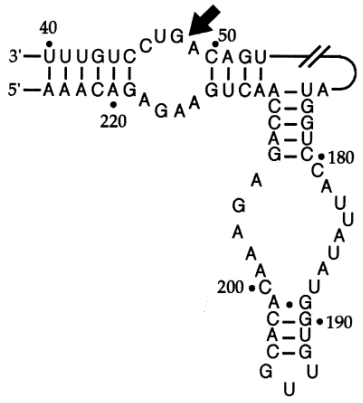

Figure 1.5. Structure of the hairpin ribozyme. Arrow indicates cleavage position. Reprinted by permission from Oxford University Press: FEMS Microbiology Reviews from reference 18, Copyright (1999).[18]

1.3.3. RNA Interference

RNA interference (RNAi) is very well-conserved, and can be found in plants, *Neurospora*, *Drosophila*, *C. elegans* and mammals, first coming to light in plants

in the 1980s.[33] However, it's mechanism and function were obscure until the late 1990s when Fire and Mello[34] found in *C. elegans* that RNAi is a natural gene-silencing mechanism. A few years later in 2002, the journal *Science* lauded RNAi as the "Scientific Breakthrough of the Year,"[33] due to the ease with which the pathway can be manipulated to knockdown genes, potentially providing control over epigenetics and stem cell differentiation.[35] RNAi functions as a viral defense mechanism, as well as a method to control mobile genetic elements such as transposons, contributing to genetic stability.[33] Later, it was also found to regulate over 30% of human genes, including those involved in cell growth, tissue differentiation, heterochromatin formation, and cell proliferation.[36]

The vehicle for RNAi is small RNAs of 21-23 nucleotides (nts) called micro RNA (miRNA). These small RNAs are processed in the nucleus from larger 1,000-nt transcripts known as the primary miRNAs or pri-miRNAs.[36] A complex of enzymes (the RNase III family enzyme Drosha and DiGeorge syndrmo critical region gene 8, or DGCR8) divide pri-mRNA into smaller precursor miRNAs (pre-miRNA) of roughly ~65-70 nts.[36] Exportin-5 and RanGTP then associate with the pre-miRNAs and export them to the cytoplasm where they undergo further processing. The enzyme Dicer trims the RNA down to a double-stranded RNA (dsRNA) of 21-25 nts, with 2-nt overhangs on the 3' termini. This new miRNA is then loaded onto an Argonaute protein, generating the RNA-induced silencing complex (RISC).[36] During loading, one of the miRNA strands is selected for binding to the RISC while the other is degraded, being referred to as the guide and passenger strands, respectively. Which strand is chosen as the guide determines the RNA silencing that follows.[36] After guide strand selection, the RISC complex is free to bind to its target RNA through the miRNA seed sequence. Binding can be complete or involve several mismatches. In the case of complementary binding, the target RNA can be cleaved, if the Argonaute protein in the RISC has ribonuclease activity.[36] Otherwise, or if there are mismatches, binding still results in silencing of the RNA through translational

repression either before or after initiation. In this case, after RISC binding, the RNA transcript is deadenylated and degraded. So far, over 1,000 miRNA have been characterized in mammalian cells.[36]

Scientists can also introduce small dsRNA into cells that can result in the same type of RNAi arising from miRNAs. These are referred to as short interfering RNA or siRNA, and are created synthetically or are of viral origin.[33] Upon entering the cytoplasm, they are processed in a similar manner to miRNAs and generally have complete complementarity with their target RNA.[33] It is important to note that in mammalian cells, dsRNA longer than 30 nts triggers the γ-interferon (IFN) pathway, part of the immune system responsible for detecting viruses. Thus, if scientists wish to use siRNA in mammalian cells, they must generate dsRNA smaller than 30 nts through chemical synthesis, enzymatic cleavage or through an expression system.[33]

As of 2012, there were over 50 RNA-based therapeutics that were in clinical trials.[37] However, more recently, due to the difficulty associated with RNAi – delivery, stability, specificity, immune activation and off-target effects – has lead to a mass exodus of pharmaceutical companies from the field. Pfizer sold its share in RNAi research in 2011, with Merck and Novartis following suit in 2014.[38] Even so, there has been one success story. The company Alnylam recently received FDA approval in August 2018 for their RNAi drug Onpattro (patisiran) to treat transthyretin-mediated amyloidosis, a rare hereditary disease with orphan status. This makes patisiran the first RNAi drug ever to be approved since research began in the field, and is a milestone for future efforts.[38]

1.3.4. Clustered Regularly Interspaced Short Palindromic Repeats (CRISPR)

The latest hot technology for DNA editing, CRISPR, was also shown to perform RNA knockdown by Feng Zhang in 2016 and 2017.[39-40] CRISPR, or **c**lustered **r**egularly **i**nterspaced **s**hort **p**alindromic **r**epeats was originally discovered as a type of bacterial immune system that

fights viral invasion. However, scientists quickly realized that CRISPR proteins could be hijacked to perform DNA editing in other systems. This led eventually to the discovery of a CRISPR protein, known as Cas13, that could perform RNA knockdown as well, with comparable efficiencies to RNAi.[39] This discovery has opened the door for perhaps an even more efficient method of RNA knockdown to be achieved than RNAi, once optimized. What follows is a short history of the discoveries leading up to CRISPR, and advances that lead the technology to where it is today.

1.3.4.1. The 1980s: Beginnings

CRISPR loci, or sequences of regularly spaced palindromic DNA repeats in bacteria, were first observed in the 1980s and given a wide variety of names. Yet, their function eluded scientists for almost twenty years after their initial discovery. With the onset of genome sequencing in the 1990s, more of these repeats were discovered in many different organisms and systematic study of them became possible. The term "CRISPR" was finally coined in 2002.[41-42]

1.3.4.2. *The 2000s: Launching the CRISPR Field*

In 2005, three different labs made the discovery that the random sequences in between the repeat DNA of the CRISPR loci matched that of DNA pathogens.[41, 43-45] From this observation, the hypothesis was proposed that the CRISPR loci formed the basis of a immune system for prokaryotes against invading nucleic acids.[41] Upon further investigation, it was found that CRISPR genotypes corresponded to bacterial resistance to certain phages.[41] Finally in 2007, a cornerstone paper[46] was published launching the rise of the CRISPR field and showed the following: (1) the spacer sequences inside CRISPR loci originated from phage DNA taken up by bacteria; (2) bacterial resistance to phage was tied to the CRISPR spacer sequence and changing this sequence led directly to the altering of bacterial resistance; (3) the addition of new spacers and the phage defense process involved CRISPR-associated (Cas) genes. After this

work, a domino effect of papers began rolling out, initially focused on the mechanism of CRISPR.[41] Among them, it was demonstrated that CRISPR RNAs guide Cas proteins to target DNAs.[41] Equally important was the discovery of the protospacer adjacent motif (PAM) located near the targeted sequences and acting as a homing beacon for the RNA guides.[47-49] Next, was the work showing that Cas9 functioned as an endonuclease to create a blunt DNA cut 3' downstream of the 3' end of PAM.[50] In 2011, work indicated that an RNA referred to as the trans-encoded crRNA (tracrRNA) is required as part of the guiding RNA strand for Cas9.[51] Additionally, CRISPR–Cas was shown to be transferrable to other bacterial species, enabling the knockdown of plasmids and phages.[52] It soon became clear that there were many common themes among CRISPR systems in different organisms, but they functioned in distinct ways, leading to a classification system for CRISPR.[41] Currently, there are two classes of CRISPR: class I involves those with a multi-protein effector complex, while class II has a single protein effector. The classes can be further divided into six main types (I – VI) and numerous subtypes.[41] The seminal work for transforming CRISPR into a gene editing tool came with two papers showing in the summer of 2012 that Cas9 uses RuvC and HNH domains to create nicks in DNA.[53] The targeting specificity could be altered by a single-guide RNA (sgRNA), created to mirror the dual crRNA:tracrRNA complex.[54]

1.3.4.3. Post 2012: Modern applications of CRISPR

Within only a few short months, several labs had demonstrated that CRISPR-Cas9 could give rise to double-stranded DNA breaks and DNA editing, with the help of DNA repair systems.[55-57] These results sparked the "CRISPR craze,[58]" greatly simplifying gene editing and making it accessible to wide range of scientists.[41] CRISPR-Cas proteins led to the ability to edit any characterized organism – specifically, Cas9, Cpf1 and dead Cas9 (dCas9, a deactivated version of Cas9).[41]

1.3.4.4. Post 2016: CRISPR for RNA knockdown

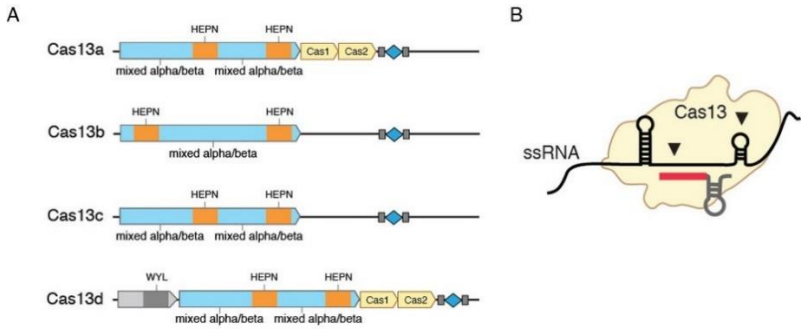

Figure 1.6. (A) Cas13 orthologs. The HEPN domains yield RNase activity. (B) Cas13 recognizes its target through complexing with a small gRNA.[59]

Although originally hailed as a gene editing tool, it soon became clear that not all CRISPR proteins targeted DNA. Some, namely Cas13 (known previously as C2c2) targeted RNA as well (Fig. 1.6.).[40] In fact, one type in each class focuses on RNA: type III of class I and type VI of class II, of which Cas13 is a member.[60] Since that initial discovery, four orthologs of Cas13 have been characterized.[61] Similar to Cas9, Cas13 also uses a guide RNA (gRNA, ~64 nts long) to find and complex with its target RNA (Fig. 1.7.). The Cas13 binds to the gRNA via a hairpin in the crRNA, attached to a spacer (~28-30 nts) that provides specificity to the target RNA.[59] After target recognition and cleavage, Cas13 remains in an activated state and will then cleave any nearby RNA transcripts, regardless of target specificity. However, this activity is seen only in bacteria, rather than in mammalian cells.[59] The most robust activity for RNA knockdown has been observed with Cas13d ortholog rather than Cas13a, although both show activity.[59, 61] For RNA knockdown, depending on the ortholog or subtype of Cas13 used, one has to modulate the gRNA and take note of differing targeting restrictions.

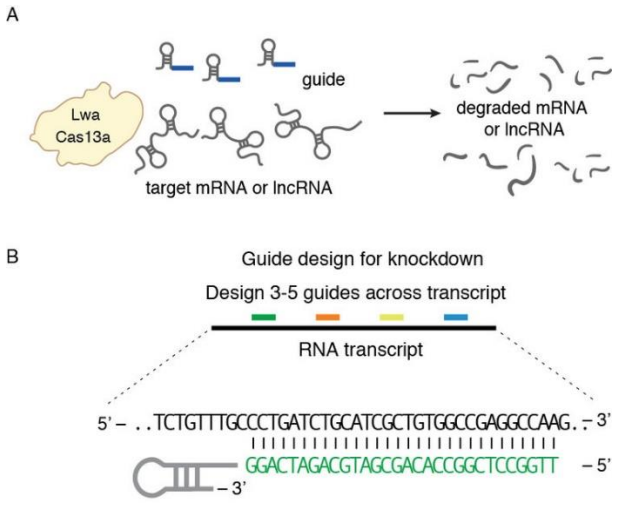

Figure 1.7. (A) RNA knockdown by Cas13. (B) Using several gRNAs along the RNA transcript increases knockdown.[59]

For example, for Cas13a, a protospacer flanking sequence (PFS), similar to PAM in Cas9, was necessary for target cleavage both in *E.coli* and *in vitro* but not in mammalian cells. The PFS required a non-G base to be present immediately 3' of it.[59] Another factor that one must consider for RNA knockdown with Cas13 is the target RNA's secondary structure. Cas13 cleaves single-stranded RNA and does not bind well to double-stranded or structured RNA regions, as it has no helicase activity.[59] The Zhang lab recommends that one test 3-5 gRNAs to find the most efficient one, as well as using several in tandem for knocking down RNA in mammalian cells.[59]

1.4. Gene Knockdown with DNAzymes

1.4.1. Why use DNAzymes?

Nucleic acids – especially DNA – would not appear to be the first choice for building new synthetic enzymes at first glance, as it has fewer functional groups than protein, for example.[62] However, clearly nature has utilized RNA enzymes or ribozymes for catalytic activity in such ribonucleoproteins as important as the ribosome[63] and other enzymes such as RNase P.[18] One reason why DNA was overlooked as an enzyme for so long is that it lacks the 2'-OH groups found on RNA, which decreases somewhat its chemical diversity. DNA enzymes are also not found in nature, as DNA has a proclivity toward being double-stranded, which prevents it from forming complex secondary and tertiary structures needed for catalytic activity.[62]

However, in the lab, scientists have had success at creating a wide-variety of DNA enzymes or DNAzymes through *in vitro* selection. The ability of DNA initially surprised scientists, but it turns out that although DNA lacks the 2'-OH groups, this deficiency is compensated for in increased flexibility of DNA over RNA, giving it a wider variety of conformations that it can form, increasing its utility in reactions.[64] There are also several reasons one might want to choose DNA over RNA or protein for building new synthetic enzymes. Namely, that DNA, because it lacks the 2'-OH group, is ~100,000 times more stable than RNA under physiological conditions.[65]

Interestingly, under the same conditions, DNA phosphodiester bonds are also more stable than peptide bonds to degradation by about 1,000 times.[66] Additionally, DNA has become inexpensive to synthesize, in comparison to both RNA and proteins, and can be amplified directly by the polymerase chain reaction (PCR). It is easily bound to surfaces or used in solution and it is simple to modify the DNA to increase its chemical stability or add functionality by increasing its number of functional groups. With these advantages, DNA becomes a versatile tool to expand the functionality of synthetic enzymes.[62] In the rest of this section, we will focus on the discovery of these enzymes, specifically focusing on DNAzymes with activity for cleaving RNA. RNA-cleaving enzymes make up the vast majority of DNAzymes[62] and are the ones most pertinent to this thesis. We will discuss the rise of the popular 10-23 DNAzyme moiety, the process of how it was selected, and a few of its applications.

1.4.2. History of RNA-cleaving DNAzymes: In vitro selection and the first DNAzyme

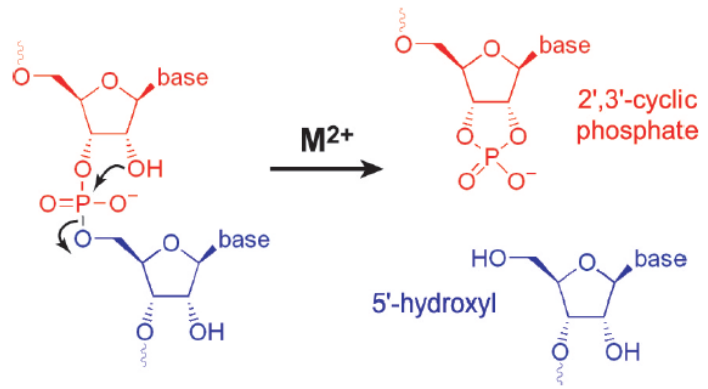

Figure 1.8. RNA cleavage reaction conducted by RNA-cleaving DNAzymes.[67]

As DNAzymes do not exist in nature, all instances of them were discovered by *in vitro* selection,[62] also known as "systematic evolution of ligands by exponential enrichment," or SELEX. However, the term SELEX is generally applied to the selection of aptamers rather than DNAzymes.[62] *In vitro* selection involves the discovery of catalytically active DNA sequences from a large, random pool of nucleic acids.[67] This is done through iterative rounds of selection until a small number of target sequences are obtained. Breaker and Joyce reported the first discovery of a DNAzyme in 1994.[68] It was able to cleave a single RNA ribonucleotide embedded within an all-DNA strand. All RNA-cleaving DNAzymes perform the same reaction

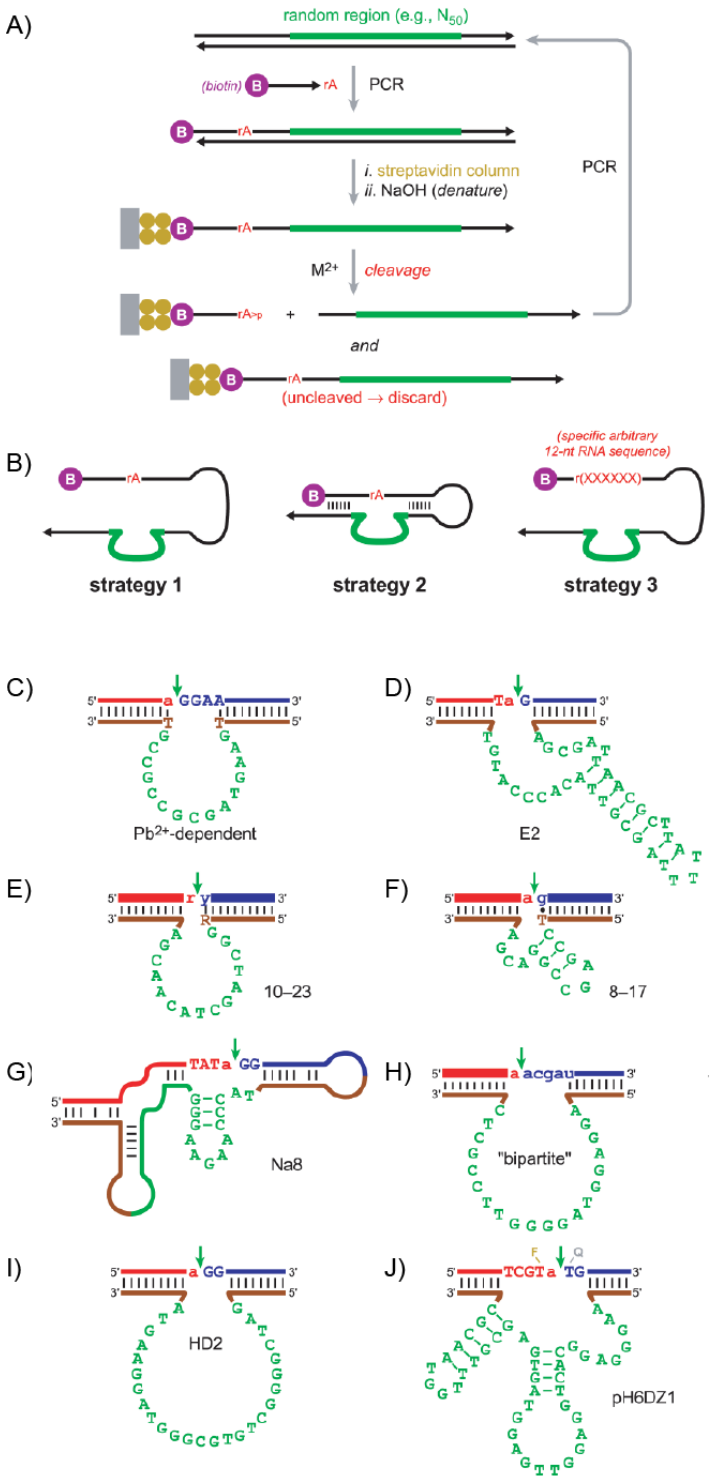

Figure 1.9. DNAzyme selection and resulting sequences discovered. (A) Route for *in vitro* selection of 10-23 DNAzymes. (B) Starting substrates used for selection, differing in how they organize the cleavage site. (C-J) RNA-cleaving DNAzymes discovered from 1994-2005.[67]

(Fig. 1.8.), catalyzing attack of the 2'-OH on the ribose onto the phosphodiester backbone, leading to 2',3'-cyclic phosphate and 5'-OH cleavage products.[67] Although this reaction can occur naturally under basic conditions, and thus, has a low energy barrier to overcome, DNAzymes can accomplish it site-specifically, making them more controlled and useful than the occurrence of random cleavage events.[67] To discover this first DNAzyme, Breaker and Joyce used strategy 1 in Figure 9B, attaching a stretch of N_{50} nucleotides, where N is a random nucleotide, to a biotinylated DNA having a single ribonucleotide (Fig. 1.9A-B.). The N_{50} region was attached to this biotinylated DNA via PCR. This DNA was then immobilized onto a streptavidin column and denatured, removing the non-biotinylated strand. A buffer containing a metal ion was flowed over the column,

allowing for active sequences to cleave at the ribonucleotide. These cleaved sequences were then collected, amplified by PCR and reattached to the biotinylated DNA support for another round of selection. At the end of all the selection rounds, individual sequences were found through cloning.[67] One might ask, why since only active sequences should cleave the target, are the DNAzymes not identified after only one round of selection? The reason lies in that each catalytically inactive DNA sequence has a random chance of having its RNA cleaved spontaneously. These spurious cleavage events act like background or noise that must be filtered out through multiple rounds of selection. Additionally, there are many variations of active sequences with a range of activities. The higher the selection round, the more likely the sequences in it are the result of genuinely active cleavage by active DNAzyme sequences.[67] The first DNAzyme discovered was identified after five rounds of selection using the metal ion Pb^{2+} (1 mM) and starting with a pool of ~10^{14} DNA sequences (Fig. 1.9C.).[68] It possessed a k_{cat} of 1 min^{-1} and a K_M of 2 µM at pH 7.0 and 23ºC, 0.5 M NaCl and KCl. Therefore, K_{cat}/K_M = 5 x 10^5 M^{-1} min^{-1} which gives a rate enhancement of k_{cat}/k_{uncat} of 10^5, approaching the value of the hammerhead ribozyme.[67] Unfortunately, since only one ribonucleotide was used in the selection process, it was found that this DNAzyme could not cleave an all-RNA substrate.[67]

Breaker and Joyce produced a follow-up paper shortly after their initial discovery, this time identifying a Mg^{2+}-dependent RNA-cleaving DNA enzyme, utilizing strategy 2 in Fig. 1.9B. In this case, for selection, a randomized N_{40} of DNA was used between binding arms on either side (Fig. 1.9B., strategy 2). However, once again, a single ribonucleotide was included as the substrate during selection, eventually leading the final DNAzyme selected not to cleave an all-RNA substrate. It was created using a hybrid of *in vitro* selection and evolution, since after six rounds of selection, the catalytic core was randomized at each nucleotide by 15%. This led to the E2 DNAzyme (Fig. 1.9D.). It had a k_{obs} = 0.01 min^{-1} at 1 mM Mg^{2+} and a k_{obs} = 0.08 min^{-1} at

>100 mM Mg^{2+} or saturating conditions. The rate enhancement was once again approximately 10^5.

Faulhammer and Famulok embarked on a third attempt to find RNA-cleaving DNAzymes, using strategy 1 of Fig. 1.9B., a single ribonucleotide cleavage and a randomized region of N_{74} with ten rounds of selection.[69] By adding histidine into the reaction buffer (20 mM), they were hoping to find a histidine-dependent DNAzyme, so only included 0.5 mM Mg^{2+} in their reaction buffer. They named their DNAzyme "Mg5" (not shown in Fig. 1.9.) and surprisingly found that it was Ca^{2+}-dependent and histidine-independent. Ca^{2+} was not used during selection. It exhibited a k_{cat} of 0.1 min^{-1} and a K_M of 6 µM at 10 mM Ca^{2+} (pH 7.0) and 37ºC. The k_{cat}/K_M = 1.6 x 10^4 M^{-1} min^{-1} giving a rate enhancement for Ca^{2+} of ~10^4.[67]

1.4.3. Second generation of DNAzymes: Birth of 10-23 and 8-17

The Joyce lab sparked a new generation of experiments when Santoro and Joyce set out to tackle the problems of a sub-optimal k_{cat}/K_M in previous DNAzymes and the fact that they were unable to cleave all-RNA targets. Using strategy number three (Fig. 1.9B.), a stretch of 12 nts of RNA in the target during selection, they would produce what are now the two most simple and popular RNA-cleaving DNAzymes: known as 10-23 (Fig. 1.9E.) and 8-17 (Fig. 1.9F.).[67, 70] These DNAzymes were named after the selection round and clone number in which they were discovered, and both were able to cleave all RNA-targets[67]. The 10-23 DNAzyme was found to have a k_{cat} of 0.15 min^{-1} and a K_M of 0.5 nM in buffer with 2 mM Mg^{2+}, 150 mM NaCl, pH 7.5 and 37ºC, simulating physiological conditions.[70] The k_{cat}/K_M = 3 x 10^8 M^{-1} min^{-1}. However, these conditions did not allow the 10-23 DNAzyme to reach maximal velocity. With 50 mM Mg^{2+}, pH 8.0 and 37ºC it was found that k_{cat} = 3 min^{-1} and K_M = 0.8 nM, giving a k_{cat}/K_M of 4 x 10^9 M^{-1} min^{-1}.[67] This value of k_{cat}/K_M beats that of hammerhead or hairpin ribozymes by 1-2 orders of magnitude, clearly showing that DNA is able to do the same type of reactions that are open to RNA.[67] Although the 10-23 DNAzyme cannot compete with an enzyme like RNase A in terms of

its k_{cat} (10^4-fold less), it's K_M is more favorable by about 10^5-fold. A favorable K_M comes from the fact that DNAzyme binding is quite stable and can be made more so by increasing the length of its binding arms, something a protein enzyme cannot modulate. Therefore, the 10-23 DNAzyme k_{cat}/K_M is competitive with RNase A if not better,[67] especially at low substrate concentrations. However, is should be noted that one can only increase the K_M by increasing the binding arms so much before it starts to limit turnover number for the DNAzyme. In DNAzymes with long binding arms, the rate limiting step becomes release of the product.[67] One must balance binding with multi-turnover kinetics.

1.4.3.1. 8-17 Variants

Three other investigators conducted searches for DNAzymes that ended up converging on the 8-17 DNAzyme motif in their catalytic cores.[67] Interestingly, it was found by Peracchi, after performing mutagenesis on 8-17, that the majority of the mutants as well as the original DNAzyme exhibited much higher k_{obs} (10-20-fold) if Ca^{2+} was used instead of Mg^{2+} in the reaction.[71] This behavior was similar to what was found with the Mg5 DNAzyme.[69] In fact, the core of the Mg5 DNAzyme was found to contain 8-17 within conserved regions. With some minor changes, it was found that Mg5 could be improved and made to cleave an all-RNA substrate, similar to the parent enzyme 8-17. The relationship between them was not obvious until after 8-17 had been discovered.[67] The hunt for DNAzyme continued with Lu and coworkers seeking to find a Zn^{2+} dependent species.[72] Interestingly, the one they identified, 17E, had a 8-17-like catalytic core as well. Why it preferred Zn^{2+} over Mg^{2+} or Ca^{2+} was not self-evident.[67] Additionally, although the 8-17 cleaves at AG dinucleotides,[70] 17E cleaves at GG with the same affinity as it cleaves at AG dinucleotides.[72] Lastly, using strategy 2 of Fig. 1.9B., Li and coworkers identified a number of 8-17 variants that can cleave any RNA dinucleotide. The plan had been to identify new DNAzymes, but 8-17 quickly rose to the forefront in all the selection pools attempted, showing that it is a favored sequence for RNA cleavage.[73]

1.4.3.2. Other RNA-cleaving DNAzymes

In 1997, Geyer and Sen began searching for an RNA-cleaving DNAzyme that did not require metal cations.[74] Considering that it was not yet well understood that their counterpart, ribozymes, were not always metallo-enzymes, their idea was rather novel.[67] After 12 rounds of selection and 6 additional rounds after cloning using strategy 2 in Fig. 1.9B., the Na8 DNAzyme was born (Fig. 1.9G.). Although it was slow cleaving, with a k_{obs} of 0.007 min^{-1} (0.5 M NaCl, pH 7.0, 25ºC), one must keep in mind that the uncatalyzed reaction rate is ~3 x 10^{-10} min^{-1}. Therefore, the k_{obs}/k_{uncat} of 2 x 10^7 is impressive. In their work, it was shown that adding the metal ions Mg^{2+}, Ca^{2+} or Zn^{2+} did not affect the DNAzyme's activity and monovalent ions other than Na^+ could be used.[74] Another DNAzyme of note, known as the 'bipartite DNAzyme' was synthesized by the Sen lab using strategy 1 (Fig. 1.9B.) and an N_{40} randomized region.[75] They did 12 rounds of selection, cloning and 7 more rounds of selection afterwards. It was unique, having no connection to 8-17 or any of the other varieties. At the cleavage site, it prefers multiple unpaired base pairs, besides the pair of binding arms.[75] In addition, the Benner lab identified another unique DNAzyme called 614 that showed itself to be Mg^{2+}-independent.[76] And finally, a few histidine-dependent DNAzymes were found (of which HD2 is one, Fig. 1.9I.) by Roth and Breaker.[77] These were identified using EDTA in the buffer, to ensure no metal ions would be present, also using strategy 2 of Fig. 1.9. and an N_{40} randomized region. The DNAzyme went through 11 rounds of selection and 5 rounds of re-selection. It was found to indeed require L-histidine as a cofactor for catalysis, as well as K^+ and imidazole, which hint at the use of G quartets in the structure.[67]

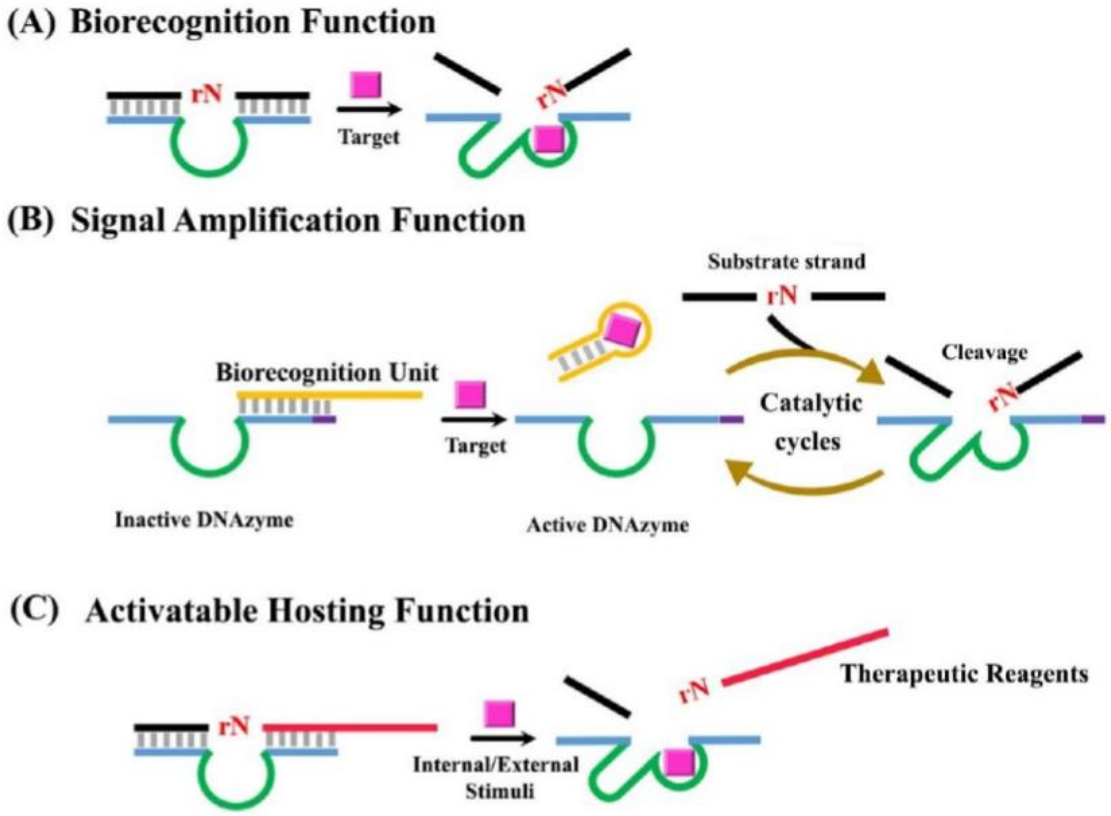

Figure 1.10. The three modes of RNA-cleaving DNAzymes that can be utilized as probes.[78]

1.4.4. Applications of RNA-cleaving DNAzymes

In addition to basic research into DNAzyme function, scientists are also interested in their applications. Generally, these fall under five different areas: 1) molecular biology tools, 2) therapeutic agents, 3) nanomotors, 4) analytical chemistry and 5) computational devices.[62] DNAzymes, as a molecular biology tool, can essentially be used as 'restriction enzymes' for RNA.[79] For this purpose, the 10-23 and 8-17 DNAzymes are most commonly used.[67] Additionally, RNA-cleaving DNAzymes can be used to knockdown mRNA in cells, alongside other therapies already discussed, such as antisense oligonucleotides, ribozymes, siRNA[67] and CRISPR. They can also be used as sensors and probes. These are the considerations that we will focus on in the rest of this thesis. First, we will give some examples of recent work with RNA-cleaving DNAzymes showing their capabilities in this area. There are three types of

probes that can be produced from RNA-cleaving DNAzymes: probes relating to biorecognition, those that rely on signal amplification, and those that detect an intracellular agent (Fig. 1.10.).[78] When used in such therapeutic studies, certain other considerations come to the fore. First, DNAzymes must be effectively delivered to cells. Once delivered, they must last long enough against the cocktail of cellular nucleases they encounter to effectively knockdown their target. For stability, modifications to the DNA can be used similar to antisense oligonucleotides, such as LNAs, 2'-*O*-Me and 2'-MOEs on either end of the DNAzyme binding arms (the gapmer concept). The biggest question facing the field then is not stability – as DNA is more stable than RNA, and with modifications, is able to effectively battle nucleases. The biggest issue to address is delivery. Being negatively charged, naked DNA cannot simply pass through the cell membrane unhindered. Studies have used DNA expression vectors, electroporation and modified delivery agents of various types to deliver DNAzymes, but each of these has its own set of problems and certainly DNA expression vectors and electroporation are not optimal for delivery in *in vivo* settings. In the work that follows, we show how we are able to address the question of delivery, while also providing an effective platform for DNAzyme activity inside cells.

1.4.5. Motivation: Our System, the DzNP Nanozyme

We solve the delivery question by attaching many copies of the 10-23 DNAzyme via a synthetic thiol linkage to a 13 nm gold nanoparticle, creating a multivalent nanozyme. The nanoparticle acts as an inert carrier, as it has been shown that DNA attached to gold particles of this size are rapidly and effectively uptaken into mammalian cells via scavenger A type receptors. Notably, it is the spherical arrangement of the DNA rather than the gold itself that provokes this recognition and uptake. Other advantages to using a gold core include that it is relatively non-toxic and easily functionalized with ligands via single mono-thiols attached to the DNA. DNAzymes, which are already more stable than their natural counterparts, ribozymes, are provided with even more stability once they are attached to a gold particle, as the particle protects the

attached ends via steric hindrance from nucleases. To better put this work in context, it will be helpful to consider the history of the nanozyme field, looking at how nanozymes are classified and how the field has evolved and grown.

1.5. References

1. Lundin, K. E.; Gissberg, O.; Smith, C. I., Oligonucleotide Therapies: The Past and the Present. *Hum Gene Ther* **2015,** *26* (8), 475-85.
2. Watts, J. K.; Corey, D. R., Gene silencing by siRNA and antisense oligonucleotides in the laboratory and the clinic. *The Journal of pathology* **2012,** *226* (2), 365-79.
3. Geary, R.; Yu, R.; Levin, A., Pharmacokinetics of phosphorothioate antisense oligodeoxynucleotides. *Current Opinion in Investigational Drugs* **2001,** *2* (4), 562-573.
4. Watanabe, T. A.; Geary, R.; Levin, A., Plasma protein binding of an antisense oligonucleotide targeting human ICAM-1 (ISIS 2302). *Oligonucleotides* **2006,** *16*, 169-180.
5. Bobst, A.; Rottman, F.; Cerutti, P., Effect of the methylation of the 2'-hydroxyl groups in polyadenylic acid on its structure in weakly acidic and neutral solutions and on its capability to form ordered complexes with polyuridylic acid. *J Mol Biol* **1969,** *46*, 221-234.
6. Oberemok, V. V.; Laikova, K. V.; Repetskaya, A. I.; Kenyo, I. M.; Gorlov, M. V.; Kasich, I. N.; Krasnodubets, A. M.; Gal'chinsky, N. V.; Fomochkina, II; Zaitsev, A. S.; Bekirova, V. V.; Seidosmanova, E. E.; Dydik, K. I.; Meshcheryakova, A. O.; Nazarov, S. A.; Smagliy, N. N.; Chelengerova, E. L.; Kulanova, A. A.; Deri, K.; Subbotkin, M. V.; Useinov, R. Z.; Shumskykh, M. N.; Kubyshkin, A. V., A Half-Century History of Applications of Antisense Oligonucleotides in Medicine, Agriculture and Forestry: We Should Continue the Journey. *Molecules* **2018,** *23* (6).
7. Paterson, B.; Roberts, B.; Kuff, E., Structural gene identification and mapping by DNA-mRNA hybrid-arrested cell-free translation. *Proceedings of the National Academy of Sciences of the United States of America* **1977,** *74* (10), 4370-4374.

8. Zamecnik, P.; Stephenson, M., Inhibition of Rous sarcoma virus replication and cell transformation by a specific oligodeoxynucleotide. *Proceedings of the National Academy of Sciences of the United States of America* **1978,** *75* (1), 280-284.

9. Donis-Keller, H., Site-specific enzymatic cleavage of RNA. *Nucleic acids research* **1979,** *7* (1), 179-192.

10. Nielsen, P. E.; Egholm, M.; Berg, R. H.; Buchardt, O., Sequence-selective recognition of a DNA by strand displacement with a thymine-substituted polyamide. *Science* **1991,** *254*, 1497-1500.

11. Obika, S.; Nanbu, D.; Hari, A.; Morio, K.; In, Y.; Ishida, T.; Imanishi, T., Synthesis of 2'-O,4'-C-Methyleneuridine and -cytidine. Novel Bicyclic Nucleosides Having a Fixed C3,-endo Sugar Puckering *Tetrahedron Letters* **1997,** *38* (50), 8735-8738.

12. Koshkina, A. A.; Singha, S. K.; Nielsen, P.; Rajwanshia, V. K.; Kumar, R.; Meldgaard, M.; Olsen, C. E.; Wengel, J., LNA (Locked Nucleic Acids): Synthesis of the adenine, cytosine, guanine, 5-methylcytosine, thymine and uracil bicyclonucleoside monomers, oligomerisation, and unprecedented nucleic acid recognition. *Tetrahedron* **1998,** *54* (14), 3607-3630.

13. Martin, P., A New Access to 2′-O-Alkylated Ribonucleosides and Properties of 2′-O-Alkylated Oligoribonucleotides. *Helv Chim Acta* **1995,** *78*, 486–504.

14. E, B.; PL, I.; Bishop MR, e. a., Systemic administration of a phosphorothioate oligonucleotide with a sequence complementary to p53 for acute myelogenous leukemia and myelodysplastic syndrome: initial results of a phase I trial. *Antisense Res Dev* **1993,** *3*, 383-390.

15. Fomivirsen approved for CMV retinitis: first antisense drug. *AIDS Treat News* **1998,** *302*, 7.

16. Kruger, K.; Grabowski, P. J.; Zaug, A. J.; Sands, J.; Gottschling, D. E.; Cech, T. R., Self-splicing RNA: autoexcision and autocyclization of the ribosomal RNA intervening sequence of Tetrahymena. *Cell* **1982,** *31*, 147-157.

17. Guerrier-Takada, C., Gardiner, K., Marsh, T., Pace, N. and Altman, S., The RNA moiety of ribonuclease P is the catalytic subunit of the enzyme. *Cell* **1983,** *35*, 849-857.

18. Tanner, N. K., Ribozymes: the characteristics and properties of catalytic RNAs. *FEMS Microbiology Reviews* **1999,** *23*, 257-275.

19. Cech, T. R., Structure and mechanism of the large catalytic RNAs: group I and group II introns and ribonuclease P. *Cold Spring Harb Laboratory Press* **1993**, 239-269.

20. Narlikar, G. J. a. H., D., Mechanistic aspects of enzymatic catalysis: lessons from comparison of RNA and protein enzymes. *Annu. Rev. Biochem.* **1997,** *66*, 19-59.

21. Saldanha, R., Mohr, G., Belfort, M. and Lambowitz, A.M., Group I and group II introns. *FASEB J.* **1993,** *7*, 15-24.

22. Cech, T. R., Self-splicing of group I introns. *Annu. Rev. Biochem.* **1990,** *59*, 543-568.

23. Michel, F. a. F., J.L., Structure and activities of group II introns. *Annu. Rev. Biochem.* **1995,** *64*, 435-461.

24. Jacquier, A., Group II introns: elaborate ribozymes. *Biochimie* **1996,** *78*, 474-487.

25. Symons, R. H., Plant pathogenic RNAs and RNA catalysis. *Nucleic acids research* **1997,** *25*, 2683-2689.

26. Symons, R. H., Small catalytic RNAs. *Annu. Rev. Biochem.* **1992,** *61*, 641-671.

27. Peña, M. d. l.; García-Robles, I.; Cervera, A., The Hammerhead Ribozyme: A Long History for a Short RNA. *Molecules* **2017,** *22* (78), 1-12.

28. Pley, H. W.; Flaherty, K. M.; McKay, D. B., Three-dimensional structure of a hammerhead ribozyme. *Nature* **1994,** *372*, 69-74.

29. Murray, J. B.; Seyhan, A. A.; Walter, N. G.; Burke, J. M.; Scott, W. G., The hammerhead, hairpin and VS ribozymes are catalytically proficient in monovalent cations alone. *Chem. Biol.* **1998,** *5*, 587–595.

30. Canny, M. D.; Jucker, F. M.; Kellogg, E.; Khvorova, A.; Jayasena, S. D.; Pardi, A., Fast Cleavage Kinetics of a Natural Hammerhead Ribozyme. *JACS Communications* **2004,** *126*, 10848-10849.

31. Jimenez, R. M.; Polanco, J. A.; Luptak, A., Chemistry and Biology of Self-Cleaving Ribozymes. *Trends Biochem Sci* **2015,** *40* (11), 648-661.

32. Esteban, J. A.; Banerjee, A. R.; Burke, J. M., Kinetic Mechanism of the Hairpin Ribozyme: Identification and Characterization of Two Non-exchangeable Conformations. *The Journal of biological chemistry* **1997,** *272* (21), 13629–13639.

33. Leung, R. K.; Whittaker, P. A., RNA interference: from gene silencing to gene-specific therapeutics. *Pharmacol Ther* **2005,** *107* (2), 222-39.

34. Fire, A.; Xu, S.; Montgomery, M. K.; Kostas, S. A.; Driver, S. E.; Mello, C. C., Potent and specific genetic interference by double-stranded RNA in Caenorhabditis elegans. *Nature* **1998,** *391*, 806-811.

35. Couzin, J., Breakthrough of the year. Small RNAs make a big splash. *Science* **2002,** *306* (5699), 1124-1125.

36. Wilson, R. C.; Doudna, J. A., Molecular mechanisms of RNA interference. *Annu Rev Biophys* **2013,** *42*, 217-39.

37. Burnett, J. C.; Rossi, J. J., RNA-based therapeutics: current progress and future prospects. *Chem Biol* **2012,** *19* (1), 60-71.

38. Conlon, N.; Royzman, I., FDA Approves First-Ever siRNA Therapy. Biologics Blog, 2018; Vol. 2018.

39. Abudayyeh, O. O.; Gootenberg, J. S.; Essletzbichler, P.; Han, S.; Joung, J.; Belanto, J. J.; Verdine, V.; Cox, D. B. T.; Kellner, M. J.; Regev, A.; Lander, E. S.; Voytas, D. F.;

Ting, A. Y.; Zhang, F., RNA targeting with CRISPR-Cas13. *Nature* **2017,** *550* (7675), 280-284.

40. Abudayyeh, O. O.; Gootenberg, J. S.; Konermann, S.; Joung, J.; Slaymaker, I. M.; Cox, D. B.; Shmakov, S.; Makarova, K. S.; Semenova, E.; Minakhin, L.; Severinov, K.; Regev, A.; Lander, E. S.; Koonin, E. V.; Zhang, F., C2c2 is a single-component programmable RNA-guided RNA-targeting CRISPR effector. *Science* **2016,** *353* (6299), aaf5573.
41. Barrangou, R.; Horvath, P., A decade of discovery: CRISPR functions and applications. *Nat Microbiol* **2017,** *2*, 17092.
42. Jansen, R., Embden, J. D., Gaastra, W. & Schouls, L. M., Identification of genes that are associated with DNA repeats in prokaryotes. *Mol Microbiol* **2002,** *43*, 1565–1575.
43. Mojica, F. J., Diez-Villasenor, C., Garcia-Martinez, J. & Soria, E., Intervening sequences of regularly spaced prokaryotic repeats derive from foreign genetic elements. *J. Mol. Evol.* **2005,** *60*, 174–182.
44. Pourcel, C., Salvignol, G. & Vergnaud, G., CRISPR elements in *Yersinia pestis* acquire new repeats by preferential uptake of bacteriophage DNA, and provide additional tools for evolutionary studies. *Microbiology* **2005,** *151*, 653–663.
45. Bolotin, A., Quinquis, B., Sorokin, A. & Ehrlich, S. D., Clustered regularly interspaced short palindrome repeats (CRISPRs) have spacers of extrachromosomal origin. *Microbiology* **2005,** *151*, 2551–2561.
46. Barrangou, R.; Fremaux, C.; Deveau, H.; Richards, M.; Boyaval, P.; Moineau, S.; Romero, D.; Horvath, P., CRISPR provides acquired resistance against viruses in prokaryotes. *Science* **2007,** *315*, 1709–1712.
47. Deveau, H.; Barrangou, R.; Garneau, J. E.; Labonté, J.; Fremaux, C.; Boyaval, P.; Romero, D. A.; Horvath, P.; Moineau, S., Phage response to CRISPR-encoded resistance in *Streptococcus thermophilus*. *J. Bacteriol.* **2008,** *190*, 1390–1400.

48. Horvath, P.; Romero, D.; Coûté-Monvoisin, A.; Richards, M.; Deveau, H.; Moineau, S.; Boyaval, P.; Fremaux, C.; Barrangou, R., Diversity, activity, and evolution of CRISPR loci in *Streptococcus thermophilus*. *J. Bacteriol.* **2008,** *190*, 1401–1412.

49. Mojica, F. J., Diez-Villasenor, C., Garcia-Martinez, J. and Almendros, C., Short motif sequences determine the targets of the prokaryotic CRISPR defence system. *Microbiology* **2009,** *155*, 733–740.

50. Garneau, J.; Dupuis, M.; Villion, M.; Romero, D.; Barrangou, R.; Boyaval, P.; Fremaux, C.; Horvath, P.; Magadán, A.; Moineau, S., The CRISPR/Cas bacterial immune system cleaves bacteriophage and plasmid DNA. *Nature* **2010,** *468*, 67–71.

51. Deltcheva, E.; Chylinski, K.; Sharma, C.; Gonzales, K.; Chao, Y.; Pirzada, Z.; Eckert, M.; Vogel, J.; Charpentier, E., CRISPR RNA maturation by trans-encoded small RNA and host factor RNase III. *Nature* **2011,** *471*, 602–607.

52. Sapranauskas, R.; Gasiunas, G.; Fremaux, C.; Barrangou, R.; Horvath, P.; Siksnys, V., The *Streptococcus thermophilus* CRISPR/Cas system provides immunity in *Escherichia coli*. *Nucleic acids research* **2011,** *39*, 9275–9282.

53. Gasiunas, G.; Barrangou, R.; Horvath, P.; Siksnys, V., Cas9–crRNA ribonucleoprotein complex mediates specific DNA cleavage for adaptive immunity in bacteria. *Proceedings of the National Academy of Sciences of the United States of America* **2012,** *109*, E2579–E2586.

54. Jinek, M.; Chylinski, K.; Fonfara, I.; Hauer, M.; Doudna, J. A.; Charpentier, E., A programmable dual-RNA-guided DNA endonuclease in adaptive bacterial immunity. *Science* **2012,** *337* (6096), 816-21.

55. Cong, L.; Ran, F.; Cox, D.; Lin, S.; Barretto, R.; Habib, N.; Hsu, P.; Wu, X.; Jiang, W.; Marraffini, L.; Zhang, F., Multiplex genome engineering using CRISPR/Cas systems. *Science* **2013,** *339*, 819–823.

56. Mali, P.; Yang, L.; Esvelt, K.; Aach, J.; Guell, M.; DiCarlo, J.; Norville, J.; Church, G., RNA-guided human genome engineering via Cas9. *Science* **2013,** *339*, 823–826.

57. Jiang, W.; Bikard, D.; Cox, D.; Zhang, F.; Marraffini, L. A., RNA-guided editing of bacterial genomes using CRISPR-Cas systems. *Nature biotechnology* **2013,** *31*, 233–239.

58. Pennisi, E., The CRISPR craze. *Science* **2013,** *341*, 833–836.

59. Abudayyeh, O. O.; Gootenberg, J. S. Tips and Tricks for Cas13. https://zlab.bio/cas13/ (accessed December 20, 2018).

60. Liu, L.; Li, X.; Ma, J.; Li, Z.; You, L.; Wang, J.; Wang, M.; Zhang, X.; Wang, Y., The Molecular Architecture for RNA-Guided RNA Cleavage by Cas13a. *Cell* **2017,** *170* (4), 714-726 e10.

61. Yan, W. X.; Chong, S.; Zhang, H.; Makarova, K. S.; Koonin, E. V.; Cheng, D. R.; Scott, D. A., Cas13d Is a Compact RNA-Targeting Type VI CRISPR Effector Positively Modulated by a WYL-Domain-Containing Accessory Protein. *Mol Cell* **2018,** *70* (2), 327-339 e5.

62. Schlosser, K.; Li, Y., Biologically inspired synthetic enzymes made from DNA. *Chem Biol* **2009,** *16* (3), 311-22.

63. Cech, T. R., The ribosome is a ribozyme. *Science* **2000,** *289*, 878-879.

64. Borman, S., After Two Decades Of Trying, Scientists Report First Crystal Structure Of A DNAzyme. In *Structural Biology: Folded conformation with product bound reveals probable mechanism of synthetic catalyst*, Chemical and Engineering News: 2016.

65. Li, Y.; Breaker, R. R., Kinetics of RNA degradation by specific base catalysis of transesterification involving the 2'-hydroxl group. *J. Am. Chem. Soc.* **1999a,** *121*, 5364-5372.

66. Smith, R. M.; Hansen, D. E., The pH-rate profile for the hydrolysis of a peptide bond. *J. Am. Chem. Soc.* **1998,** *120*, 8910-8913.

67. Silverman, S. K., In vitro selection, characterization, and application of deoxyribozymes that cleave RNA. *Nucleic Acids Res* **2005,** *33* (19), 6151-63.

68. Breaker, R. R.; Joyce, G. F., A DNA enzyme that cleaves RNA. *Chemistry and Biology* **1994,** *1*, 223-229.

69. Faulhammer, D.; Famulok, M., The Ca2+ ion as a cofactor for a novel RNA-cleaving deoxyribozyme. *Angewandte Chemie* **1996,** *35*, 2837-2841.70. Santoro, S. W., Gerald F. Joyce, A General Purpose RNA-cleaving DNAzyme. *Proceedings of the National Academy of Sciences of the United States of America* **1999,** *49* (9), 1262-1266.

71. Peracchi, A., Preferential activation of the 8-17 dexoryibozyme by Ca2+ ions. Evidence for the identity of 8-17 with the catalytic domain of the Mg5 deoxyribozyme. *J. Biol. Chem.* **2000,** *275*, 11693-11697.

72. Li, J.; Zheng, W.; Kwon, A. H.; Lu, Y., *In vitro* selection and characterization fo a highly efficient Zn(II)-dependent RNA-cleaving deoxyribozyme. *Nucleic acids research* **2000,** *28*, 481-488.

73. Cruz, R. P. G.; Withers, J. B.; Li, Y., Dinucleotide junction cleavage versatility of 8-17 deoxyribozyme. *Chem Biol* **2004,** *11*, 57-67.

74. Geyer, C. R.; Sen, D., Evidence for the metal-cofactor independence of an RNA phosphodiester-cleaving DNA enzyme. *Chem Biol* **1997,** *4*, 579-593.

75. Feldman, A. R.; Sen, D., A new and efficient DNA enzyme for the sequence-specific cleavage of RNA. *J Mol Biol* **2001,** *313*, 283-294.

76. Carrigan, M. A.; Ricardo, A.; Ang, D. N.; Benner, S. A., Quantitative analysis of a RNA-clearing DNA catalyst obtained via *in vitro* selection. *Biochemistry* **2004,** *43*, 11446-11459.

77. Roth, A.; Breaker, R. R., An amino acid as a cofactor for a catalytic poolynucleotide. *Proceedings of the National Academy of Sciences of the United States of America* **1998,** *95* (6027-6031).

78. Zhang, J., RNA-Cleaving DNAzymes: Old Catalysts with New Tricks for Intracellular and In Vivo Applications. *Catalysts* **2018,** *8* (550), 1-20.

79. Pyle, A. M.; Chu, V. T.; Janowsky, E.; Boudvillain, M., Using DNAzymes to cut, process, and map RNA molecules for structural studies or modification. *Methods Enzymol* **2000,** *317*, 140-146.

Chapter 2: Introduction of Nanozymes

2.1. Competing Definitions of "Nanozyme"

The largest use of the term "nanozyme" in literature defines it as a nanomaterial that acts as an artificial enzyme, simulating a natural enzyme's activity either through the property of the nanomaterial or its attached ligands[1-2]. The term was first coined in 2004 to describe gold nanoparticles (AuNPs) that had been functionalized with a catalytic ligand.[3-4] However, after this first mention, "nanozyme" came to refer to nanomaterials with enzymatic properties.[4] Hui Wei created a brief timeline of enzymes, natural and artificial, as well as nanozymes, illustrated below (Fig. 2.1).

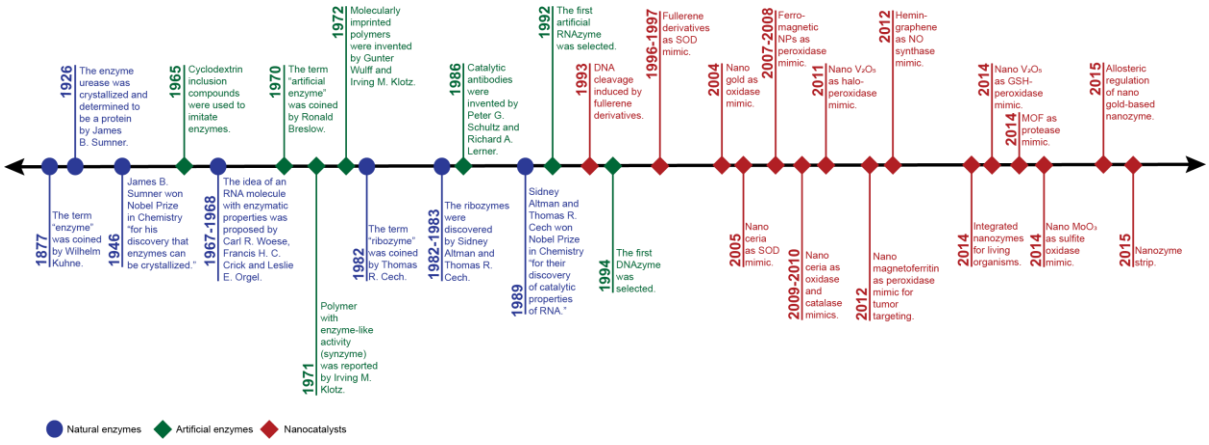

Figure 2.1. Timeline of natural and artificial enzymes and nanocatalysts. Adapted from reference 6. Copyright (2016) Royal Chemistry Society.

We prefer to classify these types of nanozymes as "nanocatalysts" rather than nanozymes, as will become clear in the following pages. The field of nanocatalysts, or nanomaterials with enzymatic properties, is quite large. They include iron oxide nanoparticles (Fe_3O_4NPs) that exhibit peroxidase-like activity; nanoceria nanoparticles (CeO_2NP) that exhibit oxidase-like activity; gold nanoparticles (AuNPs) that exhibit glucose oxidase activity, and many more.[5] Other chemistry mimics include catalase, superoxide dismutase (SOD), esterase, nuclease, phosphatase, protease and ferroxidase activities.[6] However, most of the chemistry conducted by these nanocatalysts are redox reactions.[5] In addition to naked nanomaterials performing chemical reactions, attempts have also been made to modify the surfaces of some of these

nanomaterials to improve or modify their chemical reactivity. These modifications include changes to surface charge, redox potential or acidity, addition of polymers, specific molecules or covalent attachment of ligands.[4] With the modification of nanocatalysts, one does have to be careful that the attaching ligand does not block the surface, inhibiting the material's chemical reactivity.[5] To give a summary of nanocatalyst literature and an idea of the depth of the field, see the table below listing the types of nanocatalysts that have been created, along with their surface modification and properties (Table 2.1).[4]

Table 2.1. Selection of nanocatalysts, their activity, surface modification and application. Adapted by permission from Tsinghua University Press and Springer-Verlag Berlin Heidelberg: Springer, Nano Research from reference 4, Copyright (2017).

Abbreviations: CeO_2NPs = nanoceria; Fe_3O_4NPs = iron oxide nanoparticles; BSA = bovine serum albumin; PAA = polyacrylic acid; PEG = polyethylene glycol; GO = graphene oxide; rGO = reduced graphene oxide

Nanomaterials	Enzyme-like activity	Surface modification	Activity modulation	Application	Ref
CeO_2NPs	Oxidase	Anions	Promotion by fluoride	Fluoride detection	7
	Oxidase	NTPs	Promotion; GTP > ATP > UTP > CTP	Single-nucleotide polymorphism typing	8
	Oxidase	PAA, dextran	Inhibition by thick coating; PAA coating less affected	Protein immobilization for immunoassays	9
	Oxidase	DNA	Inhibition due to blocking		10
	Oxidase	DNA	Promotion due to improve colloidal stability	Ochratoxin A detection	11
	Catalase	DNA	Retained activity	H_2O_2 and glucose detection	12
	Catalase	Phosphate	Promotion		13
	Catalase	Dextran	Retained		14
	SOD	Phosphate	inhibition		13
	SOD	Apoferritin	Promotion		15

	SOD	Dextran, PEG	Resisting inhibition by phosphate		16
	SOD	CuZn-SOD enzyme	Promotion		17
	Free radical elimination	Phosphate, chloride, sulfate	Inhibition by phosphate		18
	Free radical elimination	Bicarbonate	Inhibition		19
Fe_3O_4NPs	Peroxidase	Anions	Inhibition by phosphate	Phosphate detection	20
	Peroxidase	Catecholamines	Inhibition	Catecholamines detection	21
	Peroxidase	Dopamines	Retained activity		22
	Peroxidase	Histidine	Promotion		23
	Peroxidase	Glycine, polylysine, poly(ethylenimine)	Promoting ABTS oxidation		24
	Peroxidase	Citrate, carboxymethyl dextran, heparin	Promoting TMB oxidation		24
	Peroxidase	Dextran, PEG, APTES, SiO_2	Inhibition; dextran least affected	Protein immobilization for immunoassays	25
	Peroxidase	DNA	Inhibiting OPD oxidation		26
	Peroxidase	DNA	Promoting TMB oxidation		27
	Peroxidase	proteins	Inhibition	Proteins discrimination	28
γ-Fe_2O_3NPs	Peroxidase	Prussian blue, $Fe^{III}_4[Fe^{II}(CN)_6]_3$	Promotion		29
BSA-encapsulated AuNCs	Peroxidase	Metal ions	Inhibition by Hg^{2+}	Hg^{2+} detection	30
	Peroxidase	Metal ions	Inhibition by Ag^+, Hg^{2+}, and UO_2^{2+}	UO_2^{2+} detection	31
AuNPs	Peroxidase	Metal ions	Promotion by Hg^{2+} for TMB oxidation	Hg^{2+} detection	32
	Peroxidase	Metal ions	Promotion by Hg^{2+} and Pb^{2+} for AR oxidation		33
	Peroxidase	Anions	Inhibition by sulfide		34

	Peroxidase	Cysteamine, citrate, mercaptoacetic acid	Higher activity of cysteamine modification		35
	Peroxidase	Citrate, amino	Inhibition by modification; substrate dependent activity		36
	Peroxidase	Melamine	Promotion	Melamine detection	37
	Peroxidase	ATP	Promoting ABTS oxidation		38-39
	Peroxidase	DNA	Inhibition	Kanamycin detection	40
	Peroxidase	DNA	Promotion		41
	Catalase	Metal ions	Promotion by Ag^{+} and Hg^{2+}		42
	GOx	DNA	Inhibition	DNA detection	43
	GOx	DNA	Alter substrate selectivity		44
GO	Peroxidase	Covalent modification	Promotion and inhibition		45
	Peroxidase	Chiral supramolecular complex	Altering substrate selectivity		46
rGO	Peroxidase	Hemin	Promotion		47

Functionalizing a nanocatalyst with ligands can be important, not only for modulating the nanocatalyst's activity, but also for biosensing, targeted drug delivery, and imaging. Ligands can include small molecules, polymers and even proteins. However, as already mentioned, one must balance ligand binding with nanocatalyst activity since surface area must be left to catalyze their reactions.[5] In addition to nanocatalysts, there is a large field of work dedicated to the attaching of enzymes onto nanoparticle scaffolds to increase their catalytic rate. Confusingly, these are often also called "nanozymes." In this case, the catalytic reaction is being conducted by the enzyme(s) on the particle surface rather than by the particle itself (Fig. 2.2). These are what we would consider to be "true" nanozymes. Accordingly, we define "nanozyme" as any entity that attaches catalytic ligands or enzymes to a scaffold less than 100 nm in

diameter. The purpose of creating nanozymes includes coupling enzymatic processes, increasing the enzyme's specificity or increasing its catalytic rate. Finally, there is a separate and large body of literature looking at bioconjugation of proteins, ligands or small molecules that are not catalysts onto nanoparticle scaffolds for drug delivery purposes, rather than for the above purposes. This area is outside the scope of our review, where here we will focus specifically on gold nanoparticle-based nanozymes.

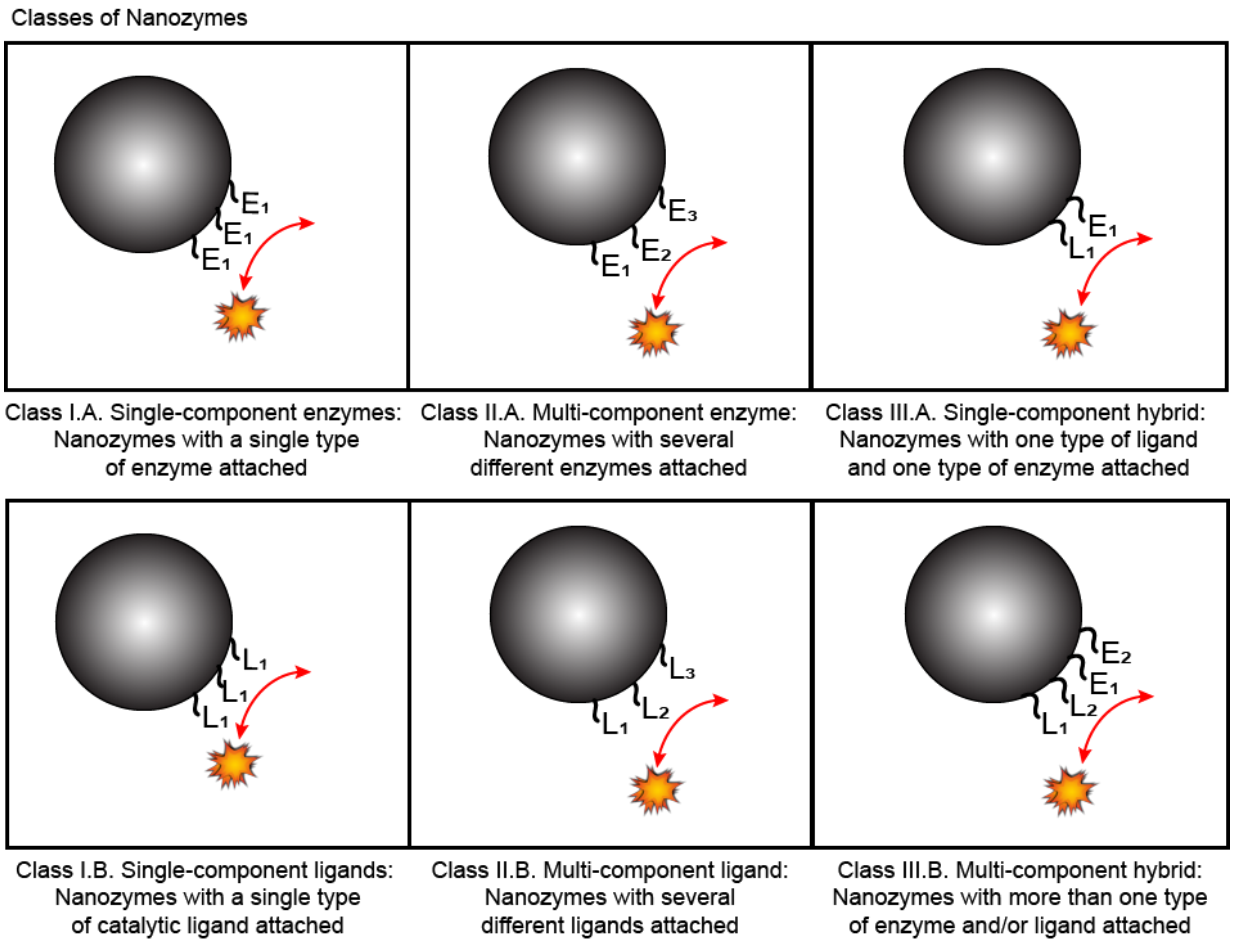

Figure 2.2. Classification of nanozymes: Class I defines single-component nanozymes. Class II defines multi-component nanozymes and Class III defines hybrid nanozymes. "L" refers to "ligand" and in this context means a molecule or collection thereof, either of biological origin or synthetic, that can catalyze a reaction or mediate a cellular response.

2.2. Advantages of Using a Gold Core

Gold nanoparticles (AuNPs), with 3 to 200 nm diameters, have become increasingly popular in biomedical research.[48] There are many reasons why gold has attracted this attention for use in nanoparticle cores. Among others, AuNPs have a unique set of optical and electronic properties that aid their use as sensors and contrast agents in microscopy.[49] Additionally, they are largely inert, biocompatible with high stability, easily synthesized in a range of sizes and shapes, and easily functionalized with proteins, DNA or other molecules.[48] Here will discuss a few aspects of these properties in a bit more depth.

2.2.1. Ease of Synthesis

One of the reasons AuNPs are so attractive to use is that they are easily synthesized through the reduction of gold salts, nucleating nanoparticles.[50] The size of the nanoparticles can be controlled based on how much reducing agent is added. A stabilizing agent is added during synthesis to keep the particles from aggregating.[50] Turkevitch first introduced this method,[51] and afterward, Frens published improvements on his technique.[52] In the Turkevitch method, sodium citrate acts as both reducing and stabilizing agent, nucleating particles and coating their surface to keep them monodisperse.[51] This method can produce particles between 10-60 nm in size.[53] A second method was developed by Brust-Schiffrin to produce even smaller particles in the range of 2 to 6 nanometers.[54] This method requires two phases and gold is transferred from aqueous to organic (toluene) with the help of a phase-transfer agent. Organic thiols are added along with a reducing agent leading to capped gold clusters whose size can be varied depending on the amount of thiol ligand added. These ligands can be exchanged for water soluble ligands if desired.[50] AuNPs can also be synthesized in a variety of shapes. In addition to the traditional nanospheres, nanorods, nanobelts, cages, prisms, cubes and stars can be formed,[55] increasing their novelty and versatility.

2.2.2. Biocompatibility and Low Toxicity Profile

Another reason why AuNPs are attractive is that they are unreactive and inert, making them biologically compatible for use as scaffolds. Unlike others such as cadmium-based nanoparticles, gold does not release toxic ions. It retains a relatively low toxicity profile. However, it should be noted that AuNP toxicity is a somewhat controversial topic with many conflicting reports. One author has noted that the conflict may arise from the ability of AuNPs to interfere with traditional dye-based assays and products.[55] AuNPs absorb and scatter light in the visible region. This absorption can interfere with assays involving colorimetry, chemiluminescence and fluorescence, leading to variable results.[55] Additionally, toxicity can also arise, not from the gold particles themselves, but from residual impurities and bioproducts of their synthesis or the capping and reducing agents.[55] For example, one report found that toxicity resulted from nanomolar concentrations of free cetyltrimethylammonium bromide (CTAB) capping ligand in solution rather than from the particles themselves and toxicity was reduced when a polymer coating was used.[56] Therefore, in any toxicity assay, it is vital to account for the amounts of free metal ions, surfactants, reactants or other biological contaminants such as endotoxins before conducting the assay.[55] It is also important to separate toxic effects that result from the material (gold) versus those that result from nanoparticles in general.[49] Toxic effects can depend on the cell line tested, on the surface chemistry of the particle and on its size.[49] In general, it appears that smaller gold nanoparticles (those under 10 nm) are toxic at lower concentrations than larger ones. This may result from small Au-clusters penetrating the nucleus of cells and binding in the grooves of DNA, leading to cytotoxic effects.[57] Nanoparticles can also affect actin fibers.[58] It should also be noted that *in vitro* cell cytotoxicity assays may or may not compare well with *in vivo* toxicity assays and biodistribution and routes of elimination for the particles in whole animals will be important to determine their relative safety. Among other things, biodistribution of AuNPs depends on their size and route of

administration.[53] In spite of the apparent conflict, gold is still known for having a relatively low toxicity profile[59] and is becoming increasingly popular for use in biomedical applications.

2.2.3. Use of Gold as a Reporter: Labeling, Sensing, Staining

Other reasons that AuNPs have been so widely used is their unique interaction with light through both absorption and scattering, making them excellent contrast agents. For this reason, AuNPs have found most frequent use in labeling applications.[49] Different sizes and shapes of AuNPs absorb light at different wavelengths, allowing for use in multi-color experiments.[49] Those larger than 20 nm can be directly observed with phase contrast optical microscopy or differential interference contrast (DIC).[49] AuNPs can also be used in staining of cells and visualizing with transmission electron microscopy (TEM).[49] Furthermore, AuNPs can be conjugated to antibodies and used to target and label cell surface structures, with or without single-particle tracking.[49] In addition to these passive applications, AuNPs can be utilized as active sensors. When AuNPs absorb light, their outer surface electrons become excited in a collective oscillation known as a surface plasmon resonance.[49] The resonance frequency will change depending on binding of molecules to the surface of the particle, leading to the possibility of detecting the bound analyte.[49] Finally, it should be noted that gold quenches the fluorescence of most fluorophores,[60] an effect that is very useful for building sensors based upon the quenching and dequenching of fluorescence.[49] In my work, we used this property of gold to quench fluorescence to measure the binding of an Alexa488-labeled enzyme to a 13 nm AuNP (see Chapter V).

2.2.4. Functionalization and Cellular Uptake

Gold readily adsorbs proteins onto its surface, making it easy to functionalize. Additionally, more controlled adsorption can occur through the thiol-gold interaction.[50] Thiolated proteins, peptides, saccharides, antibodies or oligonucleotides are readily attached to its surface via this

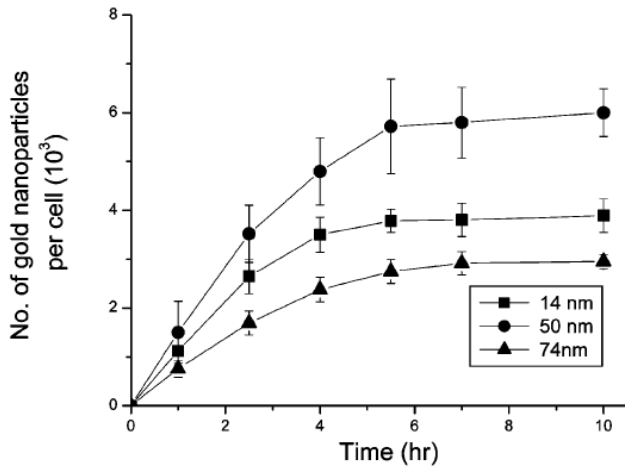

Figure 2.3. Size dependent uptake of AuNPs into HeLa cells. Adapted with permission from reference 61. Copyright (2006) American Chemical Society.[61]

chemistry.[55] Additionally, the controlled addition of proteins with histidine (His) tags can be added to gold by first attaching thiolated linkers with nitrilotriacetic acid (NTA). His_6-tagged proteins can then be attached site-specifically onto the surface of the particle.[62] In addition to being easy to functionalize, AuNPs also have the advantage that they are uptaken by cells through non-specific pathways.[61] Specific targeting can be achieved by functionalizing ligands to the particle surface that bind particular cell surface receptors.[49] However, Warren Chan and his group showed that even unfunctionalized, citrate-capped AuNPs of various sizes are taken up by cells.[61] Those taken up most readily are 50 nm in size and for all sizes tested uptake plateaus after 6 h (Fig. 2.3.). This feature of nanoparticles makes them attractive for use in therapeutic applications.[49]

2.2.5. Use of AuNPs in this Study

Therefore, for many of these reasons, our lab has chosen to work with AuNPs as the primary core for our nanozyme constructs. In particular, because of the UV absorption of AuNPs and their measured extinction coefficient, it is simple to measure their concentration. Additionally, we regularly use thiolated oligonucleotides to attach to the gold core – a modification that is easily ordered from venders like Integrated DNA Technologies (IDT). Mirkin has shown that the particles, in addition to being uptaken themselves,[61] are also readily uptaken when functionalized with DNA in a wide variety of cell types.[63] It has also been shown that attachment to a nanoparticle core confers some protection on the attached DNA, from nucleuses, likely due

to steric hindrance.[63-64] These features of AuNPs, in addition to their inert nature and low toxicity profile, make them highly attractive for building nanozymes.

2.3. Examples of Gold Core Nanozymes

2.3.1. Nanozymes Functionalized with Chemical Ligands

Emory University's own Dr. Fred Menger wrote the following in his article, "Groups of Organic Molecules That Operate Collectively":

> "…groups of molecules, properly assembled, can obviously accomplish much more than an equal number of molecules functioning separately."[65]

This statement gets at one of the goals of the nanozyme field, that enzymes attached to a scaffold can work cooperatively more efficiently than they can separately, and even arrive at novel functions. To give an idea of the breadth of this field, the following section will detail some examples of gold core nanoparticle nanozymes. One of the first nanozymes was the Class I.B. nanozymes (Fig. 2.2) produced by Paolo in 2004.[3] He synthesized AuNP conjugates functionalized with a ligand that were able to perform simple hydrolysis of p-nitrophenyl phosphate (HPNP), an RNA mimic.[3] The activities of the isolated ligand was significantly enhanced upon conjugation to AuNPs. This synthetic system formed the beginning of what would become a focus of nanozyme development.

2.3.2. Spherical Nucleic Acids

The next example of nanozymes we will discuss are known as spherical nucleic acids (SNAs) (Fig. 2.4.), pioneered by the Mirkin group. Spherical nucleic acids pre-date Paolo's nanozyme, being introduced in 1996.[66] These are formed by attaching thiolated DNA oligonucleotide ligands to gold nanoparticles through the thiol-gold interaction.[67] While the DNA is not enzymatic, these particles can still have activity against gene targets – thus mediating a cellular

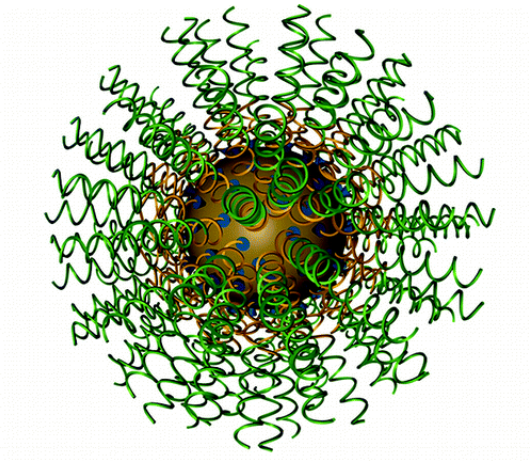

Figure 2.4. An artist's rendition of the molecular architecture of a spherical nucleic acid (SNA). Reprinted with permission from reference 67. Copyright (2012) American Chemical Society.[67]

response – if the oligonucleotides bind in antisense fashion to target RNAs. They also form the basis of other working nanozymes, such as DNAzyme and ribozyme nanoparticles. As such, spherical nucleic acids and their properties are worthy of discussion, as they form the basis of other nanozymes.

2.3.2.1. Spherical Nucleic Acid Characteristics

Notably, the characteristics of SNAs differ from their individual parts. Their binding constants for the complementary strand of DNA is higher than the individual DNAs included in the SNA.[69] Their binding is also cooperative, showing sharp melting transitions.[66, 70] SNAs are hardier than naked DNA, being resistant to nuclease degradation.[71] Additionally, they are able to transfect mammalian cells, even lacking an inorganic core (Fig. 2.5.), without any other chemical or physical aids. This feat is possible because it is the spherical arrangement of the nucleic acids – their density and orientation – that is recognized by cellular receptors.[68]

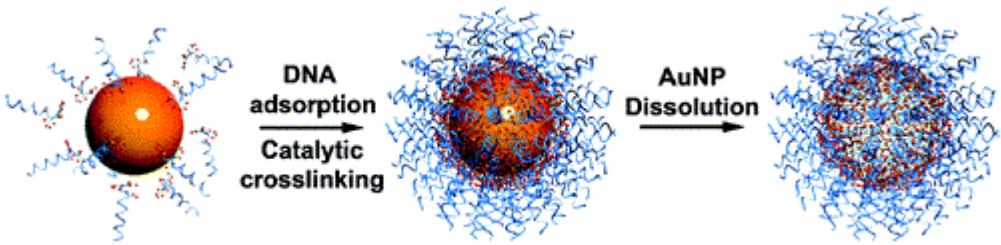

Figure 2.5. Spherical nucleic acids can be formed with or without a gold core. Reprinted with permission from reference 68. Copyright (2011) American Chemical Society.[68]

Importantly, SNAs are found to be uptaken by mammalian cells at orders of magnitude higher rates than unfunctionalized citrate-stabilized AuNPs or those passivated with bovine serum albumin (BSA).[61, 72] So far, uptake has been examined in over 50 cell types including primary

cells and been successful, except for mature red blood cells.[73] Oligonucleotides attached to make SNAs contain three common elements: an attaching functionality (in those with cores), a spacer and a recognition domain.[67] For gold core SNAs, the attaching moiety is usually a propyl- or hexylthiol- group,[67] or if one desires even greater stability, then branched thiols[74] or cyclic disulfides can be used.[75] The spacer region – usually a string of ten thymidines or adenines – separates the recognition region from the gold core surface, preventing it from binding and leaving it free to recognize its target.[67] For added buffering, the spacer can also be composed of polyethylene glycol (PEG).[76] The recognition element then, should face outward away from the particle core, available to base-pair with its target. This shell of DNA around the particle core gives the SNAs a negative zeta potential and keeps them from aggregating, helping them stay suspended in solution. SNAs, once synthesized, last on the order of months and are very stable.

2.3.2.2. Spherical Nucleic Acid Synthesis

Synthesis of spherical nucleic acids is quite simple. There are now two primary methods to prepare them. The first, referred to as salt aging, was developed by Mirkin and was subsequently improved on in another publication.[76-77] In it, one incubates thiolated oligonucleotides with AuNPs overnight (4 nmol DNA per 1 ml AuNPs) and then progressively salts them to greater salt concentrations, sonicating for 10 seconds in between each salt addition in a bath sonicator. The salt screens the charge between the DNA and helps the DNA pack onto the gold surface. Before use, the freshly prepared SNAs are washed several times to remove the excess salt. The second method to prepare SNAs was developed by Dr. Juewen Liu's group.[78] He found that one could simply add thiolated DNA to AuNPs and freeze it for about 2 h at -20ºC. After thaw, complete SNAs had formed. He speculated that the exclusion of AuNPs in the production of ice crystals locally concentrated the particles and DNA together, making their binding more favorable.[78]

2.3.2.3. Applications

SNAs are powerful gene regulation agents. With a DNA shell, they can perform RNA knockdown through the antisense pathway.[73] Additionally, RNA can be conjugated to AuNPs to form RNA SNAs rather than DNA, which can regulate mRNA through the RNAi pathway.[79] For consistent knockdown, only picomolar concentrations of the particles are necessary.[67] Additionally, other metal complexes and drugs can be conjugated to the SNA, taking advantage of its rapid internalization into cells.[67] This has worked for platinum(IV) prodrugs attached to SNAs, resulting in delivery of cisplatin to cells.[80] Other drugs that have been delivered via SNAs include paclitaxel. When attached to an SNA shell, its solubility improves by over 50 times and has lower IC_{50} values than the free drug.[81]

SNAs can also be used as probes called “nanoflares” to detect low levels of target mRNA indicative of a disease state or cellular process.[82] Nanoflares work by conjugating a short fluorophore-labeled probe to the SNA, with the fluorophore bound close to the AuNP core. Binding to the target displaces the fluorescent probe, leading to dequenching of the fluorophore and fluorescence that can be detected (Fig. 2.6.).[82] Nanoflares offer a better background fluorescence profile than molecular beacons, due to their increased nuclease resistance, and one can also knockdown an mRNA target and detect it at the same time.[67]

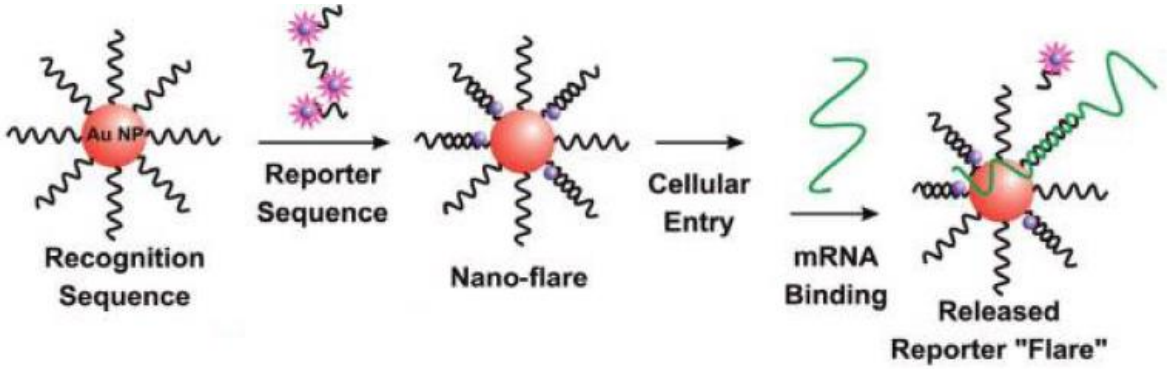

Figure 2.6. Nanoflares work through the displacing of a short “flare” sequence by the target mRNA. Adapted with permission from reference 82. Copyright (2007) American Chemical Society.[82]

The applications mentioned here merely touch on the nearly limitless possibilities that can be achieved through these simple conjugates. With the concerns about gold toxicity, hollow SNAs can step into the gap and continue to be used as potent gene regulators and drug delivery agents.[67]

2.3.3. Nanozymes Functionalized with Nucleic Acids and an Enzyme

In 2012, researchers lead by Dr. Cao at the University of Florida created an excellent example of a Class III.A. hybrid nanozyme. His team produced a site-specific ribonuclease out of the non-specific ribonuclease RNase A and DNA oligonucleotides attached to 13 nm AuNPs (Fig. 2.7.). The DNA oligonucleotides act as guide strands that bind complementary target RNA, drawing them close to the RNase A on the surface of the nanoparticle for cleavage. This activity mimicked the RNA-induced silencing complex (RISC), for specific RNA knockdown, giving the nanoparticle construct the "nanozyme" classification. Remarkably, they were able to observe 70% knockdown in cell culture and 99% knockdown in hepatitis C virus (HCV) RNA levels in mice treated with the nanozyme. In their tests, they included extensive controls, including a nanozyme without the RNase A component, a nanozyme with and without RNase A but non-specific DNA and an RNase A only particle. They were able to show that the controls did not affect the target RNA or a control non-specific RNA.

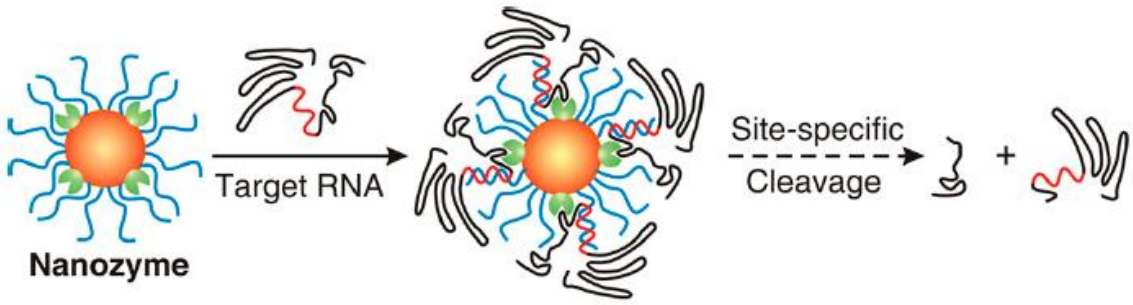

Figure 2.7. Nanozyme created by attaching RNase A and DNA complementary to target RNA, creating a site-specific ribonuclease. Reprinted with permission from reference 83. Copyright (2012) National Academy of Sciences.[83]

Furthermore, the RNase A on the particle surface retained its activity even after a 1 h incubation with proteinase K. They did not observe toxicity to the treatment in cell culture or in the mouse model.[83]

2.3.4. 10-23 DNAzyme Nanoparticle

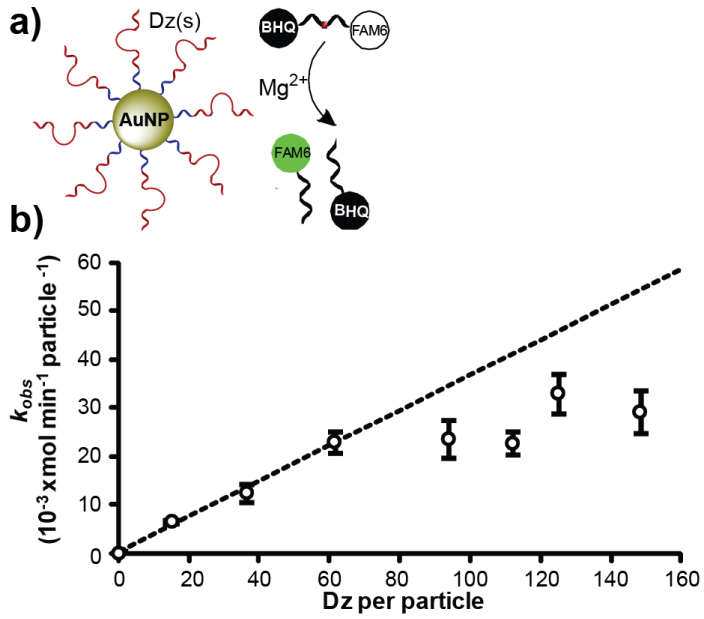

Figure 2.8. Scheme of DzNP binding and cleavage. (a) DzNP cleaving a short DNA / RNA hybrid substrate with FAM and BHQ on the ends in presence of Mg^{2+}. (b) DzNP activity as a function of DNAzyme density on the particle surface. Adapted with permission from reference 64. Copyright (2012) American Chemical Society.[64]

Also in 2012, Kevin Yehl in the Salaita Lab pioneered work on the DNAzyme-AuNP (DzNP) nanozyme,[64] also based off the SNA architecture and the foundation of my work. It's a Class I.A. nanozyme constructed by attaching 10-23 DNAzymes having a 10-nucleotide thymidine (T_{10}) spacer with a thiol modification directly to the surface of 13 nm AuNPs. Upwards of 100 strands can be attached to 13 nm AuNPs in this way, with maximal packing giving 160 strands.[64] Kevin investigated the kinetics (Fig. 2.8.) and stability of these DzNPs, showing that particles remained monodisperse upon attachment to DNAzymes by TEM and UV-Vis. To measure the DzNPs catalytic activity, he used a short DNA/RNA hybrid strand with the 5' end connected to a fluorophore and the 3' end connected to a quencher (Fig. 2.8a).[64] Upon cleavage of the strand by the DNAzyme, the fluorophore and quencher would be separated from each other, leading to an increase in fluorescence. He showed that the k_{obs} of the DzNPs increased with increasing DNAzymes per particle but plateaued after 60 strands (Fig. 2.8.).[64] Therefore, it is likely that the

steric bulk of the strands is hindering their ribonuclease activity after this packing density.[64] Kevin also tested the effect of linker length on catalysis, anticipating that longer linkers, with the reduced steric hindrance around the resulting strands, would lead to higher activities. Interestingly, he found there to be no correlation between linker length and activity.[64] In addition, PEG linkers generated the most densely packed particles with ~195 strands / NP and also the highest activity, exhibiting a 56% increase over DzNPs with T_{10}-linkers.[64] In a classic experiment, he also showed that when the DNAzyme was attached to the gold core via it's 5' end rather than its 3' end, there was a complete loss in activity. However, once the 5'-end bound DNAzymes were released from the surface, they regained their former activity.[64] He hypothesized that the 10-23 DNAzyme catalytic core was partially interacting with the gold surface in 5'-end bound DNAzymes and that residues near the 5' end in the core were sensitive to inactivation.[64] This hypothesis appeared to line up with other studies at the time demonstrating that the 10-23 DNAzyme was not tolerant of mutations in the core near the 5' end.[84] He went on to show that his DzNPs, modified on their termini with two 2'-O-methyl bases to prevent nuclease degradation, could enter HCC1954 HER2-overexpressing breast cancer cells and knockdown the levels of TGF-β related growth differentiation factor 15 (GDF15) mRNA.[64] He distinguished between antisense and non-specific knockdown by also testing a catalytically inactive DzNP with a mutation in the core and a non-specific DzNP, respectively, with scrambled binding arms. His data suggested that the active DzNP entities knockdown down GDF15 by ~57% relative to the negative control ($p < 0.005$) (Fig. 2.9.).[64]

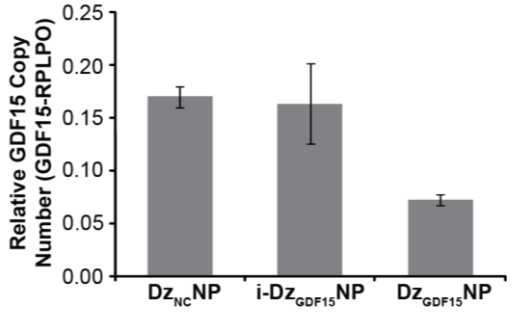

Figure 2.9. DzNP cellular activity. Active DzNPs lowered GDF15 by 57% compared to the non-specific DzNPs and the inactivated DzNPs. Adapted with permission from reference 64. Copyright (2012) American Chemical Society.[64]

2.3.5. Uranyl-specific 39E DNAzyme Nanoparticle

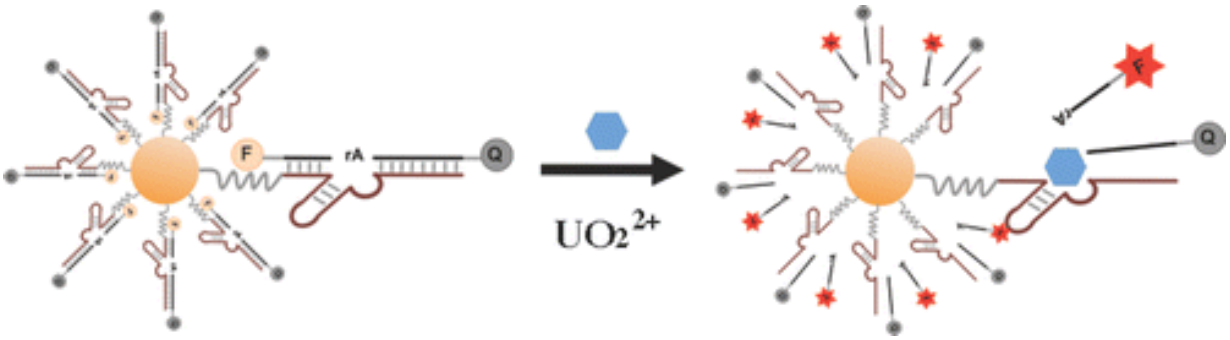

Figure 2.10. Uranyl-specific DNAzymes and their substrate bound to a 13 nm gold nanoparticle core, forming a metal-sensing nanozyme. Reprinted with permission from reference 85. Copyright (2013) American Chemical Society.[85]

Not only can RNA-cleaving DNAzymes knock down RNA targets, but they can also be used as metal ion sensors. In March of 2013, the first example of an intracellular metal sensing nanozyme was demonstrated by Dr. Yi Lu's Group, using a Class I.A. archetype.[85] It was constructed of a 13 nm AuNP core and the core was functionalized with thiolated uranyl-specific 39E DNAzymes. These DNAzymes are functionalized to the gold having already been bound to short Cy3-labeled substrates. The Cy3-label is bound to the DNAzyme near the gold surface so it is quenched by the gold (Fig. 2.10.). For good measure, there is also a quencher attached to the opposing end of the substrate that also quenches the Cy3-label.[85] These nanozymes efficiently enter cells, by a similar mechanism as SNAs. Once the UO_2^{2+} ion is bound to the DNAzyme, the DNAzyme cleaves the substrate, releasing the Cy3-labeled strand into solution and causing fluorescence. The fluorescent signal is related to the intracellular concentration of the UO_2^{2+} ion and thus, it's amount can be calculated.[85]

2.3.6. Nanoscript: Transcription Factor Nanoparticle Mimic

In 2014, Patel in Kim-Bum Lee's group developed a novel gold nanoparticle Class II.B. nanozyme composed of three different ligands designed to mimic the parts of a natural transcription factor (Fig. 2.11.).[86] The ligands included an NLS peptide, to direct the construct

into the nucleus, a synthetic peptide activation domain and a synthetic hairpin polyamide that acts as a DNA-binding domain.[86] The hairpin polyamide was made to bind specifically to a reporter plasmid that had been transfected into HeLa cells. These ligands were attached to the AuNPs via EDC/NHS coupling to mercaptoundeconic acid (MUA) that had been added to the gold surface.[86] Using inductively coupled plasma atomic emission spectroscopy (ICP-OES), they found that the Nanoscript construct entered cells after 4 h, while the control without NLS did not.[86] Additionally, Nanoscipt was able to induce expression of the reporter plasmid by 15-fold over unmodified AuNPs.[86] It was also able to induce increased expression of four endogenous genes. A year later, Ki-Bum Lee's group used this new system to target myogenic regulatory factors (MRFs) to induce mature muscle cells from adipose-derived mesenchymal stem cells in 7 days.[87] They were also able to use Nanoscript to repress *Sox9* expression in neural stem cells, helping them to differentiate into functioning neurons.[88]

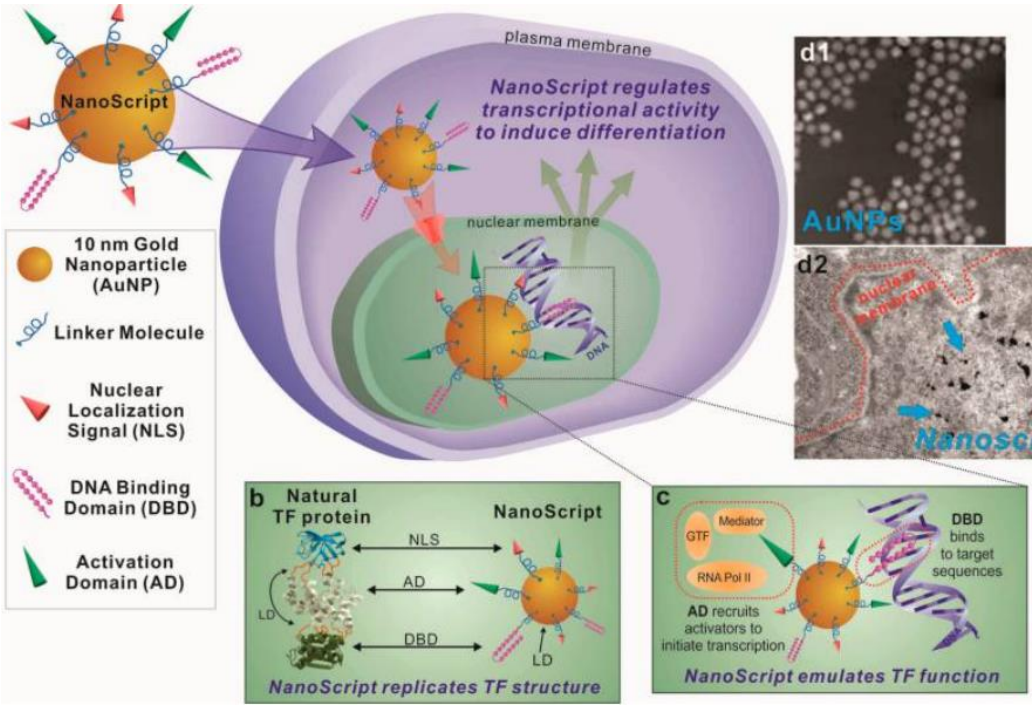

Figure 2.11. Gold nanoparticle nanozyme transcription factor mimic. It was produced by Ki-Bum Lee's Group. Ligands were attached to the particle via thiol-Au interactions with the goal of stimulating stem cell differentiation. Reprinted from reference 86. Copyright (2014) American Chemical Society.[86]

2.3.7. Ribozyme Nanoparticle

Figure 2.12. Schematic demonstrating the attachment of ribozymes to an SNA to form a novel conjugate, resulting in RNA cleavage. Reprinted with permission from reference 89. Copyright (2015) American Chemical Society.[89]

In 2015, Mirkin and his team also demonstrated a second example of a Class I.A. nanozyme utilizing a gold core and acting as a RISC mimic: the ribozyme-SNA (Fig. 2.12.).[89] Unmodified and truncated ribozymes active against the O^6-methylguanine-DNA methyltransferase (MGMT) were attached to a DNA SNA through enzymatic ligation.[89] Typically, ribozymes suffer from instability in comparison with other techniques for RNA knockdown such as siRNA and miRNA. However, as seen previously for DNA SNAs, attachment of the ribozymes to the SNA helps shield them from degradation by nucleases.[89] To show this, the team incubated the ribozyme-SNAs in 40% fetal bovine serum (FBS) for 1 hr at 37ºC. They then showed that they were still able to amplify full length ribozyme RNA by PCR.[89] While encouraging, there likely was a significant amount of degradation and this method does not give an indication of the percentage of ribozymes that survived on the surface. It only illustrates that some full-length transcript survived. Regardless, these ribozyme-SNAs were found to be active against MGMT RNA after 12-24 h exposure in 40 mM Mg^{2+} *in vitro*.[89] As a final touch, the ribozyme-SNAs also showed 75% knockdown of the target RNA in a glioma cell line after an overnight incubation.[89] As high expression of MGMT has been correlated with resistance to chemotemozolomide (TMZ) therapy

in glioblastoma multiforme (GBM), this result shows that ribozyme-SNAs can have a suitably therapeutic effect at the cellular level to a devastating disease.[89]

2.3.8. CRISPR-gold Nanozyme

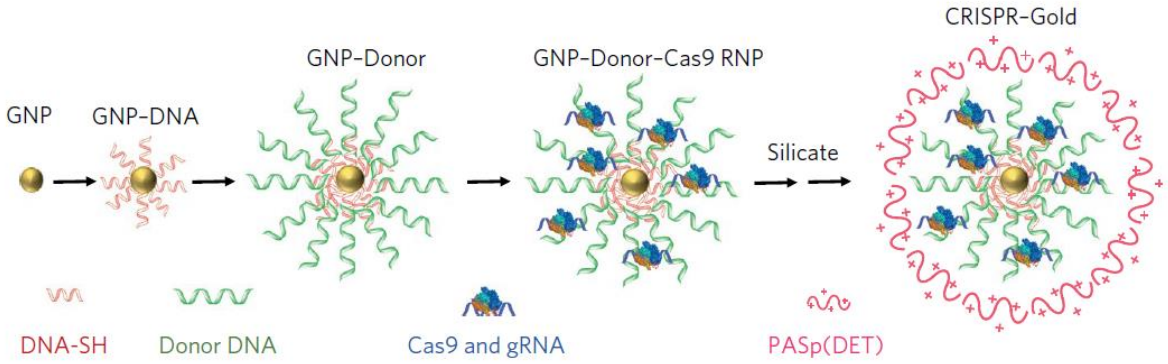

Figure 2.13. Construction of AuNPs carrying donor DNA and Cas9, capable of delivering the cargo into cells and induction of HDR. Adapted by permission from Springer Nature: Nature Publishing Group, Nature Biomedical Engineering from reference 90, Copyright (2017).[90]

In 2017, Dr. Niren Murthy's lab produced a Class III.B. CRISPR-AuNP nanozyme capable of both delivering CRISPR Cas9 and donor DNA to target cells as well as inducing homologous recombination (HDR).[90] Notably, there is a different earlier report of a CRISPR-AuNP complex by Rotello;[91] however, his featured a many particles in one large complex or "nanoassembly" and worked a bit differently than Murthy's.[91] It could be argued that even in Murthy's case, the AuNP was designed specifically for delivery of the Cas9 rather than operating as a nanozyme, since Murthy claimed the DNA and Cas9 are released from the particle once inside the cell due to glutathione reduction.[90] However, it is included here, as an important example of work done with AuNPs and CRISPR. The constructs were synthesized on a core of 15 nm AuNPs. First, 5-thiolated DNA was anchored to the particles through the thiol-Au interaction, and donor DNA was complexed to this first DNA layer (Fig. 2.13.). Then, Cas9 and guide RNA were added, and afterward, the particles were coated in a layer of silicate and the polymer poly(N-(N-(2-aminoethyl)- 2-aminoethyl) aspartamide) (PAsp(DET)), capable of endosomal disruption (Fig.

2.13).[90] The construct was tested on HEK293 cells expressing blue fluorescent protein (BFP). As proof-of-concept, the CRISPR-AuNPs were to induce HDR, changing the HEK-BFP cells to expressing green fluorescent protein (GFP). After incubation of the CRISPR-AuNPs with the cells, results were analyzed via flow cytometry and it was found that 11.3% of the cells were GFP expressing.[90] By sequencing, it was demonstrated that the donor DNA included in the CRISPR-AuNPs matched the sequence in the GFP expressing cells.[90] The construct was also able to edit the gene CXCR4 or *dystrophin* in a variety of cell lines, including stem cells, with an efficiency of between 3-4%.[90] DNA editing was also done with these particles in Ai9 and mdx mice, to show efficacy *in vivo.* In mdx mice, they saw 5.4% correction of the dystrophin gene after treatment.[90]

2.3.9. Transition Metal Catalyst Functionalized Nanozymes

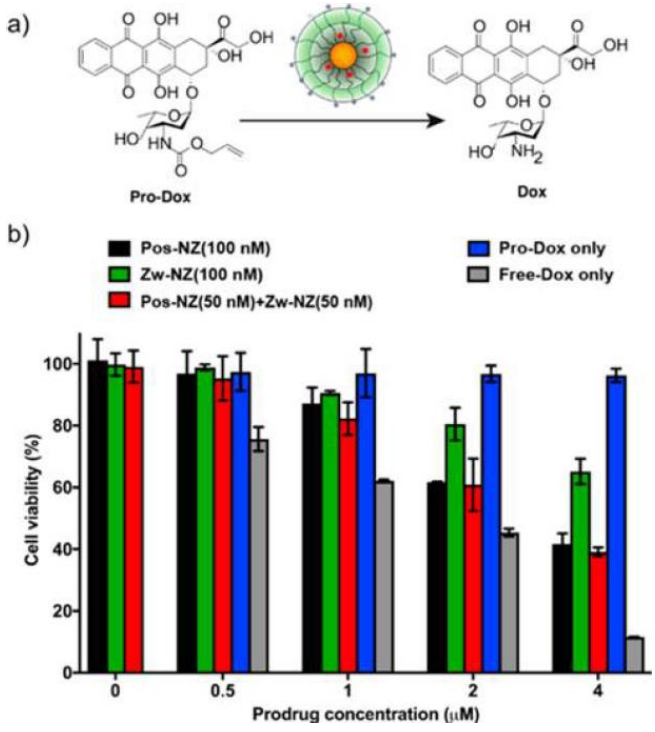

Figure 2.14. Metal functionalized nanozymes (a) Ruthenium-catalyst functionalized AuNPs catalyze DOX prodrug, (b) leading to lower cell viability. Reprinted with permission from reference 92. Copyright (2018) American Chemical Society.[92]

In 2018, Rotello's Group demonstrated the production and use of transition metal catalyst (TMC) functionalized AuNPs, a Class II.B. nanozyme, that could catalyze the activation of the prodrug allylcarbamate-protected doxorubicin.[92] To produce the nanozymes, he used 2 nm AuNP cores with a series of ligands: 1) a hydrophobic alkane chain capable of encapsulating the TMC, which in this case is a ruthenium-based catalyst 2) a tetraethylene glycol spacer 3) a terminal ligand that provided the particles with

either a positive or zwitterionic charge.[92] The positive NPs were uptaken by cells while the zwitterionic ones were not, allowing for intracellular and extracellular catalysis, respectively.[92] He was able to show that cell viability decreased when incubated with pro-drug and the nanozymes, indicating activation of the prodrug, when compared to controls (Fig. 2.14).[92] Rotello's group has a history of producing AuNP conjugate sensors[93] and nanozymes[94-96] of many varieties.

2.4. References

1. Lin, Y.; Ren, J.; Qu, X., Nano-gold as artificial enzymes: hidden talents. *Adv Mater* **2014,** *26* (25), 4200-17.
2. Lin, Y.; Ren, J.; Qu, X., Catalytically active nanomaterials: a promising candidate for artificial enzymes. *Acc Chem Res* **2014,** *47* (4), 1097-105.
3. Manea, F.; Houillon, F. B.; Pasquato, L.; Scrimin, P., Nanozymes: gold-nanoparticle-based transphosphorylation catalysts. *Angew Chem Int Ed Engl* **2004,** *43* (45), 6165-9.
4. Liu, B.; Liu, J., Surface modification of nanozymes. *Nano Research* **2017,** *10* (4), 1125-1148.
5. Zhou, Y.; Liu, B.; Yang, R.; Liu, J., Filling in the Gaps between Nanozymes and Enzymes: Challenges and Opportunities. *Bioconjug Chem* **2017,** *28* (12), 2903-2909.
6. Wang, X.; Hu, Y.; Wei, H., Nanozymes in bionanotechnology: from sensing to therapeutics and beyond. *Inorg. Chem. Front.* **2016,** *3* (1), 41-60.
7. Liu, B.; Huang, Z.; Liu, J., Boosting the oxidase mimicking activity of nanoceria by fluoride capping: rivaling protein enzymes and ultrasensitive F(-) detection. *Nanoscale* **2016,** *8* (28), 13562-7.
8. Xu, C.; Liu, Z.; Wu, L.; Ren, J.; Qu, X., Nucleoside Triphosphates as Promoters to Enhance Nanoceria Enzyme-like Activity and for Single-Nucleotide Polymorphism Typing. *Advanced Functional Materials* **2014,** *24* (11), 1624-1630.
9. Asati, A.; Santra, S.; Kaittanis, C.; Nath, S.; Perez, J. M., Oxidase-like activity of polymer-coated cerium oxide nanoparticles. *Angew Chem Int Ed Engl* **2009,** *48* (13), 2308-12.
10. Pautler, R.; Kelly, E. Y.; Huang, P. J.; Cao, J.; Liu, B.; Liu, J., Attaching DNA to nanoceria: regulating oxidase activity and fluorescence quenching. *ACS Appl Mater Interfaces* **2013,** *5* (15), 6820-5.

11. Bulbul, G.; Hayat, A.; Andreescu, S., ssDNA-Functionalized Nanoceria: A Redox-Active Aptaswitch for Biomolecular Recognition. *Adv Healthc Mater* **2016,** *5* (7), 822-8.

12. Liu, B.; Sun, Z.; Huang, P. J.; Liu, J., Hydrogen peroxide displacing DNA from nanoceria: mechanism and detection of glucose in serum. *J Am Chem Soc* **2015,** *137* (3), 1290-5.

13. Singh, S.; Dosani, T.; Karakoti, A. S.; Kumar, A.; Seal, S.; Self, W. T., A phosphate-dependent shift in redox state of cerium oxide nanoparticles and its effects on catalytic properties. *Biomaterials* **2011,** *32* (28), 6745-53.

14. Perez, J. M.; Asati, A.; Nath, S.; Kaittanis, C., Synthesis of biocompatible dextran-coated nanoceria with pH-dependent antioxidant properties. *Small* **2008,** *4* (5), 552-6.

15. Liu, X.; Wei, W.; Yuan, Q.; Zhang, X.; Li, N.; Du, Y.; Ma, G.; Yan, C.; Ma, D., Apoferritin-CeO2 nano-truffle that has excellent artificial redox enzyme activity. *Chem Commun (Camb)* **2012,** *48* (26), 3155-7.

16. Karakoti, A. S.; Singh, S.; Kumar, A.; Malinska, M.; Kuchibhatla, S. V. N. T.; Wozniak, K.; Self, W. T.; Seal, S., PEGylated nanoceria as radical scavenger with tunable redox. *JACS Communications* **2009,** *131*, 14144–14145.

17. Li, Y.; He, X.; Yin, J. J.; Ma, Y.; Zhang, P.; Li, J.; Ding, Y.; Zhang, J.; Zhao, Y.; Chai, Z.; Zhang, Z., Acquired superoxide-scavenging ability of ceria nanoparticles. *Angew Chem Int Ed Engl* **2015,** *54* (6), 1832-5.

18. Xue, Y.; Zhai, Y.; Zhou, K.; Wang, L.; Tan, H.; Luan, Q.; Yao, X., The vital role of buffer anions in the antioxidant activity of CeO2 nanoparticles. *Chemistry* **2012,** *18* (35), 11115-22.

19. Zhai, Y.; Zhang, Y.; Qin, F.; Yao, X., An electrochemical DNA biosensor for evaluating the effect of mix anion in cellular fluid on the antioxidant activity of CeO2 nanoparticles. *Biosens Bioelectron* **2015,** *70*, 130-6.

20. Chen, C.; Lu, L.; Zheng, Y.; Zhao, D.; Yang, F.; Yang, X., A new colorimetric protocol for selective detection of phosphate based on the inhibition of peroxidase-like activity of magnetite nanoparticles. *Analytical Methods* **2015,** *7* (1), 161-167.

21. Liu, C. H.; Yu, C. J.; Tseng, W. L., Fluorescence assay of catecholamines based on the inhibition of peroxidase-like activity of magnetite nanoparticles. *Anal Chim Acta* **2012,** *745*, 143-8.

22. Liu, Y.; Purich, D. L.; Wu, C.; Wu, Y.; Chen, T.; Cui, C.; Zhang, L.; Cansiz, S.; Hou, W.; Wang, Y.; Yang, S.; Tan, W., Ionic Functionalization of Hydrophobic Colloidal Nanoparticles To Form Ionic Nanoparticles with Enzymelike Properties. *J Am Chem Soc* **2015,** *137* (47), 14952-8.

23. Fan, K.; Wang, H.; Xi, J.; Liu, Q.; Meng, X.; Duan, D.; Gao, L.; Yan, X., Optimization of Fe3O4 nanozyme activity via single amino acid modification mimicking an enzyme active site. *Chem Commun (Camb)* **2016,** *53* (2), 424-427.

24. Yu, F.; Huang, Y.; Cole, A. J.; Yang, V. C., The artificial peroxidase activity of magnetic iron oxide nanoparticles and its application to glucose detection. *Biomaterials* **2009,** *30* (27), 4716-22.

25. Gao, L.; Zhuang, J.; Nie, L.; Zhang, J.; Zhang, Y.; Gu, N.; Wang, T.; Feng, J.; Yang, D.; Perrett, S.; Yan, X., Intrinsic peroxidase-like activity of ferromagnetic nanoparticles. *Nat Nanotechnol* **2007,** *2* (9), 577-83.

26. Park, K. S.; Kim, M. I.; Cho, D. Y.; Park, H. G., Label-free colorimetric detection of nucleic acids based on target-induced shielding against the peroxidase-mimicking activity of magnetic nanoparticles. *Small* **2011,** *7* (11), 1521-5.

27. Liu, B.; Liu, J., Accelerating peroxidase mimicking nanozymes using DNA. *Nanoscale* **2015,** *7* (33), 13831-5.

28. Li, X.; Wen, F.; Creran, B.; Jeong, Y.; Zhang, X.; Rotello, V. M., Colorimetric protein sensing using catalytically amplified sensor arrays. *Small* **2012,** *8* (23), 3589-92.

29. Zhang, X.-Q.; Gong, S.-W.; Zhang, Y.; Yang, T.; Wang, C.-Y.; Gu, N., Prussian blue modified iron oxide magnetic nanoparticles and their high peroxidase-like activity. *Journal of Materials Chemistry* **2010,** *20* (24).

30. Zhu, R.; Zhou, Y.; Wang, X. L.; Liang, L. P.; Long, Y. J.; Wang, Q. L.; Zhang, H. J.; Huang, X. X.; Zheng, H. Z., Detection of Hg2+ based on the selective inhibition of peroxidase mimetic activity of BSA-Au clusters. *Talanta* **2013,** *117*, 127-32.

31. Zhang, D.; Chen, Z.; Omar, H.; Deng, L.; Khashab, N. M., Colorimetric peroxidase mimetic assay for uranyl detection in sea water. *ACS Appl Mater Interfaces* **2015,** *7* (8), 4589-94.

32. Long, Y. J.; Li, Y. F.; Liu, Y.; Zheng, J. J.; Tang, J.; Huang, C. Z., Visual observation of the mercury-stimulated peroxidase mimetic activity of gold nanoparticles. *Chemical communications* **2011,** *47* (43), 11939-41.

33. Wang, C. I.; Huang, C. C.; Lin, Y. W.; Chen, W. T.; Chang, H. T., Catalytic gold nanoparticles for fluorescent detection of mercury(II) and lead(II) ions. *Anal Chim Acta* **2012,** *745*, 124-30.

34. Deng, H. H.; Weng, S. H.; Huang, S. L.; Zhang, L. N.; Liu, A. L.; Lin, X. H.; Chen, W., Colorimetric detection of sulfide based on target-induced shielding against the peroxidase-like activity of gold nanoparticles. *Anal Chim Acta* **2014,** *852*, 218-22.

35. Jv, Y.; Li, B.; Cao, R., Positively-charged gold nanoparticles as peroxidase mimic and their application in hydrogen peroxide and glucose detection. *Chemical communications* **2010,** *46* (42), 8017-9.

36. Wang, S.; Chen, W.; Liu, A. L.; Hong, L.; Deng, H. H.; Lin, X. H., Comparison of the peroxidase-like activity of unmodified, amino-modified, and citrate-capped gold nanoparticles. *Chemphyschem* **2012,** *13* (5), 1199-204.

37. Ni, P.; Dai, H.; Wang, Y.; Sun, Y.; Shi, Y.; Hu, J.; Li, Z., Visual detection of melamine based on the peroxidase-like activity enhancement of bare gold nanoparticles. *Biosens Bioelectron* **2014,** *60*, 286-91.

38. Lin, Y.; Huang, Y.; Ren, J.; Qu, X., Incorporating ATP into biomimetic catalysts for realizing exceptional enzymatic performance over a broad temperature range. *NPG Asia Materials* **2014,** *6* (7), e114-e114.

39. Shah, J.; Purohit, R.; Singh, R.; Karakoti, A. S.; Singh, S., ATP-enhanced peroxidase-like activity of gold nanoparticles. *J Colloid Interface Sci* **2015,** *456*, 100-7.

40. Sharma, T. K.; Ramanathan, R.; Weerathunge, P.; Mohammadtaheri, M.; Daima, H. K.; Shukla, R.; Bansal, V., Aptamer-mediated 'turn-off/turn-on' nanozyme activity of gold nanoparticles for kanamycin detection. *Chemical communications* **2014,** *50* (100), 15856-9.

41. Hizir, M. S.; Top, M.; Balcioglu, M.; Rana, M.; Robertson, N. M.; Shen, F.; Sheng, J.; Yigit, M. V., Multiplexed Activity of perAuxidase: DNA-Capped AuNPs Act as Adjustable Peroxidase. *Anal Chem* **2016,** *88* (1), 600-5.

42. Lien, C. W.; Chen, Y. C.; Chang, H. T.; Huang, C. C., Logical regulation of the enzyme-like activity of gold nanoparticles by using heavy metal ions. *Nanoscale* **2013,** *5* (17), 8227-34.

43. Zheng, X.; Liu, Q.; Jing, C.; Li, Y.; Li, D.; Luo, W.; Wen, Y.; He, Y.; Huang, Q.; Long, Y. T.; Fan, C., Catalytic gold nanoparticles for nanoplasmonic detection of DNA hybridization. *Angewandte Chemie* **2011,** *50* (50), 11994-8.

44. Zhan, P.; Wang, Z.-G.; Li, N.; Ding, B., Engineering Gold Nanoparticles with DNA Ligands for Selective Catalytic Oxidation of Chiral Substrates. *ACS Catalysis* **2015,** *5* (3), 1489-1498.

45. Sun, H.; Zhao, A.; Gao, N.; Li, K.; Ren, J.; Qu, X., Deciphering a nanocarbon-based artificial peroxidase: chemical identification of the catalytically active and substrate-binding sites on graphene quantum dots. *Angewandte Chemie* **2015,** *54* (24), 7176-80.

46. Xu, C.; Zhao, C.; Li, M.; Wu, L.; Ren, J.; Qu, X., Artificial evolution of graphene oxide chemzyme with enantioselectivity and near-infrared photothermal effect for cascade biocatalysis reactions. *Small* **2014,** *10* (9), 1841-7.

47. Guo, Y.; Deng, L.; Li, J.; Guo, S.; Wang, E.; Dong, S., Hemin−graphene hybrid nanosheets with intrinsic peroxidase-like activity for label-free colorimetric detection of single-nucleotide polymorphism. *ACS nano* **2011,** *5* (2), 1282–1290.

48. Conde, J.; Dias, J. T.; Grazu, V.; Moros, M.; Baptista, P. V.; de la Fuente, J. M., Revisiting 30 years of biofunctionalization and surface chemistry of inorganic nanoparticles for nanomedicine. *Front Chem* **2014,** *2*, 48.

49. Sperling, R. A.; Gil, P. R.; Zhang, F.; Zanella, M.; Parak, W. J., Biological applications of gold nanoparticles. *Chemical Society Reviews* **2008,** *37*, 1896-1908.

50. Arvizo, R.; Bhattacharya, R.; Mukherjee, P., Gold nanoparticles: opportunities and challenges in nanomedicine. *Expert Opin Drug Deliv* **2010,** *7* (6), 753-63.

51. J., T.; P.C., S.; J., H., A study of the nucleation and growth processes in the synthesis of colloidal gold. *Discuss Faraday Soc* **1951,** *11*, 55–75.

52. Frens, G., Controlled nucleation for the regulation of the particle size in monodisperse gold suspensions. *Nature Phys Sci* **1973,** *241*, 20–22.

53. Khlebtsov, N.; Dykman, L., Biodistribution and toxicity of engineered gold nanoparticles: a review of in vitro and in vivo studies. *Chem Soc Rev* **2011,** *40* (3), 1647-71.

54. M, B.; M, W.; D, B.; DJ, S.; RJ, W., Synthesis of Thiol-derivatised Gold Nanoparticles in a Two-phase Liquid-Liquid System. *J Chem Soc, Chem Commun* **1994**, 801-802.

55. Sasidharan, A.; Monteiro-Riviere, N. A., Biomedical applications of gold nanomaterials: opportunities and challenges. *Wiley Interdiscip Rev Nanomed Nanobiotechnol* **2015,** *7* (6), 779-96.

56. AM, A.; PK, N.; CR, H.; TJ, S.; CJ, M.; MD, W., Cellular uptake and cytotoxicity of gold nanorods: molecular origin of cytotoxicity and surface effects. *Small* **2009,** *5* (701-708).

57. Y, P.; S, N.; A, L.; M, F.; F, W.; U, S.; G, S.; W, B.; W., J.-D., Size-dependent cytotoxicity of gold nanoparticles. *Small* **2007,** *3* (11), 1941-1949.

58. N, P.; X, F.; Y, S.; A, B.; A, R.; J, S.; A, U.; M., R., Adverse effects of citrate/gold nanoparticles on human dermal fibroblasts. *Small* **2006,** *2* (6), 766-773.

59. Connor, E. E.; Mwamuka, J.; Gole, A.; Murphy, C. J.; Wyatt, M. D., Gold nanoparticles are taken up by human cells but do not cause acute cytotoxicity. *Small* **2005,** *1* (3), 325-7.

60. Lakowicz, J. R., *Principles of Fluorescence Spectroscopy*. 3rd ed.; Springer: New York, 2006.

61. Chithrani, B. D.; Ghazani, A. A.; Chan, W. C. W., Determining the Size and Shape Dependence of Gold Nanoparticle Uptake into Mammalian Cells. *Nano letters* **2006,** *6* (4), 662-668.

62. Vranish, J. N.; Ancona, M. G.; Walper, S. A.; Medintz, I. L., Pursuing the Promise of Enzymatic Enhancement with Nanoparticle Assemblies. *Langmuir* **2018,** *34* (9), 2901-2925.

63. Choi, C. H.; Hao, L.; Narayan, S. P.; Auyeung, E.; Mirkin, C. A., Mechanism for the endocytosis of spherical nucleic acid nanoparticle conjugates. *Proc Natl Acad Sci U S A* **2013,** *110* (19), 7625-30.

64. Yehl, K.; Joshi, J. P.; Greene, B. L.; Dyer, B.; Nahta, R.; Salaita, K., Catalytic deoxyribozyme-modified nanoparticles for RNAi-independent gene regulation. *ACS nano* **2012,** *6* (10), 9150–9157.

65. Menger, F. M., Groups of Organic Molecules That Operate Collectively. *Angew. Chem. Int. Ed. Engl.* **1991,** *30*, 1086-1099.

66. CA, M.; RL, L.; RC, M.; JJ., S., A DNA-based method for rationally assembling nanoparticles into macroscopic materials. *Nature* **1996,** *382* (6592), 607-609.

67. Cutler, J. I.; Auyeung, E.; Mirkin, C. A., Spherical nucleic acids. *J Am Chem Soc* **2012,** *134* (3), 1376-91.

68. Cutler, J. I.; Zhang, K.; Zheng, D.; Auyeung, E.; Prigodich, A. E.; Mirkin, C. A., Polyvalent Nucleic Acid Nanostructures. *JACS* **2011,** *133* (24), 9254–9257.

69. Lytton-Jean, A. K. R.; Mirkin, C. A., A Thermodynamic Investigation into the Binding Properties of DNA Functionalized Gold Nanoparticle Probes and Molecular Fluorophore Probes. *JACS Communications* **2005,** *127* (37), 12754–12755.

70. Jin, R.; Wu, G.; Li, Z.; Mirkin, C. A.; C. Schatz, G., What Controls the Melting Properties of DNA-Linked Gold Nanoparticle Assemblies? *JACS* **2003,** *125* (6), 1643–1654.

71. Seferos, D. S.; Prigodich, A. E.; Giljohann, D. A.; Patel, P. C.; Mirkin, C. A., Polyvalent DNA nanoparticle conjugates stabilize nucleic acids. *Nano Lett* **2009,** *9* (1), 308-11.

72. Giljohann, D. A.; Seferos, D. S.; Patel, P. C.; Millstone, J. E.; Rosi, N. L.; Mirkin, C. A., Oligonucleotide Loading Determines Cellular Uptake of DNA-Modified Gold Nanoparticles. *Nano letters* **2007,** *7* (12), 3818-3821.

73. Rosi, N. L.; Giljohann, D. A.; Thaxton, C. S.; Lytton-Jean, A. K.; Han, M. S.; Mirkin, C. A., Oligonucleotide-modified gold nanoparticles for intracellular gene regulation. *Science* **2006,** *312* (5776), 1027-30.

74. Li, Z.; Jin, R.; Mirkin, C. A.; Letsinger, R. L., Multiple thiol-anchor capped DNA–gold nanoparticle conjugates. *Nucleic acids research* **2002,** *30* (7), 1558–1562.

75. Dougan, J. A.; Karlsson, C.; Smith, W. E.; Graham, D., Enhanced oligonucleotide–nanoparticle conjugate stability using thioctic acid modified oligonucleotides. *Nucleic acids research* **2007,** *35* (11), 3668–3675.

76. Hurst, S. J.; Lytton-Jean, A. K.; Mirkin, C. A., Maximizing DNA Loading on a Range of Gold Nanoparticle Sizes. *Anal Chem* **2006,** *78* (1), 8313-8318.

77. Hill, H. D.; Mirkin, C. A., The bio-barcode assay for the detection of protein and nucleic acid targets using DTT-induced ligand exchange. *Nat Protoc* **2006,** *1* (1), 324-36.

78. Liu, B.; Liu, J., Freezing Directed Construction of Bio/Nano Interfaces: Reagentless Conjugation, Denser Spherical Nucleic Acids, and Better Nanoflares. *Journal of the American Chemical Society* **2017,** *139* (28), 9471-9474.

79. Giljohann, D. A.; Seferos, D. S.; Prigodich, A. E.; Patel, P. C.; Mirkin, C. A., Gene Regulation with Polyvalent siRNA-Nanoparticle Conjugates. *JACS Communications* **2009,** *131* (6), 2072–2073.

80. Dhar, S.; Daniel, W. L.; Giljohann, D. A.; Mirkin, C. A.; Lippard, S. J., Polyvalent Oligonucleotide Gold Nanoparticle Conjugates as Delivery Vehicles for Platinum(IV) Warheads. *JACS* **2010,** *132* (48), 17335–17335.

81. Zhang, X.-Q.; Xu, X.; Lam, R.; Giljohann, D.; Ho, D.; Mirkin, C. A., Strategy for Increasing Drug Solubility and Efficacy through Covalent Attachment to Polyvalent DNA–Nanoparticle Conjugates. *ACS nano* **2011,** *5* (9), 6962–6970.

82. Seferos, D. S.; Giljohann, D. A.; Hill, H. D.; Prigodich, A. E.; Mirkin, C. A., Nano-Flares, Probes for Transfection and mRNA Detection in Living Cells. *JACS Communications* **2007,** *129* (50), 15477–15479.

83. Wang, Z., Hongyan Liu, Soon Hye Yang, Tie Wang, Chen Liu and Y. Charles Cao, Nanoparticle-based artificial RNA silencing machinery for antiviral therapy. *Proceedings of the National Academy of Sciences of the United States of America* **2012,** *109* (31), 12387-12392.

84. Zaborowska, Z.; Furste, J. P.; Erdmann, V. A.; Kurreck, J., Sequence Requirements in the Catalytic Core of the “10-23” DNA Enzyme. *J. Biol. Chem.* **2002,** *277*, 40617–40622.

85. Wu, P.; Hwang, K.; Lan, T.; Lu, Y., A DNAzyme-gold nanoparticle probe for uranyl ion in living cells. *J Am Chem Soc* **2013,** *135* (14), 5254-7.

86. Patel, S.; Jung, D.; Yin, P.; Carlton, P.; Yamamoto, M.; Bando, T.; Sugiyama, H.; Lee, K. B., NanoScript: A Nanoparticle-Based Artificial Transcription Factor for Effective Gene Regulation. *ACS nano* **2014,** *8* (9), 8959–8967.

87. Patel, S.; Yin, P. T.; Sugiyama, H.; Lee, K. B., Inducing Stem Cell Myogenesis Using NanoScript. *ACS nano* **2015,** *9* (7), 6909-6917.

88. Patel, S.; Chueng, S. T.; Yin, P. T.; Dardir, K.; Song, Z.; Pasquale, N.; Kwan, K.; Sugiyama, H.; Lee, K. B., Induction of stem-cell-derived functional neurons by NanoScript-based gene repression. *Angew Chem Int Ed Engl* **2015,** *54* (41), 11983-8.

89. Rouge, J. L.; Sita, T. L.; Hao, L.; Kouri, F. M.; Briley, W. E.; Stegh, A. H.; Mirkin, C. A., Ribozyme-Spherical Nucleic Acids. *J Am Chem Soc* **2015,** *137* (33), 10528-10531.

90. Lee, K.; Conboy, M.; Park, H. M.; Jiang, F.; Kim, H. J.; Dewitt, M. A.; Mackley, V. A.; Chang, K.; Rao, A.; Skinner, C.; Shobha, T.; Mehdipour, M.; Liu, H.; Huang, W. C.; Lan, F.; Bray, N. L.; Li, S.; Corn, J. E.; Kataoka, K.; Doudna, J. A.; Conboy, I.; Murthy, N., Nanoparticle delivery of Cas9 ribonucleoprotein and donor DNA in vivo induces homology-directed DNA repair. *Nat Biomed Eng* **2017,** *1*, 889-901.

91. Mout, R.; Ray, M.; Yesilbag Tonga, G.; Lee, Y. W.; Tay, T.; Sasaki, K.; Rotello, V. M., Direct Cytosolic Delivery of CRISPR/Cas9-Ribonucleoprotein for Efficient Gene Editing. *ACS nano* **2017,** *11* (3), 2452-2458.

92. Das, R.; Landis, R. F.; Yesilbag Tonga, G.; Cao-Milan, R.; Luther, D. C.; Rotello, V. M., Control of Intra- versus Extracellular Bioorthogonal Catalysis using Surface-Engineered Nanozymes. *ACS Nano* **2018**.

93. Ehrenberg, M. S.; Friedman, A. E.; Finkelstein, J. N.; Oberdorster, G.; McGrath, J. L., The influence of protein adsorption on nanoparticle association with cultured endothelial cells. *Biomaterials* **2009,** *30* (4), 603-10.

94. You, C.-C.; Arvizo, R. R.; Rotello, V. M., Regulation of a-chymotrypsin activity on the surface of substrate-functionalized gold nanoparticles. *Chemical Communcations* **2006,** (27), 2905–2907.

95. Gupta, A.; Das, R.; Yesilbag Tonga, G.; Mizuhara, T.; Rotello, V. M., Charge-Switchable Nanozymes for Bioorthogonal Imaging of Biofilm-Associated Infections. *ACS Nano* **2018,** *12* (1), 89-94.

96. Tonga, G. Y.; Jeong, Y.; Duncan, B.; Mizuhara, T.; Mout, R.; Das, R.; Kim, S. T.; Yeh, Y. C.; Yan, B.; Hou, S.; Rotello, V. M., Supramolecular regulation of bioorthogonal catalysis in cells using nanoparticle-embedded transition metal catalysts. *Nat Chem* **2015,** *7* (7), 597-603.

Chapter 3: Mechanism of DNAzyme Nanoparticles for RNA Knockdown

Contributions: Tom Pickel synthesized 3-azidopropan-1-thiol. Nusaiba Baker isolated RNA from T47D cells for Figure 3.11.

3.1. Introduction

Deoxyribozyme (DNAzyme) conjugated gold nanoparticle (AuNP) nanozymes (DzNPs) have been built for a wide range of applications. For example, Niazov and colleagues synthesized a DzNP that detects the activity of telomerase.[1] Yin and coworkers produced a DzNP that senses the concentration of Cu^{2+} and Pb^{2+} ions.[2] Our lab synthesized the first example of a DzNP that knocks down levels of a cellular mRNA target *in vitro*[3] and *in vivo*.[4] Zagorovsky *et al.* made a DzNP that detects a particular nucleic acid analyte as a point-of-care diagnostic,[5] and Wu and colleagues developed a DzNP for uranyl ion sensing in cells.[6] Finally, Yang and Wu separately with their own collaborators made DzNPs that detect cellular micro RNA (miRNA).[7-8] Yet, one question that has intrigued researchers from this field's infancy is how DzNPs operate inside the cell – their mechanism of action. Some of this story is addressed in the work of colleagues in the Mirkin lab, who investigated the fate of spherical nucleic acids (SNAs): how they are taken up and processed by cells.[9-13] DzNPs can be classified as an SNA and thus share the same fate, as they are formed by attaching DNAzymes (which are DNA) to an AuNP core.

The first glimpse of how cells responded to SNAs was found by Massich and colleagues.[9] Massich determined that HeLa cells incubated with 10 nM citrate stabilized AuNPs drastically changed their gene expression – 119 genes were downregulated and 8 were upregulated compared to control cells.[9] However, HeLa cells exposed to SNAs, or AuNPs that had been functionalized with single-stranded DNA (ssDNA), double-stranded DNA (dsDNA), dsRNA or bovine serum albumin (BSA) did not have a significant change in their gene expression profile.[9] Therefore, Massich postulated that the citrate was the cause of the change in gene expression, showing how the change in a surface ligand could have a significant impact on the cell.[9] This work, however, did not touch on how the SNA particles were uptaken by cells. This question began to be addressed by Mirkin lab members in 2007,[14] after which several critical papers would be published on the topic by their group.[10-13] It had already been shown by Zhu and

coworkers from the Rotello lab that small changes in surface ligands on an AuNP lead to changes in cellular uptake.[15] However, Zhu did not analyze DNA-functionalized AuNPs, looking at alkyl chain functionalized AuNPs with varying charges. Giljohann and coworkers first investigated SNA uptake, and found that uptake increased with the number of oligonucleotides bound to the AuNP.[14] Uptake plateaued when SNAs were coated with 60 strands per particle.[14] They also found that serum proteins bound to the attached SNAs and speculated that the protein recruitment to the particle was what led to higher amounts of uptake.[14] However, Patel and coworkers in a follow-up paper a few years later showed that protein adsorption to the SNAs actually decreased uptake.[10] When absorbing BSA to the SNAs, uptake decreased with increasing concentration of BSA.[10] When incubating SNAs with cells in serum-free media, they found uptake to increase by 150% compared to serum-containing media.[10] Patel and coworkers speculated that scavenger receptors may be involved in SNA recognition and uptake. Interestingly, when they knocked down levels of scavenger receptor class A (SR-A) and class B (SR-B1) in HeLa cells, the uptake of SNAs was not affected.[10] They hypothesized that there were other undiscovered scavenger receptors uptaking the particles.[10]

A much more detailed paper on this topic would come out in 2013 by Choi and coworkers.[11] Using inductively coupled plasma mass spectrometry (ICP-MS), and incubating C166 mouse endothelial cells in reduced serum media, they quantified uptake and intracellular transport.[11] They found that the most critical window for association and uptake of the SNAs was in the first 30 min. After just 5 min, each cell takes in ~3.6×10^4 NPs. As the 30 min interval increases, particle uptake increases, but at a slower rate.[11] To localize the SNAs within cells, transmission electron microscopy (TEM) was used. After 15 min, SNAs are found inside small 50 nm vesicles and invaginations, becoming clearer after the 30 min mark.[11] Indeed, after 1 h, the SNA vesicles have grown to 100-250 nm, and appear to be early endosomes.[11] This idea was confirmed in that early endosome antigen-1 colocalizes with these SNA vesicles, showing that SNAs are

indeed sorted into early endosomes in these cells.[11] Clathrin-dependent endocytosis was ruled out when the C166 cells were treated with chlorpromazine, an inhibitor of clathrin-coated pits. This treatment only resulted in a 12% reduction in SNA uptake.[11] However, when cells were incubated with filipin, which sequesters cholesterol, SNA uptake decreased by 70%.[11] This result implicated caveolae as the endocytosis mechanism. Indeed, when caveolin-1 was knocked down, SNA uptake decreased by 60%.[11] This data suggests that lipid rafts and caveolae mediate the endocytosis of the bulk of SNAs in this cell type.[11] This result was interesting, considering that Patel and coworkers ruled out caveolae-mediated endocytosis for HeLa cells.[10] In continuing to look at SNA uptake, Choi then focused on the cellular receptors involved. It was found that treatment with the scavenger receptor (SR) inhibitors fucoidan (FCD) and polyinosinic acid (Poly I) did inhibit as much as 80-90% of SNA uptake,[11] similar to the findings of Patel and coworkers in HeLa cells.[10] When inhibiting SR-B1, Choi found there to be only a 25% reduction in SNA uptake; whereas inhibiting SR-A resulted in an 80% loss in uptake.[11] This result contrasts with that of Patel, as neither of these receptors appeared to play a role in HeLa cells.[10] Choi then attempted to generalize this observation to other cell types besides C166, examining SNA uptake in human lung adenocarcinoma epithelium (A549), mouse fibroblast (3T3) and human keratinocyte (HaCaT).[11] It was found that SNA uptake correlated with the amount of caveolae and SR-A expressed in these cell types, with the highest expressor of both, HaCaT cells, uptaking the most SNAs.[11]

A third paper, by Wu and coworkers, focuses on SNA fate after endocytosis.[12] He was able to show that SNAs are slowly trafficked from early to late endosomes, being grouped together into clusters of 20-30 NPs at 4 h and then large clusters of aggregated particles (300-500 NPs) after 16 h (Fig. 3.1.).[12] Only a relative few escape to the cytosol, where they perform their therapeutic function.[12]

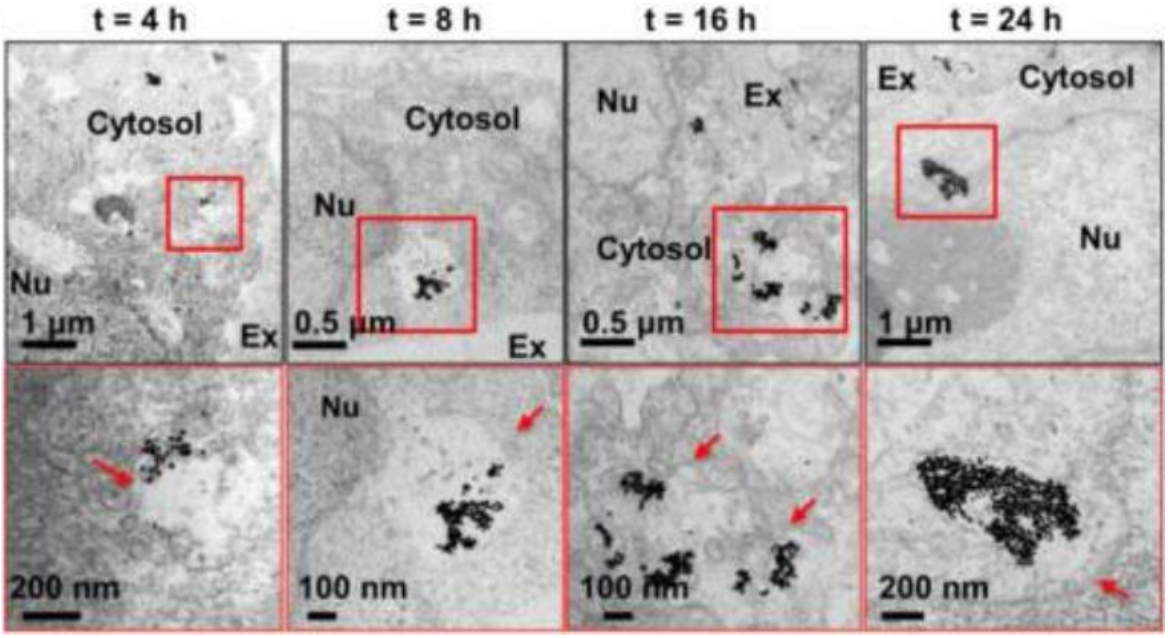

Figure 3.1. SNAs once uptaken by cells are trafficked to endosomes, forming larger and larger clusters. Reprinted from reference 12. Copyright (2014) American Chemical Society.[12]

He showed that the inorganic core and the sequence of the attached nucleic acid did not have any bearing on where the particles ended up in the cell.[12] Additionally, the length of time the cells were incubated with SNAs and whether the incubation was continuous or discontinuous also did not affect localization.[12] Wu also tested differing conditions to examine whether and how SNAs are degraded in late endosomes. Incubation in pH buffers ranging from 7.4 to 4.5 for 3 days did little to degrade the SNAs, as did incubation in concentrations of glutathione (1-10 mM, 24 h).[12] However, when the SNAs were subjected to treatment with DNase I and DNase II, they saw a 25% and 60% loss in nucleic acid coverage, respectively.[12] Therefore, Wu and coworkers concluded that it was primarily DNase II that is responsible for degradation of the SNAs inside cells.[12]

Finally, Narayan and coworkers demonstrated that there is a sequence partiality in SNA uptake,[13] though perhaps not for cellular localization.[12] They tested uptake in C166 cells of a 30-mer poly-G rich strand, a poly-C rich strand, a poly-A strand and a poly-T strand, finding that poly-G was uptaken the best and the poly-T strand had the lowest uptake.[13] The other strands

had intermediate amounts of uptake.[13] Narayan also found that the poly-G strand was likely taken up better due to the formation of G-quadruplexes, which are hypothesized to interact with SR-A receptors.[13] Additionally, Narayan implicated the 10 bases closest to the surface for causing cellular recognition and uptake, as when a string of G's was buried close to the surface of the AuNPs by a string of T's, uptake was markedly decreased.[13]

In addition to the reports on SNA uptake and cellular trafficking by the Mirkin group, there is also a report by Mason and Lévy that argues that the majority of SNAs are retained in endosomes. Therefore, they argue that SNAs cannot possibly report on cellular mRNA concentrations,[16] as the SNA nanoflares are said to do.[17-18] Another report, by Czarnek and Bereta supports this idea – showing experiments that suggest nanoflares do not report on mRNA concentration in their hands.[19] However, even the Mirkin group agrees that a significant population of SNAs are sequestered in endosomes.[11-12] Therefore, there is a debate as to the degree of endosomal escape, and accordingly whether nanoflares can function to detect messenger RNA (mRNA). This point pertaining to nanoflares is outside the scope of this review; therefore, we will not examine in detail the arguments by Mason and Czarnek here.

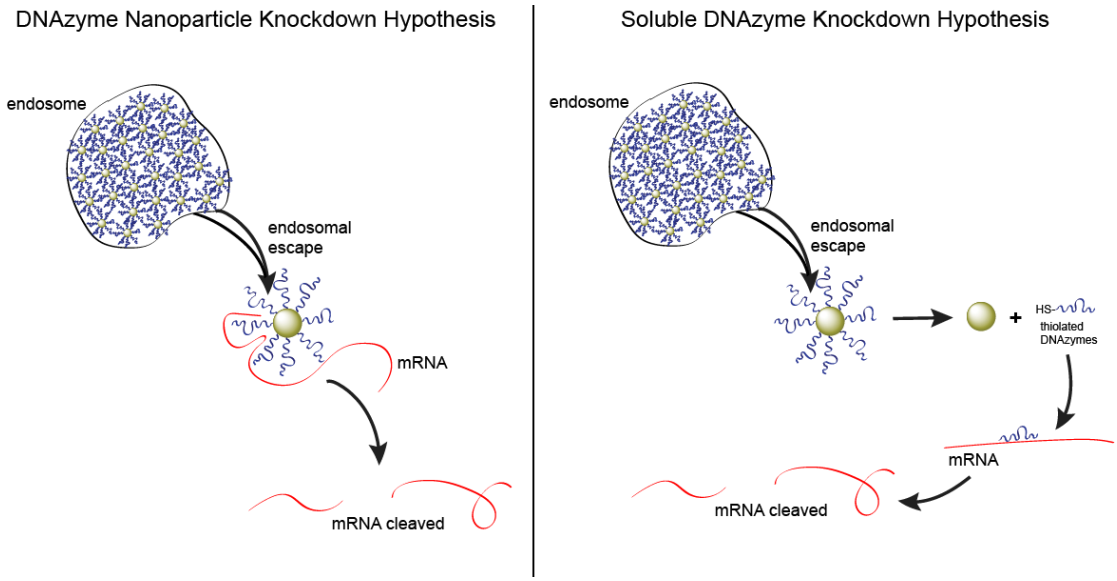

Figure 3.2. The two primary hypotheses illustrated for how DzNPs operate inside the cell.

Even with these important reports, it has still yet to be confirmed the mechanism by which the active SNAs or DzNP nanozymes operate inside the cell once they escape the endosome and migrate to the cytosol. Are DzNPs hydrolyzing target mRNA while attached to their gold nanoparticle scaffold or do DzNPs dissociate in the cytosol to function via their soluble strands (Fig. 3.2.)? Wu *et al.* would seem to suggest that DzNPs remain attached to their gold cores inside the cell, as exposure to varying concentrations of glutathione for 24 h did nothing to dissociate the SNAs tested.[12] Additionally, one of the first reports of SNAs, made via antisense strands attached to 13 nm AuNPs, showed that they likely remained on the AuNP inside cells.[20] In this work, the authors attached a Cy3 dye to the DNA strands near the gold core where it would be quenched and theorized that if the DNA came off the gold particles inside the cell, they would see Cy3 fluorescence. However, even after a 48 h incubation, very little Cy3 fluorescence was observed.[20] Nevertheless, the idea that attached DNA remains on the AuNP surface inside the cell is contradicted by at least one report. For instance, Kunwoo Lee and coworkers in the Murthy lab, in their paper on the CRISPR-gold construct state that, “Importantly, once in the cytoplasm, glutathione releases the DNA from the gold core of CRISPR–Gold, which causes the rapid release of Cas9 RNP and donor DNA.”[21] However, the team did not perform direct controls to support this claim, and the reference cited, a paper by the Rotello group,[22] does not conclusively answer this question. Therefore, we aimed to tackle this problem to better understand how DzNP conjugates operate, to broaden our understanding of this class of nanozymes. To answer this question, we synthesized an inactive DzNP whose DNAzymes become active once released from the particle. To accomplish this goal, we custom synthesized a DNAzyme with an alkyne modified uracil base in the middle of its catalytic core (Fig. 3.3.). We found in literature that the eighth T in the core from the 5’ end was able to tolerate mutations well.[23] We then clicked a 3-azidopropan-1-thiol ligand to it, giving it a single thiol group in the middle of the catalytic core. We hypothesized that when incubated with AuNPs, these

DNAzymes would attach to the gold by the core of the DNAzyme, rather than the 3' end, the anchor point typically used (Fig. 3.4.).

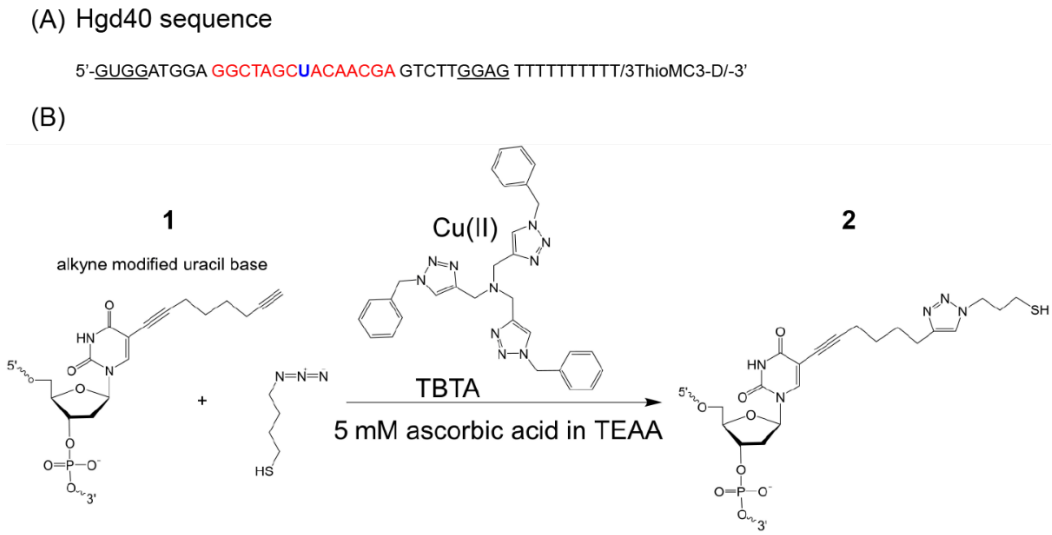

Figure 3.3. Synthetic strategy for the core-attached DNAzymes. (A) Sequence of the Hgd40 DNAzyme. Catalytic core is in red. Alkyne modified uracil base is in blue. Placement of 2'-O-methyl modifications are in red. (B) Synthesis of the thiol modified uracil base in the core of the Hgd40 DNAzyme. Reaction conditions: 60 µl 2M TEAA, 60 µl Nanopure water, 60 µl of 1 mM DNA alkyne suspended in Nanopure water, 60 µl of 5 mM fresh ascorbic acid, 330 µl dimethyl sulfoxide (DMSO), 6 µl if 3 azido-1-propanethiol (66% pure) and 24 µl Cu·TBTA. The reaction was incubated 24 h at room temperature in the dark. TBTA = Tris[(1-benzyl-1H-1,2,3-triazol-4-yl)methyl]amine, TEAA = triethylammonium acetate.

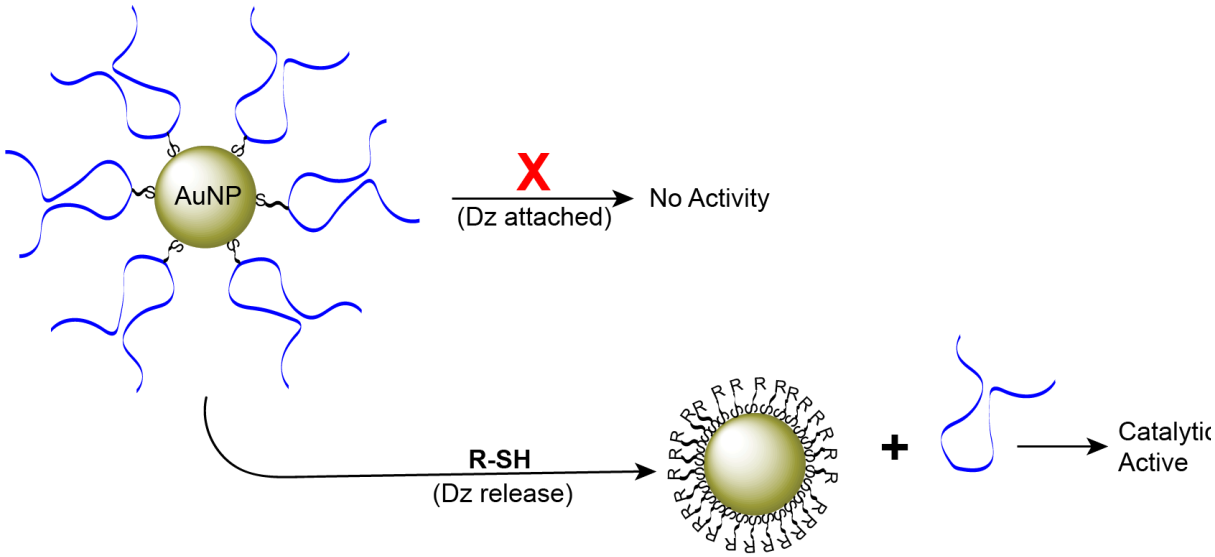

Figure 3.4. A schematic showing the lack of activity with core-attached-DzNPs. When the DNAzymes are displaced by a reducing agent and released from the AuNP, they become catalytically active.

After incubating these constructs with cells, we measured the levels of gene knockdown via quantitative real-time polymerase chain reaction (qRT-PCR). Given that the intact DzNP is catalytically inactive, the observation of knockdown activity would suggest that the soluble DNAzyme species mediates mRNA cleavage rather than the intact construct. Controls include a non-specific DNAzyme, targeting human papillomavirus (HPV) – a target which does not exist within the cells tested. This non-specific DNAzyme reports on whether there is a change in gene expression due to the presence of the DNAzyme, rather than due to its activity on the target. We also include a control DNAzyme with a mutation in the catalytic core that abolishes activity. The inactivated DNAzyme control group reports on the fraction of activity mediated by antisense mechanisms, rather than catalytic DNAzyme cleavage. Antisense activity refers to the binding of the DNAzyme to the target, preventing translation, in the absence of cleavage.

3.2. Optimizing DzNP Synthesis

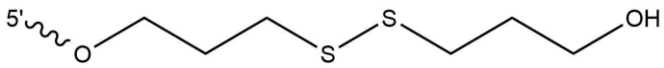

Figure 3.5. Thiol modification attached to the 3' end of the DNAzyme.

Before synthesizing an inactive DzNP, we chose to validate two approaches for synthesizing DzNPs to determine which method produced the highest density particle. The two synthetic approaches tested were salt aging[24-25] and the freezing method.[26] Literature suggests that the freezing method produces particles with higher DNA loading than the salt aging method (20-30% greater).[26] We prepared DzNPs from the DNAzyme targeting the mRNA GATA-3 known as 2251 via the salt aging method and found that there were an average of 119 $\pm$ 1 strands per particle. However, using the freezing method, we quantified 141 $\pm$ 4 strands per particle (an 18% increase). In both cases, to achieve the greatest packing density, it is critical to reduce the disulfide protecting group that is required for solid phase DNA synthesis (Fig. 3.5.). Otherwise, the number of strands per particle was reduced. For example, using Hgd40, another GATA-3 mRNA targeting DNAzyme,[27] DzNPs produced via the freezing method without reduction to remove the protecting group produced densities of 70 strands per particle. As a second check, we also measured the activity of DzNPs produced by the salt aging and freezing methods. As one might expect, 3'-thiolated

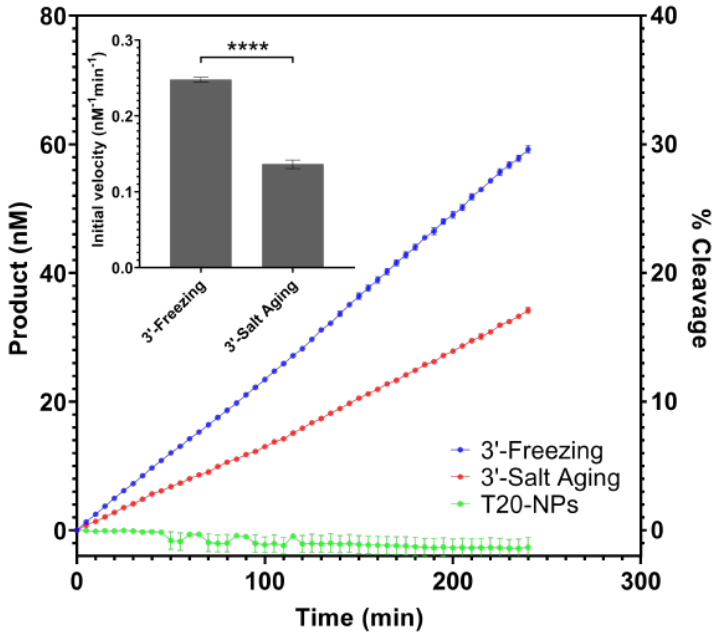

Figure 3.6. Activity of 3'-thiolated DzNPs (2251) made via the freeze method or salt method shown by cleaving a short reporter strand. Data is reported in triplicate with SEM. In some cases, error bars are too small to be seen. [100 µl of 1x PBS, 200 nM substrate, 2 mM Mg^{2+}, 0.5 nM DzNPs] Inset shows initial velocities (nM^{-1} min^{-1}) are significantly different (p = 0.0001).

and attached DzNPs produced by the freezing method exhibited higher initial velocities (p = 0.0001) and cleaved 55% more substrate in 4 h than those produced by the salt aging method (Fig. 3.6.), likely due to their higher DNA densities. Thus, to produce the core-attached DzNP, we chose the freezing method for its simplicity, as well as, for its resulting in particles with greater DNAzyme packing density.

3.3. Synthesizing Inactivated DNAzyme Nanoparticles

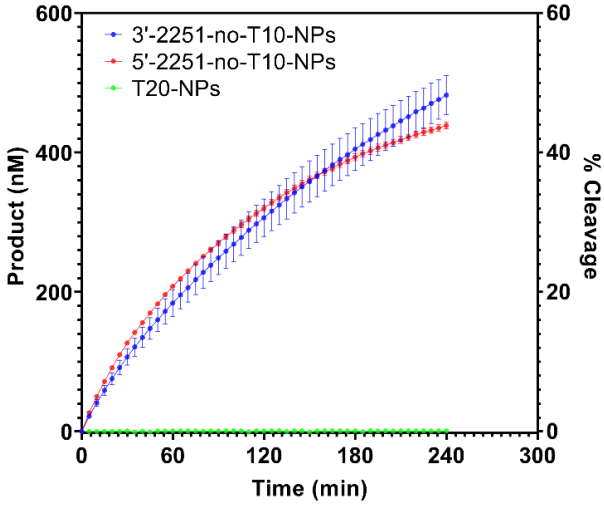

Figure. 3.7. 2251 without a T10 linker 3'-attached or 5'-attached to AuNPs still show activity under the conditions used by Yehl [100 µl of 1x PBS, 1 µM substrate 50 mM Mg^{2+}, 0.5 nM DzNP][3] Data is reported in triplicate with SEM.

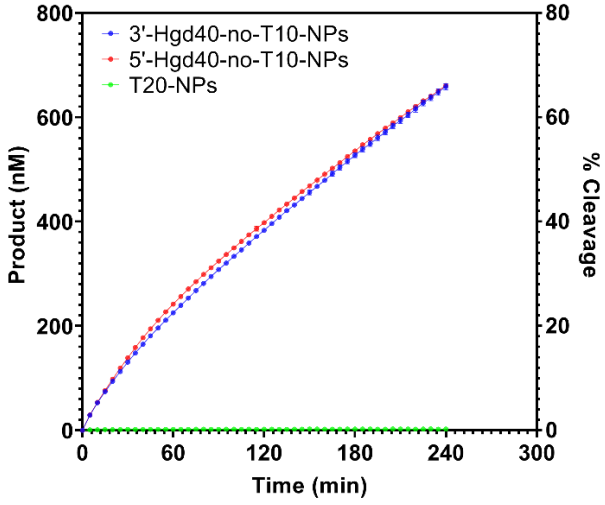

Figure 3.8. Hgd40 without a T10 linker 3'-attached or 5'-attached to AuNPs still show activity under the conditions used by Yehl [100 µl of 1x PBS, 1 µM substrate, 50 mM Mg^{2+}, 0.5 nM DzNP][3] Data is reported in triplicate with SEM.

To synthesize an inactive DNAzyme nanoparticle, we searched for DNAzymes that were inactive on the particle surface but showed a restoration in activity once detached. Yehl reported[3] that if one reversed the orientation of binding of the DNAzyme from the 3' to the 5' end on an AuNP, the DNAzyme would be entirely inactivated.[3] However, in our hands, we discovered that this property failed to hold for the 10-23 DNAzymes 2251 and Hgd40 that target the GATA-3 mRNA using different binding arms. We also tried removing the thymidine (T_{10}) linker that acts as a spacer between the AuNP surface and the DNAzymes; however, both 5'

and 3' attached 2251 and Hgd40 retained activity even without the T_{10} linkers and when reproducing the same conditions as used by Yehl and coworkers[3] (Fig. 3.7. – Fig. 3.8.). As a next step, we hypothesized that attaching the DNAzyme to the AuNP by its catalytic core would inactivate it, due to the proximity of the core residues to the gold surface. To produce core-attached DzNPs, we custom synthesized DNAzymes with an alkyne modified uracil in the middle of the catalytic core and clicked a thiolated propyl azide to it (Fig. 3.3.). Afterward, we incubated the DNAzymes with AuNPs and found they made stable DzNPs with only 40 strands per particle. The reduced density is expected, since attachment via the core will increase the oligo footprint thus reducing density on the AuNP surface. Moreover, the conformational rigidity of the surface-bound core would likely result in the reduction in activity we desired. We found that these DzNPs were indeed largely inactive (Fig. 3.9.). However, once the DNAzymes were released from the AuNP core with DTT, they re-gained their activity (Fig. 3.10.).

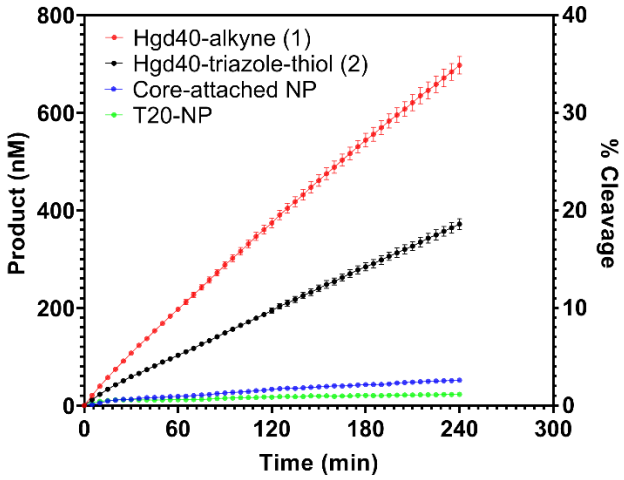

Figure 3.9. Activity assay showing product formation over time for the core-attached NP (DNAzymes attached to AuNP via catalytic core), the pre-cursor strands and a control T_{20}-NP strand as a baseline for no activity. [100 µl of 1x PBS, 2 µM substrate, 50 mM Mg^{2+}, 0.5 nM DzNP][3] Data is reported in triplicate with SEM.

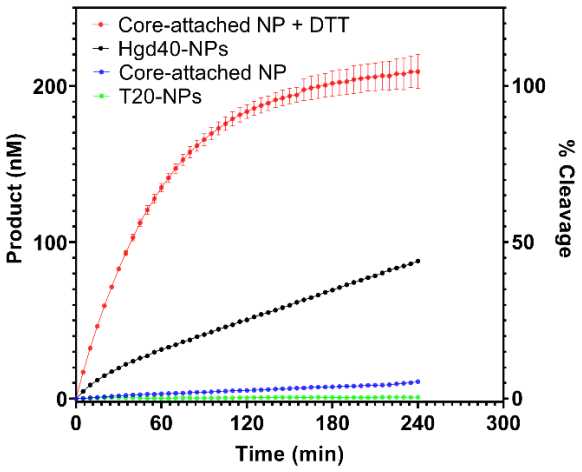

Figure 3.10. Activity assay showing inactive core-attached NP (blue) compared to core-attached-NP when strands are released with 5 mM DTT incubation (red). 3'-attached Hgd40-NPs (black) were synthesized using freeze method in a different experiment, in same conditions, shown here for comparison. [100 µl of 1x PBS, 200 nM substrate, 2 mM Mg^{2+}, 0.5 nM DzNP.] Data is reported in triplicate with SEM.

3.4. Testing Whether DzNPs Degrade mRNA While Intact

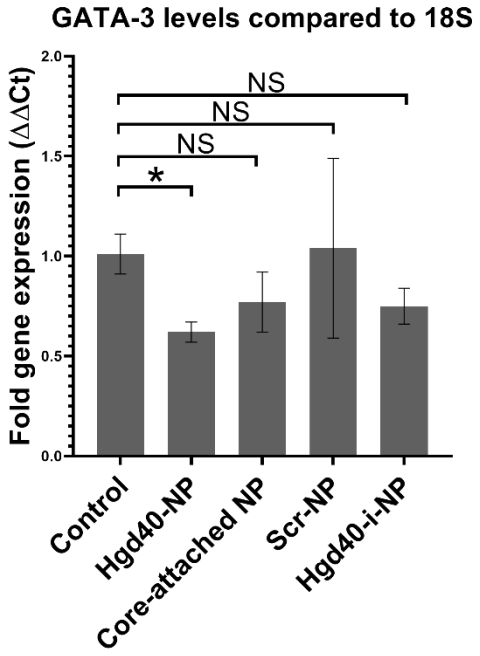

Figure 3.11. DzNP knockdown of GATA-3 in T47D cells. Control vs Hgd40-NP is significant ($p<0.05$). The other values are not significant. All DzNPs were incubated at 5 nM concentration. Hgd40-NPs had 141±4 strands per NP. Core-attached NPs had 40 strands per NP. Scr-NP refers to the HPV targeting DzNPs. Hgd40-i-NPs refers to Dz(s) with a mutation in the catalytic core making them inactive. Data is from triplicate wells, except for Scr-NP and Hgd40-i-NP which had duplicate wells.

As a preliminary test of core-attached DzNPs, we incubated the following sets of DzNPs with T47D cells, a breast cancer cell line known to highly express our target gene GATA-3[28]: Hgd40-active-DzNPs, Hgd40-inactive-DzNPs, HPV-DzNPs and Hgd40-core-attached-DzNPs (Fig. 3.11.). These particles were each made using the freezing method. The active Hgd40-DzNPs contain the active 3'-thiolated DNAzyme, with a T_{10}-linker, bound to the AuNP. The inactivated DzNPs contain a point mutation in the catalytic core that abolishes activity of the DzNP and should report on what portion of the knockdown is due to antisense. The HPV DzNP is active against HPV and not genes in mammalian cells. Thus, it acts as a non-specific control to determine what effect a DzNP itself may have inside the cell, apart from its activity. Finally, the core-attached Hgd40-DzNPs are those that had a thiolated linker clicked to the core of the DNAzyme, allowing the DNAzyme to attach to the AuNPs via the core, rather than the 3' end. In an initial experiment, 5 nM of the DzNPs were incubated with T47D cells. The cells were then harvested, and real-time PCR was performed (qPCR) on the resulting cDNA to measure fold gene expression of GATA-3 compared to 18S. Each DzNP group had three replicates, except for the non-specific HPV control and the inactivated DzNPs (Hgd40-i-NP), which had two replicates. Note that 0.5 units of 18S were used

in this experiment, to prevent spurious amplification. It was found that there was 39% knockdown in the Hgd40-NP group, not all of which could be accounted for as antisense, when compared to knockdown in the Hgd40-i-NP group which showed 26% knockdown. There was no observable knockdown for the non-specific HPV DzNPs, as would be expected, and there was 24% knockdown in the Hgd40-core-attached-DzNPs group. It is difficult to know if this observed activity is due to antisense or cleavage by the DNAzymes, as the Hgd40-core-attached-DzNPs were incubated at the same gold concentration (5 nM) as the other NPs; however, the packing density of the Hgd40 on their surface was much less: only 40 strands per particle, compared to 129 strands per particle in the active Hgd40 DzNPs attached via the 3' end. The number of strands per particle in the HPV-DzNPs and the Hgd40-i-NPs were not quantified. In any case, only the Hgd40-NP data compared to the control was found to be significant ($p<0.05$). The other data sets were not statistically significant in any of the groups, most likely due to the large error bars in the non-specific control and the fact that there were only two replicates for the non-specific and Hgd40-i-NP controls.

3.5. Proposed Experiments for Future Work

Table 3.1. Layout of Experiment

Type	Sample Name	Concentration	Cells
Control	1x PBS	NA	T47D
Active	Hdg40-NPs	5 nM	T47D
Inactive control	Hgd40-i-NPs	5 nM	T47D
Scrambled control	Scr-NPs	5 nM	T47D
Core inactivated	Click-NPs	5 nM	T47D

With the initial troubleshooting phase of this project complete, it is now ready to be taken into a more complete series of experiments to determine the levels of GATA-3 in the presence of

Hgd40-DzNPs and Hgd40-core-attached-DzNPs. Hgd40-DzNPs will be synthesized using the freezing method. Instead of an HPV sequence for a non-specific control, a scrambled sequence will be produced from the Hgd40 DNAzyme, scrambling both the binding arms and the catalytic core, to determine if these nucleotides modulate GATA-3 levels. The other groups will be kept the same (Table 1.). The DzNPs will be incubated with T47D cells at 5 nM concentration for 48 h. qPCR will be run on the resulting cDNA using 0.5 units of 18S and GATA-3. Note that 18S is one of the most stable overall housekeeping genes to use with T47D cells and GAPDH should be avoided.[28] GAPDH was shown not to be a stable housekeeping gene for ER^+ breast cancer cell lines, of which T47D is one.[28] Additionally, an experiment can be performed to control the number of strands per particle, with PEG-thiol as a backfilling molecule. We can synthesize all DzNPs with 40 strands per particle, so that the concentration of DzNP does not need to be adjusted, to account for differing DNAzyme density on the particle surface.

In addition to these groups, it will be important to analyze DzNPs synthesized with DNAzymes containing stronger binding di- and tri-thiol linkers for AuNP attachment. If we find that mono-thiol anchored DNAzymes dissemble in the cytoplasm, it is possible that di- or tri-thiol linkers could prove more stable. In addition to cell experiments, it will be important to perform several *in vitro* experiments. First, we will run a kinetic experiment with DzNPs in 5 mM glutathione in 1x PBS. This experiment will more accurately simulate the cellular environment, rather than using DTT, allowing us to reproduce what Wu, Mirkin and colleagues observed upon incubation of SNAs with glutathione for 24 h.[12] Secondly, we will perform a stability assay exposing modified DzNPs to DNase I and II, to determine if they are more nuclease resistant than unmodified DzNPs, as the SNAs Wu *et al.* tested were not modified.[12] It may be beneficial to test differently modified DzNPs to determine which modification is best able to protect against digestion, while still retaining activity of the DzNP.

3.6. Conclusion

These assays give a better picture of the mechanism of DzNPs once they escape the endosome inside cells. As it has been shown that endosomes have an oxidizing environment,[29] it is unlikely that DzNPs are being reduced off the AuNP in the endosome. However, degradation by DNase I or DNase II is always a possibility. These experiments will pave the way for a better mechanistic understanding of both DzNPs and SNAs and may lead to improved drugs and targeted strategies to approach drug release in the future.

3.7. Materials and Methods

Table 3.2. Sequences Used in this Study

Name	Sequence (5'→3')
3'-SH-Hgd40	GTGGATGGA GGCTAGCTACAACGA GTCTTGGAG TTTTTTT TTT/3ThioMC3-D/
3'-SH-2251	ATTCCTTAAAggctagctacaacgaTTCTTGGCTTTTTTTTTT/3ThioMC3-D/
5'-SH-2251	/5ThioMC6-D/TT TTT TTT TTA TTC CTT AAA GGC TAG CTA CAA CGA TTC TTG GC
2251 substrate	/56-FAM/GCCAAGAArGrUTTAAGGAAT/3IABkFQ/
Hgd40 substrate	/56-FAM/CTCCAAGACrGrUCCATCCAC/3IABkFQ/
3'-SH-T20	TTTTTTTTTTTTTTTTTTT/3ThioMC3-D/
Hgd40-alkyne	mGmUmGmGATGGA GGCTAGC/i5OctdU/ACAACGA GTCTTmGmGmAmG
5'-SH-Hgd40	/5ThioMC6-D/TT TTT TTT TTG TGG ATG GAG GCT AGC TAC AAC GAG TCT TGG AG
5'-SH-Hgd40 no T10	/5ThioMC6-D/G TGG ATG GAG GCT AGC TAC AAC GAG TCT TGG AG
3'-SH-2251 no T10	ATTCCTTAAAggctagctacaacgaTTCTTGGC/3ThioMC3-D/
5'-SH-2251 no T10	/5ThioMC6-D/A TTC CTT AAA GGC TAG CTA CAA CGA TTC TTG GC
5'-SH-2251	/5ThioMC6-D/TTTTTTTTTTA TTC CTT AAA GGC TAG CTA CAA CGA TTC TTG GC
Hgd40-i-SH	GTGGATGGA GGCTACCTACAACGA GTCTTGGAG TTTTTTT TTT/3ThioMC3-D/
Hgd40-scr	CAAGTCAGAAGTGGTCTGGTTAGAGAGCGGTCG TTTTTTTTTT/3ThioMC3-D/
HPV non-specific DNAzyme	GTT TCT CTA GGC TAG CTA CAA CGA GTG TTC TTG

3.7.1. Synthesizing 3-azidopropan-1-thiol

To a scintillation vial capped with an air tight teflon lid containing 3-Chloropropan-1-thiol (700 mg, 616 µL, 6.3 mmol) in a 2:1 mixture of EtOH and water (10 mL total), NaN3 was added (800 mg, 12.2 mmol) and the reaction was heated overnight at 110 °C. After ~24h, the reaction was removed from heat and diluted with ~ 10 mL of ether and ~10 mL of brine, and the organics were separated. The organics were dried with Na_2SO_4, filtered, and concentrated to afford a

pale, yellow oil. The desired compound was obtained in pure form as a pale, yellow oil after purification by column (flash) chromatography with 20% diethyl ether in hexanes (r_f = 0.3). Yield: 157 mg, 22% (See Chapter Appendix for NMR).

3.7.2. Clicking 3-azidopropan-1-thiol to alkyne modified Hgd40 DNAzyme

This protocol was adapted from a paper by Yehl *et al.*[30] To click the 3-azidopropan-1-thiol to alkyne modified Hgd40, the following reaction was setup in the order described: 60 µl 2M triethylammonium acetate (TEAA), 60 µl Nanopure water, 60 µl of 1 mM DNA alkyne suspended in Nanopure water, 60 µl of 5 mM fresh ascorbic acid, 330 µl dimethyl sulfoxide (DMSO), 6 µl of 3 azido-1-propanethiol (66% pure) and 24 µl Cu·TBTA. It was incubated at room temperature in the dark overnight. Later, a 1 h reaction was found to be sufficient for coupling. After coupling, the reaction was purified as follows: it was spun down at 15,000 rpm 20 min. The supernatant was removed to a 15 ml falcon tube and 250 µl 3M sodium acetate was added. The reaction was split into 25 Eppendorf tubes in 100 µl aliquots. To these, 1 mL of 100% ethanol was added to each tube and the tubes were frozen at -80ºC for 2 h. After, the tubes were spun down at 15,000 rpm for 30 min, the supernatant was removed, and each was washed with 500 µl 70% room temperature RNase free ethanol. The tubes were then spun down again at the same speed for 15 min, the supernatant was removed and speed vacced for 30 min. Each tube was then resuspended in 100 µl Ultrapure water, collecting all the tubes together. The UV-Vis absorbance at 260 nm was then taken on a Nanodrop instrument. The yield of the click reaction was found to be 57%.

3.7.3. Synthesizing DzNPs by the freeze method

To synthesize DzNPs by the freezing method, 60 nmol of each thiolated DNAzyme was reduced in 1 mM DTT in disulfide cleavage buffer (170 mM phosphate buffer (pH = 8.0)) for 2 h at room temperature in the dark. Afterward, DNAzymes were purified on a nap-25 column (GE

Healthcare) according to the manufacturer's instructions in Nanopure water. To 1 ml aliquots of AuNPs (average 8-10 nM concentration) 4 nmol of purified DNAzyme were added. The aliquots were then frozen at -20ºC 2 h and allowed to thaw at room temperature prior to use.

3.7.4. Synthesizing DzNPs by the salting method

To synthesize DzNPs by salt aging, 60 nmol thiolated DNAzyme were reduced with 1 mM DTT in disulfide cleavage buffer (170 mM phosphate buffer (pH = 8.0)) 2 hrs in the dark at room temperature. The samples were then purified on a nap-25 column (GE Healthcare) according to the manufacturer's instructions in Nanopure water. While running the column, the Eppendorf tubes used to collect the sample were weighed, the weight recorded, and the tubes were weighed again after the sample was collected. The resulting purified DNAzyme was quantified on a NanoDrop 2000c spectrophotometer. Afterward, the nmol/ul of the sample using the volume was found and 4 nmol of DNAzyme to 1 ml AuNPs (typically between 8 – 10 nM) was added and incubated in an appropriate glass vessel overnight. The next day, phosphate adjustment buffer (100 mM phosphate buffer (pH 7.0)) was added to a final phosphate concentration of 9 mM and 10% sodium dodecyl sulfate (SDS) was added to a final concentration of ~0.1% (wt/vol). After this addition, the DzNPs were incubated at room temperature on an orbital shaker 30 min. Next, salting buffer (10 mM phosphate buffer + 2 M NaCl (pH 7.0)) was added to final concentrations of NaCl (0.05, 0.1, 0.2, 0.3, 0.4, 0.5, 0.6 and 0.7 M) every 20 min with 10-15 sec of sonication. The DzNPs were then incubated overnight on an orbital shaker.

3.7.5. In vitro activity assay of the DzNPs

To perform activity assays for the DzNPs as shown, each DzNP was incubated with a short DNA/RNA hybrid that was complementary either to 2251 or Hgd40 as follows: For Hgd40, 5'-/56-FAM/CTCCAAGACrGrUCCATCCAC/3IABkFQ/-3' and for 2251, 5'-/56-FAM/GCCAAGAArGrUTTAAGGAAT/3IABkFQ/-3'. These strands have a fluorescein dye on the

5’ end (FAM) and an Iowa black quencher on the 3’ end. The respective DNAzyme can hybridize to this target and cleave it, leading to an increase in fluorescence. The conditions for each activity experiment were standardized to 100 µl of 1x PBS, 200 nM substrate, 2 mM Mg^{2+}, and 0.5 nM DzNPs. If conditions differed, they were noted in the caption of the appropriate figure. T20-NPs were used as a control inactive DzNP. If soluble strands were tested alongside the particles, T20-functionalized NPs were added at 0.5 nM concentration to the soluble strand wells, so that all wells had the same absorbance due to the particles and could be compared. Soluble strand concentration was adjusted depending on the number of strands per particle. The wells were run in triplicate and imaged on a Cytation 5 Biotek reader, using the extended gain setting. Data was averaged across the wells and the standard error of the mean calculated for each sample.

3.7.6. Standard curve for the in vitro DzNP activity assay

To produce a standard curve to calibrate the data from fluorescence over time to nM product over time, completely cleaved substrate was simulated by mixing a 5’-FAM-2251 strand and a black hole quencher™ 1 (BHQ1) strand in triplicate wells between the concentrations tested: 2 uM and 50 nM. The 5-FAM strand sequence is as follows: /56-FAM/AT TCC TTA AAG GCT AGC TAC AAC GAT TCT TGG CTT TTT TTT TT/3ThioMC3-D/. The BHQ1 strand is as follows: 5’-/5BHQ1/CGC ATC TGT GCG GTA TTT CAC TTT-3’. These strands did not have high complementarity, as measured by Integrated DNA Technology’s OligoAnalyzer tool. The strands were measured and a 100 µM and 10 µM stock of both were made. Using these stocks, the strands were added in equimolar amounts in triplicate wells in total volume of 100 µl 1x PBS, with 2 mM Mg^{2+} and 0.5 nM T20-NPs, at the following concentrations: 2 µM, 1.75 µM, 1.5 µM, 1.25 µM, 1.0 µM, 0.75 µM, 0.5 µM, 0.25 µM, 0.20 µM, 0.15 µM, 0.10 µM and 0.05 µM. The standard curve was then imaged on a Cytation 5 Biotek reader on the extended gain setting. The wells were averaged and a standard curve was produced in Excel. Note that this standard

curve is not accurate where a different concentration of DzNPs was used. To convert the fluorescence observed in my experiments to nM product, the following equation was used:

$Ft = F_0(1 – p) + Ff(p)$

Where Ft = the measured fluorescence, F_0 = the initial fluorescence measured at time 0, Ff = the maximum fluorescence when all the substrate at the concentration is cleaved (which value can be obtained from the standard curve), and p = the fraction of cleaved substrate. Solved for p then, the equation is as follows:

$p = (Ff – F_0) / (Ff – F_0)$

Using Excel, this equation was used to find the % cleavage of each dataset, from the measured fluorescence. Then, the % cleavage could be converted into nM product by multiplying by the total substrate concentration.

3.7.7. Washing of the DzNPs before incubation with cells

To prepare the DzNP samples, 1 ml aliquots were spun down at 13,000 rpm 20 min. The supernatant was removed, and the sample was resuspended in 500 µl Nanopure water and sonicated for 10 sec. The samples were then spun down at 13,000 rpm 20 min. The supernatant was removed and the sample was resuspended in 500 µl of Nanopure water. Sonication is not necessary at this point. The sample was then washed twice more. The final time, it is resuspended in the desired volume of Nanopure water, which differs depending on the number of tubes one is spinning down and combining. The UV-Vis absorption of the tubes is then measured via Nanodrop to find the final gold concentration. A one in three dilution in Nanopure water is often necessary, to prevent saturation of the Nanodrop.

3.7.8. Incubating DzNPs with T47D cells

T47D cells acquired from ATCC were grown in RPMI-1640 with 10% fetal bovine serum (FBS), 0.2 units/mL insulin and 1% pen-strep. They were split 1 to 3 every 4 to 5 d. They were counted and seeded into either a 12-well plate at 50,000 cells per well or a 6-well plate at 100,000 cells

per well, and grown at 37ºC at 5% CO_2 until 80% confluent. Afterwards, 5 nM of DzNPs were added to 3 replicate wells and allowed to incubate at 37ºC at 5% CO_2 for 48 h.

3.7.9. RNA extraction of T47D cells

Our RNA extraction protocol was adapted from the Qiagen RNeasy Mini-kit. After 48 h of incubation with the DzNPs, the media was aspirated off the cells in the 6-well plate. To each well, 700 µl of trypsin was added and incubated for 5 min at 37 ºC 5% CO_2. Afterward, 700 µl of RPMI media was added to quench the reaction. The cells were transferred to sterile 1.5 ml Eppendorf tubes and spun at 1,000 rpm 5 min. The supernatant was aspirated off and 1 ml 1x PBS was added to gently resuspend the cells. The cells were spun down once more and the supernatant was removed. While the tubes were centrifuging, we prepared 1,500 µl of RLT-plus with 15 µl of beta-mercaptoethanol (BME) added. Afterward, 300 µl of the RLT-plus / BME mixture was added to each tube of cells. The sample was homogenized with a needle 20 times. It is important to pull the syringe quickly so as to make a squeaking noise. The lysate was transferred to a DNA mini-spin column and spun at 10,000 rpm 1 min, to remove DNA and cellular debris. To the flow through, 300 µl of 70% ethanol was added and transferred to sterile, pink RNA columns. The samples were spun at 10,000 rpm 1 min and the flow through was discarded. Afterward, 700 µl of RW1 buffer was pipetted onto the column and centrifuged as previously, discarding the flow through. Then, 500 µl of RPE buffer was added to each tube and centrifuged, discarding the flow through. This step was repeated. The column was removed from the tube and added to a new collection tube, spinning at 10,000 rpm 1 min empty, to remove residual traces of wash buffer. The column was then added to a sterile tube and 30 µl of RNase free water was applied directly to the center of the column and incubated 1 min. The tubes were spun at 10,000 rpm 1 min and Nanodropped. They could then be stored at -20ºC for short periods or at -80ºC until needed, if storing longer than 1 week.

3.7.10. Synthesis of cDNA from T47D cell total RNA

The protocol for this reaction was modified from Biorad's iScript cDNA synthesis kit (catalog number #1708891). If not previously done, the RNA is first Nanodropped to determine its concentration. Afterward, add 1 µg RNA, 4 µl iScript, 1 µl reverse transcriptase and Nanopure water up to 20 µl. Be sure to add the Nanopure water first. Incubate the cDNA reaction in a thermocycler at 25ºC 5 min, 46ºC 20 min, 95ºC 1 min and 4ºC 60 min or until removal from the instrument. Store at -20ºC.

3.7.11. Taqman probe qPCR

For each qPCR 20 µl reaction, 6 µl of Nanopure water, 1 µl of GATA3 Taqman primer, 1 µl 18S Taqman primer and 10 µl of Master Mix was added. Each of these components is multiplied by the number of samples and done in triplicate for each sample. After a master mix containing all the components is mixed, it is aliquoted into a 365-well plate and 2 µl of cDNA are added afterward to each well. Wells without cDNA and master mix only with and without primers are used as negative controls.

3.8. Appendix

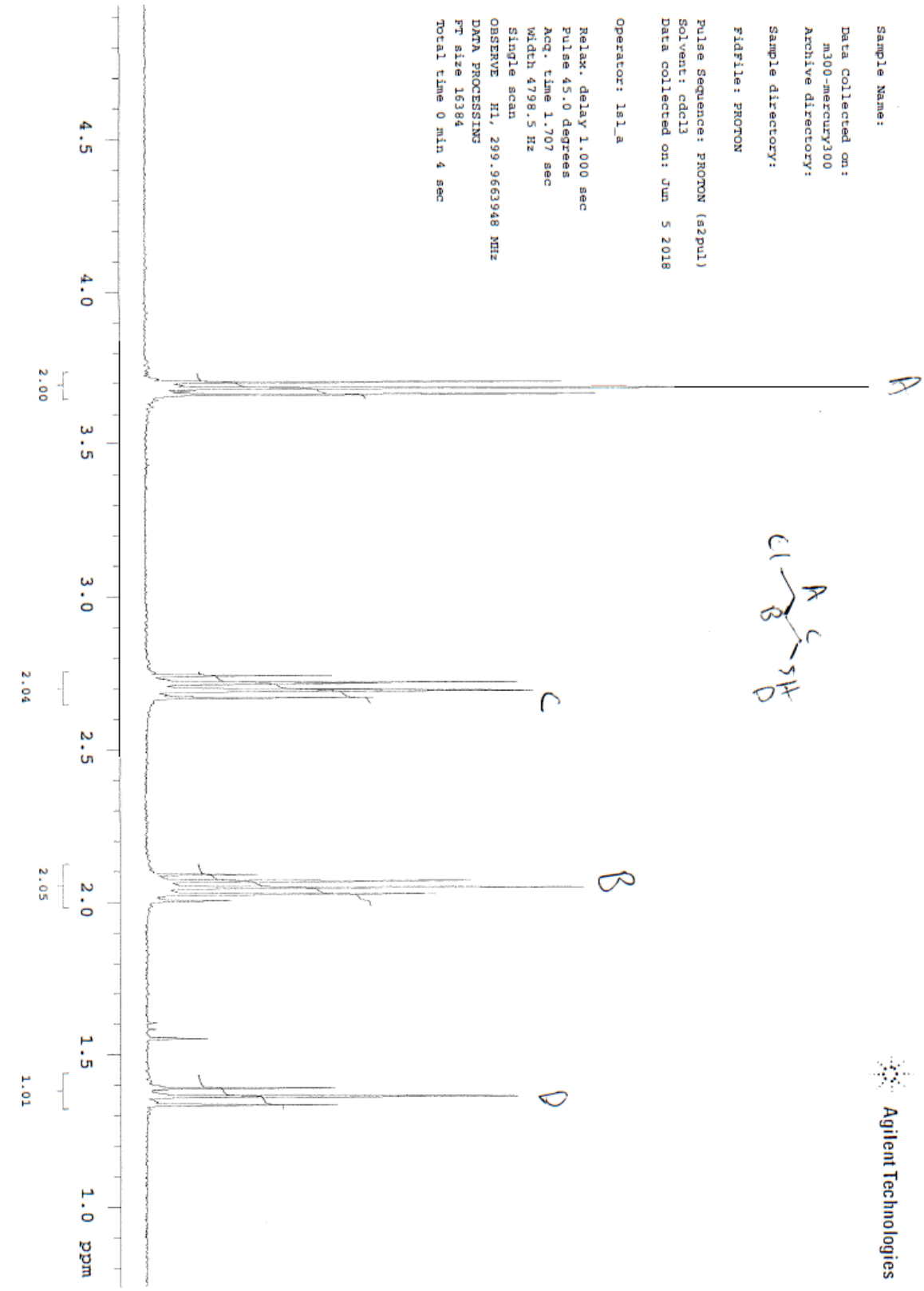
Sample Name:
Data Collected on:
m300-mercury300
Archive directory:
Sample directory:
FidFile: PROTON
Pulse Sequence: PROTON (s2pul)
Solvent: cdcl3
Data collected on: Jun 5 2018
Operator: lsl_a
Relax. delay 1.000 sec
Pulse 45.0 degrees
Acq. time 1.707 sec
Width 4798.5 Hz
Single scan
OBSERVE H1, 299.9663948 MHz
DATA PROCESSING
FT size 16384
Total time 0 min 4 sec
A
B
C
D
Cl
A
C
B
H
D
4.5
4.0
3.5
3.0
2.5
2.0
1.5
1.0 ppm
2.00
2.04
2.05
1.01
Agilent Technologies

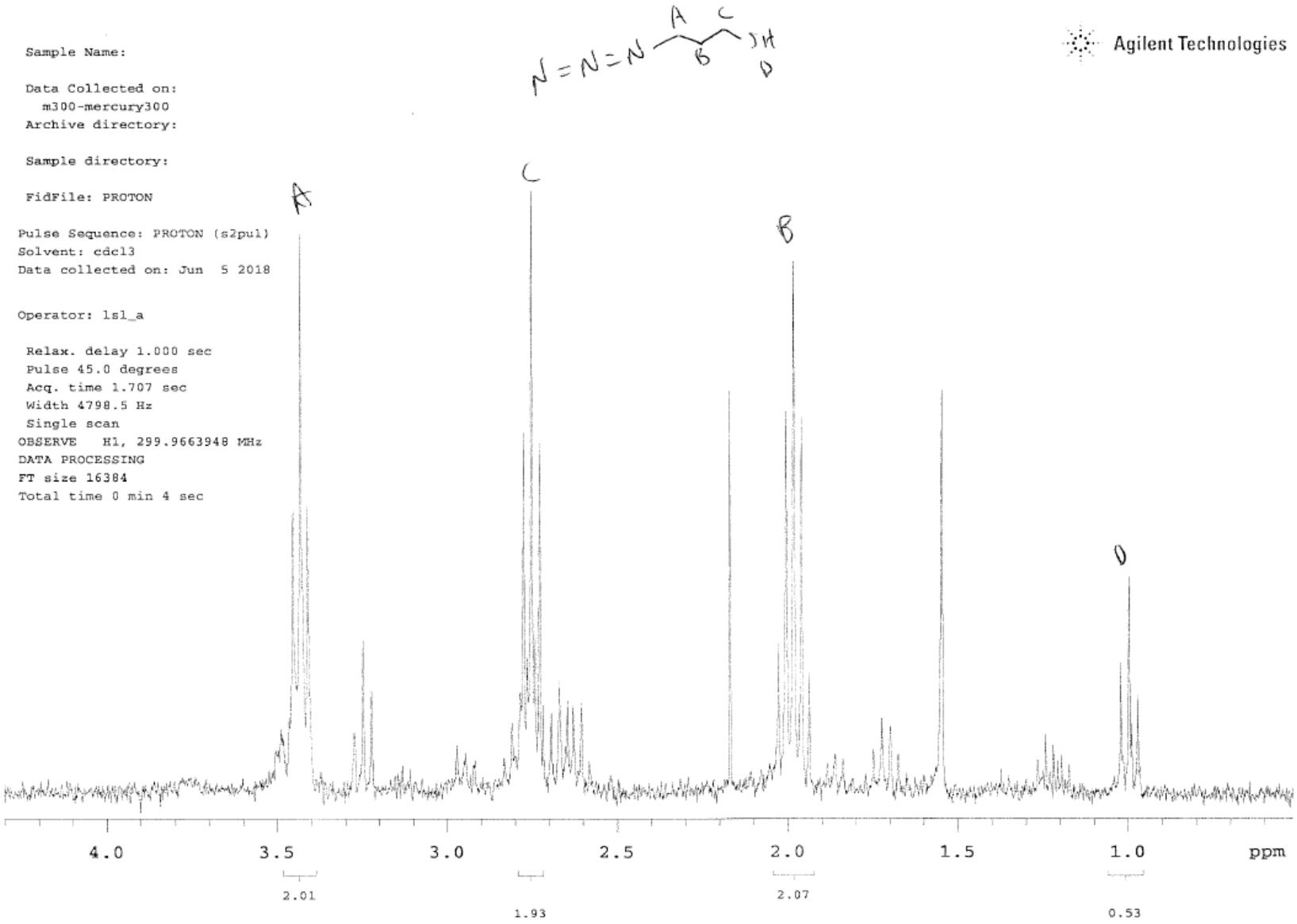
Sample Name:
Data Collected on:
m300-mercury300
Archive directory:
Sample directory:
FidFile: PROTON
Pulse Sequence: PROTON (s2pul)
Solvent: cdcl3
Data collected on: Jun 5 2018
Operator: lsl_a
Relax. delay 1.000 sec
Pulse 45.0 degrees
Acq. time 1.707 sec
Width 4798.5 Hz
Single scan
OBSERVE H1, 299.9663948 MHz
DATA PROCESSING
FT size 16384
Total time 0 min 4 sec
A
C
B
D
4.0
3.5
3.0
2.5
2.0
1.5
1.0
ppm
2.01
1.93
2.07
0.53

3.9. References

1. Niazov, T.; Pavlov, V.; Xiao, Y.; Gill, R.; Willner, I., DNAzyme-Functionalized Au Nanoparticles for the Amplified Detection of DNA or Telomerase Activity. *Nano letters* **2004,** *4* (9), 1683-1687.
2. Yin, B. C.; Zuo, P.; Huo, H.; Zhong, X.; Ye, B. C., DNAzyme self-assembled gold nanoparticles for determination of metal ions using fluorescence anisotropy assay. *Anal Biochem* **2010,** *401* (1), 47-52.
3. Yehl, K.; Joshi, J. P.; Greene, B. L.; Dyer, B.; Nahta, R.; Salaita, K., Catalytic deoxyribozyme-modified nanoparticles for RNAi-independent gene regulation. *ACS nano* **2012,** *6* (10), 9150–9157.
4. Somasuntharam, I.; Yehl, K.; Carroll, S. L.; Maxwell, J. T.; Martinez, M. D.; Che, P. L.; Brown, M. E.; Salaita, K.; Davis, M. E., Knockdown of TNF-alpha by DNAzyme gold nanoparticles as an anti-inflammatory therapy for myocardial infarction. *Biomaterials* **2016,** *83*, 12-22.
5. Zagorovsky, K.; Chan, W. C. W., A Plasmonic DNAzyme Strategy for Point-of-Care Genetic Detection of Infectious Pathogens. *Angewandte Chemie* **2013,** *52*, 3168 –3171.
6. Wu, P.; Hwang, K.; Lan, T.; Lu, Y., A DNAzyme-gold nanoparticle probe for uranyl ion in living cells. *J Am Chem Soc* **2013,** *135* (14), 5254-7.
7. Yang, Y.; Huang, J.; Yang, X.; He, X.; Quan, K.; Xie, N.; Ou, M.; Wang, K., Gold Nanoparticle Based Hairpin-Locked-DNAzyme Probe for Amplified miRNA Imaging in Living Cells. *Anal Chem* **2017,** *89* (11), 5850-5856.
8. Wu, Y.; Huang, J.; Yang, X.; Yang, Y.; Quan, K.; Xie, N.; Li, J.; Ma, C.; Wang, K., Gold Nanoparticle Loaded Split-DNAzyme Probe for Amplified miRNA Detection in Living Cells. *Anal Chem* **2017,** *89* (16), 8377-8383.

9. Massich, M. D.; Giljohann, D. A.; Schmucker, A. L.; Patel, P. C.; Mirkin, C. A., Cellular response of polyvalent oligonucleotide-gold nanoparticle conjugates. *ACS Nano* **2010,** *4* (10), 5641-6.

10. Patel, P. C.; Giljohann, D. A.; Daniel, W. L.; Zheng, D.; Prigodich, A. E.; Mirkin, C. A., Scavenger receptors mediate cellular uptake of polyvalent oligonucleotide-functionalized gold nanoparticles. *Bioconjug Chem* **2010,** *21* (12), 2250-6.

11. Choi, C. H.; Hao, L.; Narayan, S. P.; Auyeung, E.; Mirkin, C. A., Mechanism for the endocytosis of spherical nucleic acid nanoparticle conjugates. *Proc Natl Acad Sci U S A* **2013,** *110* (19), 7625-30.

12. Wu, X. A.; Choi, C. H.; Zhang, C.; Hao, L.; Mirkin, C. A., Intracellular fate of spherical nucleic acid nanoparticle conjugates. *J Am Chem Soc* **2014,** *136* (21), 7726-33.

13. Narayan, S. P.; Choi, C. H.; Hao, L.; Calabrese, C. M.; Auyeung, E.; Zhang, C.; Goor, O. J.; Mirkin, C. A., The Sequence-Specific Cellular Uptake of Spherical Nucleic Acid Nanoparticle Conjugates. *Small* **2015,** *11* (33), 4173-82.

14. Giljohann, D. A.; Seferos, D. S.; Patel, P. C.; Millstone, J. E.; Rosi, N. L.; Mirkin, C. A., Oligonucleotide Loading Determines Cellular Uptake of DNA-Modified Gold Nanoparticles. *Nano letters* **2007,** *7* (12), 3818-3821.

15. Zhu, Z. J.; Ghosh, P. S.; Miranda, O. R.; Vachet, R. W.; Rotello, V. M., Multiplexed screening of cellular uptake of gold nanoparticles using laser desorption/ionization mass spectrometry. *JACS* **2008,** *130* (43), 14139-14143.

16. Mason, D.; Carolan, G.; Held, M.; Comenge, o.; Cowman, S.; Levy, R., The Spherical Nucleic Acids mRNA Detection Paradox. *ScienceOpen Research* **2016**.

17. Seferos, D. S.; Giljohann, D. A.; Hill, H. D.; Prigodich, A. E.; Mirkin, C. A., Nano-Flares, Probes for Transfection and mRNA Detection in Living Cells. *JACS Communications* **2007,** *129* (50), 15477–15479.

18. Briley, W. E.; Bondy, M. H.; Randeria, P. S.; Dupper, T. J.; Mirkin, C. A., Quantification and real-time tracking of RNA in live cells using Sticky-flares. *Proc Natl Acad Sci U S A* **2015,** *112* (31), 9591-5.

19. Czarnek, M.; Bereta, J., SmartFlares fail to reflect their target transcripts levels. *Sci Rep* **2017,** *7* (1), 11682.

20. Rosi, N. L.; Giljohann, D. A.; Thaxton, C. S.; Lytton-Jean, A. K.; Han, M. S.; Mirkin, C. A., Oligonucleotide-modified gold nanoparticles for intracellular gene regulation. *Science* **2006,** *312* (5776), 1027-30.

21. Lee, K.; Conboy, M.; Park, H. M.; Jiang, F.; Kim, H. J.; Dewitt, M. A.; Mackley, V. A.; Chang, K.; Rao, A.; Skinner, C.; Shobha, T.; Mehdipour, M.; Liu, H.; Huang, W. C.; Lan, F.; Bray, N. L.; Li, S.; Corn, J. E.; Kataoka, K.; Doudna, J. A.; Conboy, I.; Murthy, N., Nanoparticle delivery of Cas9 ribonucleoprotein and donor DNA in vivo induces homology-directed DNA repair. *Nat Biomed Eng* **2017,** *1*, 889-901.

22. Ding, Y.; Jiang, Z.; Saha, K.; Kim, C. S.; Kim, S. T.; Landis, R. F.; Rotello, V. M., Gold nanoparticles for nucleic acid delivery. *Molecular therapy : the journal of the American Society of Gene Therapy* **2014,** *22* (6), 1075-1083.

23. Zaborowska, Z.; Furste, J. P.; Erdmann, V. A.; Kurreck, J., Sequence requirements in the catalytic core of the "10-23" DNA enzyme. *J Biol Chem* **2002,** *277* (43), 40617-22.

24. Hurst, S. J.; Lytton-Jean, A. K.; Mirkin, C. A., Maximizing DNA Loading on a Range of Gold Nanoparticle Sizes. *Anal Chem* **2006,** *78* (1), 8313-8318.

25. Hill, H. D.; Mirkin, C. A., The bio-barcode assay for the detection of protein and nucleic acid targets using DTT-induced ligand exchange. *Nat Protoc* **2006,** *1* (1), 324-36.

26. Liu, B.; Liu, J., Freezing Directed Construction of Bio/Nano Interfaces: Reagentless Conjugation, Denser Spherical Nucleic Acids, and Better Nanoflares. *Journal of the American Chemical Society* **2017,** *139* (28), 9471-9474.

27. Krug, N.; Hohlfeld, J. M.; Kirsten, A. M.; Kornmann, O.; Beeh, K. M.; Kappeler, D.; Korn, S.; Ignatenko, S.; Timmer, W.; Rogon, C.; Zeitvogel, J.; Zhang, N.; Bille, J.; Homburg, U.; Turowska, A.; Bachert, C.; Werfel, T.; Buhl, R.; Renz, J.; Garn, H.; Renz, H., Allergen-induced asthmatic responses modified by a GATA3-specific DNAzyme. *N Engl J Med* **2015,** *372* (21), 1987-95.

28. Liu, L.-L.; Zhao, H.; Ma, T.-F.; Ge, F.; Chen, C.-S.; Zhang, Y.-P., Identification of Valid Reference Genes for the Normalization of RT-qPCR Expression Studies in Human Breast Cancer Cell Lines Treated with and without Transient Transfection. *PloS one* **2015**, 1-15.

29. Austin, C. D. W., Xiaohui; Gazzard, Lewis; Nelson, Christopher; Scheller, Richard H.; and Scales, Suzie J., Oxidizing potential of endosomes and lysosomes limits intracellular cleavage of disulfide-based antibody–drug conjugates. *PNAS* **2005,** *102* (50), 17987-17992.

30. Yehl, K.; Mugler, A.; Vivek, S.; Liu, Y.; Zhang, Y.; Fan, M.; Weeks, E. R.; Salaita, K., High-speed DNA-based rolling motors powered by RNase H. *Nat Nanotechnol* **2016,** *11* (2), 184-90.

Chapter 4: Deoxyribozyme-Mediated Knockdown of GATA-3

Contributions: Aaron Blanchard coded an algorithm for locating DNAzyme binding sites in GATA-3.

4.1. Introduction

Asthma is defined as an allergic inflammatory disease of the lung airways, with three primary signs: inflammation, bronchial hyperresponsiveness and reversible obstruction of the lower respiratory tract.[1-2] While asthma has typically been characterized by bronchial hyperresponsiveness, the key aspect is inflammation.[2] This observation is validated by the fact that the severity of asthma is correlated to the degree of inflammation.[2-4] In years prior, mast cells and eosinophils were thought to be the key players in modulating asthma, but later the tide began to shift, instead implicating CD4+ T helper cells, especially Th2 cells.[2] Th2 cells secrete cytokines such as IL-3, 4, 5, 10 and 13 that control the activity of other cell types such as mast cells, eosinophils and basophils.[2, 5-8] Additionally, CD4+ T cells have been found in bronchoalveolar lavage (BAL) fluid from asthmatics, as well as in lung biopsies.[2-4, 9-10] Targeting CD4+ T cells has been shown to decrease the number of eosinophils recruited to inflamed tissue.[2, 11] Other evidence pointing to Th2 cells has been found in that IL-5 knockout mice or those treated with IL-5 antibodies show dampening of allergen induced asthma and airway hyperresponsiveness.[2, 11] Thus, it appears that decreasing Th2 cytokine production, as well as decreasing IgE levels and increasing Th1 production (based on other data) may help abrogate and treat asthma.[2, 12] Th2-positive asthma constitutes 50% of all patients with asthma, while the other 50% have asthma whose source has not yet been well-characterized.[13] Rather than targeting these cytokines individually, researchers began targeting factors upstream of these cytokines, to stop them at their source. In the case of Th2 mediated cytokines, that means targeting the transcription factor GATA-3, as GATA-3 was shown to be sufficient for Th2 cytokine expression in both humans and murine models.[13-15] GATA-3 is one of several transcription factors that bind to the sequence ‘GATA’ in the promotor regions of target genes

and are involved in a large array of signaling processes in different cell types.[13, 16] GATA-3 itself is a C4 zinc finger protein that is expressed in T cells, mast cells, eosinophils, basophils, and embryonic brain and kidney.[1] It can be found expressed in Th2 cells but not Th1 cells[1] and has been called the 'master regulator' or 'master transcription factor' regulating Th2 cell differentiation.[17] Furthermore, GATA-3 was found to be over-expressed in asthma patients, making it a prominent target for knockdown and to decrease Th2 cytokine production.[13] However, the type of treatment that should target GATA-3 was not at first self-evident. Many common treatments were not able to reach the target intracellularly or failed at specificity. For instance, monoclonal antibodies do not readily enter cells.[13] Small molecule inhibitors failed as therapeutics because they were not selective enough between the different GATA-3 family members.[13] Thus, antisense technology came to the fore, as both highly selective and having made headway toward clinical application.[13, 18] The first use, to our knowledge, of antisense against the GATA-3 pathway came with the work of Finotto and coworkers, who explored the effects of a phosphorothioate antisense oligonucleotide in a mouse model of asthma.[1] These mice were sensitized to ovalbumin (OVA) and

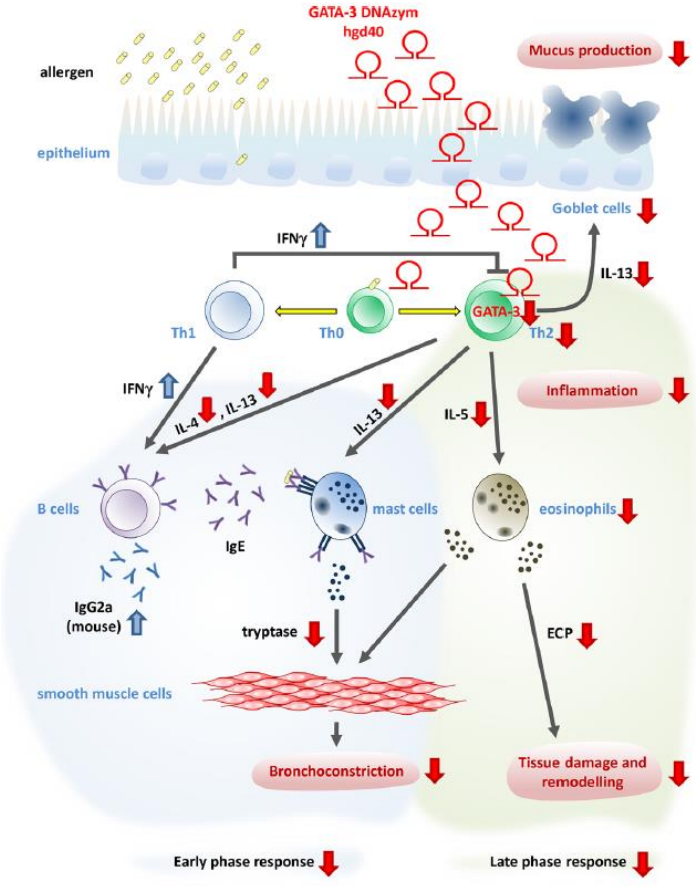

Figure 4.1. The Hgd40 DNAzyme inhibits GATA-3, downregulating a variety of pathways inside the cell, leading to lower levels of inflammation in the lung. Adapted by permission from John Wiley and Sons: Wiley Online Library, European Journal of Immunology, from reference 13, Copyright (2017).[13]

labeled antisense oligonucleotides targeting GATA-3 were given to them intranasally.[1] Finotto found that eosinophil counts in the BAL fluid were decreased, as were Th2 cytokine concentrations.[1] Inflammation in the airways went down and airway hyperresponsiveness decreased to levels similar to the saline control mice.[1] In another key paper, Sel and colleagues examined different types of antisense technology – DNA, siRNA and DNAzymes – against GATA-3.[19] All reduced inflammation, confirming the importance of GATA-3 as a drug target; however, the best results were obtained with DNAzymes.[19] They announced two DNAzymes in particular – gd21 and hgd40 – as the best of 70 tested against the target in a large multiplex assay (Fig. 4.1.).[19] There were some concerns, since DNAzymes have a CpG motif in their catalytic core, that they could trigger inflammation through activating the toll-like receptor 9 (TLR9) signaling pathway.[13, 20] When DNAzymes were tested for activation of the innate immune system, no activation or inflammation was detected, when measured in mast cells, basophils, neutrophils, dendritic cells and human and mouse macrophages.[13, 21] The safety of Hgd40 was then tested in mice, rats and dogs, finding it to be well-tolerated by inhalation and intravenously.[22] Hgd40 went on to phase I[23] and phase II[24] clinical trials in human asthma patients.[13] In the phase II trial, Hgd40 – referred to as the drug SB010 – was able to show efficacy, lowering the late asthmatic response (LAR) by 34% and the early asthmatic response (EAR) by 11% compared to controls.[24] These results speak well for this DNAzyme in continued therapy and for other drugs targeting GATA-3.

4.2. In Vitro Activity of GATA-3 Targeted DzNPs

For the purposes of this work, we were interested in finding a DNAzyme that was more potent against GATA-3 than the previously published DNAzyme Hgd40 (also called SB010).[24] As mentioned above, Sel and colleagues analyzed 70 DNAzymes active against GATA-3 using a multiplex cleavage assay and found that Hgd40 and another DNAzyme named gd21 were the most highly active.[19] Hgd40 went on to be tested in a phase 2 trial to determine its efficacy in asthmatic patients.[24] However, these studies did not employ computer modeling when conducting their DNAzyme screen. Therefore, our lab tackled this problem with custom software coded by Blanchard in our lab. This code looks for possible DNAzyme binding sites in a target RNA transcript, and attempts to find and exclude areas on the mRNA where there is a high degree of secondary structure. The code specifically seeks AU/GU junctions and optimizes the DNAzyme arms to bind with a ΔG of -9 kcal/mol. Using this code, Blanchard identified 50 potential DNAzyme binding sites in GATA-3. Note that the code searched for DNAzymes that could bind both the human and mouse GATA-3 transcripts. We screened these hits in T47D cells, known to highly express GATA-3.[25] This work was largely conducted

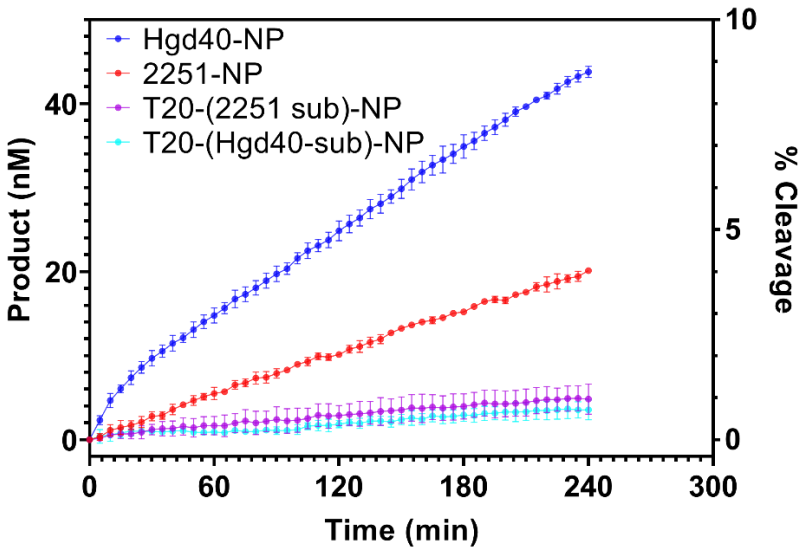

Figure 4.2. Compared to control inactive T20-NP strands, 2251-DzNPs show less activity than Hgd40-DzNPs *in vitro*. [500 nM substrate, 2 mM Mg^{2+}, 1 nM DzNPs, 1x PBS, room temperature (RT)] Note that nM product and % cleavage may be an underestimate, since standard curve used to calibrate this data was performed with 0.5 nM DzNPs, rather than 1 nM DzNPs. Initial velocities were taken by measuring slope of the first 15 min of the reaction. Error bars represent SEM of triplicate wells.

by Galior, Blanchard, Baker and Deal. They found that the DNAzyme known as 2251 had greater activity in T47D cells than did the previously published Hgd40 DNAzyme (data not shown). The goal of this work was to validate the 2251 DNAzyme activity *in vitro.* Afterward, we could move forward with *in vivo* asthma model tests of 2251-DzNPs in mice. To test *in vitro* particle activity, we used a fluorophore/quencher paired substrate that could be cleaved by the DNAzyme, leading to an increase in fluorescence upon cleavage. Interestingly, the *in vitro* results suggested that Hgd40 was faster than 2251, conflicting with the results in the cell studies (v_0 = 0.409 and 0.101 nM^{-1} min^{-1}, respectively, p = 0.0013) (Fig. 4.2.). However, there are several possible reasons for this difference. The DNA density for each DNAzyme was not measured for these batches of NPs, and if they are unequal, it could explain the different velocities. A second explanation is that possibly the 2251-DzNPs are better at endosomal escape, leading them to be more highly active inside the cell than they are in a simple *in vitro* test. Furthermore, it is possible that the Hgd40 sequence is less stable inside the cell than the 2251 sequence. More experiments will need to be conducted to confirm which of these hypotheses is valid.

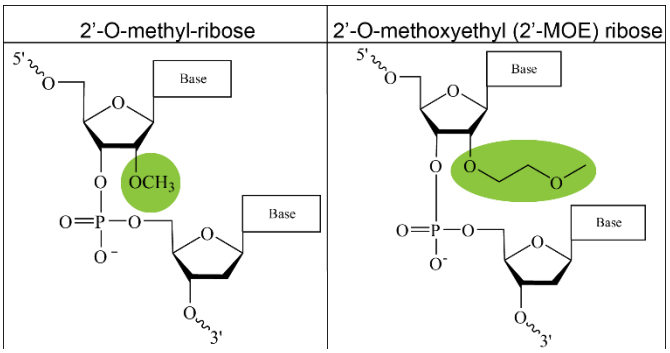

Figure 4.3. Some common modifications to increase nuclease resistance: 2'-O-methyl (left, in green), 2'-O-methoxyethyl (2'-MOE) (right, green).

In addition to comparing the 2251-DzNPs to the Hgd40-DzNPs, we performed experiments to characterize which 2251 DNAzyme modifications to increase nuclease resistance would retain the greatest activity of the DNAzyme *in vitro.* This experiment verified that the modification to the DNAzyme did not interfere with its activity in any way. The modifications tested included the 2'-O-methyl modification, four modifications on each terminus of the DNAzyme, as well as the 2'-O-methoxyethyl bases (2'-MOE) (Fig. 4.3.).

(A) 2251 sequence

5'-**AT**TCCTTAAA *GGCTAGCTACAACGA* TTCTTG**GC** TTTTTTTTTT/3ThioMC3-D/-3'

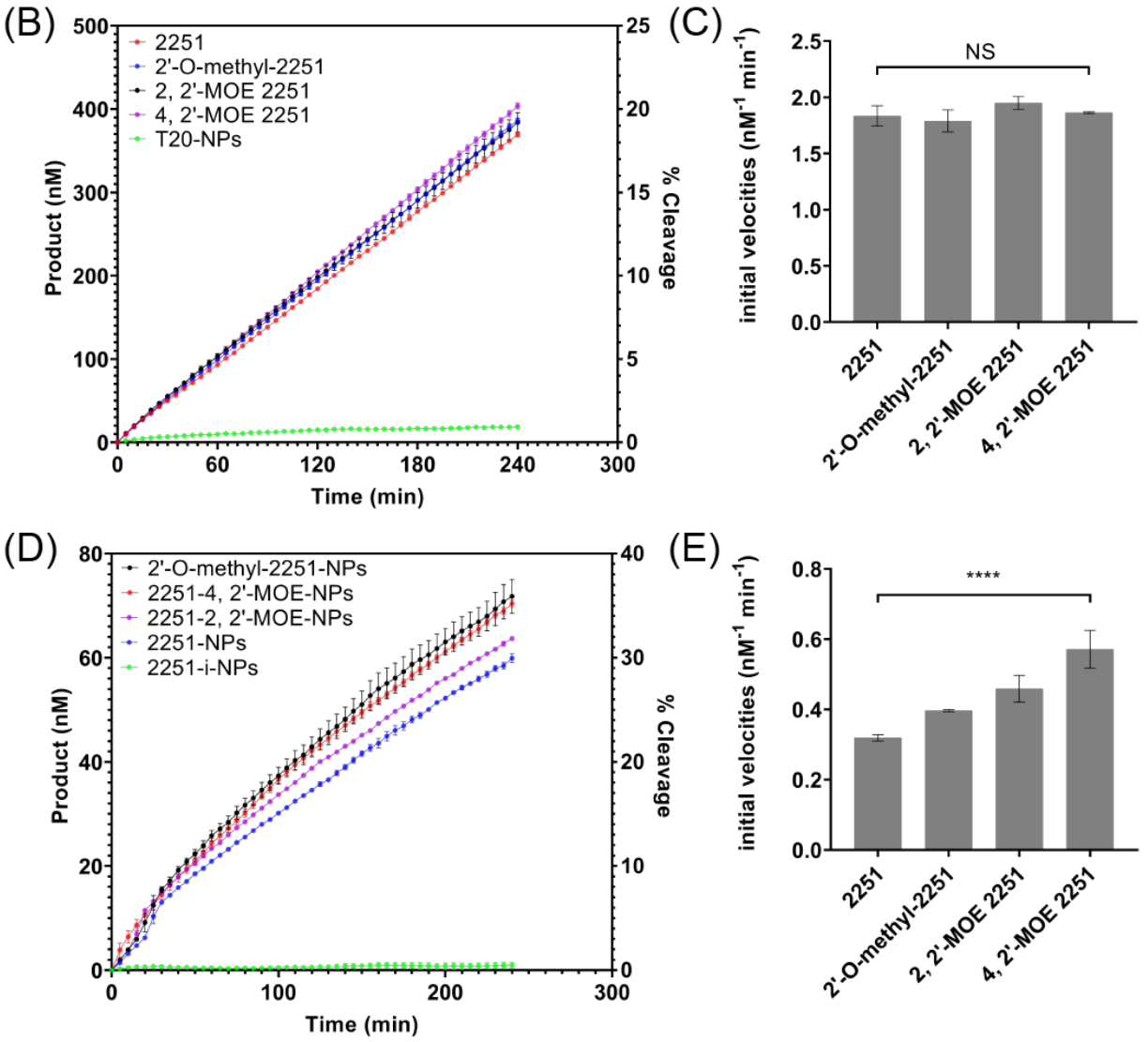

Figure 4.4. Kinetics of modified 2251 on and off AuNPs. (A) Sequence of the 2251 DNAzyme. Catalytic core is italicized in red. Bolding indicates placement of the two 2'-O-methoxyethyl modifications. Underlining indicates placement of either four 2'-O-methyl or four 2'-methoxyethyl modifications. (B) Differently modified soluble 2251 activity were tested. (C) Initial velocities were not significant. Reaction conditions: 2 µM substrate, 2 mM Mg^{2+}, 60 nM soluble Dz(s), 100 µl 1x PBS at RT. (D-E) When 2251 DNAzymes were attached to AuNPs, activity indicated that four 2'-MOE 2251 had greatest initial velocity. One-way ANOVA indicated significance ($p<0.0001$). Reaction conditions: 200 nM substrate, 2 mM Mg^{2+}, 0.5 nM DzNPs, 1x PBS at RT. In these tests (B-E), error bars represent SEM of triplicate wells. Initial velocities were found by taking the slope of the first 15 min of the reaction.

Either two or four of the 2'-O-methoxyethyl modifications were tested on the DNAzyme ends. Interestingly, results differed depending on whether the modified DNAzyme activity was measured on or off gold nanoparticles (AuNPs) (Fig. 4.4.). When the DNAzyme activities are measured off the AuNPs, there is no significant difference between their initial velocities (Fig. 4.4B-C.). However, when the DNAzymes are attached to AuNPs, their initial velocities are significantly different ($p < 0.05$) (Fig 4.4D-E.). The only exception is 2'-O-methyl 2251-NPs which are not significantly different from the 2251-NPs with two 2'-MOE modifications. The fastest initial velocity measured was for the four 2'-MOE modifications ($p < 0.05$) (Fig. 4.4E.). Unfortunately, when samples are measured, there is a 2 min delay on average in the first reading due to the addition of the metal ion Mg^{2+}. Therefore, there is a lag time before sample fluorescence can be measured in which the DNAzymes have started cleaving their substrate. In the future, to offset this effect, a plate reader with a mixing function could be used that automatically adds and mixes the metal ion. Regardless, the data suggest that in future the four 2'-MOE modifications should be used in further *in vitro* studies, as they led to the highest initial velocities.

4.3. Characterization of GATA-3 2251 DzNPs

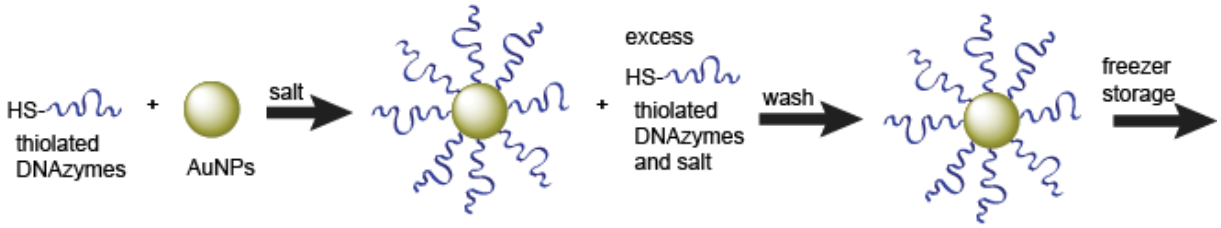

Figure 4.5. DzNPs are synthesized, stored in excess salt and thiolated DNAzyme and washed before use. We wanted to test the stability of the DzNPs if they were frozen and stored after the wash step.

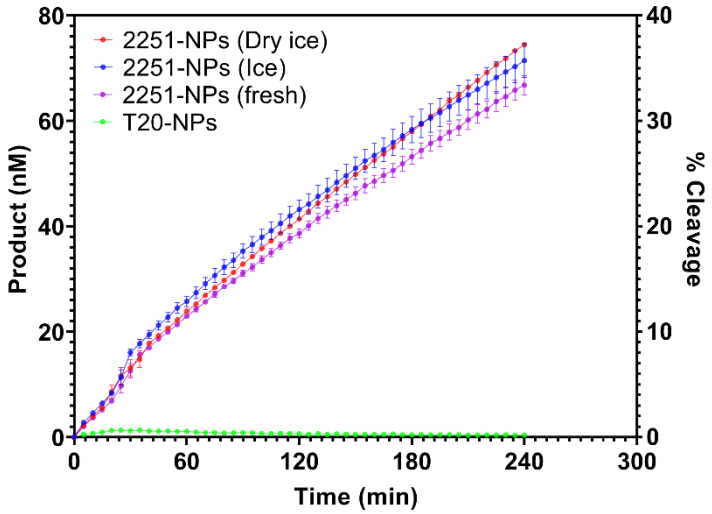

Figure 4.6. Activity of 2251-DzNPs after washing, freezing and storage four days. Washed DzNPs were stored on ice or dry ice and compared to freshly washed 2251 DzNPs. [100 µl of 1x PBS, 200 nM substrate, 2 mM Mg^{2+}, 0.5 nM DzNPs, RT] Data reported in triplicate with SEM. Initial velocities in first 15 min for dry ice, ice and fresh 2251-NPs were 0.3739, 0.4231, and 0.3458 nM^{-1} min^{-1}, respectively. Only ice and fresh 2251-NPs were significantly different ($p < 0.05$).

To better understand, characterize and extend the stability of 2251-DzNPs, we assayed whether they could be frozen after the washing step (Fig. 4.5.). The washing step removes the excess salt and DNAzymes (in the case of salt aged particles) or excess DNAzymes alone (in the case of DzNPs made by the freezing method). Being able to freeze the DzNPs after the wash step would increase their utility, as it would allow particles to be thawed and used immediately. To answer this question, we washed 2251 DzNPs and retained them in storage for four days on either ice or dry ice. We then compared them to DzNPs that had been freshly washed (Fig. 4.6.). We found that both sets of DzNPs, either on ice or dry ice, retained their activity. Thus, freezing the DzNPs after washing them does not lead to aggregation. However, we did find that in storage DzNPs could stick to the

sides of the Eppendorf tube leading to an apparent drop in concentration. To solve this problem and re-solubilize the DzNPs, we tried sonication, vortexing or both techniques. Sonicating 10-15 sec had the best result at resuspending the particles overall; although, some of the particles resuspended by simple vortexing and others did not respond to either method (data not shown). Regardless, sonicating the DzNPs for a short time after storage will likely improve their overall yield and is highly recommended.

Secondly, to further characterize the 2251-DzNPs, we also assayed how long they retain their activity over time. Hill and Mirkin suggested that traditional SNAs could be stable over a period of one month in excess salt and DNA.[26] Additionally, Somasuntharam *et al.* tested DzNP stability after washing the DzNPs in Nanopure water and found that they decreased in activity about 1.5% per day.[27] Bhatt and coworkers analyzed SNA stability after washing;[28] however, only Hill and Mirkin[26] addressed storage conditions before washing, when SNAs were kept in excess DNA.

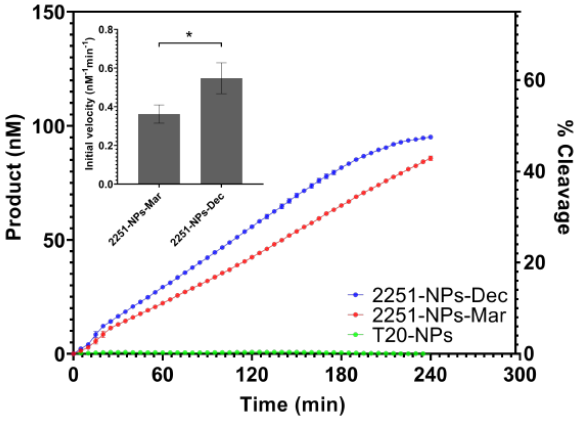

Figure 4.7. Activity of 2251-DzNP tested 3 months apart. Reaction conditions: 100 µl of 1x PBS, 200 nM substrate, 2 mM Mg^{2+}, 0.5 nM DzNPs, RT. Data is reported in triplicate with SEM. Inset shows initial velocities ($nM^{-1}min^{-1}$) taken by finding slope of first 15 min of reaction. DzNPs (3 mo old) are significantly faster (p = 0.0360).

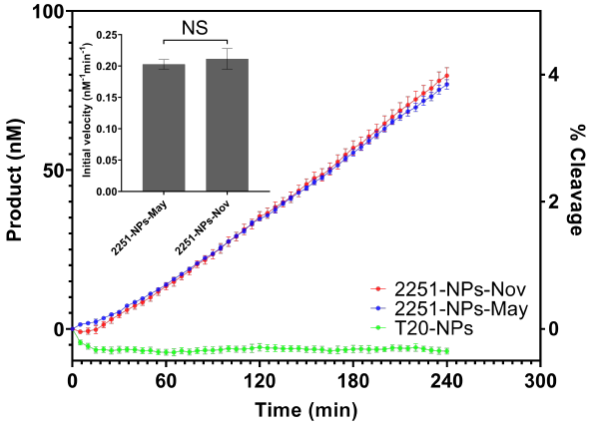

Figure 4.8. Activity of 2251-DzNPs tested 6 months apart. Reaction conditions: 100 µl of 1x PBS, 2 µM substrate, 2 mM Mg^{2+}, 0.5 nM DzNPs, RT. Data is reported in triplicate with SEM. Inset shows initial velocities ($nM^{-1}min^{-1}$) taken by finding the slope of the first 40 min of the reaction. DzNPs initial velocities are not significantly different (p = 0.6649).

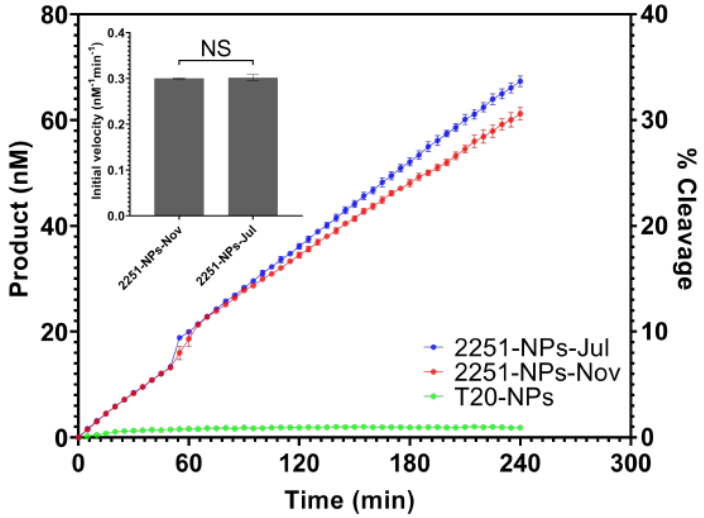

Figure 4.9. Activity of 2251-DzNPs tested 9 months apart. Reaction conditions: 100 µl of 1x PBS, 200 nM substrate, 2 mM Mg^{2+}, 0.5 nM DzNPs, RT. Data is reported in triplicate with SEM. Inset shows initial velocities ($nM^{-1}min^{-1}$) taken by finding slope of first 15 min of the reaction. DzNPs initial velocities are not significantly different (p = 0.7477).

To look at the longevity of salt aged 2251 DzNPs in more detail, our lab performed a series of experiments over the course of a few months, comparing older batches of particles stored in excess salt and DNAzyme at 4ºC to newer batches. We found that older batches of particles, when stored for 3 months, had an increase in activity over fresh batches (Fig. 4.7.) We hypothesized that this effect might occur due to the particles coming to an equilibrium over time with increased packing on the AuNPs surface. The DzNPs are stored in excess salt, which screens charge, as well as excess thiolated DNAzyme. Thus, packing density may increase over time. However, DzNPs tested 6 months apart (Fig. 4.8.) had similar activities, and the difference between their activities was not significant (p = 0.6649). Additionally, after 9 months, DzNP activity was also similar to freshly washed particles (Fig. 4.9.), with no significant difference (p = 0.7477). It is interesting to note, that the activity of the particles seems to vary batch to batch, when examining nM product formed.

Finally, we examined which synthesis method – freezing or salt aging – could produce the highest packing density and activity for 2251 DzNPs. The data obtained using attached 3'-thiolated 2251, showed that freezing mediated synthesis produced the superior density. We determined the number of DNAzyme strands per particle on the DzNPs produced by either method. The salt aging method produced 119 $\pm$ 1 strands per particle while the freezing method

produced 141 ± 4 strands per particle (n of three measurements per batch). The greater packing density of 2251-DzNPs synthesized via the freezing method could also be evaluated via kinetics. DzNPs produced via the freezing method were measurably faster at cleaving substrate than salt aged particles (Fig. 4.10.) ($p = 0.0005$). However, when comparing 5'-thiolated and immobilized 2251 (both 3' and 5' attached DzNPs include a T_{10}-linker) the result is more complicated. In both cases, DzNPs synthesized via the freezing method proved faster than salt aged DzNPs. However, 5'-attached salt aged DzNPs are faster than 3'-attached salted DzNPs, at least for this sequence ($p = 0.0003$) (Fig 4.11). It is interesting that when attached via the 5'-end, freezing and salt aging appear to give DzNPs that result in very similar activities, close to the activity of 3'-attached 2251 DzNPs synthesized via the freezing method (Fig. 4.10B.) Based on these results, there may be sequence bias toward either freezing or salt aging.

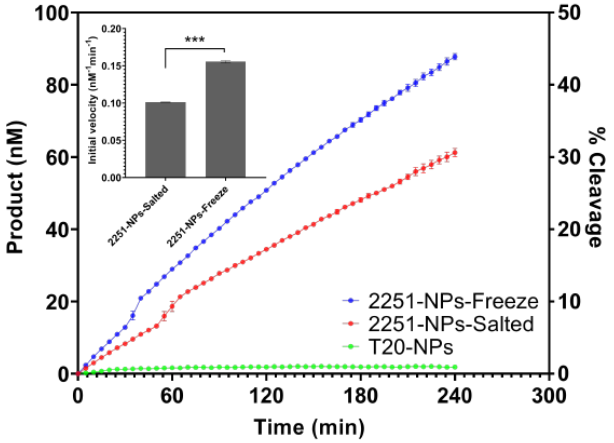

Figure 4.10. The activity of salt aged versus freezing method synthesized 2251-DzNPs. Reaction conditions: 100 µl of 1x PBS, 200 nM substrate, 2 mM Mg^{2+}, 0.5 nM DzNPs, RT. Data is reported in triplicate with SEM. DzNPs initial velocities are found by taking the slope in the first 15 min of the reaction. The initial velocities are significantly different ($p = 0.0005$).

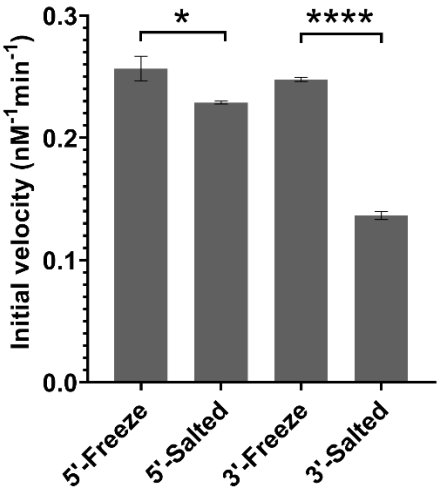

Figure 4.11. The initial velocities in the first 15 min, comparing 3' and 5' attached salt aged and freezing synthesized DzNPs. 5'-attached DzNPs produced by the freezing method are significantly faster than 5'-attached salt aged DzNPs ($p = 0.0365$) and likewise for 3'-attached DzNPs ($p < 0.0001$). Error bars indicate the standard error of the slope.

Note that 3’ and 5’ anchored DNAzymes displayed the same binding arms and only differed in the orientation of binding. More experiments will have to be conducted in order to determine the origin of this effect.

4.4. Conclusion

Overall, we showed that among the nucleotide modifications tested, four 2’-MOE modifications on the DNAzymes on each arm provide the greatest initial DNAzyme velocity. Washed 2251 DzNP remains active after freezing, and can be resuspended after thawing, provided there is a small amount of vortexing and sonication to help the resuspension. Salt aged 2251 DzNPs can last up to 9 months, stored at 4ºC in excess salt and DNAzyme. We speculate that the frozen 2251 DzNPs have a similar shelf-life, although this question has not yet been tested. 2251 DzNPs made using the freezing method display higher DNAzyme densities and are correspondingly more active than salt aged 2251 DzNPs, when immobilized via their 3’ end. However, when immobilized via their 5’ end, the activity of freeze mediated and salt mediated synthesis is similar. In future experiments, we would like to explore the longevity of frozen 2251 DzNPs. We could also perform experiments to determine why Hgd40 does not function as well in cells as 2251. Even so, with these experiments, we have come much closer to understanding the properties of 2251 DzNPs as a model system and are able to more readily apply them to cells and *in vivo* mouse models.

4.5. Materials and Methods

Table 4.3. Sequences used in this study

Name	Sequence (5'→3')
3'-SH-Hgd40	GTGGATGGA GGCTAGCTACAACGA GTCTTGGAG TTTTTTT TTT/3ThioMC3-D/
3'-SH-2251	ATTCCTTAAAggctagctacaacgaTTCTTGGCTTTTTTTTTT/3ThioMC3-D/
5'-SH-2251	/5ThioMC6-D/TT TTT TTT TTA TTC CTT AAA GGC TAG CTA CAA CGA TTC TTG GC
2251 substrate	/56-FAM/GCCAAGAArGrUTTAAGGAAT/3IABkFQ/
Hgd40 substrate	/56-FAM/CTCCAAGACrGrUCCATCCAC/3IABkFQ/
3'-SH-T20	TTTTTTTTTTTTTTTTTTTT/3ThioMC3-D/
2'-O-methyl 3'-SH-2251	mAmTmTmCCTTAAAggctagctacaacgaTTCTmTmGmGmCTTTTTTTTTT/3ThioMC3-D/
2 MOE-2251	/52MOErT//i2MOErA/TCCTTAAAggctagctacaacgaTTCTTG/i2MOErG//i2MOErC/TTTTTTTTTT/3ThioMC3-D/
4 MOE-2251	/52MOErT//i2MOErA//i2MOErT//i2MOErC/CTTAAAggctagctacaacgaTTCT/i2MOErT//i2MOErG//i2MOErG//i2MOErC/TTTTTTTTTT/3ThioMC3-D/

4.5.1. Synthesizing DzNPs by the freezing method

To synthesize DzNPs by the freezing method, 60 nmol of each thiolated DNAzyme was reduced in 1 mM DTT in disulfide cleavage buffer (170 mM phosphate buffer (pH = 8.0)) for 2 h at room temperature in the dark. Afterward, DNAzymes were purified on a nap-25 column (GE Healthcare) according to the manufacturer's instructions in Nanopure water. To 1 ml aliquots of AuNPs (average 8-10 nM concentration) 4 nmol of purified DNAzyme were added. The aliquots were then frozen at -20ºC 2 h and allowed to thaw at room temperature prior to use.

4.5.2. Synthesizing DzNPs by the salt aging method

To synthesize DzNPs by salt aging, 60 nmol thiolated DNAzyme were reduced with 1 mM DTT in disulfide cleavage buffer (170 mM phosphate buffer (pH = 8.0)) 2 hrs in the dark at room temperature. The samples were then purified on a nap-25 column (GE Healthcare) according to the manufacturer's instructions in Nanopure water. While running the column, the Eppendorf

tubes used to collect the sample were weighed, the weight recorded, and the tubes were weighed again after the sample was collected. The resulting purified DNAzyme was quantified on a NanoDrop 2000c spectrophotometer. Afterward, the nmol/ul of the sample using the volume was found and 4 nmol of DNAzyme to 1 ml AuNPs (typically between 8 – 10 nM) was added and incubated in an appropriate glass vessel overnight. The next day, phosphate adjustment buffer (100 mM phosphate buffer (pH 7.0)) was added to a final phosphate concentration of 9 mM and 10% sodium dodecyl sulfate (SDS) was added to a final concentration of ~0.1% (wt/vol). After this addition, the DzNPs were incubated at room temperature on an orbital shaker 30 min. Next, salting buffer (10 mM phosphate buffer + 2 M NaCl (pH 7.0)) was added to final concentrations of NaCl (0.05, 0.1, 0.2, 0.3, 0.4, 0.5, 0.6 and 0.7 M) every 20 min with 10-15 sec of sonication. The DzNPs were then incubated overnight on an orbital shaker.

4.5.3. Washing of the DzNPs

To prepare the DzNP samples, 1 ml aliquots were spun down at 13,000 rpm 20 min. The supernatant was removed, and the sample was resuspended in 500 µl Nanopure water and sonicated for 10 sec. The samples were then spun down at 13,000 rpm 20 min. The supernatant was removed and the sample was resuspended in 500 µl of Nanopure water. Sonication is not necessary at this point. The sample was then washed twice more. The final time, it is resuspended in the volume of Nanopure water of one's choice, which differs depending on the number of tubes one is spinning down and combining. The user then measures the UV-Vis absorbance at 520 nm of each tube using a NanoDrop 2000c spectrophotometer, to find the final gold concentration. A one in three dilution in Nanopure water is often necessary, to prevent saturation of the Nanodrop.

4.5.4. In vitro activity assay of the DzNPs

To perform activity assays for the DzNPs as shown, each DzNP was incubated with a short DNA/RNA hybrid that was complementary either to 2251 or Hgd40 as follows: For Hgd40, 5'-/56-FAM/CTCCAAGACrGrUCCATCCAC/3IABkFQ/-3' and for 2251, 5'-/56-FAM/GCCAAGAArGrUTTAAGGAAT/3IABkFQ/-3'. These strands have a fluorescein dye on the 5' end (FAM) and an Iowa black quencher on the 3' end. The respective DNAzyme can hybridize to this target and cleave it, leading to an increase in fluorescence. The conditions for each activity experiment were standardized to 100 µl of 1x PBS, 200 nM substrate, 2 mM Mg^{2+}, and 0.5 nM DzNPs. If conditions differed, they were noted in the caption of the appropriate figure. T20-NPs were used as a control inactive DNA-NP. If soluble strands were tested alongside the particles, T20-functionalized NPs were added at 0.5 nM concentration to the soluble strand wells, so that all wells had the same absorbance due to the particles and could be compared. Soluble strand concentration was adjusted depending on the number of strands per particle. The wells were run in triplicate and imaged on a Cytation 5 Biotek reader, using the extended gain setting. Data was averaged across the wells and the standard error of the mean calculated for each sample.

4.5.5. Standard curve for the in vitro DzNP activity assay

To produce a standard curve to calibrate the data from fluorescence over time to nM product over time, completely cleaved substrate was simulated by mixing a 5'-FAM-2251 strand and a black hole quencher™ 1 (BHQ1) strand in triplicate wells between the concentrations tested: 2 uM and 50 nM. The 5'-FAM strand sequence is as follows: /56-FAM/AT TCC TTA AAG GCT AGC TAC AAC GAT TCT TGG CTT TTT TTT TT/3ThioMC3-D/. The BHQ1 strand is as follows: 5'-/5BHQ1/CGC ATC TGT GCG GTA TTT CAC TTT-3'. These strands did not have high complementarity, as measured by Integrated DNA Technology's OligoAnalyzer tool. The strands were measured and a 100 µM and 10 µM stock of both were made. Using these stocks, the strands were added in equimolar amounts in triplicate wells in total volume of 100 µl 1x

PBS, with 2 mM Mg^{2+} and 0.5 nM T20-NPs, at the following concentrations: 2 µM, 1.75 µM, 1.5 µM, 1.25 µM, 1.0 µM, 0.75 µM, 0.5 µM, 0.25 µM, 0.20 µM, 0.15 µM, 0.10 µM and 0.05 µM. The standard curve was then imaged on a Cytation 5 Biotek reader on the extended gain setting. The wells were averaged and a standard curve was produced in Excel. Note that this standard curve is not accurate where a different concentration of DzNPs was used. To convert the fluorescence observed in my experiments to nM product, the following equation was used:

$Ft = F_0(1 – p) + Ff(p)$

Where Ft = the measured fluorescence, F_0 = the initial fluorescence measured at time 0, Ff = the maximum fluorescence when all the substrate at the concentration is cleaved (which value can be obtained from the standard curve), and p = the fraction of cleaved substrate. When solved for p, the equation becomes as follows:

$p = (Ff – F_0) / (Ff – F_0)$

Using Excel, this equation was used to find the % cleavage of each dataset, from the measured fluorescence. Then, the % cleavage could be converted into nM product by multiplying by the total substrate concentration.

4.5.6. Analysis of kinetics data

The slope of the line from the first 15 min of the kinetics data was taken by calculating a linear regression, to find the initial velocities of the reactions. Statistical t-tests were performed on the slopes to identify significance (p equal to or greater than 0.05). The only plot that differed was in Fig. 4.9. in which we drew a linear regression over the first 40 min of the reaction, because in the first 15 min, one of the slopes was negative due to an initial dip in fluorescence.

4.6. References

1. Finotto, S.; De Sanctis, G. T.; Lehr, H. A.; Herz, U.; Buerke, M.; Schipp, M.; Bartsch, B.; Atreya, R.; Schmitt, E.; Galle, P. R.; Renz, H.; Neurath, M. F., Treatment of Allergic Airway Inflammation and Hyperresponsiveness by Antisense-Induced Local Blockade of Gata-3 Expression. *The Journal of Experimental Medicine* **2001,** *193* (11), 1247-1260.
2. Mazzarella, G.; Bianco, A.; Catena, E.; De Palma, R.; Abbate, G. F., Th1/Th2 lymphocyte polarization in asthma. *Allergy* **2000,** *55* (61), 6-9.
3. Jeffery, P. K.; Wardlaw, J.; Nelson, F. C.; Collins, J. V.; Kay, A. B., Bronchial biopsies in asthma. *Am Rev Respir Dis* **1989,** *140*, 1745-1753.
4. Holgate, S. T., Asthma: past, present and future. *Eur Respir J* **1993,** *6*, 1507-1520.
5. Fiorentino, D. F.; Bond, M. W.; Mosmann, T. R., Two types of mouse T helper cell. IV. Th2 clones secrete a factor that inhibits cytokine production by Th1 clones. *J Exp Med* **1989,** *170*, 2081-2095.
6. Trinchieri, G., Interleukin-12: a cytokine produced by antigen-presenting cells with immunoregulatory functions in the generation of T-helper cells type 1 and cytotoxic lymphocytes. *Blood* **1994,** *84*, 4008-4027.
7. Manetti, R.; Parronchi, P.; Giudizi, M. G.; Piccinni, M.; Maggi, E.; Tinchieri, G.; Romagnani, S., Natural killer cell stimulatory factor (interleukin 12 [IL-12]) induces T helper type 1 (TH1)-speci®c immune responses and inhibits the development of IL-4-producing Th cells. *J Exp Med* **1993,** *177*, 1199-1204.
8. Wenner, C. A.; Güler, M. L.; Macatonia, S. E.; O'Garra, A.; Murphy, K. M., Roles of IFN-gamma and IFN-alpha in IL-12-induced T helper cell-1 development. *J Immunol* **1996,** *156* (4), 1442-1447.

9. Bochner, B.; Undem, B. J.; Lichtenstein, L. M., Immunological aspects of allergic asthma. *Annu Rev Immunol* **1994,** *12*, 295-335.

10. Wierenga, E. A.; Snoek, M.; de Groot, C.; Chrétien, I.; Bos, J. D.; H.M., J.; Kapsenberg, M. L., Evidence for compartmentalization of functional subset of CD4+ T lymphocytes in atopic patients. *J Immunol* **1990,** *144*, 4651-4656.

11. Gleich, G. J.; Kita, H., Bronchial asthma: lessons from murine models. *Proc Natl Acad Sci U S A* **1997,** *94*, 2101-2102.

12. Wills-Karp, M., Immunological basis of antigen-induced airway hyperresponsiveness. *Annu Rev Immunol* **1999,** *17*, 255-281.

13. Garn, H.; Renz, H., GATA-3-specific DNAzyme - A novel approach for stratified asthma therapy. *Eur J Immunol* **2017,** *47* (1), 22-30.

14. Zhang, D. H.; Cohn, L.; Ray, P.; Bottomly, K.; Ray, A., Transcription factor GATA-3 is differentially expressed inmurine Th1 and Th2 cells and controls Th2-specific expression of the interleukin-5 gene. *J. Biol. Chem.* **1997,** *272*, 21597–21603.

15. Maneechotesuwan, K.; Xin, Y.; Ito, K.; Jazrawi, E.; Lee, K.-Y.; Usmani, O. S.; Barnes, P. J.; Adcock, I. M., Regulation of Th2 cytokine genes by p38 MAPK-mediated phosphorylation of GATA-3. *J. Immunol.* **2007,** *178*, 2491–2498.

16. Patient, R. K.; McGhee, J. D., The GATA family (vertebrates and invertebrates). *Curr. Opin. Genet. Dev.* **2002,** *12*, 416–422.

17. Ho, I. C.; Tai, T. S.; Pai, S. Y., GATA3 and the T-cell lineage: essential functions before and after T-helper-2-cell differentiation. *Nat Rev Immunol* **2009,** *9* (2), 125-35.

18. Potaczek, D. P.; Garn, H.; Unger, S. D.; Renz, H., Antisense molecules: a new class of drugs. *J. Allergy Clin. Immunol.* **2016,** *137*, 1334–1346.

19. Sel, S.; Wegmann, M.; Dicke, T.; Sel, S.; Henke, W.; Yildirim, A. O.; Renz, H.; Garn, H., Effective prevention and therapy of experimental allergic asthma using a GATA-3-specific DNAzyme. *J Allergy Clin Immunol* **2008,** *121* (4), 910-916 e5.

20. Moschos, S. A.; Usher, L.; Lindsay, M. A., Clinical potential of oligonucleotide-based therapeutics in the respiratory system. *Pharmacology & Therapeutics* **2016,** *169*, 83-103.

21. Dicke, T.; Pali-Scholl, I.; Kaufmann, A.; Bauer, S.; Renz, H.; Garn, H., Absence of unspecific innate immune cell activation by GATA-3-specific DNAzymes. *Nucleic Acid Ther* **2012,** *22*, 117-126.

22. Turowska, A.; Librizzi, D.; Baumgartl, N.; Kuhlmann, J.; Dicke, T.; Merkel, O.; Homburg, U.; Hoffken, H.; Renz, H.; Garn, H., Biodistribution of the GATA-3-specific DNAzyme hgd40 after inhalative exposure in mice, rats and dogs. *Toxicol Appl Pharmacol* **2013,** *272* (2), 365-72.

23. Homburg, U.; Renz, H.; Timmer, W.; Hohlfeld, J. M.; Seitz, F.; Luer, K.; Mayer, A.; Wacker, A.; Schmidt, O.; Kuhlmann, J.; Turowska, A.; Roller, J.; Kutz, K.; Schluter, G.; Krug, N.; Garn, H., Safety and tolerability of a novel inhaled GATA3 mRNA targeting DNAzyme in patients with TH2-driven asthma. *J Allergy Clin Immunol* **2015,** *136* (3), 797-800.

24. Krug, N.; Hohlfeld, J. M.; Kirsten, A. M.; Kornmann, O.; Beeh, K. M.; Kappeler, D.; Korn, S.; Ignatenko, S.; Timmer, W.; Rogon, C.; Zeitvogel, J.; Zhang, N.; Bille, J.; Homburg, U.; Turowska, A.; Bachert, C.; Werfel, T.; Buhl, R.; Renz, J.; Garn, H.; Renz, H., Allergen-induced asthmatic responses modified by a GATA3-specific DNAzyme. *N Engl J Med* **2015,** *372* (21), 1987-95.

25. Neve, R. M.; Chin, K.; Fridlyand, J.; Yeh, J.; Baehner, F. L.; Fevr, T.; Clark, L.; Bayani, N.; Coppe, J. P.; Tong, F.; Speed, T.; Spellman, P. T.; DeVries, S.; Lapuk, A.; Wang, N. J.; Kuo, W. L.; Stilwell, J. L.; Pinkel, D.; Albertson, D. G.; Waldman, F. M.; McCormick, F.; Dickson, R. B.; Johnson, M. D.; Lippman, M.; Ethier, S.; Gazdar, A.; Gray, J. W., A collection of breast cancer cell lines for the study of functionally distinct cancer subtypes. *Cancer Cell* **2006,** *10* (6), 515-27.

26. Hill, H. D.; Mirkin, C. A., The bio-barcode assay for the detection of protein and nucleic acid targets using DTT-induced ligand exchange. *Nat Protoc* **2006,** *1* (1), 324-36.

27. Somasuntharam, I.; Yehl, K.; Carroll, S. L.; Maxwell, J. T.; Martinez, M. D.; Che, P. L.; Brown, M. E.; Salaita, K.; Davis, M. E., Knockdown of TNF-alpha by DNAzyme gold nanoparticles as an anti-inflammatory therapy for myocardial infarction. *Biomaterials* **2016,** *83*, 12-22.

28. Bhatt, N.; Huang, P. J.; Dave, N.; Liu, J., Dissociation and degradation of thiol-modified DNA on gold nanoparticles in aqueous and organic solvents. *Langmuir* **2011,** *27* (10), 6132-7.

Chapter 5: Site-Selective RNA Splicing Nanozyme: DNAzyme and RtcB Conjugates on a Gold Nanoparticle

Adapted with permission from Petree, J.R.; Yehl, K.; Galior, K.; Glazier, R.; Deal, B. and Salaita, K.S., Site-Selective RNA Splicing Nanozyme: DNAzyme and RtcB Conjugates on a Gold Nanoparticle, *ACS Chem. Biol.* **2018**, 13 (1), 215-224. Contributions: Jessica Petree, Khalid Salaita and Kevin Yehl discussed experiments and controls. Jessica Petree performed experiments. Kornelia Galior expressed RtcB-Cys shown in Figure 5.5f. Brendan Deal performed flow cytometry on Dz1Dz2NPs and nanozymes shown in Figure 5.S17. Roxanne Glazier performed FLIM on nanozymes shown in Figure 5.S14.

5.1. Introduction

Tools that can manipulate nucleic acids are very powerful, capable of controlling almost all cellular outcomes. RNA in particular is a desirable and accessible target, as it is in the cytoplasm, not bound by histones and chromatin, and is thus more accessible than DNA.[2] Modulating RNA can have tremendous potential for elucidating RNA biology, gene knockdown and regulating splicing. Two major methods have been developed to manipulate RNA. The first operates by modulating the activity of the spliceosome,[3-4] while the second approach employs RNA modifying enzymes[2, 5] and ribozymes.[6] Key examples of the latter approach include adenosine deaminase[2, 7] and the tRNA endonuclease from *Methanococcus jannaschii* (MJ-EndA).[5, 8] Adenosine deaminases that act on RNA (ADAR) have been shown to create A to G point mutations by converting adenosine to inosine,[2] which can be used to correct RNA errors. For example, by coupling to an antisense RNA strand and a λ-phage RNA binding protein, it can target and correct nonsense mutations in the cystic fibrosis transmembrane conductance regulator (CFTR), restoring translation at 100% efficiency.[2] Alternatively, MJ-EndA functions by cleaving bulge-helix-bulge (BHB) regions in RNA. Artificial BHBs can be created in *trans* by introducing a guide RNA strand that recruits MJ-EndA to these RNA sequences. The cleavage product is then repaired by cellular ligases. MJ-EndA has demonstrated activity for splicing *in vitro*.[5] This approach requires delivery of a plasmid encoding the endonuclease, along with the guide RNA strand, and has shown an efficiency as high as 30% splicing.[8]

In addition to protein enzymes, ribozymes[6, 9-10] or catalytic RNAs, are also actively used to control RNA splicing. Originally discovered as self-splicing group I introns,[11] ribozymes have been modified and used for RNA knockdown,[10] intron removal,[6] as well as *trans*-splicing of 3'[12] and 5' segments.[13] Thus far, ribozyme-based editing has shown 10-50% efficiency in mammalian cells under ideal conditions.[14] Given the importance of manipulating RNA in cell and

molecular biology and biochemistry, the development of new approaches to modify RNA is highly desirable.

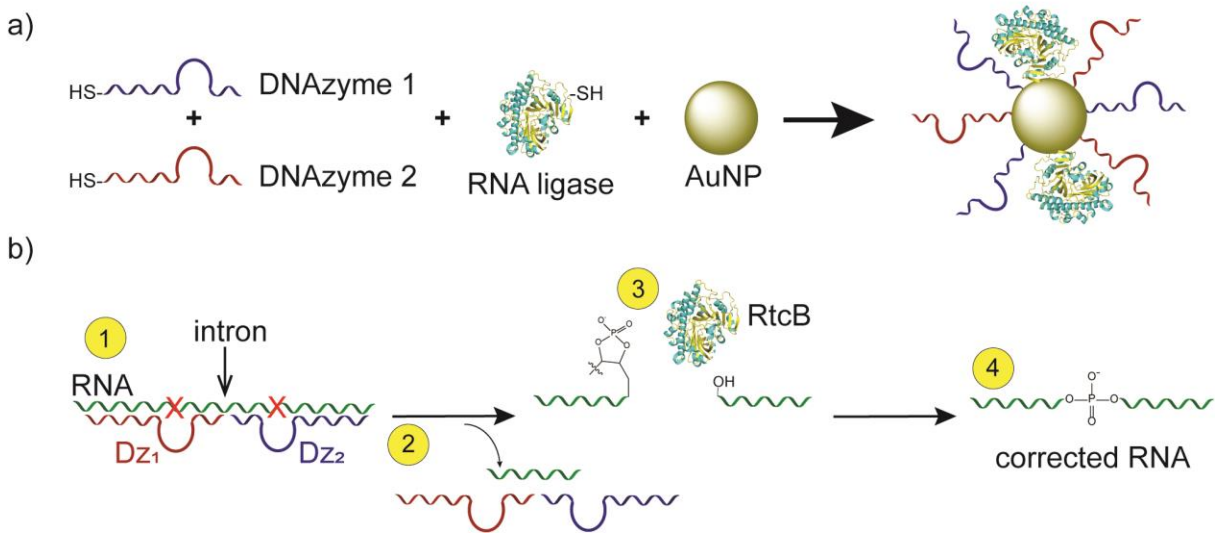

Scheme 5.1. DNAzymes and RtcB can work together in an RNA splicing reaction. (a) Nanozymes are constructed of two DNAzymes and an RNA ligase (RtcB) attached to a gold nanoparticle (AuNP) scaffold. (b) DNAzymes cleave target RNA at purine / pyrimidine junctions (red "X"), removing an intron and leaving 2'-3'-cyclic phosphates that RtcB can ligate to produce corrected RNA. Note: Crystal structure is from the *P. horikoshii* RtcB species [PDB=4ISZ].[1]

Herein, we developed a new method for RNA splicing by generating a nanozyme, (Scheme 2.1) which generally refers to a particle that mimics enzymatic activity either through the property of the particle or its attached ligands.[15-16] In our case, we built a splicing nanozyme by attaching RNA cleaving and ligating enzymes onto a gold nanoparticle (AuNP) scaffold. To the best of our knowledge, this technique is the first RNA splicing nanozyme.

We chose the 10-23 DNAzyme[17] as the site-specific RNA-cleaving component of this nanozyme (Fig. 5.S1), since mammalian cells also readily internalize DNAzyme-AuNP conjugates, allowing efficient gene knockdown *in vitro* and *in vivo*.[18-19] DNAzymes are not found in nature, and are synthetic constructs generated through rounds of selection (SELEX) for a

specific enzymatic activity – in this case, for RNA cleavage.[17] The 10-23 DNAzyme is composed of a Mg/Mn^{2+} dependent[20] 15-nucleotide (nt) catalytic core flanked by two 6-10 nt binding arms. The binding arms can be tuned to bind any RNA target with high specificity. DNAzymes cleave at purine / pyrimidine junctions – most often AU or GU residues. After cleavage, the binding arms dissociate as they are no longer thermally stable, allowing for a new round of binding and cleavage to take place.[17]

RtcB was selected as the RNA ligating enzyme of the nanozyme because it is the only known ligase that can directly ligate the termini produced by DNAzymes: 2'3'-cyclic phosphate and 5'-OH.[21] RtcB is well-conserved throughout bacteria, archaea and metazoa,[22] having functions in bacteria for RNA repair,[23] and in metazoa, for splicing of tRNAs[24] and upregulating the unfolded protein response.[25] RtcB's natural substrate for ligation is hydrolyzed stem-loop RNA. Since it is expressed in most mammalian cells for RNA ligation and ligates the products of DNAzyme cleavage, it is well-suited for generating our nanozyme.

In principle, this nanozyme obviates the need for genetic engineering, providing a potential delivery vehicle into cells. It also sequesters its enzyme cargo onto the AuNP surface, away from degrading proteases and nucleases, increasing stability over current strategies.[18, 26] The spliced product is not a substrate for the DNAzymes, helping to move the reaction toward completion. This technique opens the door to a new method of cellular splicing heretofore unexplored in the literature: that of coupling a natural and synthetic enzyme to splice RNA targets. Herein, we investigate and characterize the splicing of these combined enzymes, both separately and integrated onto a gold nanoparticle scaffold.

5.2. Results and Discussion

5.2.1. RtcB is more active on stem-loops than linear RNA

To test the activity of RtcB, the ligase was isolated using a lacI inducible plasmid expressing *E.coli* N-terminal hexahistidine-tagged RtcB (Fig. 5.S2). Throughout this work, RtcB activity was assayed using fluorescein-labeled target RNAs and the products were quantified using 15% polyacrylamide gel electrophoresis (PAGE).

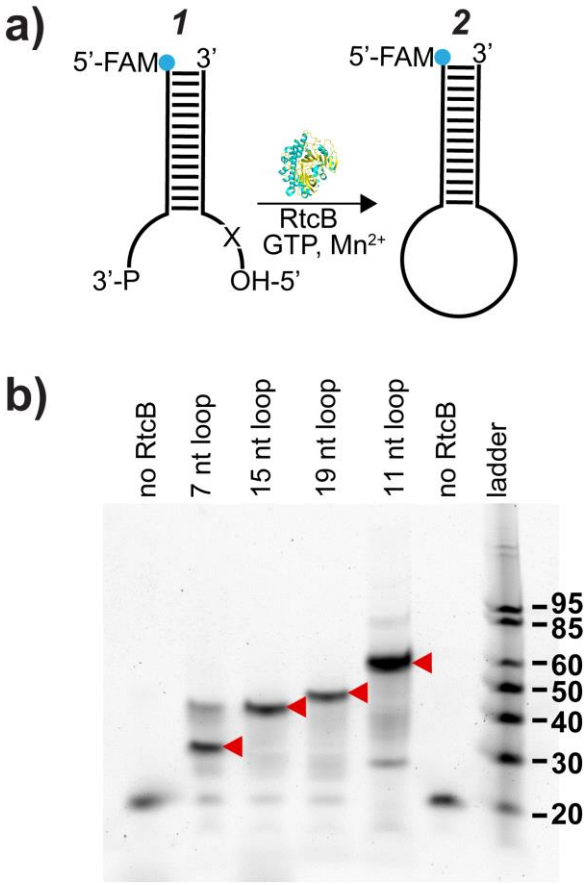

Figure 5.1. Testing the role of loop size in ligation efficiency. (a) Schematic showing model RNA substrate for testing RtcB activity as a function of loop size. "X" indicates added nucleotides (see Table S2). (b) Reaction was conducted at 37 ºC for 1 hr, 200 nM FAM-labeled strand, 250 nM unlabeled strand, 150 mM NaCl, 1 mM Mn^{2+}, 0.1 mM GTP and 1 µM RtcB. Lane 1: 19 nt FAM-labeled strand alone; lane 6, stem-loop of 7 nt without RtcB to ligate. Red arrows indicate ligation products. Note that RtcB can ligate either 2'3'-cyclic phosphates or 3' phosphates.

Inspired by Desai and Raines's experiments, we first tested the action of RtcB using a 7 mer stem-loop $tRNA^{glu}$ mimic and found that RtcB ligated this substrate with 100% efficiency, while it ligated two 10 mer linear RNA strands with an efficiency of up to 46% (Fig. 5.S3-5.S4). Additionally, we found that the stem-loop target ligation was rapid, reaching completion within 2 min (Fig. 5.S5). Our results agree with Desai and Raines, who demonstrated that RtcB is more active on stem-loops than on linear RNA substrates[27] and postulated that this selectivity is due to the proximity of the stem-loop termini.

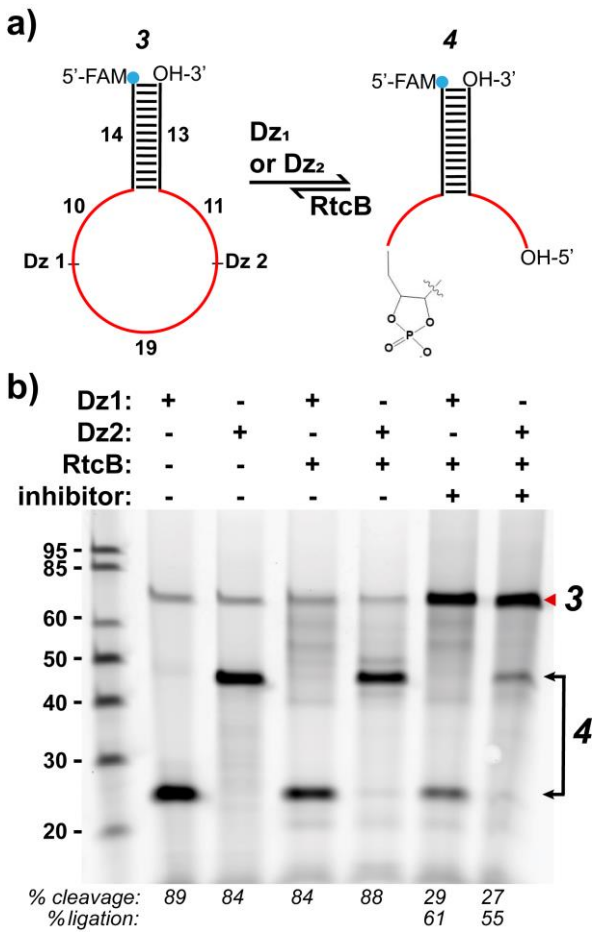

Figure 5.2. Reversible DNAzyme cleavage with RtcB. (a) Schematic showing DNAzyme cleavage and ligation back to substrate ***3***. RNA is shown in red and DNA in black. (b) Gel showing single cleavage reactions and ligation back to substrate. Lanes 2-3: single Dz digests; lanes 4-5: single Dz digests after RtcB addition; lanes 6-7: same reaction shown in lanes 4-5 after addition of inhibitor strands complementary to the Dz(s). Ligation reactions contain 150 mM NaCl, 2 mM Mn2+, 0.4 µM substrate 3, 0.4 µM Dz_1 or Dz_2, 0.42 µM Dz inhibitor (lane 6-7), 0.4 mM GTP and 2.2 µM RtcB. Red arrow indicates ligation product. Note that lanes were loaded evenly.

In subsequent studies on RtcB by Tanaka and Chakravarty, the majority of RtcB substrates tested were stem-loops or linear strands that were allowed to cyclize.[23, 28] Our results further confirm that the stem loop is the preferred substrate for RtcB mediated ligation, suggesting that it will also be the preferred substrate for splicing reactions.

Given the strong dependence on substrate geometry, we next examined the efficiency of RtcB ligation as a function of stem-loop size (7, 11, 15, 19 nts), to determine if RtcB could ligate stem-loops larger than tRNA anticodon loops. We modified the $tRNA^{glu}$ stem-loop with increasing numbers of unpaired base pairs and introduced additional unpaired nucleotides on the 5'-end (Fig. 5.1a, ***1***), increasing loop size. We found that all the stem-loops tested were ligated to near 100% efficiency (Fig. 5.1b). To interrogate the ligation of loops larger than 19 nts, we used DNAzymes to cleave a DNA / RNA hybrid stem-loop target (Fig. 5.2a, ***3***), producing single-stranded overhangs of 10 and 30 nts or 11 and 29 nts, with a total loop size of 40 nts. As proof-of-concept, we chose model DNAzymes known to have a relatively high k_{cat} (Dz_1)[29] or operate at low Mg^{2+} concentration (Dz_2)[30] for use throughout this work (Fig. 5.S1). We also

confirmed the specificity of Dz1 and Dz2 by introducing single and double nucleotide mutations in the binding arms and measured the nuclease activity (Fig. 5.S6). After DNAzyme cleavage of the RNA / DNA hybrid substrate for 2 hrs, an aliquot of the reactions was taken (Fig. 5.2b, lanes 2-3) and an inhibitor strand complementary to the DNAzymes was introduced along with RtcB. The reaction was then allowed to proceed for another 1 hr (Fig. 5.2b, lanes 6-7). Using PAGE, we assayed the efficiency of RtcB ligation of these cleavage products with and without inhibitor strand. Analysis of the resulting gel showed that when an inhibitor strand was present, these stem-loops were ligated back to substrate ***3*** with 55-60% efficiency (Fig. 5.2b, lanes 6-7). The inhibitor strands to inactivate the DNAzymes were necessary to block DNAzyme action and allow for RtcB ligation. The reduction in efficiency is likely due to the enlarged loop, as well as the limited cyclic phosphodiesterase activity of RtcB (*vide infra*).[31] Importantly, this data indicates that RtcB is amenable for ligation of stem-loops as large as 40 nts and shows that it can process the products of DNAzyme cleavage.

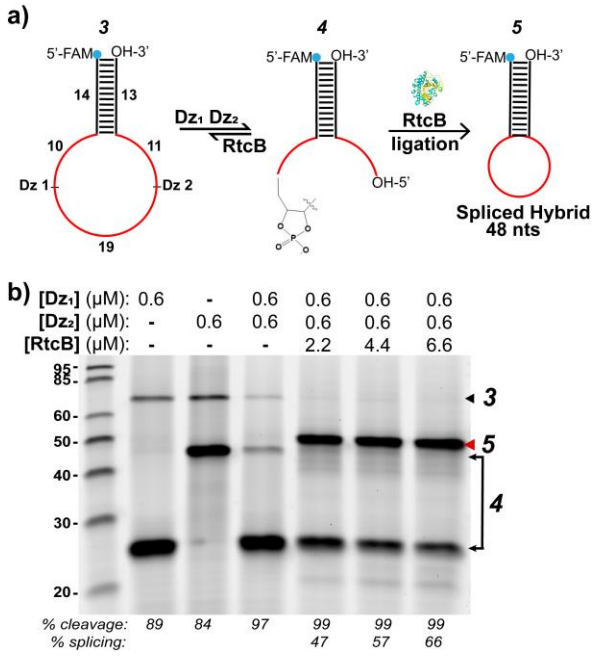

Figure 5.3. RtcB ligation of DNAzyme cleavage products and splicing. (a) Schematic showing reactions used to test splicing. 5'-FAM-labeled *in vitro* splice substrate ***3*** is cleaved, removing 19 nt intron to produce ***4***. RtcB addition produces spliced stem-loop ***5***. RNA is shown in red. (b) Cleavage and splice reaction with soluble Dz(s) and RtcB. Dz_1 (lane 2) and Dz_2 (lane 3) single cleavage produces bands at 24 and 43 nts. Addition of RtcB to a Dz_1Dz_2 double digest produces splice product (red arrow). Reaction conditions: 150 mM NaCl, 0.6 μM each Dz, 0.6 μM substrate ***3***, 2 mM Mn^{2+}, 0.4 mM GTP, 2.2, 4.4 or 6.6 μM RtcB. DNAzyme cleavage (2 hrs) and RtcB ligation (1 hr) proceeded at 37ºC.

5.2.2. DNAzymes and RtcB splice an RNA stem-loop

Next, we tested whether it was possible for DNAzymes and RtcB to splice in a one-pot reaction. We first incubated substrate ***3*** with an equimolar concentration (0.6 μM) of both

Dz_1 and Dz_2 for 2 hrs in the presence of 2 mM Mn^{2+}. The DNAzymes bound adjacent sites in the loop region of the stem-loop substrate ***3*** and cleaved, removing a 19 nt intron (Fig. 5.3a, ***4***). After cleavage, RtcB was added to the reaction at different concentrations (2.2, 4.4 and 6.6 µM). Upon addition of RtcB, a smaller spliced stem-loop product ***5*** was produced (48 nts) at 47-66% yield, depending on the concentration of the enzyme (Fig. 5.3b). In general, splicing yield varied between 45-68% with 2.2 µM of RtcB (data not shown). Yield was calculated by integrating the splice product band intensity and dividing by the integrated intensity of all the bands per lane. All values were background subtracted using the integrated intensity above and below each band (Fig. 5.S7). Note that in this case a hybrid RNA / DNA substrate was used for splicing; however, all RNA substrates can also be used (Fig. 5.4). Interestingly, RtcB and DNAzymes spliced RNA targets both in sequential reactions (with DNAzyme addition followed by RtcB addition) and in one-pot reactions, with similar yields (Fig. 5.S8). As with the ligation of RNA stem-loops, the splice reaction is also relatively fast, and splice product was observed 5 min after adding RtcB enzyme (Fig. 5.S9).

There are two possible reasons that likely limit splice yield. The first is that the DNAzymes could be binding to the target and not dissociating adequately, thus inhibiting RtcB binding and ligation. Additionally, stalled or inactive RtcB enzyme may sequester RNA ends, binding them but not effectively performing the ligation reaction. To test whether DNAzymes could be inhibiting the splice reaction, we bound the DNAzymes with a complementary strand after cleavage and then added RtcB. The yield of this reaction showed a 5% increase (Fig. 5.S10) over reactions with free DNAzymes. We thus shortened the DNAzyme arms from 9 nts to 8 and 7 nts, to decrease the T_m, reducing DNAzyme-target stability and enhancing product dissociation. We observed a 12% increase in splicing (from 48 to 60%) (Fig. 5.S11) upon using

8 nt arms over 9 nt arms. However, no additional improvement in splicing was observed for the 7 nt arm DNAzyme. Only Dz_2 was tested with 7 nt arms, since Dz_1's T_m was already significantly reduced with 8 nt arms, and further shortening the arms would likely limit binding to the target (Table 2.S1). Therefore, these experiments appear to justify our hypothesis that the DNAzyme arms inhibit splicing, but that factor alone cannot account for the observed lower yield.

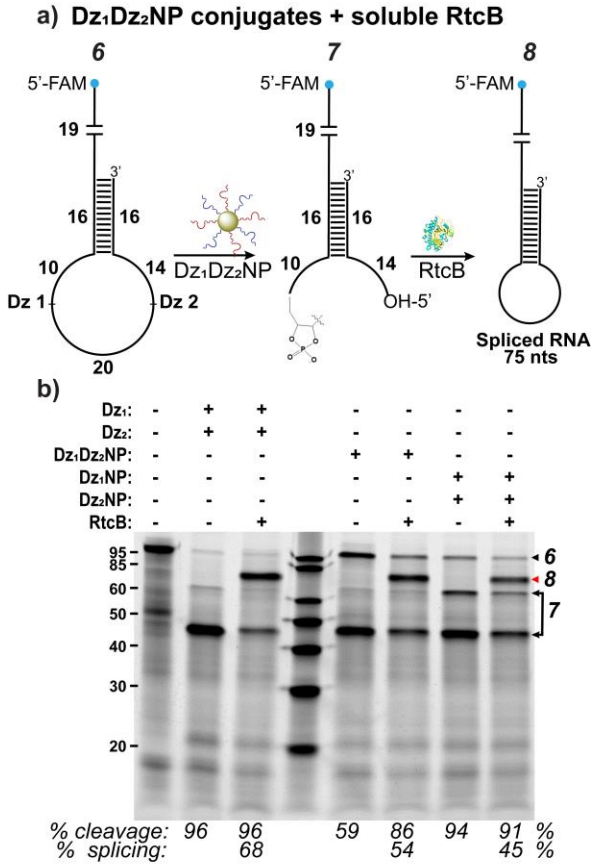

Figure 5.4. DNAzyme conjugates (Dz_1Dz_2NPs) can splice with excess soluble RtcB. (a) Scheme showing splicing by Dz_1Dz_2NPs and RtcB on RNA substrate. (b) Splicing by soluble DNAzymes is compared to NPs with either both or single Dz's attached. Red arrow indicates splice product. Reaction conditions: 150 mM NaCl, 1 mM Mn^{2+}, 0.4 µM substrate ***6***, 0.4 mM GTP, 2.2 µM RtcB, lanes 2-3, 0.4 µM Dz(s), lanes 5-6, 9 nM Dz_1Dz_2NPs, lanes 7-8, 9 nM Dz_1NP and Dz_2NP. Cleavage was conducted at 37ºC for 2 hrs and splicing at 37ºC for 1 hr. Note that the cleavage yield increased in lane 6 compared to lane 5 likely due to the additional 1 hr incubation time following treatment with RtcB.

Interestingly, ligation efficiency was nearly quantitative when 3'-P termini were used for the stem-loop ligation (Fig. 5.1b), suggesting that the 2'3'-cyclic phosphates formed as the DNAzyme cleavage products reduce the yield of splicing. As RtcB first converts the 2'3'-cyclic phosphate to a 3'-P before ligation,[31] it is possible the cyclic phosphatase reaction stalls splicing yield. Nevertheless, these splice reactions show that DNAzymes and RtcB are indeed able to function under identical conditions to splice RNA stem-loop targets, removing a 19 nt intron. These results confirm the potential for a splicing nanozyme system employing both classes of enzymes.

5.2.3. Dz_1Dz_2NP splicing using excess RtcB

As a first step toward splicing with a nanozyme composed of both DNAzymes and RtcB conjugated to a gold nanoparticle scaffold, we first tested whether soluble RtcB could splice in the presence of DNAzyme-functionalized gold nanoparticle conjugates (Dz_1Dz_2NPs). To produce Dz_1Dz_2NPs, we adopted previously reported protocols for single component DzNPs.[18] Briefly, thiolated DNA was incubated with citrate stabilized AuNP and progressively salted.[32-33] After washing to remove excess salt, mature Dz_1Dz_2NPs were then incubated with an RNA substrate (Fig. 5.4, ***6***), allowing cleavage to proceed. We found that Dz_1Dz_2NPs cleaved target RNA producing ***7*** with an efficiency between 86-94%, in the presence of 1 mM Mn^{2+}. When RtcB was added to these digests, a 54% splicing yield was observed (Fig. 5.4, ***8***), similar to what was obtained for splicing with soluble DNAzymes and RtcB (Fig. 5.3b; Fig. 5.4b, lane 3). Additionally, mixing Dz_1NPs and Dz_2NPs also resulted in efficient cleavage. These products were spliced at a yield of 45% (Fig. 5.4b, lanes 7-8). The yield was lower in this case possibly due to the added steric bulk of two AuNPs being involved in the cleavage reaction. For single component DzNPs, the number of Dz(s) per NP was quantified using a fluorescence assay, which showed that there were 102 ± 9 strands of Dz_1 and 54 ± 6 strands of Dz_2 on the AuNPs. Since for Dz_1Dz_2NPs each Dz was added in equimolar amounts, the number of strands of each on the NP may be estimated at half their number on single component DzNPs. Overall, these experiments show that splicing is effectively achieved with DNAzyme-nanoparticle conjugates and excess soluble RtcB.

5.2.4. Nanozyme synthesis

To produce complete nanozymes we needed to attach both DNAzymes and RtcB to a single particle. The RtcB enzyme was engineered with two cysteine residues at the N-terminus to enhance AuNP binding through thiol-Au chemistry. Dz_1Dz_2NPs were first synthesized as described (see Methods). Afterward, RtcB-Cys (4.7 μM) was attached to these Dz_1Dz_2NPs in an overnight incubation at 4ºC in 100 mM Tris-HCl (Fig. 5.5a), thus allowing RtcB binding by thiol

exchange and production of nanozymes. The zeta potential of the Dz_1Dz_2NPs and nanozymes was also measured (Fig. 5.5a). These measurements suggest that RtcB alters the zeta potential of the Dz_1Dz_2NP particles. A fluorescence assay indicated that an average of 1.4 RtcB molecules were bound to each Dz_1Dz_2NP. However, when the thiol exchange was performed in the presence of 1x PBS, 5.2 RtcB were bound per Dz_1Dz_2NP (Fig. 5.S12). This greater degree of binding is likely due to charge screening, as 1x PBS has a greater ionic strength than the Tris buffer used for binding studies. As expected, the cysteine residues were critical in the binding of the RtcB to the AuNPs to produce complete nanozymes, since His-tagged RtcB failed to bind to AuNPs, as shown by failure to generate splice product after washing the particles (Fig. 5.S13). Fluorescence lifetime spectroscopy was also used to confirm the association between the RtcB and the gold nanoparticle surface. Gold nanoparticles are known to reduce the fluorescence lifetime of organic dyes due to the process of nanometal surface energy transfer (NSET). To perform this experiment, we labeled RtcB-Cys and RtcB-His ligases with NHS-Alexa488. The fluorescence lifetime of Alexa488 was then measured when the enzyme was soluble and compared to that of enzyme incubated with the DNAzyme-functionalized gold nanoparticles. The measurements show a significant reduction in the fluorescence lifetime of RtcB-Cys upon incubation with gold nanoparticles, which is in contrast to RtcB-His enzymes that were indistinguishable regardless of nanoparticle interaction (Fig. 5.S14). This result confirms that the engineered Cys residues are important in mediated binding to the gold nanoparticle. Finally, the AuNPs, Dz_1Dz_2NPs and nanozymes were characterized by transmission electron microscopy (TEM) and dynamic light scattering (DLS) (Fig. 5.5b, c). TEM shows that the Dz_1Dz_2NPs and nanozymes were not aggregated by addition of DNA and protein to the surface of the gold. Additionally, DLS provided another confirmation that these species were attached to the particle surface, in addition to the fluorescence and spectroscopy assays that we performed (Fig. 5.S12, S14).

5.2.5. Nanozyme conjugates splice RNA stem-loop targets

Despite the low copy number of RtcB molecules per nanozyme, we next tested the activity of our nanozyme in splicing an RNA substrate ***3*** (Table 5.S2). Soluble DNAzymes with and without RtcB enzyme were used as positive and negative controls, respectively. After overnight RtcB-Cys incubation, the fresh nanozymes were washed three times with 100 mM Tris-HCl buffer, to remove excess soluble RtcB-Cys. After each wash, nanozyme aliquots were then mixed with substrate ***3*** and incubated at 37ºC for 2 hrs (Fig. 5.S15). Nanozymes digested the RNA target and showed a splicing efficiency of 3% after the third wash (Figure 5.S15, lane 6, ***5***) at 24 nM concentration of nanozyme. Another set of experiments was conducted, concentrating the nanozymes in each reaction up to ~200 nM. In this case, nanozyme splicing reactions were performed in triplicate and splice product was as high as 10% (Fig. 5.5e), as determined by band intensities. We found that increasing the amount of nanozymes did increase the amount of splice product within the range of nanozyme concentrations tested, although the increase was not linear, due, in part, to decreasing activity of RtcB-Cys as it ages. Further experiments were then conducted with additional controls, such as creation of a nanozyme with RtcB-Cys and non-specific DNAzymes. This construct was unable to cleave or splice target RNA, as expected (Fig. 5.5f, lane 7). Additionally, we found that RtcB-Cys must be located on the same particle as the target-specific DNAzymes to effect splicing. Non-specific nanozymes, that included RtcB-Cys, were unable to splice the target even after active Dz_1Dz_2NPs were introduced (Fig. 5.5f, lane 8). To further explore the finding that the nanozyme splicing reaction is most optimal when the nuclease and ligase activity are localized to the same particle, we performed an additional set of experiments where we compared the activity of the complete nanozyme against that of a binary mixture of particles where the nuclease and ligase activities are isolated onto different particles (Fig. 5.S16). Taken together, the lower yield when using binary mixtures of particles is likely due to the substrate associating with the Dz_1Dz_2NPs and thus reducing the association with the RtcB. Finally, we tested splice reactions with excess DNAzymes and soluble RtcB

equivalent to the amount of RtcB on nanozymes. Splicing was found to be equivalent to nanozyme splicing (Fig. 5.5f, lane 9-10), indicating that RtcB activity is maintained on the AuNP surface. These experiments suggest that *E.coli* RtcB is likely a single-turnover enzyme[34] and thus, the limiting reagent in the splice reaction.

Overall, this nanozyme shows utility in splicing RNA stem-loops. For cellular splicing, it is possible that RtcB does not need to be included on the nanozyme, since endogenous RtcB is already expressed and may be recruited to the particle for splicing. Future work will focus on increasing the efficiency of the nanozyme and transitioning toward *in vivo* splicing.

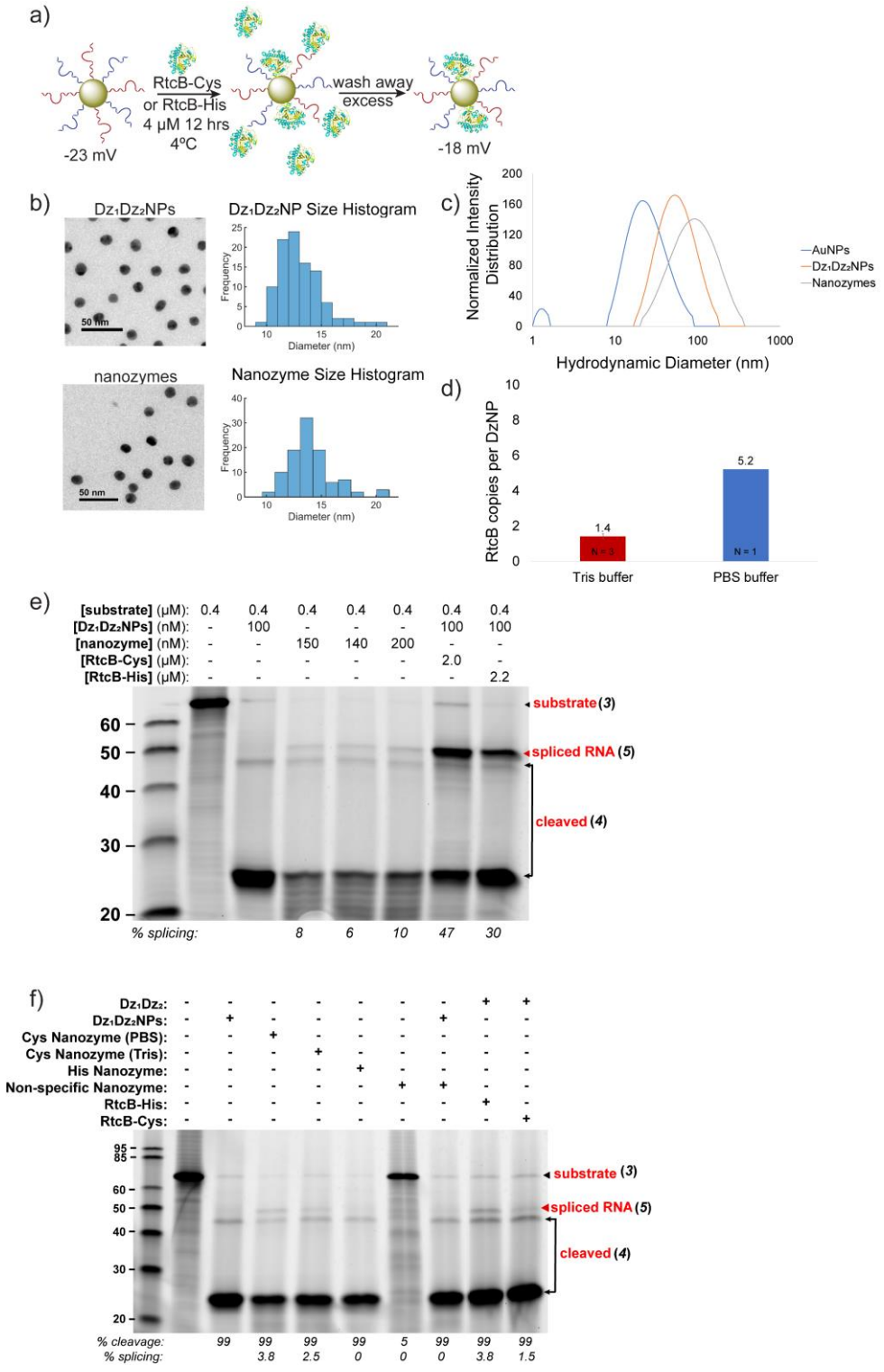

Figure 5.5. Characterizing the splicing of nanozyme constructs.

(a) Scheme illustrating nanozyme synthesis. Zeta potential = -22.5±1.5 for Dz1Dz2NPs and -17.7±1.4 for nanozymes in 10 mM Tris-HCl, pH 7.4. (b) Transmission electron microscope (TEM) characterization of Dz1Dz2NPs and nanozymes. DNAzymes and RtcB are not visible in unstained TEM; however, no aggregation was observed. (c) DLS of unmodified AuNPs, Dz1Dz2NPs and nanozymes. (d) Plot showing the measured density of RtcB on nanozymes. Measurement was performed using fluorescence spectrometry. (e) Triplicate nanozyme splicing reactions. Lane 2: RNA / DNA hybrid substrate 3 only; lane 3: Negative control containing Dz_1Dz_2NPs and no RtcB; lane 4-6: nanozymes after washing 3 times yields splice product (red arrow); lane 7: positive control with Dz_1Dz_2NPs and 2 µM soluble RtcB-Cys; lane 8: positive control with Dz_1Dz_2NPs and 2.2 µM soluble RtcB-His. Reaction conditions: 0.4 µM substrate, 150 mM NaCl, 0.4 mM GTP, 2 mM Mn^{2+}, 37ºC for 2 hrs. (f) Gel showing the role of buffer and immobilization chemistry in tuning nanozyme efficiency. Lane 2: DNA / RNA hybrid substrate ***3*** alone; lane 3, negative control with Dz_1Dz_2NPs without RtcB; lane 4, nanozyme, produced by RtcB incubated in 1x PBS; lane 5, nanozyme produced by RtcB incubated in 100 mM Tris; lane 6, nanozymes produced by incubation with RtcB-His; lane 7, inactive nanozyme, produced with non-specific DzNPs incubated with RtcB-Cys in 100 mM Tris; lane 8, inactive nanozyme supplemented with active Dz_1Dz_2NP; lane 9, soluble 37.5 nM RtcB-His in presence of excess Dz_1 / Dz_2; lane 10, soluble 37.5 nM RtcB-Cys in presence of excess Dz_1 / Dz_2. Nanozyme concentration was 25 nM in all lanes. Red arrow indicates splice product.

5.3. Conclusion

In summary, we demonstrate that RtcB and DNAzymes – natural and synthetic enzymes, respectively – can be coupled to a gold nanoparticle and work together to splice RNA targets with up to a 10% yield. This activity is observed despite direct coupling of the RtcB to the gold nanoparticle surface. This nanozyme is the first example of a splicing nanoparticle system and the only known combination of a natural and synthetic enzyme for splicing. We demonstrate that RtcB and DNAzymes must be on the same particle to achieve splicing and cannot complement each other on separate particles. We also demonstrate that the cysteine residues on RtcB are essential for RtcB binding to the Dz_1Dz_2NPs, without which, no nanozyme is formed; and after washing of Dz_1Dz_2RtcB-His-NPs, no detectable splicing is observed (Fig. 5.S12). Labeled His-nanozymes also do not show a change in their fluorescence lifetime (Fig. 5.S14c-d). Additionally, DNAzymes and RtcB also splice RNA targets up to 45-66% yield when including excess RtcB in solution. This system provides a completely new method of RNA splicing that adds to the toolkit for *in vitro* work. Since DNAzyme-NP conjugates and nanozymes readily enter cells *in vitro*[18] (Fig. 5.S17) and DNAzyme-NP conjugates have shown uptake *in vivo*,[19] it

also provides a platform with which to conduct cellular splicing. In future work, we plan to increase splicing efficiency inside cells by arraying more RtcB around the particle using a linker strand, as well as recruiting endogenously expressed RtcB (HSPC117) to the particle surface for specific splicing.

5.4. Materials and Methods

5.4.1. Expression and Purification of RtcB-His

To express, isolate and purify hexahistidine-tagged RtcB enzyme, we adapted protocols from both the Raines and Shuman labs.[23, 27] RtcB with an N-terminal hexahistidine tag under a lac-I inducible promoter (pQE-70) was obtained from the Raines lab[27] and transformed into Keio JW5688-1 (ΔrtcA::kan) from the E. coli Genetic Stock Center (Yale). Briefly, 5 ml of LB (100 µg/ml Amp, 50 µg/ml Km) was inoculated with a single colony of the above transformant and grown at 37ºC overnight. This culture was used to inoculate 1L of LB (100 µg/ml AMP, 50 µg/ml Km) which grew at 37ºC shaking until OD_{600} = 0.6 – 0.8. Expression was then induced by addition of 0.5 mM IPTG and grown for 2.5 hours at 32ºC. The culture was spun down at 3,100 g at 6ºC for 30 min. Pellet was transferred to a 50 ml Falcon tube and resuspended in 10 ml lysis buffer. Lysis buffer was prepared by mixing 100 µl of protease inhibitor cocktail (PIC, Sigma Aldrich, P8849) in 50 ml buffer A [50 mM Tris-HCl, pH 7.4, 250 mM NaCl, 10% sucrose] on ice. Culture was sonicated on a probe sonicator, 10 sec pulse, 20 sec rest (11-14 mM, lvl 4) for 4 min. The lysate was cleared by centrifuging on an Optima XE-90 ultracentrifuge for 30 min at 24,100 rpm (67,000 g). The lysate was then added to a Falcon tube with 15 ml buffer A and 3 ml Ni:NTA beads (QIAGEN, cat. no. 30210) equilibrated in 15 ml buffer A. Lysate was then allowed to rock on a nutating mixer at 4ºC for 1 hr. After incubation, Ni:NTA beads were centrifuged at 4,000 g for 15 min and resuspended in buffer B_1 [50 mM Tris-HCl, pH 7.4, 150 mM NaCl, 10% glycerol, 25 mM imidazole]. This wash was repeated two more times. The beads were then added to a column (Bio-rad, #737-4156) and washed with ~20 ml wash buffer [50 mM Tris-HCl, pH 7.4, 2 M KCl], 10 ml buffer B_1, 10 ml buffer B_2 [buffer B_1, 40 mM imidazole], 10 ml buffer B_1 and eluted with 7 ml elution buffer [buffer B_1, 300 mM imidazole]. Protein elution was estimated by the Bradford Assay and dialyzed against 500 ml of buffer C [10 mM Tris-HCl, pH 8.0, 350 mM NaCl, 1 mM DTT, 10% glycerol] for two hours. Buffer was changed four times at

two hour intervals and finally dialyzed overnight at 4ºC. After dialysis, aliquots of RtcB enzyme were frozen in liquid nitrogen and stored at -80ºC.

5.4.2. Expression and Purification of Cysteine-modified RtcB

RtcB that had been modified with two cysteine residues before the N-terminal His-tag was expressed under a lac-I inducible promoter (pQE-70) and transformed into *E.coli* BL21. Briefly, 5 ml of LB (100 µg/ml Amp) was inoculated with a single colony of the above transformant and grown at 37ºC overnight. This culture was then used to inoculate 250 mL of LB (100 µg/ml Amp) which grew at 37ºC shaking until OD_{600} = 0.6. Expression was then induced by addition of 0.1 mM IPTG and grown for 4 hrs at 37ºC. Culture was spun down at 4,000 rpm 6ºC for 20 min and the pellet kept on ice. Cell pellets were resuspended in a total of 10 ml lysis buffer [50 mM sodium phosphate, 300 mM NaCl, 10 mM imidazole], supplemented with 100 µl Protease Inhibitor Cocktail (PIC), 60 µl lysozvme [20 mg/mL stock], 5-10 µl benzonase. The resuspended cells were incubated on ice for 20 min, then sonicated for 3.5 minutes: 15 sec pulse, 15 sec rest. The lysate was then centrifuged at 4ºC, 4,000 rpm for 30 min. Ni-NTA beads (QIAGEN, cat. no. 30210) were prepared by adding 1.2 mL of the resin slurry into a 15 mL Falcon tube. Slurry was centrifuged at 4,000 rpm for 2 min, and the ethanol was decanted and the beads resuspended in 4 mL of lysis buffer. The tube was shaken for 2 min, centrifuged for 2 min, and decanted and rinsed with lysis buffer two more times. The cell lysate was added to the Ni-NTA beads and the beads were resuspended and rotated on a nutating mixer at 4ºC for 0.5-1.5 hrs. The beads were then transferred to a 30 mL propylene column and the initial flow through was collected. The column was washed, with the elutions collected, as follows: 20 mL wash 1: 50 mM potassium phosphate (pH 7.8), 150 mM NaCl, 10 mM imidazole; 15 mL wash 2: 50 mM potassium phosphate (pH 7.8), 150 mM NaCl, 50 rnM imidazole; 1 ml elution 1: 50 mM potassium phosphate (pH 7.8), 150 mM NaCl, 250 mM imidazole; 1 mL elution 2: 50 mM potassium phosphate (pH 7.8), 150 mM NaCl, 500 mM imidazole; 1 mL elution 3: 50 mM potassium phosphate (pH 7.8), 150 mM NaCl, 1,000 mM imidazole. A 12% PAGE gel was run

for each fraction to determine which fraction contained the majority of the protein. 10 µl of each fraction was mixed with 10 µl of SDS loading dye and boiled in a thermocycler on the boil cycle for 10 min at 95ºC. 15 µl were loaded onto a 12% SDS-PAGE gel and run for 40 min at 220 V, 60 mA. The resulting gel was stained with Coomassie blue 30 min, then destained [40% methanol, 10% glacial acetic acid]. Fractions with protein were dialyzed against 1 L of cold storage buffer (50 mM HEPES / 10 mM $MgCl_2$). The concentration of the protein was verified by a NanoDrop 2000c spectrophotometer. 50 µl aliquots of RtcB protein was flash frozen in liquid nitrogen and stored in a -80ºC freezer.

5.4.3. DNAzyme Design

Two DNAzymes were adopted from the literature[29-30] for our study. These were selected because of either relatively rapid catalysis or good activity at low Mg^{2+} concentration. The first DNAzyme (Dz_1), DT-99, has 9 nt binding arms and is active against HPV, with a k_{obs} of 0.21 min^{-1} at 10 mM Mg^{2+}.[29] The sequence is 5'-GTTTCTCTAGGCTAGCTACAACGAGTGTTCTTG-3', with the catalytic core underlined. The second DNAzyme also has 9 nt binding arms and is active against the VEGF receptor, at 0.01 mM Mg^{2+}.[30] The sequence is 5'-TGCTCTCCA GGCTAGCTACAACGACCTGCACCT-3'.

5.4.4. Designing Construct 3

In order to confirm splicing on another platform, a 5'-FAM-labeled 67 nt synthetic DNA / RNA hybrid was ordered from IDT as shown ("r" indicates ribonucleotides): 5'-AGACGAGTCTCACGr*CrArArGrArArCrArC***rGrU***rArGrArGrArArArC*rArGrGrUrGrCrArGrG **rGrU**rGrGrArGrArGrCrAGTCGTGAGACTCGTC-3'. This sequence contained a DNA stem-loop and the recognition sites for both the DT-99 (italicized) and VEGFR DNAzymes (underlined) described previously, allowing the removal of a 19-bp intron. Cleavage sites for each DNAzyme are in bold (see Table S2, ***3***).

5.4.5. Synthesis of Gold Nanoparticles

Citrate-stabilized gold nanoparticles of 13.1 ± 1.9 nm were made using the Turkevich method as described by the Mirkin lab.[32] Briefly, all glassware to be used was washed with aqua regia and rinsed with Nanopure water. First, 300 ml of 1 mM hydrogen tetrochloroaurate (III) trihydrate was prepared with Nanopure water in a three-prong 500-ml round-bottom flask. The flask was boiled with condenser attached until reflux was achieved at 1 drip / sec, stirring continuously. In a 50 mL Falcon tube, 30 ml of 38.8 mM sodium citrate tribasic dehydrate was prepared with Nanopure water. The sodium citrate was quickly dumped into the refluxing solution. The flask was re-sealed and refluxed for 15 min. The solution rapidly changed color: yellow to black, to purple to deep red. The reaction was taken off the heat and cooled to room temperature (~2-4 hrs). The particles were filtered through a 0.45-μm acetate filter, producing monodisperse AuNPs, and transferred into a clean flask. The absorbance of the particles was verified by a Nanodrop 2000c spectrophotometer. Correctly synthesized 13 nm particles should have a λ_{max} of ~519 nm and a peak width of ~50 nm.

5.4.6. Preparation of DNAzyme-Functionalized Gold Nanoparticles (Dz_1Dz_2NPs)

To prepare maximally packed Dz_1Dz_2NPs, we followed previous protocols.[18, 32-33] Briefly, the 3'-thiolated T_{10}-linker DNAzymes were first ordered from Integrated DNA Technologies (IDT). Their sequences are as follows: for the DT-99 DNAzyme: GTT TCT CTA GGC TAG CTA CAA CGAGTG TTC TTGTTTTTTTTTT/3ThioMC3-D/, and for the VEGFR DNAzyme: TGC TCT CCA GGC TAG CTA CAA CGA CCT GCA CCT TTTTTTTTTT/3ThioMC3-D/. Next, 60 nmol of each DNAzyme were reduced in 1 ml of 0.1 M DTT in disulfide cleavage buffer [170 mM phosphate buffer (pH = 8.0)] and allowed to incubate at room temperature for 2 hrs with occasional vortexing. A Nap-25 column (GE Healthcare) was flushed with four column volumes of Nanopure water. 1 ml of reduced sample was applied to the column and allowed to flow through completely. Then, 1.5 ml of Nanopure water was allowed to enter the column completely. Samples were eluted with 2.5 ml Nanopure water, collecting 4 drops at a time in microcentrifuge

tubes. Tubes were Nanodropped and fractions with DNAzymes were combined. The volume of the sample was recorded and DNAzymes concentrations were determined from UV absorbance. To each 1 ml of AuNPs, 2 nmol of each of the reduced DNAzymes were added in a cleaned EPA vial (4 nmol total DNAzymes). The vial was wrapped in foil and allowed to equilibrate on an orbital shaker overnight at room temperature. The following day, phosphate adjustment buffer [100 mM phosphate buffer (pH 7.0)] was added to the Dz_1Dz_2NPs to 9 mM final phosphate concentration. SDS was added to ~0.1% (wt/vol). The tubes were wrapped in foil and incubated on an orbital shaker for 30 min at room temperature. Afterward, NaCl was added to the Dz_1Dz_2NPs with salting buffer [10 mM phosphate buffer (pH 7.0), 2M NaCl] in eight increments of final concentration as follows: 0.05 , 0.1, 0.2, 0.3, 0.4, 0.5, 0.6 and 0.7 M. After each addition, the Dz_1Dz_2NPs were sonicated in a bath sonicator (VWR 97043-968) 20-30 sec, wrapped in foil and incubated on an orbital shaker 20 min. Salt additions were continued until 0.7 M NaCl was reached. Dz_1Dz_2NPs were stored in 4ºC cold room until use.

5.4.7. Dz_1Dz_2NP Washing Procedure

In an Eppendorf tube, 1 mL of Dz_1Dz_2NPs were spun down in a table top centrifuge at 13,000 rpm 4ºC. Supernatant was removed by pipetting and the pellet was resuspended in 500 µl of Nanopure water, with $\leq$ 1 min sonication. The wash was repeated two more times and the pellet resuspended in the desired volume and buffer. Sonication is only necessary for the first resuspension.

5.4.8. DNAzyme-Functionalized Gold Nanoparticle Splicing Assay

To test whether or not Dz_1Dz_2NPs plus soluble RtcB were active for splicing (Fig. 5.3), 20 µl reactions were setup with either gold conjugates containing both DNAzymes, or single DNAzyme gold particles mixed as follows: 50 mM Tris-HCl (pH 7.4 at 37˚C), 1.5 mM $MnCl_2$,150 mM NaCl, 9.09 nM DNAzyme-conjugates (each conjugate) 0.4 µM 5'-FAM labeled stem-loop RNA (see SI). This reaction was incubated in a water bath at 37˚C for 2 hours, after which 2.2 µM RtcB and 0.4 mM GTP were added, and the reaction continued for another 1 hr. After

incubation, 10 µl samples were quenched in stop solution (5 µl 95% formamide, 10 mM EDTA and 5 µl Ultrapure water (Invitrogen)). Samples were run on a 15% polyacrylamide gel electrophoresis (PAGE) in 1x Tris-borate EDTA (TBE) buffer pre-heated to 70˚C for 30 min. PAGE gel was imaged on a Typhoon TRIO Variable Mode Imager (Amersham Biosciences) at 600 PMT.

5.4.9. Denaturing RNA Polyacrylamide Gel Electrophoresis

RNA reactions were imaged on 8%, 10% or 15% polyacrylamide electrophoresis gels (PAGE) using a Mini-PROTEAN Tetra Cell (Bio-rad). To prepare a 15% gel, the following recipe was used (10 ml): 4.2 g urea, 1 ml 1x TBE, 5 ml 37.5:1 acrylamide/bis solution (#1610158, Bio-rad), 3.5 µl TEMED, 70 µl 10% APS. The ingredients were mixed except for TEMED and APS and allowed to dissolve, with stirring. The gel solution was filtered through a 0.20 µm filter (if the gel was being stained with SYBR gold or Diamond stain). Upon addition of TEMED and APS, the solution was mixed by stirring for 10 s and poured, setting for 45 min or until use. Gel plates were prepared by washing with antibacterial soap, rinsing in Nanopure water, and RNase zapped (Ambion) 5 min. They were then rinsed with regular water, Nanopure water and 100% ethanol and sonicated in isopropanol for 7 min. After sonication, the gel plates were rinsed in 100% ethanol and allowed to dry in a dust free area. To avoid leaking, plates were prepared with a thin layer of halocarbon grease on the sides and the bottom of the gel was parafilmed before pouring. Combs were RNase zapped for 5 min and rinsed in regular, then Nanopure water.

5.4.10. TEM Imaging of DzNPs and nanozymes

Samples were prepared by depositing 5 µl of 11 nM AuNPs, washed Dz_1Dz_2NPs or washed nanozymes, onto a carbon film 200 mesh copper grid (CF200-Cu, lot #150318, Electron Microscopy Sciences). Samples were then allowed to sit 5 min and excess liquid was wicked away with a tip of filter paper. Samples were imaged on a JEOL JEM-1210 transmission

electron microscope. The extinction coefficient was estimated from the particle diameter and used to determine particle concentrations by a NanoDrop 2000C spectrophotometer.

5.4.11. Measurement of Dz_1Dz_2NP Activity

Activity of Dz_1Dz_2NPs was determined through digestion of a fluorescein labeled RNA / DNA hybrid substrate (construct ***3***), as follows ("r" indicates ribonucleotides): 5'-FAM-AGACGAGTCTCACG*rCrArArGrArArCrArC***rG*rU***rArG *rArGrArArArC*rArGrGrUrGrCrArGrG**rGrU**rGrGrArGrArGrCrAGTCGTGAGACTCGTC-3'. DNAzyme cleavage sites are in bold. Dz_1 recognition site is italicized. Dz_2 recognition site is underlined. Each digest was run on a 15% RNA polyacrylamide gel as described and imaged on a Typhoon TRIO Variable Mode Imager. Cleavage products were estimated in size compared to a ladder. Band intensity was determined using ImageJ, and percent cleavage products determined as indicated (Fig. 5.S6).

5.4.12. Calculation of DNAzymes per AuNP

The number of DNAzymes per AuNP was approximated using the Quant-iT™ OliGreen® ssDNA Reagent and Kit (ThermoFisher, Grand Island, NY), after releasing the DNAzymes from the gold core. Briefly, 100 µl of DzNPs were aliquoted in 0.2, 0.4, 0.6 and 0.8 nM amounts in TE buffer (10 mM Tris-HCl, 1 mM EDTA, pH 7.5), and the gold core dissolved with 1 µl of 5 M potassium cyanide (KCN), that was added to each well. Note that KCN is hazardous and must be kept away from acid to avoid producing noxious cyanide fumes. It should be used in the hood and disposed of separately. A well with TE buffer but no DzNPs served as the control. The AuNP core was allowed to dissolve for 30 min, releasing the DNAzymes. An equal volume (100 µl) of 1x OliGreen reagent made up in TE buffer was added to each well and pipetted up and down to mix. The resulting wells were imaged immediately on a Bio-Tek Synergy HT plate reader with an approximately 2 min lag time. The fluorescence intensity at 485/528 nm excitation/emission were compared to a standard curve of soluble DNAzymes. This standard curve was produced by diluting a stock of each DNAzyme (4 µg/ml) to known concentrations

(0.1, 0.2, 0.5, 0.75, 1, and 2 µg/mL) in 100 µl of TE buffer. After adding 1x OliGreen reagent, fluorescence intensities at each concentration were measured and plotted. Using this plot, the fluorescence intensity corresponding to the number of DNAzymes per well could be determined and this number was divided by the AuNP concentration to approximate the number of DNAzymes per NP.

5.4.13. Nanozyme Synthesis

Salted Dz_1Dz_2NPs (1 mL) were washed as follows: The NPs were spun down at 13,000 rpm (15,871 g) for 20 min and resuspended in 500 µl Nanopure water. Afterward, they were sonicated in a bath sonicator 1 min, vortexed and spun down as above. This wash was repeated three more times. After the second wash, Dz_1Dz_2NPs were resuspended in 500 µl of 100 mM Tris-HCl pH 7.43 at 37ºC rather than Nanopure water. Sonication is not necessary after the first wash. After the final wash, the Dz_1Dz_2NPs were resuspended in 100 mM Tris-HCl pH 7.43 at 37ºC up to 100 µl total volume. They were then incubated with 20 µl of 28.3 µM cysteine-modified RtcB to a final concentration of 4.72 µM, and allowed to incubate at 4ºC overnight. The following day, the nanozymes were spun down 13,000 rpm (15,871 g) in a microcentrifuge 20 min at 4ºC and the supernatant was pipetted off. The particles were resuspended in 500 µl 100 mM Tris-HCl buffer, pH 7.43 at 37ºC. This wash was repeated two more times. Note: Never sonicate the nanozymes. Pipetting up and down should be sufficient to resuspend. If the pellet does not resuspend, attempt to break it up with a pipette tip, wait 20 sec, then gently pipette up and down again.

5.4.14. Measurement of RtcB on Nanozyme Conjugates

To 100 µl of 50.5 µM RtcB-Cys in 1x PBS, 0.1 mg of dried Alexa488 was added and allowed to react 2.5 hrs on ice. The resulting mixture was run through a P4 gel in 1x PBS. The degree of labeling (DOL) was calculated with the equation DOL = $\frac{A_{max} \times MW}{[protein] \times \varepsilon_{dye}}$, where MW = the molecular weight of the protein, ε_{dye} = the extinction coefficient of the dye at its absorbance

maximum 488 nm, and the protein concentration is in mg/mL. Dz_1Dz_2NPs (1 mL) were washed as previously described, and resuspended in 100 µl of PBS (30 µl Nanopure, 70 µl 1x PBS). To this sample, 13.6 µl of 41.8 µM (DOL=1.4) Alexa488-RtcB-Cys was added and allowed to incubate overnight at 4ºC. The Dz_1Dz_2NP-Alexa488-RtcB-Cys in 100 mM Tris-HCl (pH 7.43 at 37ºC) was washed three times by first voluming the sample to 500 µl, spinning down at 13,000 rpm in a table top centrifuge, removing the supernatant and repeating twice more. After the last removal of the supernatant, 40 µl 100 mM Tris-HCl were added and the sample absorbance at 520 nm was measured with a NanoDrop 2000c spectrophotometer. Next, 5 µl of 5 M potassium cyanide (KCN) was added to a final volume of 52 µl and incubated on ice 45 min. The sample was volumed to 100 µl in 100 mM Tris-HCl. Additionally, a standard curve was then aliquoted of Alexa488-RtcB-Cys in 0, 10, 50, 100, 200 and 400 nM concentrations. The fluorescence emission of Alexa488-RtcB-Cys samples was measured in a Horiba Scientific Dual-FL fluorometer with 10 accumulations. The data was plotted in Excel and the emission at 488 nm for each sample was recorded. Using the standard curve, the average number of RtcB on each Dz_1Dz_2NP was calculated.

5.4.15. Dynamic Light Scattering and Zeta Potential of Dz_1Dz_2NPs and nanozymes

Dynamic light scattering and zeta potential experiments were performed on a NanoPlus zeta/nano particle analyzer. For DLS, Dz_1Dz_2NPs and nanozymes were synthesized as described, washed 3 times in 100 mM Tris-HCl buffer, pH 7.43 at 37ºC, and 60 µl samples were run at room temperature using 150 accumulations. Samples were kept on ice until collecting the DLS spectrum. The same procedure was used to collect zeta potential measurements, except nanozymes were created in 1x PBS buffer and washed in 10 mM Tris-HCl, pH 7.43 at 37ºC as described, and 150 µl sample was measured.

5.5. Author Contributions and Acknowledgements

Author Contributions

J.P. and K.S. were responsible for writing this manuscript. J.P., K.S. and K.Y. discussed experiments and controls. J.P. performed experiments. K.G. expressed RtcB-Cys shown in Figure 5.5f. B.D. performed flow cytometry on Dz1Dz2NPs and nanozymes shown in Figure 5.S17. R.G. performed FLIM on nanozymes shown in Figure 5.S14. All authors have given approval to the final version of the manuscript.

Acknowledgements

K.S. would like to thank the NIH (R01-GM097399) and the NSF CAREER Award (1350829) for financial support. J.P. would like to thank the ARCS Foundation and S. and F. Burke for their generous support. R.G. would like to thank NIH (NIGMS GM124472) and the NSF Fellowship for financial support. J.P. and K.S. would like to thank K. Desai and R. Raines for the gift of the RtcB-lacI plasmid. We thank O. Laur for technical expertise in construction and synthesis of plasmid constructs. We thank K. Yehl, E. Weinert and G. Conn for helpful discussions about the data. We thank V. Ma for production of the cy3b-labeled construct for nanozyme cell uptake experiments. We thank H. Su, B. Deal and N. Baker for assistance with nanozyme uptake experiment and flow cytometry. We thank G. Raghunath for assistance with DLS and zeta potential measurements. We thank J. Brockman for production of particle construct size histograms using MatLab. We thank S. Druzak for technical expertise during the early stages of this project. We acknowledge the work of I. Bolin, G. Thomsen, B. Bohannon and Z. Mousavi – students trained during this work. We thank K. Clarke, V. Ma and B. Fontaine for critical reading of the manuscript.

5.6. Supplementary Materials and Methods

5.6.1. Generating construct 6 (Fig. 5.3)

i. **Designing construct *6*.** To produce stem-loop RNA ***6***, a 95 bp stem-loop RNA was designed retaining the stem loop from $tRNA^{Glu}$, and adding the recognition sites of Dz_1 and Dz_2 to form a 42 nt single-stranded loop region that can be spliced by the removal of a 20 nt intron segment. The cDNA sequence with an attached 3' T7 promoter (underlined) was custom synthesized by Integrated DNA Technologies (IDT) as an Ultramer oligo, as follows: 5'-TGGCTCCGATATCACGCTTACTGCTCTCCACCCTGCA CCTGGTTTCTCTACGTGTTCTTGCGTGATATCGGAGCCAGATCAGTCGATACATCA GGTATAGTGAGTCGTATTAA-3' (see Table 2, cDNA ***6***).

ii. **Transcription of construct *6*.** To produce stem-loop RNA ***6*** for *in vitro* splicing experiments as shown in Figure 3, the 95 bp RNA was transcribed using the AmpliScribe T7-flash kit (Epicentre, Madison, WI). Briefly, the following 20 µl reaction was setup: 1 µg cDNA, 1.43 µg promoter, 2 µl 10x reaction buffer, 1.8 µl 100 mM ATP, CTP, GTP and UTP, 2 µl 100 mM DTT, 0.5 µl RiboGuard RNase inhibitor, 2 µl enzyme solution. The reaction was incubated at 42˚C for 2 hrs. Afterward, 1 µl DNase I was added and incubated at 37˚C for 1 – 2 hrs. RNA was purified from the reaction using a spin column from the RNA clean and concentrator-25 kit (Zymo Research, Irvine, CA). RNA was stored at -80ºC until needed.

iii. **RNA 5'-end FAM labeling of construct *6*.** After *in vitro* transcription, the stem-loop RNA was 5'-end labeled with a fluorescein using a previous published protocol.[3] Briefly, the RNA was dephosphorylated with 3 units of recombinant shrimp alkaline phosphatase (rSAP) from NEB in a 50 µl reaction using rSAP reaction buffer (20 mM Tris-HCl, 10 mM $MgCl_2$, pH 8 @ 25˚C) at 37ºC for 2 hours. Afterwards, the following were added: 1 µl 26 mM ATPγS, 5 µl T4 polynucleotide kinase (PNK) 10x reaction buffer (70 mM Tris-HCl,

10 mM $MgCl_2$, 5 mM DTT pH 7.6 @ 25ºC), 2.5 µl 100 mM DTT and 40 units of T4 PNK. This reaction was further incubated at 37ºC overnight. The reaction was then ethanol precipitated (1 µl 5 mg/ml LPA, 0.01 M $MgCl_2$, 0.3 M sodium acetate, 200 µl ethanol), resuspended in 50 µl 25 mM HEPES pH 7.44 and quantified on a Nanodrop 2000c spectrophotometer. Subsequently, 7.5 µl of 10 mM of 5-IAF suspended in DMSO was added and the reaction incubated in the dark for 2 hrs. The reaction was ethanol precipitated twice to remove excess 5-IAF. If additional purification was required, it was run through a NucAway™ Spin Column (ThermoFisher, Grand Island, NY) and stored at -80ºC.

5.6.2. Nanozyme uptake into MDA-MB-231 cells

An experiment was performed to determine whether complete nanozymes could enter a model mammalian cell line (MDA-MB-231). Nanozymes and Dz_1Dz_2NPs were synthesized as previously described. The thiolated-oligonucleotides added per 1 mL AuNPs were as follows: 1 nmol of a Cy3b-labeled strand (see Table S2, ***9***), 1.5 nmol Dz_1 and 1.5 nmol Dz_2. MDA-MB-231 cells were plated in a 24-well plate 50,000 cells per well in 500 µl of DMEM + 10% FBS, 2% L-glutamine and 1% penicillin-streptomycin and grown for 24 hrs at 37ºC, 5% CO_2. Afterward, 5.6 nM of washed Cy3b-labeled Dz_1Dz_2NPs and 6.2 nM of Cy3b-labeled nanozyme were added to a total volume of 300 µl media (see above) and added to 3 wells and 1 well of MDA-MB-231 cells, respectively. (Note: Both were washed in 1x PBS. The nanozymes were only washed 1 time, to remove excess RtcB-Cys). The cells were then incubated for 24 hrs at 37ºC, 5% CO_2. After the incubation period, the cells were washed with 500 µl 1x PBS and trypsonized (300 µL) (Gibco, ThermoFisher Scientific) for 5 min at 37ºC, 5% CO_2. Afterward, 700 µl media was added to the wells and the cells were spun down at 300 g for 5 min in a tabletop centrifuge and washed two times with 1 mL 1x PBS. The cells were then transported on ice and 10,000 cells were measured for each sample

on a BD LSR II flow cytometer. Triplicate cells without exposure to NPs were measured as a control.

5.6.3. Fluorescence lifetime imaging of nanozymes

Specific binding of RTCB to AuNPs through gold-thiol interaction was validated using fluorescence lifetime imaging microscopy (FLIM). Alexa 488 is quenched by near surface energy transfer (NSET) when in close proximity to AuNPs. This effect causes a decrease in fluorescence lifetime. Therefore, we hypothesized that Alexa 488-labeled RtcB bound to AuNPs would have a shorter average fluorescence lifetime than Alexa 488-labeled RtcB in solution. RtcB with and without N-terminal cysteine residues was labeled nonspecifically using Alexa 488 NHS ester, incubated on ice for 2 hrs. Excess dye was removed with a P4 gel. RtcB-Cys-488 and RtcB-His-488 was added to AuNPs at 4.27 µM concentration and incubated overnight at 4ºC. Excess RtcB was rinsed away in four consecutive washes, leaving an estimated 0.07 nM soluble RtcB. The fluorescence lifetime was measured in the presence and in the absence of AuNPs.

Fluorescence lifetime measurements were performed on a Nikon Ti Eclipse Inverted confocal microscope with a Picoquant Laser Scanning Microscope Time Correlated Single Photon Counting Upgrade. Samples were imaged using a 20 MHz pulsed 514 nm laser, and the average fluorescence lifetime was calculated according to the Fast FLIM algorithm in SymphoTime 64. The IRF was collected using quenched Erythrosine B in saturated potassium iodide. Data is reported as the average of three measurements. Representative normalized decay curves were plotted for regions of interest containing ~10^5 photons in the peak.

SI Table 5.1: DNAzymes used in this study

**Conditions for Tm analysis (0.4 µM oligo, 150 mM Na^+, 2 mM Mg^{2+}, 0.4 mM NTP)*
r=ribonucleotide, red=catalytic core, NS=non-specific

ID	Sequence (5'-3')	5' T_m(ºC)	3' T_m(ºC)	Both T_m(ºC)
Dz1, 9/9	GTTTCTCTAGGCTAGCTACAACGAGTGTTCTTG	24.4	30.5	54.6
Dz1, 8/8	TTTCTCTAGGCTAGCTACAACGAGTGTTCTT	14.9	22.5	50.6
Dz2, 9/9	TGCTCTCCAGGCTAGCTACAACGACCTGCACCT	38.3	41.7	68.1
Dz2, 8/8	GCTCTCCAGGCTAGCTACAACGACCTGCACC	31.9	36.7	64.6
Dz2, 7/7	CTCTCCAGGCTAGCTACAACGACCTGCAC	18.3	27.0	57.6
Dz_{NS}	GTGGATGGAGGCTAGCTACAACGAGTCTTGGAG	35.4	32.9	61.2
Dz1, NP	GTTTCTCTAGGCTAGCTACAACGAGTGTTCTTG TTTTTTTTTT/3ThioMC3-D/			
Dz2, NP	TGCTCTCCAGGCTAGCTACAACGACCTGCACCT TTTTTTTTTT/3ThioMC3-D/			
Dz_{NS}, NP	GTGGATGGAGGCTAGCTACAACGAGTCTTGGAG TTTTTTTTTT/3ThioMC3-D/			

SI Table 5.2: Constructs used in this study

Construct	Strand Designation	Sequence (5'-3')
1	5'	FAM/rUrGrGrCrUrCrCrGrArUrArUrCrArCrGrCrUrU/3Phos/
1	3', 7 nt loop	rUrCrArCrCrGrUrGrArUrArUrCrGrGrArGrCrCrA
1	3', 15 nt loop	rUrCrArCrArCrArCrCrArUrArUrArUrCrGrGrArGrCrCrA
1	3', 19 nt loop	rUrCrArCrUrCrArCrArCrArCrCrArUrArUrArUrCrGrGrArGrCrCrA
1	3', 11 nt loop	rUrGrGrArGrArGrCrArGrUrArArGrCrGrUrGrArUrArUrCrGrGrArGrCrCrA
3	substrate	FAM/AGACGAGTCTCACGrCrArArGrGrArArCrArCrGrUrArGrArGrArArArC rArGrGrUrGrCrArGrGrGrUrGrGrArGrArArGrCrA GTCGTGAGACTCGTC
4	5' cleaved	FAM/AGACGAGTCTCACGrCrArArGrGrArArCrArCrG>P

4	3’ cleaved	**rU**rGrGrArGrArGrCrAGTCGTGAGACTCGTC
5	spliced	FAM/AGACGAGTCTCACGrCrArArGrArArCrArCrGrUrGrGrArGrArGrCrA GTCGTGAGACTCGTC
6	cDNA	TGGCTCCGATATCACGCTTACTGCTCTCCACCCTGCACCTGGTT TCTCTACGTGTTCTTGCGTGATATCGGAGCCAGATCAGTCGATACA TCAGGTATAGTGAGTCGTATTAA
6	substrate	FAM/rCrCrUrGrArUrGrUrArUrCrGrArCrUrGrArUrCrUrGrGrCrUrCrCrGrA rUrArUrCrArCrGrCrArArGrArArCrArC**rGrU**rArGrArGrArArArCrCrArGrG rUrGrCrArGrG**rGrU**rGrGrArGrArArGrCrArGrUrArArGrCrGrUrGrArUrArUrC rGrGrArGrCrCrA
7	5’, cleaved	FAM/rCrCrUrGrArUrGrUrArUrCrGrArCrUrGrArUrCrUrGrGrCrUrCrCrGrA rUrArUrCrArCrGrCrArArGrArArCrArC**rG**>P
7	3’, cleaved	**rU**rGrGrArGrArGrCrArGrUrArArGrCrGrUrGrArUrArUrCrGrGrArGrCrCrA
8	spliced	FAM/rCrCrUrGrArUrGrUrArUrCrGrArCrUrGrArUrCrUrGrGrCrUrCrCrGrA rUrArUrCrArCrGrCrArArGrArArCrArCrGrUrGrGrArGrArGrCrArGrUrArA rGrCrGrUrGrArUrArUrCrGrGrArGrCrCrA
9	Cy3b-labeled strand	/5ThioMC6-D/TTTTTTTTTTAAAGTGAAATACCGCACAGATGCG/3AmMO/Cy3b
10	pre-cleaved substrate 5’	FAM/AGACGAGTCTCACGrCrArArGrArArCrArC**rG**-P
11	pre-cleaved substrate 3’	**rU**rGrGrArGrArGrCrAGTCGTGAGACTCGTC
12	non-specific T10 DNA	TTTTTTTTTT/3ThioMC3-D/
13	non-specific T20 DNA	TTTTTTTTTTTTTTTTTTTT/3ThioMC3-D/

*******Bolded sequences are the recognition sites of Dz_1 and Dz_2, respectively. r=ribonucleotide, FAM=5’6’-carboxyfluorescein, >P=2’-3’ cyclic phosphate, underlining=stem-loop, orange=Dz_1 recognition site, blue=Dz_2 recognition site, green=T7 promoter*

5.6.4. Sequence of E.coli RtcB-Cys used in this study (Accession #P46850)

5’-
ATGCACCATCATCATCACCATTGTTGCGGTAATTACGAATTACTGACCACTGAAAATGCCCC
GGTAAAAATGTGGACCAAAGGCGTGCCGGTAGAGGCCGATGCGCGTCAGCAACTTATTAA
TACGGCGAAGATGCCGTTTATTTTCAAACATATTGCGGTAATGCCTGATGTACACCTGGGT
AAAGGTTCCACCATTGGTAGCGTGATCCCGACCAAAGGGGCGATTATTCCGGCGGCGGTG
GGCGTGGATATTGGCTGTGGAATGAACGCGCTGCGTACCGCGTTAACGGCGGAAGACCT
GCCTGAAAACCTGGCAGAGCTGCGTCAGGCGATTGAAACGGCCGTGCCGCACGGGCGTA
CCACTGGCCGTTGTAAACGTGATAAAGGTGCCTGGGAAAATCCACCTGTTAACGTCGATGC
TAAATGGGCTGAGCTTGAAGCCGGTTATCAGTGGTTAACGCAAAAATATCCCCGTTTCCTG
AATACCAATAACTATAAACACCTGGGAACGCTGGGAACCGGTAACCACTTTATTGAAATCT
GCCTTGATGAGTCGGACCAGGTGTGGATTATGCTGCACTCCGGTTCACGCGGAATTGGTA
ACGCCATCGGGACTTACTTTATCGATCTGGCACAAAAAGAGATGCAGGAAACGCTTGAGAC
GTTGCCGTCGCGTGATCTGGCGTACTTTATGGAAGGTACGGAATACTTTGATGATTACCTG
AAAGCCGTGGCCTGGGCGCAGCTTTTTGCCAGCCTTAACCGCGATGCGATGATGGAAAAC
GTGGTAACGGCATTGCAGAGCATTACGCAGAAAACGGTCAGACAGCCACAAACGCTGGCG
ATGGAAGAGATCAACTGTCACCACAACTATGTGCAAAAAGAACAGCACTTTGGTGAAGAGA
TCTACGTGACGCGTAAAGGCGCGGTGTCTGCGCGTGCTGGTCAATATGGAATTATTCCCG
GTTCGATGGGAGCAAAAAGCTTTATCGTCCGTGGGCTGGGAAATGAAGAGTCGTTCTGTTC
GTGCAGCCACGGTGCCGGGCGGGTAATGAGCCGAACTAAAGCGAAAAAACTGTTCAGCGT
GGAAGATCAAATTCGTGCCACCGCGCATGTGGAATGCCGTAAAGATGCCGAAGTGATCGA
CGAAATCCCGATGGCGTATAAAGATATTGATGCGGTGATGGCGGCACAAAGCGATCTGGT
GGAAGTTATCTATACCCTGCGTCAGGTGGTGTGCGTAAAAGGATAA-3’

Note: Blue is the hexahistidine-tag and codons colored red are the two cys residues.

5.7. Supplementary Figures

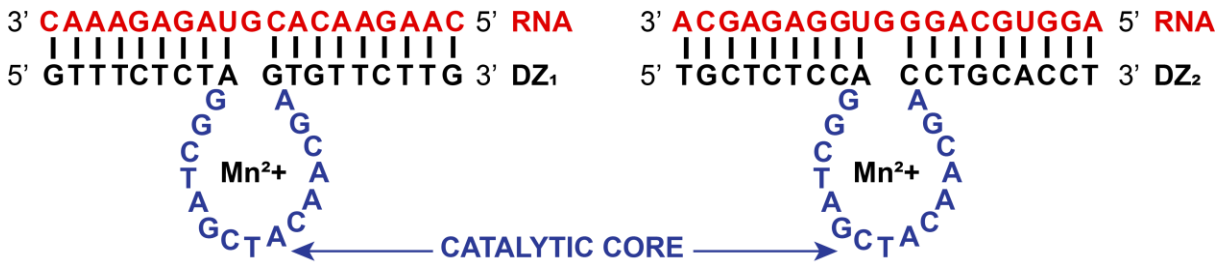

Figure 5.S1. Model DNAzymes used for the splice experiments in this study. Dz_1 was known to have a relatively high k_{cat} (Dz_1)[1] of 0.21 min^{-1} at 10 mM Mg and Dz_2 operates at low Mg^{2+} concentration (0.01 mM).[2] In our studies, we used Mn^{2+} as the metal ion cofactor rather than Mg^{2+}.

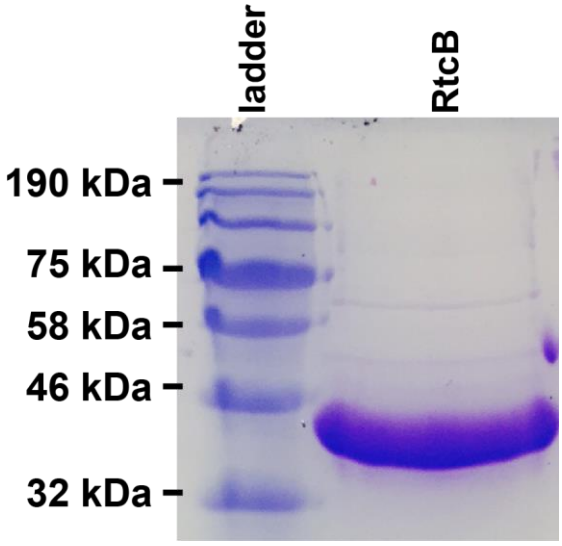

Figure 5.S2. SDS-PAGE of RtcB. RtcB shows up at approximately 45 kDa, which is its expected molecular weight.

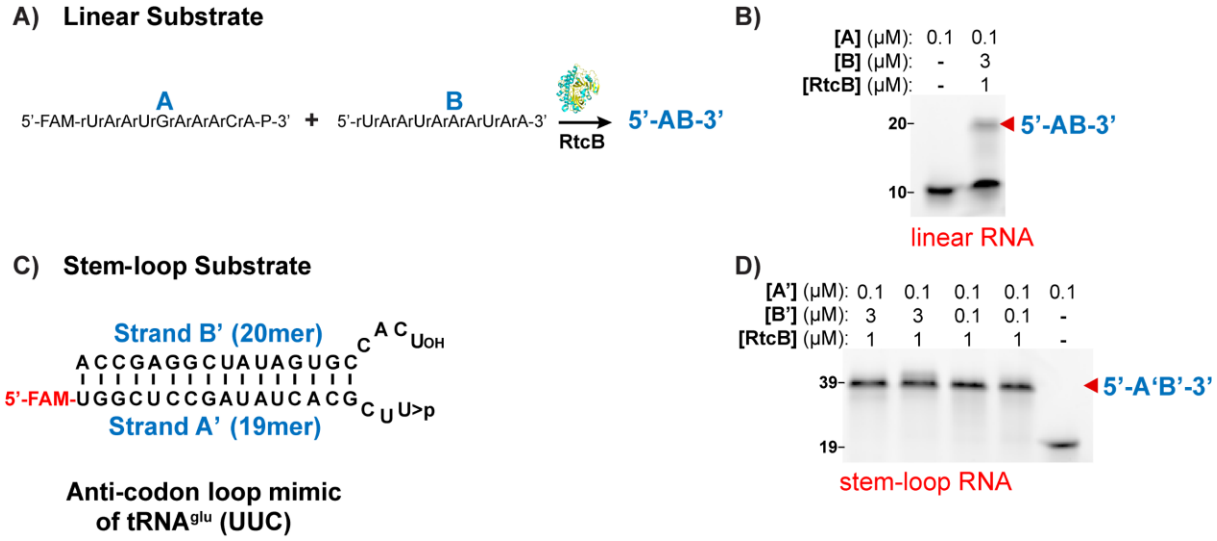

Figure 5.S3. RtcB is active on linear and stem-loop RNA substrates. (A) 5'-FAM labeled linear RNA substrate to test RtcB activity. (B) Gel showing RtcB activity when ligating linear substrate shown in (A). (C) 5'-FAM-labeled stem-loop substrate to test RtcB activity. (D) Gel showing RtcB activity when ligating stem-loop substrate shown in (C). Red arrow indicates ligation product. In addition to substrate and RtcB, reaction lanes contain 150 mM NaCl, 0.1 mM GTP, 1 mM Mn^{2+} and 40 units of RNase inhibitor in 50 mM Tris-HCl, pH 7.43 at 37ºC for 3 hrs.

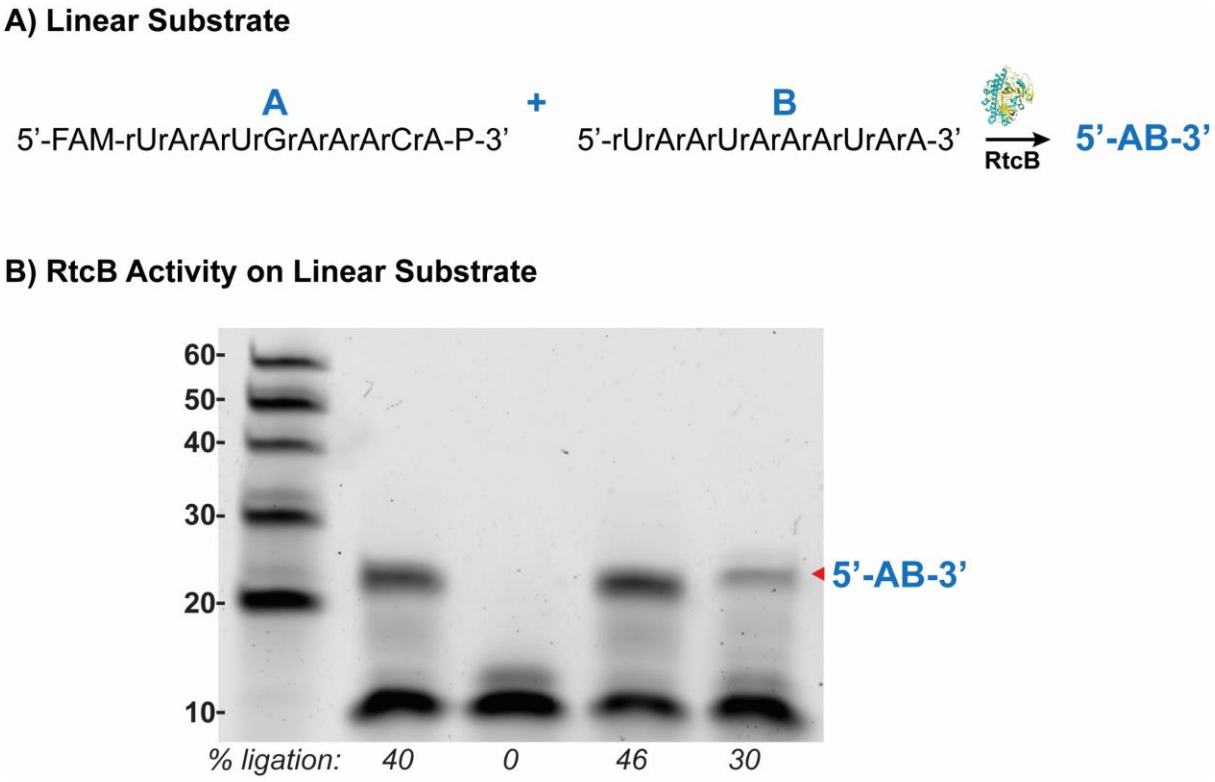

Figure 5.S4. Quantifying RtcB ligation yield on linear 10mer RNA substrates (A) with 3'-P and 5'-OH groups. (B) Gel showing RtcB activity upon ligating linear RNA substrates. Red arrow indicates ligation product. Reaction contained 50 mM Tris-HCl, pH 7.4 at 37ºC, 150 mM NaCl, 100 nM strand A, 3 µM strand B, 40 units RNase inhibitor, 0.4 mM GTP, 1 mM Mn^{2+}, 1 µM RtcB incubated at 37ºC for 4 hrs. Note cyclization of strand A is blocked, since the 5' end is modified with FAM. Also, note that in order to achieve a yield greater than 10%, a significant excess of one strand was needed.

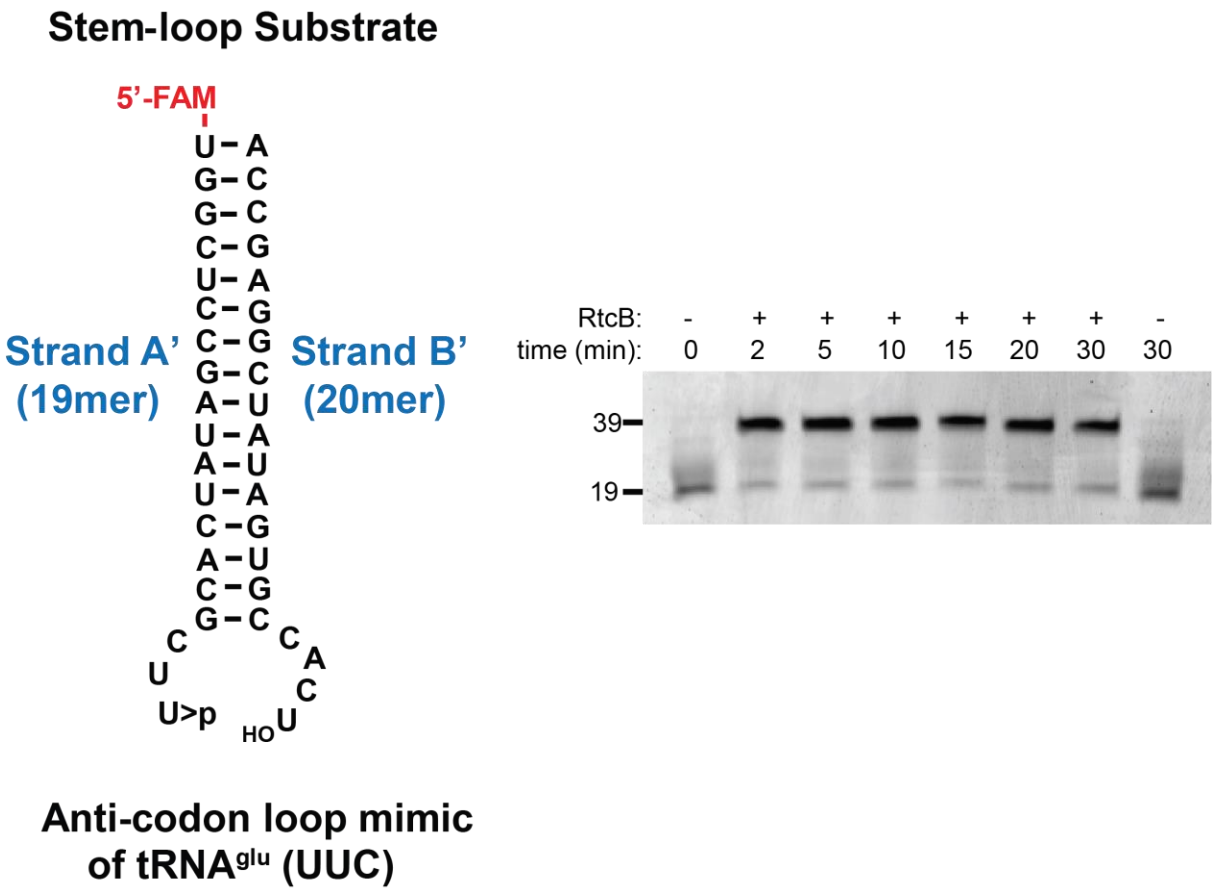

Figure 5.S5. Quantifying RtcB ligation kinetics on stem-loop substrate. A stem-loop 19mer 3'-P RNA (A') and unlabeled 20mer 5'-OH RNA strand (B') were incubated for the indicated amount of time to determine ligation kinetics. Gel shows near complete ligation within 2 min. The reaction included 100 nM each strand, 150 mM NaCl, 1 mM Mn^{2+}, 0.1 mM GTP, 40 units RNase inhibitor and 1 µM RtcB.

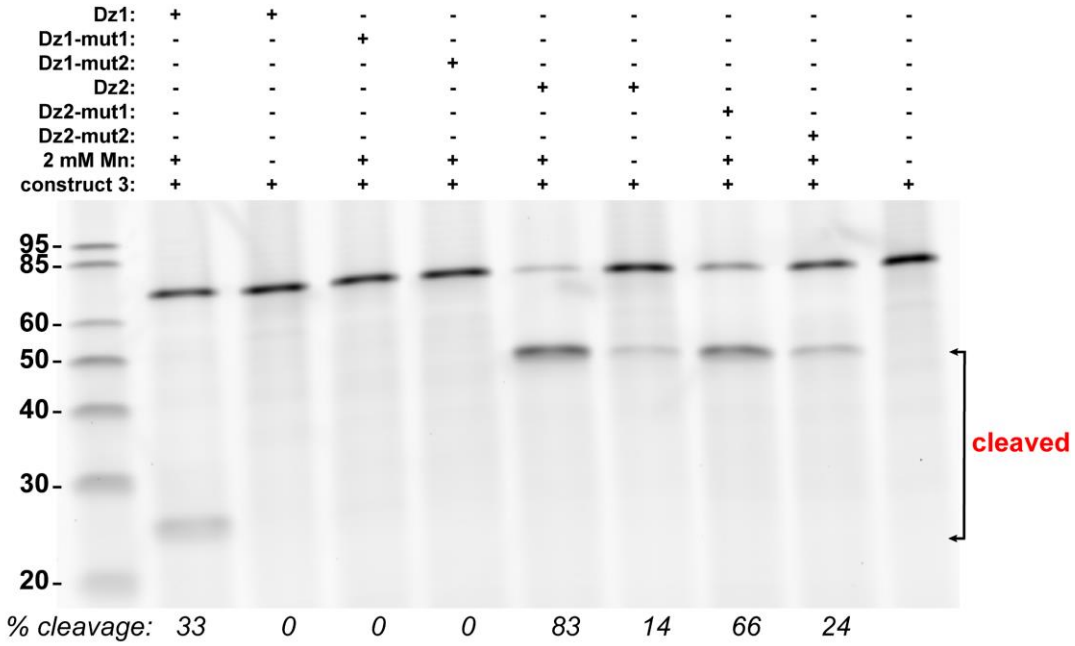

Dz2-mut2: GCTCGCCA GGCTAGCTACAACGA CCTGAACC TTTTTTTTTT/3ThioMC3-D/
T→G C→A

Dz2-mut1: GCTCGCCA GGCTAGCTACAACGA CCTGCACC TTTTTTTTTT/3ThioMC3-D/
T→G

Dz1-mut2: TTTATCTA GGCTAGCTACAACGA GTGGTCTT TTTTTTTTTT/3ThioMC3-D/
C→A T→G

Dz1-mut1: TTTATCTA GGCTAGCTACAACGA GTGTTCTT TTTTTTTTTT/3ThioMC3-D/
C→A

Figure 5.S6. Dz_1NPs and Dz_2NPs with select mutations show lowered activity. Reaction was conducted for 2 hrs at 37ºC in 100 mM Tris-HCl, pH 7.43 at 37ºC, 150 mM NaCl, 2 mM Mn^{2+}. Lane 2: Dz_1NPs; lane 3: Dz_1NPs without Mn^{2+}; lane 4: Dz_1NPs with mutated 5' arm; lane 5: Dz_1NPs with mutated 5' and 3' arms; lane 6: Dz_2NPs; lane 7: Dz_2NPs without Mn^{2+}; lane 8, Dz_2NPs with mutated 5' arm; lane 9, Dz_2NPs with mutated 5' and 3' arms; lane 10: construct 3 only.

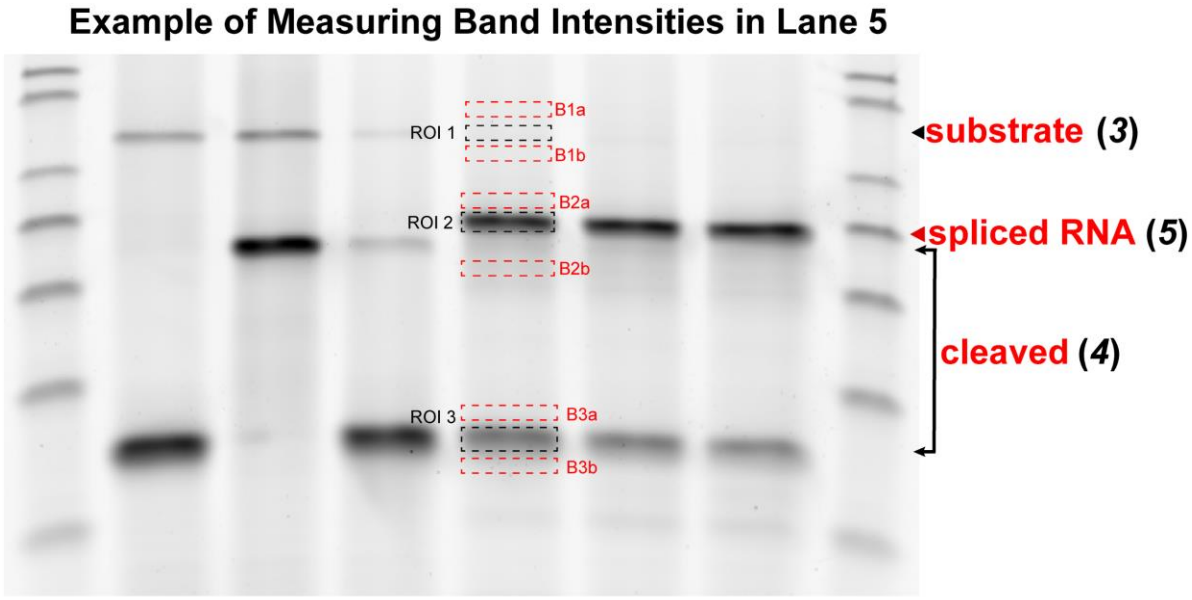

ROI1 Band Intensity = Mean intensity of ROI1 - Mean background intensity ((B1a + B1b) / 2)

$$\% \text{ splice yield} = \frac{ROI2}{ROI1+ROI2+ROI3} \times 100\%$$

Figure 5.S7. Image analysis for calculating percent splicing yield or percent cleavage in each lane. The band intensities are measured in ImageJ and integrated over the measured area. The background intensity was determined by measuring the average intensity of a band above and below the ROI. The ROI intensity was then background subtracted. The splice yield was determined by measuring the splice band ROI and dividing by the intensities of all the bands x 100%. ROI=region of interest, B=background

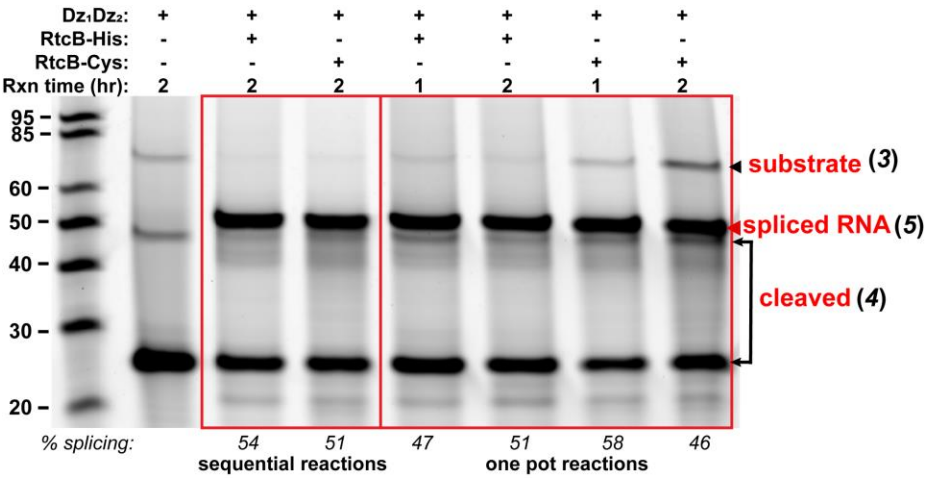

Figure 5.S8. Sequential splicing reactions show similar yield as one-pot splicing. Lane 2: negative control, with soluble Dz(s); lane 3, splicing with RtcB-His; lane 4, splicing with RtcB-Cys; lane 5-6, one pot 1-2 hr reaction with RtcB-His; lane 7-8, one pot 1-2 hr reaction with RtcB-Cys. Red arrow indicates splice product. Reaction contained 50 mM Tris-HCl, pH 7.43 at 37ºC, 150 mM NaCl, 2 mM Mn^{2+}, 0.4 µM splice substrate (see Table S2, ***3***), 0.4 µM each Dz, 0.4 mM GTP, 2.2 µM RtcB.

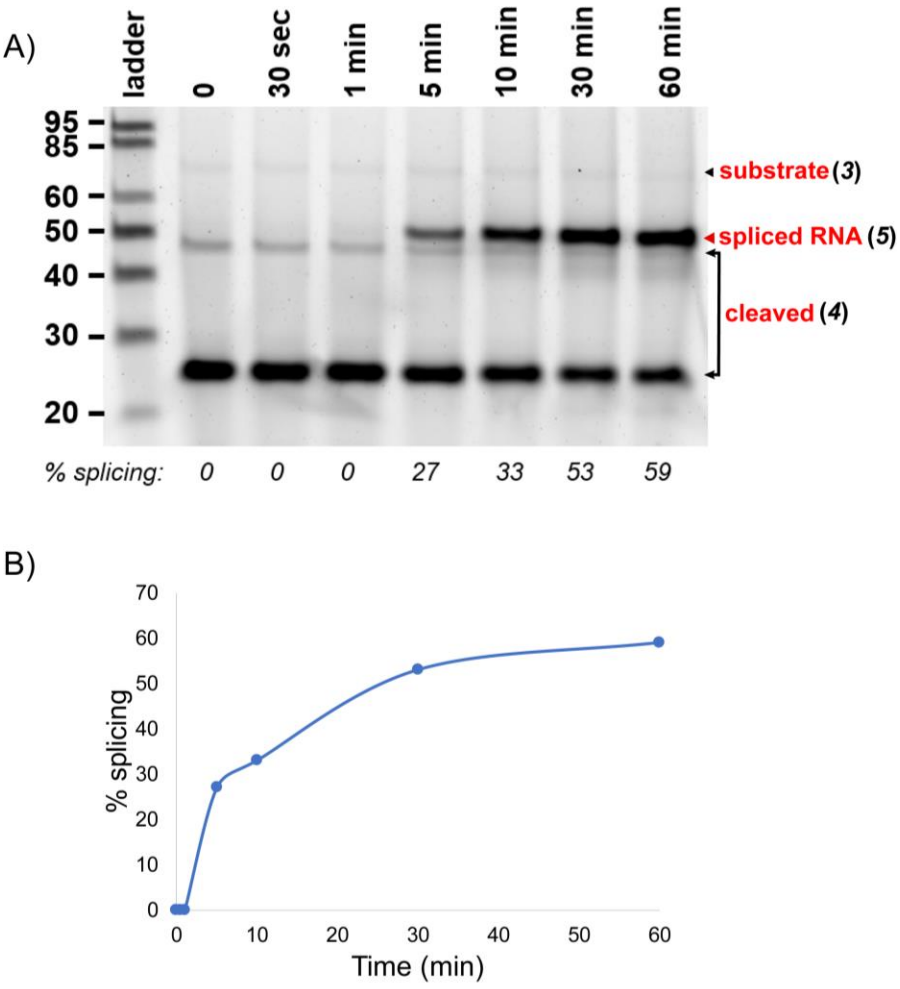

Figure 5.S9. RtcB splicing kinetics on substrate *3* (see Table S2, *3*). (A) Gel showing splicing kinetics with a reaction containing 50 mM Tris-HCl, pH 7.43 at 37ºC, 150 mM NaCl, 2 mM Mn^{2+}, 0.4 µM splice substrate, 0.4 µM each Dz, 0.4 mM GTP, 2.2 µM RtcB. DNAzymes were allowed to react for 2 hrs at 37ºC, after which GTP and RtcB were added, and 10 µl aliquots taken at the specified time points and quenched in 95% formamide, 10 mM EDTA. (B) Plot of splice product versus time (min). Line connecting data points is not a fit, but rather a guide for the reader.

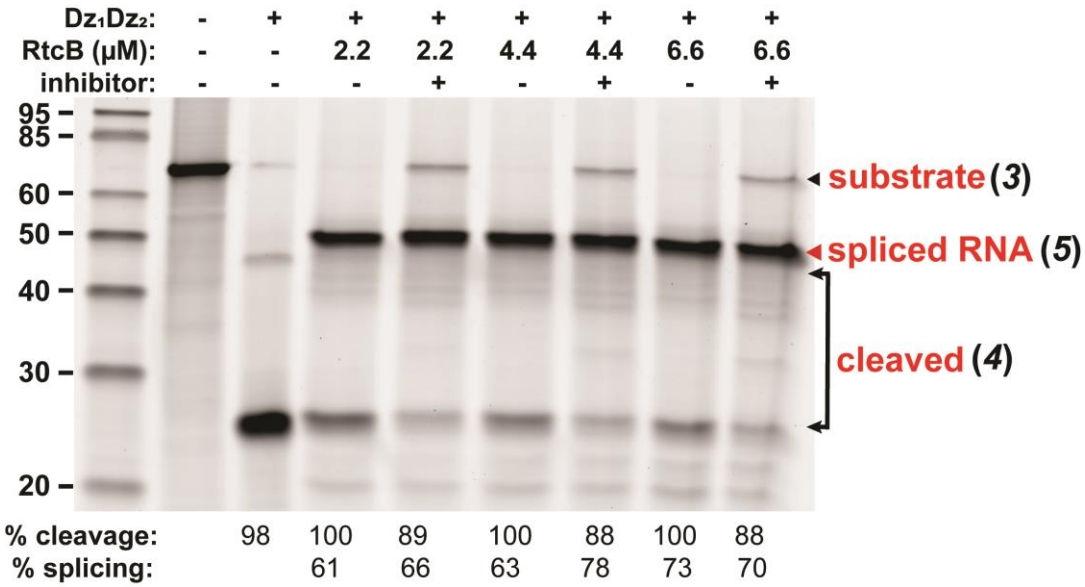

Figure 5.S10. RtcB splicing as a function of ligase concentration and DNAzyme inhibition. Reactions contain 50 mM Tris-HCl, pH 7.43 at 37ºC, 150 mM NaCl, 2 mM Mn^{2+}, 0.4 μM splice substrate ***3***, 0.4 μM each Dz and 0.38 mM GTP. DNAzymes were allowed to react for 2 hrs at 37ºC, after which reaction was divided into 10 μl aliquots. RtcB was added, with and without 0.42 μM inhibitor strand (complementary strand that binds and inactivates the DNAzyme) and allowed to react 1 hr at 37ºC.

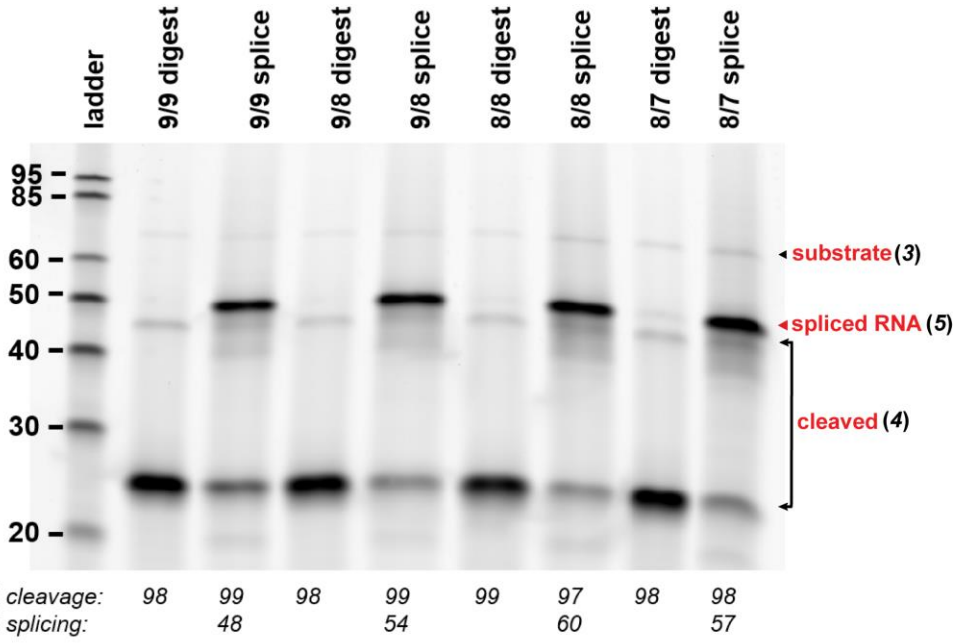

Figure 5.S11. RtcB splicing upon digestion with DNAzymes of decreasing arm length. "9/9" indicates the length of the binding arms of Dz_1 and Dz_2 are both 9 nts, respectively. Reactions contain 150 mM NaCl, 2 mM Mn^{2+}, 0.4 µM splice substrate (see Table S2, ***3***) and 0.4 µM each Dz, in 50 mM Tris-HCl, pH 7.43 at 37ºC for 3 hrs.

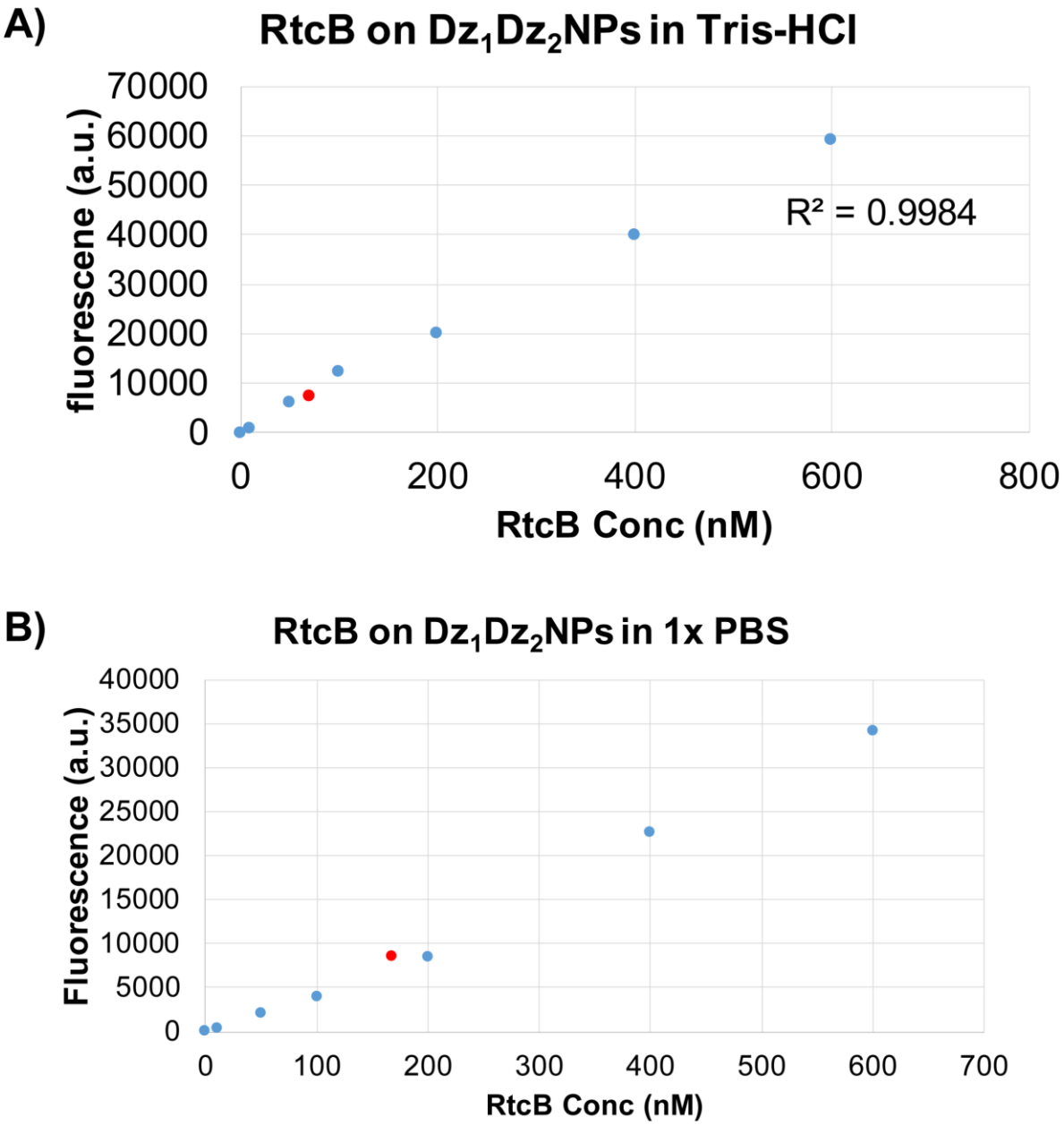

Figure 5.S12. Fluorescence calibration curve to determine RtcB bound to nanozyme. RtcB was labeled with Alexa488. (A) Red dot indicates the nanozyme sample emission, after dissolving the AuNPs and corresponds to a 69 nM concentration. Nanozymes were constituted in 100 mM Tris-HCl, pH 7.43 at 37ºC. No NaCl was added in the buffer. (B) Red dot indicates the nanozyme sample emission, after dissolving the AuNPs, and corresponds to a 167 nM concentration. Nanozymes were constituted in 1x PBS.

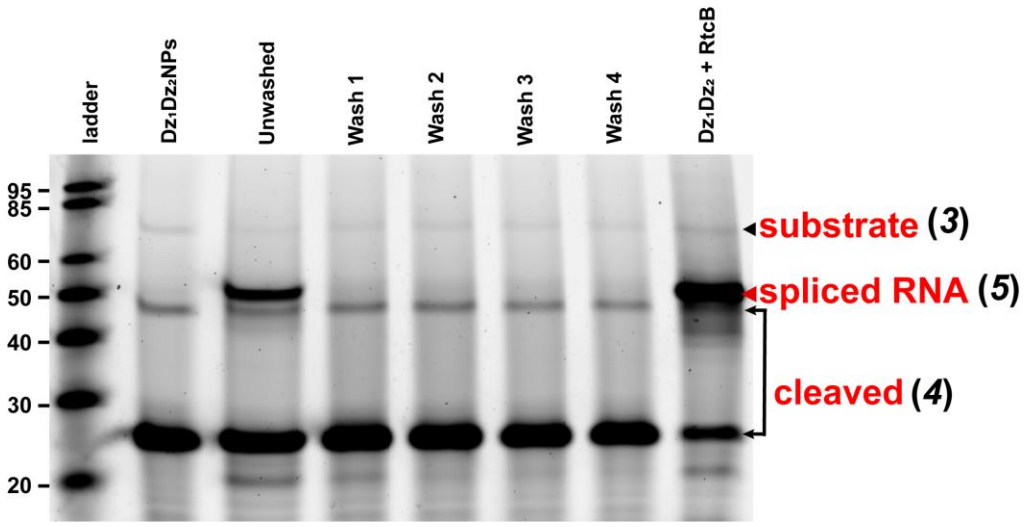

Figure 5.S13. Dz_1Dz_2NPs with His-tagged RtcB not form a detectable splice product. Lane 2: Negative control, Dz_1Dz_2NPs without RtcB; lane 3: unwashed RtcB-His nanozymes; lane 8: positive control with soluble DNAzymes and RtcB. Reaction included 50 mM Tris-HCl, pH 7.43 at 37ºC, 150 mM NaCl, 2 mM Mn^{2+}, 0.4 µM substrate (see Table S2, ***3***), 0.4 µM Dz_1 and Dz_2, 0.4 mM GTP at 37ºC for 2 hrs.

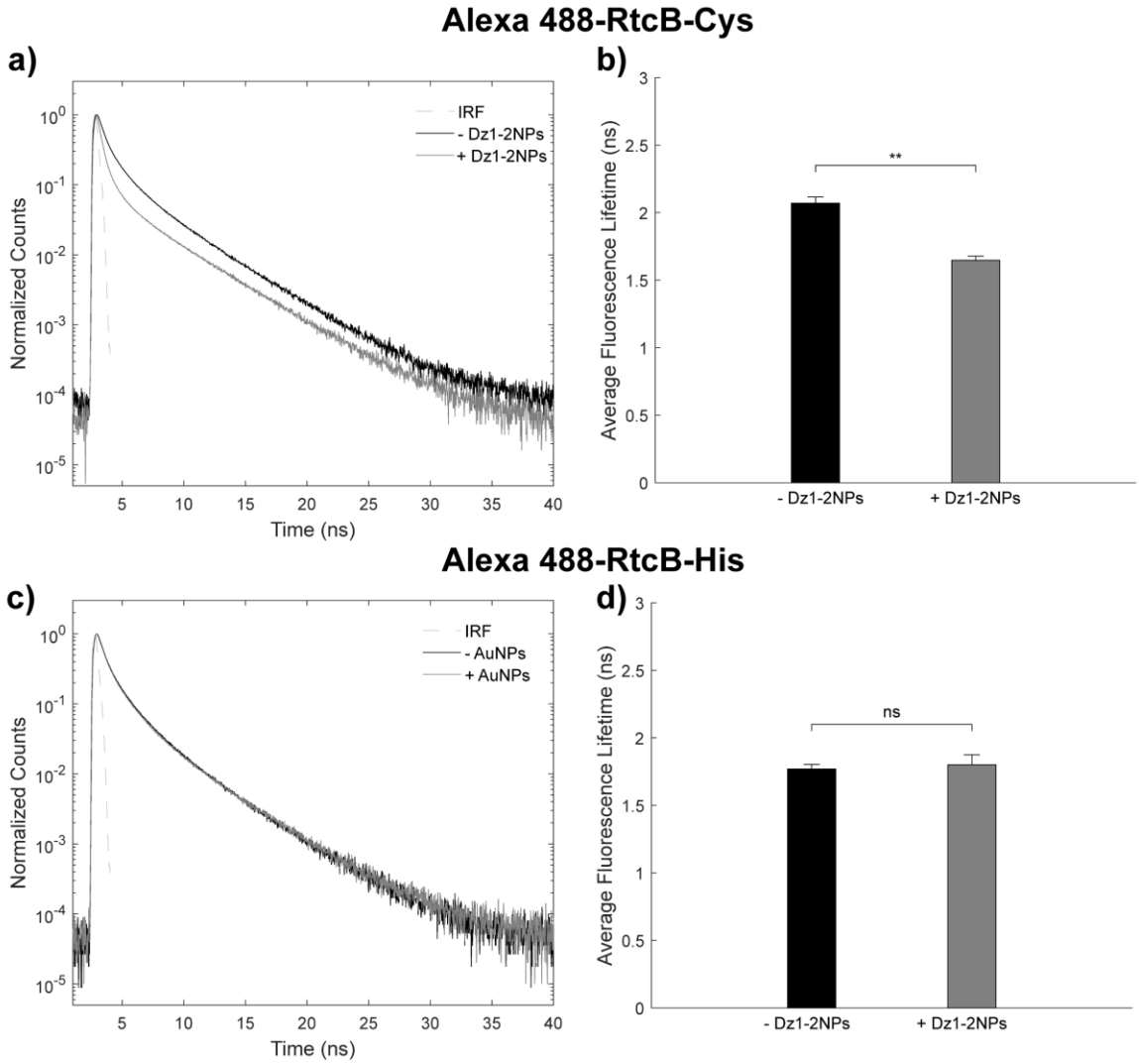

Figure 5.S14. RtcB is specifically bound to Dz1-2NPs. (a) Fluorescence lifetime decay traces demonstrate that Alexa 488-RTCB is quenched by near surface energy transfer when bound to Dz1-2NPs. (b) Average Alexa 488 fluorescence lifetime is reduced by 22.9% when RtcB is bound to Dz1-2NPs. (c). Fluorescence lifetime decay traces demonstrate no significant changes in Alexa 488 lifetime in the presence of Dz1-2NPs when RtcB lacks Cys, which is required to bind to Dz1-2NPs (d). Average fluorescence lifetime of Alexa 488-RtcB without Cys remains unchanged in the presence of Dz1-2NPs.

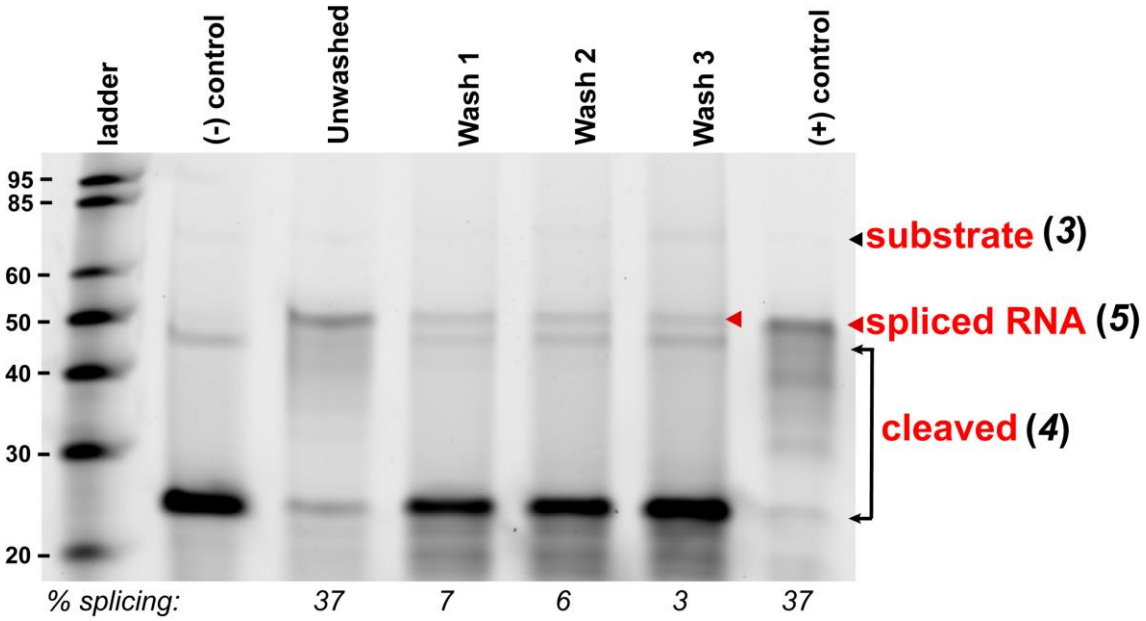

Figure 5.S15. The effect of multiple washes on nanozyme splice yield. Lane 2: Negative control with soluble Dz(s) and no RtcB; lane 3: unwashed nanozyme positive control after overnight RtcB incubation; lane 4-6: successive washes of nanozymes after addition of RtcB yields splice product (red arrow); lane 7 positive control, RtcB-Cys with soluble DNAzymes. Reaction conditions: 0.4 µM substrate (see Table S2, ***3***), 150 mM NaCl, 0.4 mM GTP, 2 mM Mn^{2+}, 37ºC for 2 hrs. Nanozyme concentration was 40 nM (wash 1) and 24 nM (wash 2-3).

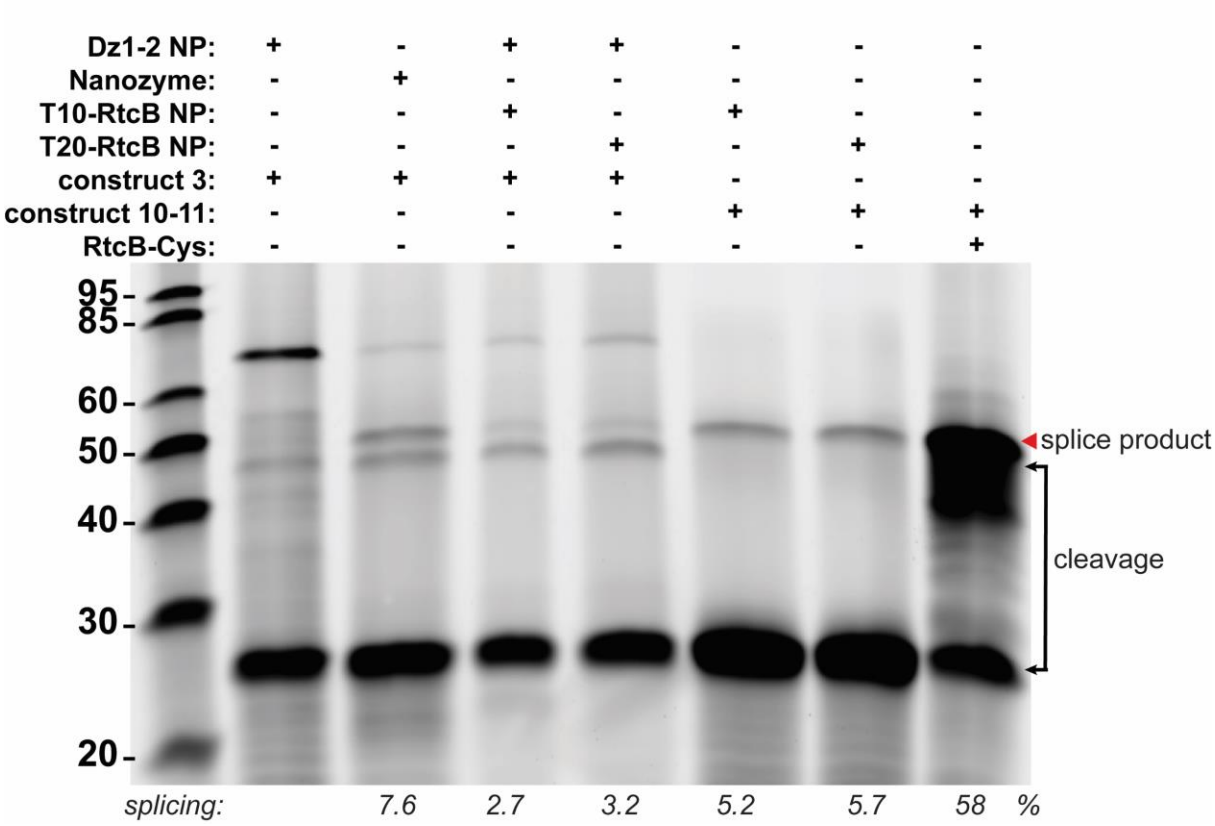

Figure 5.S16. RtcB on non-specific NPs is still active on pre-cleaved substrate. Reaction was conducted in 50 mM Tris-HCl, pH 7.43 at 37ºC, 150 mM NaCl, 2 mM Mn^{2+}, 0.4 mM GTP and 0.4 µM construct 3 or pre-cleaved substrate (construct 10-11). Lane 2: Dz1-2 NPs alone [0.13 µM]; lane 3: nanozyme [0.6 µM]; lane 4: non-specific T10-RtcB-NPs mixed with Dz1-2NPs, each [0.38 µM]; lane 5: non-specific T20-RtcB-NPs mixed with Dz1-2NPs, each [0.53 µM]; lane 6: non-specific T10-RtcB-NPs [0.48 µM] supplemented with pre-cleaved substrate [0.4 µM]; lane 7: non-specific T20-RtcB-NPs [0.78 µM] supplemented with pre-cleaved substrate [0.4 µM]; lane 8: positive control RtcB-Cys [2.5 µM] with pre-cleaved substrate [0.4 µM].

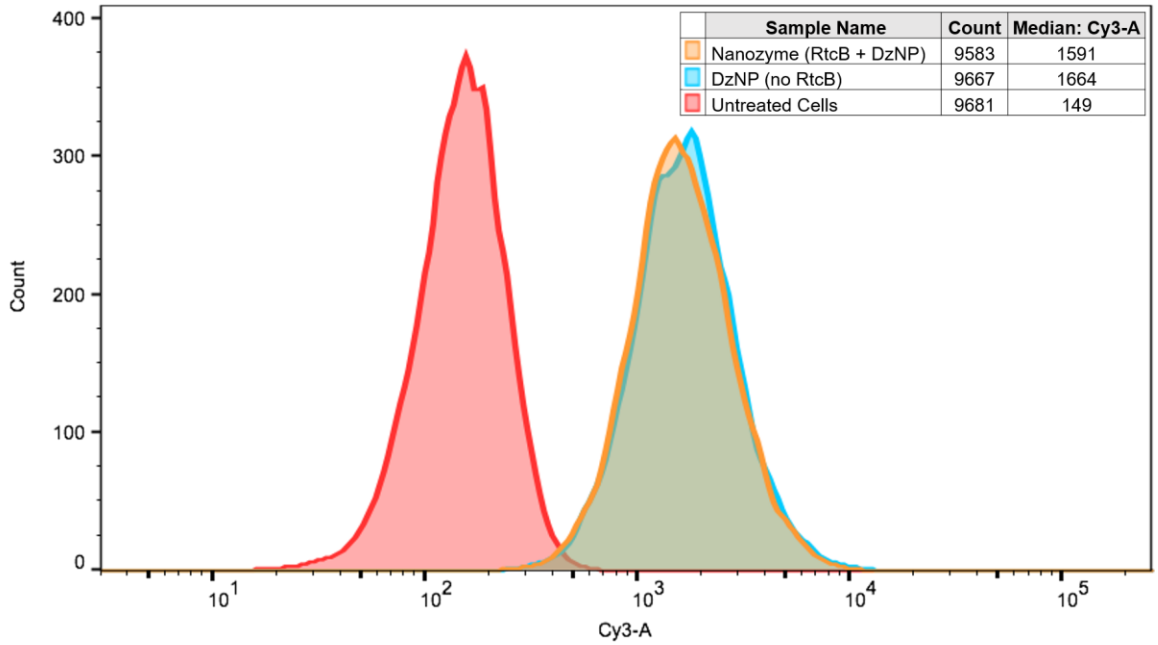

Figure 5.S17. Flow cytometry of Dz_1Dz_2NPs and nanozymes entering MDA-MB-231 cells. Red indicates non-fluorescent control cells without exposure to nanoparticles. Blue indicates MDA-MB-231 cells exposed to 5.6 nM Cy3b-labeled Dz_1Dz_2NPs for 24 hrs. Yellow indicates cells exposed to 6.2 nM Cy3b-labeled nanozymes for 24 hrs. Both sets of Cy3b-labeled NPs suggest uptake, as indicated by a shift to the right as compared to control non-fluorescent cells. Therefore, RtcB does not appear to inhibit nanozyme uptake into this cell line.

5.8. References

1. Desai, K. K.; Bingman, C. A.; Phillips, G. N., Jr.; Raines, R. T., Structures of the noncanonical RNA ligase RtcB reveal the mechanism of histidine guanylylation. *Biochemistry* **2013,** *52* (15), 2518-25.
2. Montiel-Gonzalez, M. F.; Vallecillo-Viejo, I.; Yudowski, G. A.; Rosenthal, J. J., Correction of mutations within the cystic fibrosis transmembrane conductance regulator by site-directed RNA editing. *Proceedings of the National Academy of Sciences of the United States of America* **2013,** *110* (45), 18285-90.
3. Evers, M. M.; Toonen, L. J.; van Roon-Mom, W. M., Antisense oligonucleotides in therapy for neurodegenerative disorders. *Advanced drug delivery reviews* **2015,** *87*, 90-103.
4. Havens, M. A.; Duelli, D. M.; Hastings, M. L., Targeting RNA splicing for disease therapy. *Wiley interdisciplinary reviews. RNA* **2013,** *4* (3), 247-66.
5. Deidda, G.; Rossi, N.; Tocchini-Valentini, G. P., An archaeal endoribonuclease catalyzes cis- and trans- nonspliceosomal splicing in mouse cells. *Nature biotechnology* **2003,** *21* (12), 1499-504.
6. Amini, Z. N., Karen E. Olson, Ulrich F. Muller, Spliceozymes: Ribozymes that Remove Introns from Pre-mRNAs in Trans. *PloS one* **2014,** *9* (7), 1-11.
7. Reenan, R., Correcting Mutations by RNA Repair. *The New England Journal of Medicine* **2014,** *370* (2), 172-174.
8. Putti, S.; Calandra, P.; Rossi, N.; Scarabino, D.; Deidda, G.; Tocchini-Valentini, G. P., Highly efficient, in vivo optimized, archaeal endonuclease for controlled RNA splicing in mammalian cells. *FASEB journal : official publication of the Federation of American Societies for Experimental Biology* **2013,** *27* (9), 3466-77.
9. Lewin, A. S.; Hauswirth, W. W., Ribozyme gene therapy: applications for molecular medicine. *Trends in molecular medicine* **2001,** *7* (5), 221-228.

10. Mitsuyasu, R. T.; Merigan, T. C.; Carr, A.; Zack, J. A.; Winters, M. A.; Workman, C.; Bloch, M.; Lalezari, J.; Becker, S.; Thornton, L.; Akil, B.; Khanlou, H.; Finlayson, R.; McFarlane, R.; Smith, D. E.; Garsia, R.; Ma, D.; Law, M.; Murray, J. M.; von Kalle, C.; Ely, J. A.; Patino, S. M.; Knop, A. E.; Wong, P.; Todd, A. V.; Haughton, M.; Fuery, C.; Macpherson, J. L.; Symonds, G. P.; Evans, L. A.; Pond, S. M.; Cooper, D. A., Phase 2 gene therapy trial of an anti-HIV ribozyme in autologous CD34+ cells. *Nature medicine* **2009,** *15* (3), 285-92.

11. Kruger, K.; Grabowski, P. J.; Zaug, A. J.; Sands, J.; Gottschling, D. E.; Cech, T. R., Self-splicing RNA: autoexcision and autocyclization of the ribosomal RNA intervening sequence of Tetrahymena. *Cell* **1982,** *31*, 147-157.

12. Fiskaa, T.; Birgisdottir, A. B., RNA reprogramming and repair based on trans-splicing group I ribozymes. *New biotechnology* **2010,** *27* (3), 194-203.

13. Alexander, R. C.; Baum, D. A.; Testa, S. M., 5′ Transcript Replacement in Vitro Catalyzed by a Group I Intron-Derived Ribozyme. *Biochemistry* **2005,** *44* (21), 7796-7804.

14. Olson, K. E.; Muller, U. F., An in vivo selection method to optimize trans-splicing ribozymes. *Rna* **2012,** *18* (3), 581-9.

15. Lin, Y.; Ren, J.; Qu, X., Nano-gold as artificial enzymes: hidden talents. *Advanced materials* **2014,** *26* (25), 4200-17.

16. Lin, Y.; Ren, J.; Qu, X., Catalytically active nanomaterials: a promising candidate for artificial enzymes. *Accounts of chemical research* **2014,** *47* (4), 1097-105.

17. Santoro, S. W., Gerald F. Joyce, A General Purpose RNA-cleaving DNAzyme. *Proceedings of the National Academy of Sciences of the United States of America* **1999,** *49* (9), 1262-1266.

18. Yehl, K.; Joshi, J. P.; Greene, B. L.; Dyer, B.; Nahta, R.; Salaita, K., Catalytic deoxyribozyme-modified nanoparticles for RNAi-independent gene regulation. *ACS nano* **2012,** *6* (10), 9150–9157.

19. Somasuntharam, I.; Yehl, K.; Carroll, S. L.; Maxwell, J. T.; Martinez, M. D.; Che, P. L.; Brown, M. E.; Salaita, K.; Davis, M. E., Knockdown of TNF-alpha by DNAzyme gold nanoparticles as an anti-inflammatory therapy for myocardial infarction. *Biomaterials* **2016,** *83*, 12-22.

20. Silverman, S. K.; Baum, D. A., Use of Deoxyribozymes in RNA Research. *Methods Enzymol* **2009,** *469*, 95-117.

21. Chakravarty, A. K.; Subbotin, R.; Chait, B. T.; Shuman, S., RNA ligase RtcB splices 3'-phosphate and 5'-OH ends via covalent RtcB-(histidinyl)-GMP and polynucleotide-(3')pp(5')G intermediates. *Proceedings of the National Academy of Sciences of the United States of America* **2012,** *109* (16), 6072-7.

22. Tanaka, N.; Meineke, B.; Shuman, S., RtcB, a novel RNA ligase, can catalyze tRNA splicing and HAC1 mRNA splicing in vivo. *The Journal of biological chemistry* **2011,** *286* (35), 30253-7.

23. Tanaka, N.; Shuman, S., RtcB is the RNA ligase component of an Escherichia coli RNA repair operon. *The Journal of biological chemistry* **2011,** *286* (10), 7727-31.

24. Popow, J.; Englert, M.; Weitzer, S.; Schleiffer, A.; Mierzwa, B.; Mechtler, K.; Trowitzsch, S.; Will, C. L.; Luhrmann, R.; Soll, D.; Martinez, J., HSPC117 is the essential subunit of a human tRNA splicing ligase complex. *Science* **2011,** *331* (6018), 760-4.

25. Kosmaczewski, S. G.; Edwards, T. J.; Han, S. M.; Eckwahl, M. J.; Meyer, B. I.; Peach, S.; Hesselberth, J. R.; Wolin, S. L.; Hammarlund, M., The RtcB RNA ligase is an essential component of the metazoan unfolded protein response. *EMBO reports* **2014,** *15* (12), 1278-85.

26. Wadhwani, P.; Heidenreich, N.; Podeyn, B.; Burck, J.; Ulrich, A. S., Antibiotic gold: tethering of antimicrobial peptides to gold nanoparticles maintains conformational flexibility of peptides and improves trypsin susceptibility. *Biomater Sci* **2017,** *5* (4), 817-827.

27. Desai, K. K.; Raines, R. T., tRNA ligase catalyzes the GTP-dependent ligation of RNA with 3'-phosphate and 5'-hydroxyl termini. *Biochemistry* **2012,** *51* (7), 1333-5.

28. Chakravarty, A. K.; Shuman, S., The sequential 2',3'-cyclic phosphodiesterase and 3'-phosphate/5'-OH ligation steps of the RtcB RNA splicing pathway are GTP-dependent. *Nucleic acids research* **2012,** *40* (17), 8558-67.

29. Cairns, M. J., Toni M. Hopkins, Craig Witherington, Li Wang and Lun-Quan Sun, Target site selection for an RNA-cleaving catalytic DNA. *Nature biotechnology* **1999,** *17*, 480-486.

30. Ruble, B. K.; Richards, J. L.; Cheung-Lau, J. C.; Dmochowski, I. J., Mismatch Discrimination and Efficient Photomodulation with Split 10-23 DNAzymes. *Inorganica Chim Acta* **2012,** *380*, 386-391.

31. Tanaka, N.; Chakravarty, A. K.; Maughan, B.; Shuman, S., Novel mechanism of RNA repair by RtcB via sequential 2',3'-cyclic phosphodiesterase and 3'-Phosphate/5'-hydroxyl ligation reactions. *The Journal of biological chemistry* **2011,** *286* (50), 43134-43.

32. Hill, H. D.; Mirkin, C. A., The bio-barcode assay for the detection of protein and nucleic acid targets using DTT-induced ligand exchange. *Nature protocols* **2006,** *1* (1), 324-36.

33. Hurst, S. J.; Lytton-Jean, A. K.; Mirkin, C. A., Maximizing DNA Loading on a Range of Gold Nanoparticle Sizes. *Anal Chem* **2006,** *78* (1), 8313-8318.

34. Desai, K. K.; Beltrame, A. L.; Raines, R. T., Coevolution of RtcB and Archease created a multiple-turnover RNA ligase. *Rna* **2015,** *21* (11), 1866-72.

Chapter 6: Cellular Splicing – Using DzNPs to Splice the XBP1 Intron

Contributions: Victor Ma aliquoted polyethylenimine (PEI) for transfection of HEK293T cells.

6.1. Introduction

Being able to manipulate RNA inside cells is a useful diagnostic tool for both basic research and RNA gene therapy. Having built a nanozyme that could splice RNA (see chapter 5), the next goal was to perform the same reaction using DNAzyme-nanoparticles (DzNPs) inside cells. The first method pursued to test this concept involved the use of a tRNA scaffold to express a stem loop region that could be cleaved by DNAzymes (Fig. 6.1.). Expressing the desired RNA inside a tRNA minimizes RNase-mediated degradation. This process was introduced by Luc Ponchon and coworkers[1-3] and later improved on by Nelissen and colleagues.[4] Their techniques allow the large scale synthesis of a great quantity of RNA inside cells, rather than relying on expensive synthetic methods.[2] The RNA can then be purified, removed from the scaffold, and used appropriately. For our purposes, we wanted to use the tRNA scaffold approach to express a substrate inside cells that would avoid cellular RNases but could be cleaved and spliced by DNAzymes. Unfortunately, although we successfully expressed our RNA hybrid, our RNAs were found to be degraded upon purification (data not shown). We hypothesized that the loop region did not have sufficient secondary structure to keep it hidden from RNases. Indeed, the literature suggests that this technique works optimally with structured RNAs.[2] If the RNA contains large, unstructured loop regions, these loops are accessible to cellular enzymes and thus susceptible to RNA degradation.

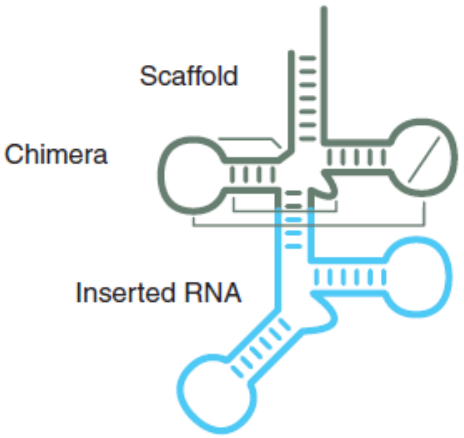

Figure 6.1. tRNA scaffold (gray) into which a donor RNA (blue) can be inserted and expressed inside cells. Adapted by permission from Springer Nature: Nature Publishing Group, Nature Protocols from reference 1, Copyright (2009).[1]

Therefore, we turned to an alternate method to measure splicing with DzNPs, using the natural gene spliced by the ligase RtcB, in our nanozyme: X-box binding protein 1 (XBP1). XBP1 is a transcription factor that is spliced in the

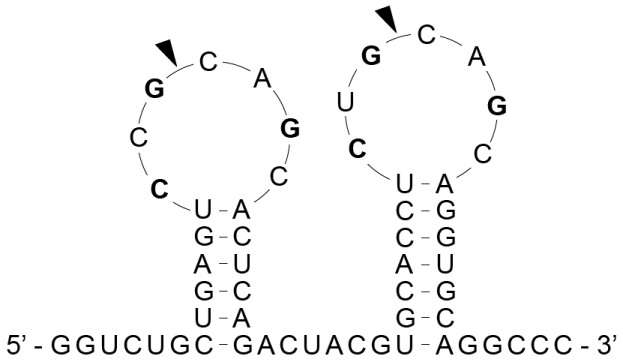

human XBP1

Figure 6.2. The sequence and secondary structure of the recognition motif CNGNNG in the intron of XBP1. Black arrows indicate IRE1α cleavage sites. Bold letters indicate the CNGNNG recognition motif for IRE1α. Redrawn by permission from Mary Ann Liebert, Inc., New Rochelle, NY: Antioxidants & Redox Signaling from reference 5, Copyright (2007).[5]

cytoplasm by inositol-requiring protein-1 α (IRE1α) in mammalian cells (Fig. 6.2.).[6-7] IRE1α is one of three stress receptors located in the endoplasmic reticulum (ER) that regulates the unfolded protein response (UPR).[6] It is a transmembrane protein composed of three domains: a luminal domain, a cytoplasmic kinase domain and an RNase domain.[7] The amino-terminal domain is on the luminal side of the ER and senses built up unfolded proteins.[7] Unfolded proteins trigger the dimerization of IRE1α's luminal domain, allowing *trans*-autophosphorylation through the kinase domain in the cytoplasm.[7] This chain reaction then stimulates RNase cleavage of XBP1 by the carboxyl-terminal RNase domain also in the cytoplasm.[7] IRE1α recognizes the consensus sequence CNGNNG in XBP1, located in a pair of stem-loops in the intron (Fig 6.2.).[5] The intron that is spliced out of XBP1 is only 26-nucleotides long, separating the DNA-binding domain (DBD) from the activation domain (AD).[5] Being so short, it does not prevent translation of the unspliced transcript.[5] Rather, there is a delicate balance between the spliced and unspliced transcripts of XBP1, leading to regulation feedback loops. Unspliced XBP1 sequesters and downregulates spliced XBP1, shutting off UPR upregulation.[5] However, once spliced, XBP1 becomes an active transcription factor, with its DBD connected to the AD, and localizes to the nucleus where it transcribes chaperone proteins that mediate the unfolded protein response, including more XBP1.[5] Interestingly, in addition to cleaving XBP1, IRE1α also cleaves its own mRNA and 28S rRNA.[7]

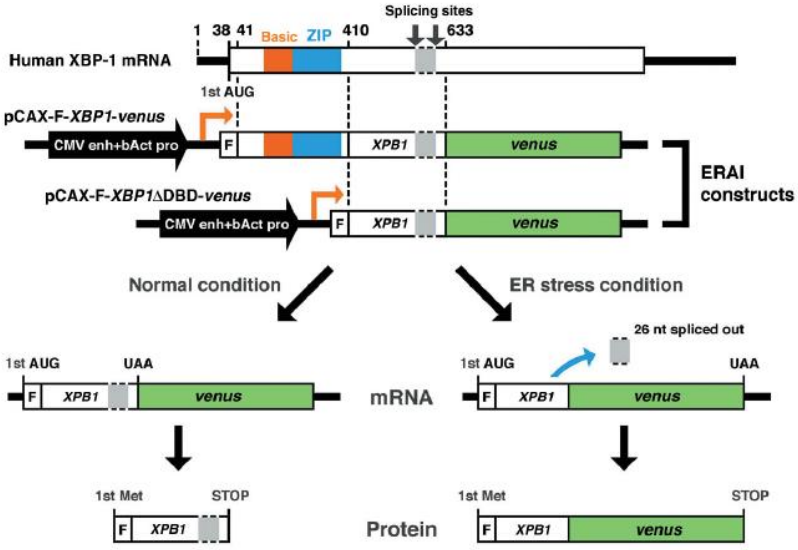

Figure 6.3. XBP1 reporter constructed by Iwawaki and colleagues, fusing Venus onto truncated XBP1. Reprinted by permission from Springer Nature: Nature Publishing Group, Nature Medicine from reference 7, Copyright (2004).[8]

Iwawaki and colleagues constructed a Venus-based XBP1 splicing reporter that could work in cells and in mice.[8] To construct this reporter, they attached Venus, a variant of green fluorescent protein (GFP), to the C-terminus of a truncated XBP1 (Fig. 6.3.).[8]

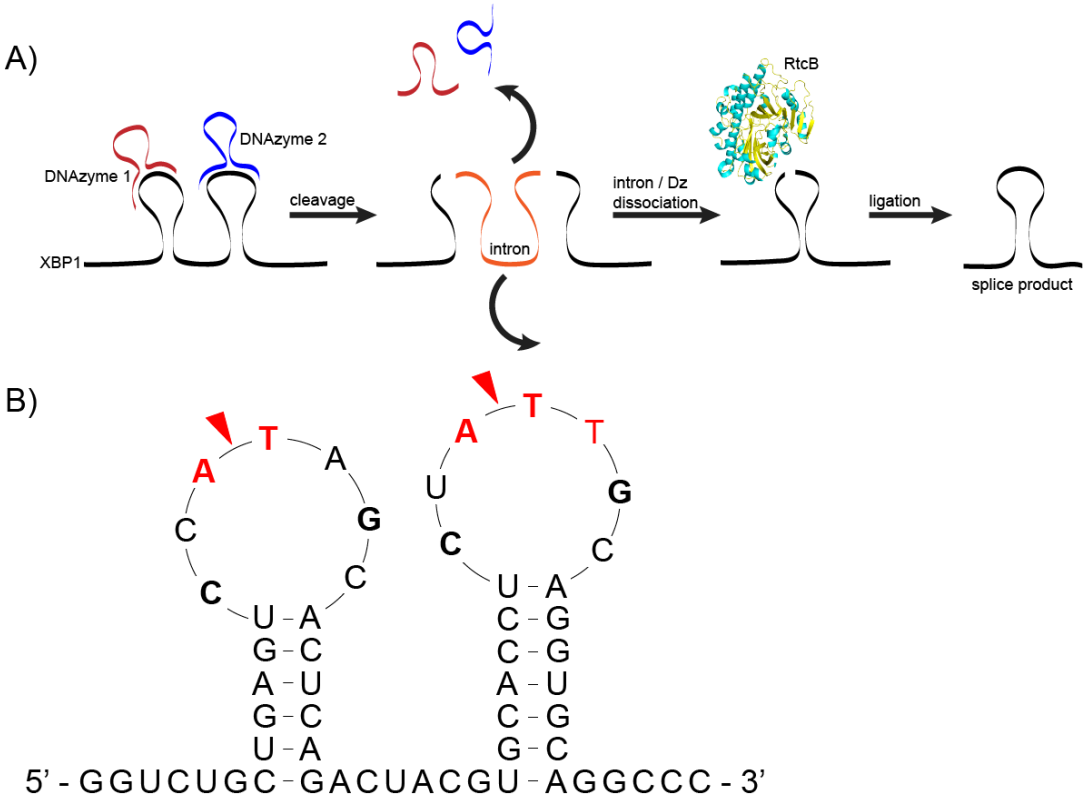

Figure 6.4. Schemes showing modified XBP1 construct cleavable by DNAzymes. (A) XBP1 is cleaved by DNAzymes and then ligated by cellular RtcB ligase (B) Sequence of the modified XBP1 construct (modifications in red), allowing DNAzymes to cleave at the sites indicated by the red arrows.

In the absence of stress, XBP1 is expressed but stops at a stop codon before Venus. During stress, the intron is spliced out, leading to a frame shift that abolishes the stop codon and allows Venus to be transcribed and attached to XBP1.[8] The authors used this reporter as a stress indicator in HEK293T cells and mice.[8] Our goal was to have DzNPs cleave this reporter at the XBP1 exon / intron junction, allowing cellular RtcB ligase to re-join the two ends, fusing XBP1 with Venus (Fig. 6.4.).

6.2. Results and Discussion

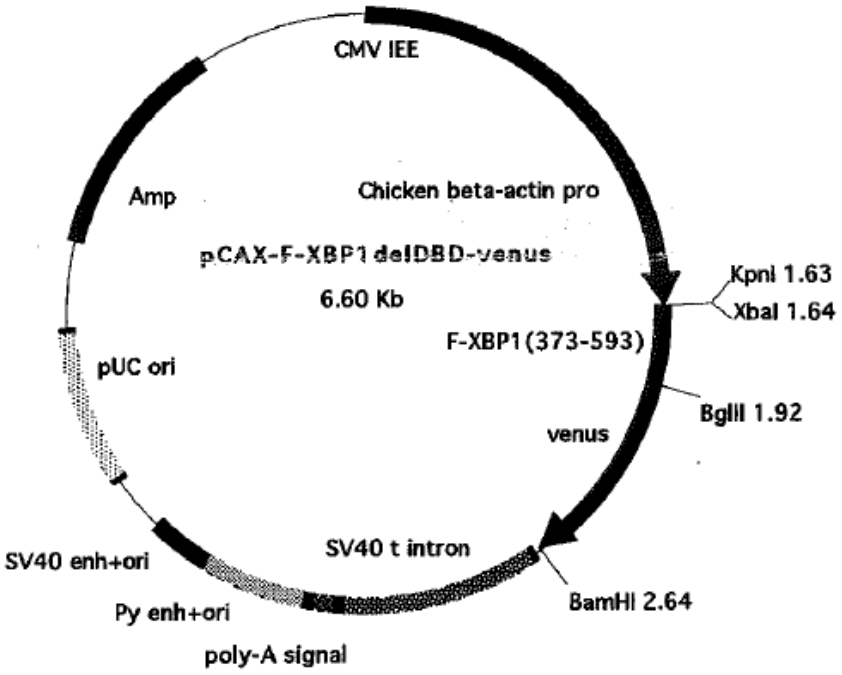

Figure 6.5. The plasmid map of the XBP1-Venus reporter.

6.2.1. Modifying the construct

For our research, we chose to modify Iwawaki's Venus-based reporter plasmid (Fig. 6.5.) for DzNP splicing in HEK293FT cells by modifying it to include a DNAzyme cleavage site in the intron. The DNAzyme cleavage site was added by mutating the G on the 5' side of the IRE1α cleavage site to an A. Literature suggests that this change should abolish IREα's recognition of the substrate.[9] Thus, a point mutation changes the cleavage site to a DNAzyme's recognition site with a purine / pyrimidine junction and removes IRE1α's recognition at the same time.

6.2.2. Control Experiment: Transfecting Original Plasmid

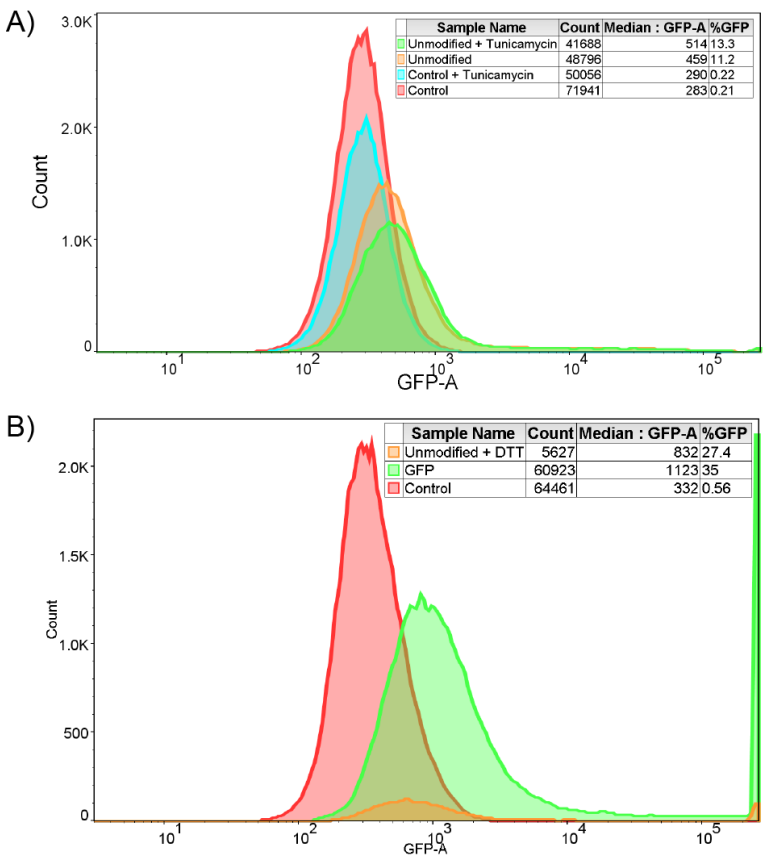

Figure 6.6. HEK293FT transfection experiments. (A) HEK293FT cells transfected with the unmodified plasmid with (green) and without (orange) tunicamycin treatment. Blue and red are control cells not exposed to plasmid with and without tunicamycin treatment, respectively. (B) Fluorescence of HEK293FT cells transfected with unmodified plasmid and exposed to DTT. Untreated control cells are in red. GFP positive control is green. Cells exposed to the unmodified plasmid and DTT to stimulate the stress response are labeled orange.

Before using the modified plasmid, we transfected the original plasmid into HEK293FT cells using Lipofectamine 2000 to determine if we could reproduce the literature results.[8] In our first round of experiments, we stimulated the cells with and without tunicamycin, an inhibitor of N-linked glycosylation,[8] causing ER stress. However, there was little difference between the fluorescence of the transfected cells with and without exposure to tunicamycin (Fig. 6.6A.). In the next round of experiments, we introduced a constitutively expressing enhanced green fluorescent protein (eGFP) as a positive control. We also used 1 mM of the reducing agent DTT as a stress inducing drug rather than tunicamycin. In the second transfection, 35% of the eGFP positive control cells were fluorescent (Fig. 6.6B.) and there was a slight shift in HEK cells exposed to DTT; however, the cell count was very low because the DTT killed most of the cells in the overnight incubation. Reducing the incubation time with DTT improved cell viability, but toxicity

A)

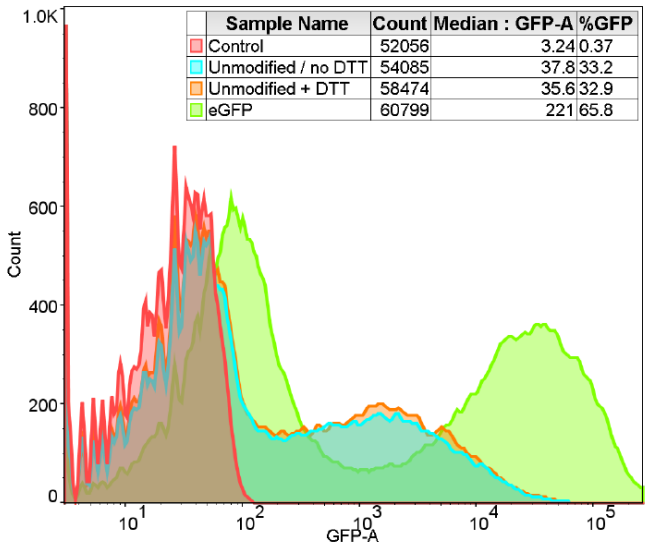

B)

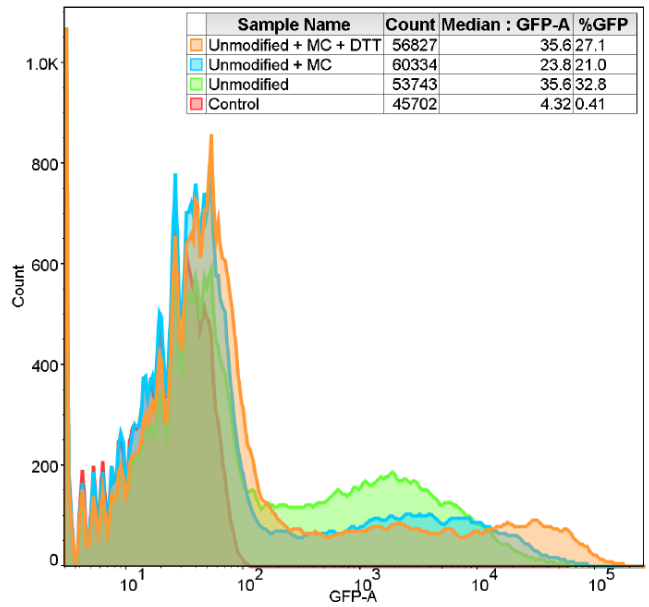

Figure 6.7. HEK293FT transfection experiments with and without media changes. (A) Flow cytometry of HEK293FT cells transfected with unmodified plasmid with (orange) and without (blue) DTT incubation, compared to eGFP positive control (green) and untreated cells (red). (B) Flow cytometry of HEK293FT cells exposed to the unmodified plasmid (green) after performing media changes (MC) every 6 h, with (orange) and without (blue) DTT incubation. Untreated control cells are in red.

was still high. In a personal communication with the study author,[8] he recommended limiting incubation times and performing a titration of the DTT either in concentration or time, to determine what was tolerable to our cells. In these experiments, we found that any incubation longer than 1 h appeared toxic based on microscopy cell counts. We did not want to change the concentration of the DTT, as this change could result in the stress response not being properly induced. In a third round of experiments, we used polyethylenimine (PEI) as a different transfection method to compare to lipofectamine. However, in our PEI transfection of HEK293FT cells with the unmodified plasmid, we continued to see no difference between cells with and without DTT stimulation (Fig. 6.7A.) We hypothesized the difference was small due to cell stress already being high from lack of media changes. After transfection, the cells were incubated for 48 h with no change in media. This

procedure raised concerns that the cells could be becoming glucose starved, leading to activation of the stress response. The literature suggested that changing the media on the cells every 6 h was necessary to avoid glucose starvation.[8] Therefore, we attempted another experiment in which we changed the media every 6 h as suggested, transfecting the unmodified plasmid with PEI. In this case, flow cytometry appeared to indicate that fluorescence did decrease with the addition of media changes compared to cells without media changes, but cells that had received media changes and DTT incubation did not show an increase in fluorescence (Fig. 6.7B.).

6.2.3. Comparing Modified Plasmid to Unmodified Plasmid

As another control, we next incubated HEK293FT cells with the unmodified plasmid and the modified plasmid. The former had the recognition site for IRE1α in the intron changed to DNAzyme cleavage sites. Thus, IRE1α should no longer recognize it, uncoupling the plasmid from the stress response and leading to no splicing or fluorescence. We used this plasmid as a negative control to compare alongside the unmodified plasmid, which is still coupled to the stress response and IRE1α splicing. This experiment was designed to determine if we could see a difference in fluorescence levels. Instead, we saw that the negative control plasmid appeared to have more overall fluorescence than the unmodified plasmid (Fig. 6.8A.). This data directly contradicted what we expected. We spoke with several experts in the field about this issue and made a few hypotheses as to why we saw this result. Firstly, it is possible that the IRE1α recognition site is not completely inactivated by the point mutations, as the literature claimed.[9] Peschek *et al.*'s IRE1α cleavage studies were done *in vitro* with recombinant protein.[9] It is possible that in cells IRE1α is more difficult to inactivate than *in vitro* and more mutations in the recognition site are necessary. Thus, the negative control may still be being cleaved and spliced by IRE1α, resulting in cellular fluorescence. Others suggested that we should use the same cell line as used in the literature.[8] We also found that when introducing the DNAzyme cleavage

sites, another stop codon had accidentally been added. Another plasmid was cloned to address this issue. We switched the cell line to HEK293T and used calcium phosphate (CaP) transfection, as had been done in literature.[8] We theorized that this transfection was gentler on the cells and did not spuriously activate the stress response by damaging the membrane, as lipofectamine and PEI could do. We then performed the CaP transfection with the corrected plasmid three separate times in triplicate, with the following results. The first trial showed no difference between the negative control and unmodified plasmid, as before (Fig. 6.8B.). In our other replicate experiments, we noticed an anomally. Each time we repeated the experiment, one of the three wells showed data consistent with the literature: the negative control showed less fluorescence than the unmodified plasmid (Fig. 6.8C.). However, the other two wells showed high fluorescence in the negative control as before (Fig. 6.8D.).

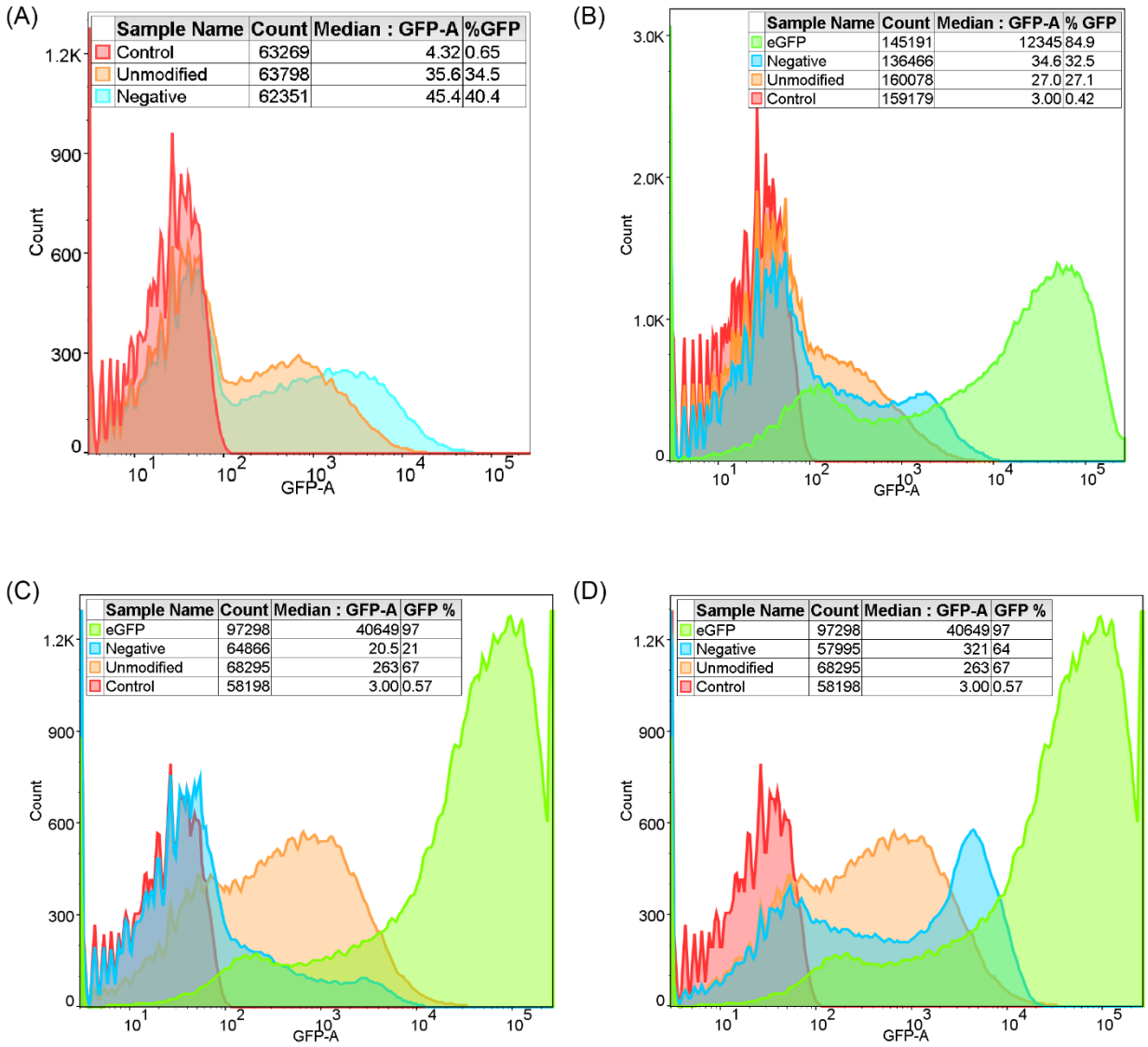

Figure 8. Transfections comparing negative control modified plasmid to unmodified plasmid. (A) Flow cytometry of HEK293FT cells transfected with the unmodified plasmid (orange) and the negative control plasmid (blue), compared to untreated cells (red). Data indicates that the negative control is more fluorescent than the positive control. (B, D) Flow cytometry of HEK293T cells transfected by CaP transfection with the unmodified plasmid (orange) and the negative control plasmid (blue), compared to untreated cells (red). eGFP (green) is used as the positive control. Data indicates that the negative control shows equal or greater fluorescence than the unmodified plasmid. Data in (D) is from two wells. (C) Flow cytometry of HEK293T cells transfected by CaP transfection to the unmodified plasmid (orange) and the negative control plasmid (blue), compared to untreated cells (red). eGFP (green) is used as the positive control. Data indicates that the negative control is less fluorescent than the unmodified plasmid. Data is from one well.

This inconsistency could perhaps be explained by transfection efficiency. Because we do not have a dual reporter, it is impossible to determine the transfection efficiency of the plasmid in each cell. It is possible that in one isolated instance, conditions were not optimal and the plasmid transfected poorly in those population of cells, leading to lower fluorescence in the negative control.

6.3. Future Work

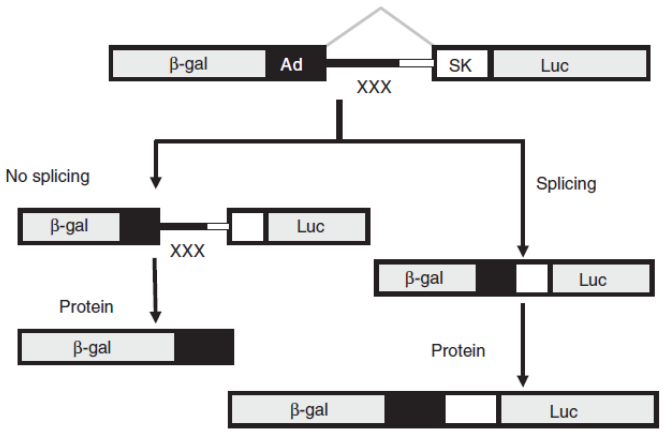

Figure 6.9. Dual reporter splicing system developed by Nasim and Eperon, using β-galactosidase and luciferase. Adapted by permission from Springer Nature: Nature Publishing Group, Nature Protocols from reference 10, Copyright (2006).[10]

In future work, we would like to further mutate the IRE1α recognition site. In addition, we could add two more stop codons before Venus, to make a string of three stop codons, which is more likely to prevent spurious translational read-through. We could also place stop codons inside the intron itself. In theory, since the intron will be removed by the DNAzymes, the additional stop codons will only prevent translation when the intron is still present, which will have the desired effect. The other change we could make is adding another GFP variant like mCherry to the beginning of the XBP1 gene, so it would be constituitively expressed. The mCherry could then report on the transfection efficiency of the plasmid and act as a ratiometric reporter with Venus.

6.4. Other Systems to Detect Splicing in Cells

It should be noted that there are other systems for measuring splicing in cells. One example in particular that stood out uses a dual-reporter structure with β-galactosidase and luciferase

between the genes for adenovirus and the skeletal muscle isoform of human tropomysin (Fig. 6.9.).[10] It includes three stop codons in between the two reporters, that when spliced out, lead to luciferase fluorescence.

6.5. Conclusion

In summary, we were unable to consistently reproduce the data in the literature[8] using the plasmid obtained directly from the Miura lab, and the negative control showed large background signal, generating fluorescence similar to the unmodified plasmid. In future work, it would be best to re-engineer the plasmid entirely into a dual reporter system similar to Nasim's design, so that transfection efficiency could be measured along with splicing efficiency.[10] This ratiometric approach would allow us to correct for transfection efficiency when viewing splicing results.

6.6. Materials and Methods

6.6.1. Sephadex tRNA pull down

The following procedure details the sephadex pulldown technique used when attempting to overexpress our RNA of interest inside a tRNA. This protocol was adapted and modified from several papers. First, the protocol for the tRNA pulldown was used from Ponchon and coworker's Nature paper.[1] For the RNA isolation, we used sephadex beads and followed the protocol found in Ponchon and coworker's 2007 paper in the affinity purification section.[2] Finally, for swelling the beads we used a partial protocol from the work by Walker *et al.*[11] First, we expressed the tRNA plasmid in DH5α in 1L of 2x YT media overnight at 37ºC. Then, we spun down 1L of culture at 6ºC 30 min at 3,100 g. At this point, we took out protease inhibitor cocktail (PIC) to thaw on ice, checked the sephadex beads and chilled the column to be used. After the culture was done centrifuging, we poured off the supernatant and scooped out the pellet with a spatula, transferring it to a tared 50 ml Falcon tube. We weighed the tube to find the mg weight of the pellet and calculated the amount of sephadex beads to use. We then added 100 µl PIC to 50 ml buffer A [100 mM sodium phosphate, 100 mM NaCl, 5 mM $MgCl_2$, pH 7.2] freshly prepared and chilled. After mixing, we added a maximum of 10 mL buffer A to the pellet and resuspended it. We sonicated the resulting slurry on a probe sonicator with a 10 sec pulse and 20 sec rest at the settings 11-14 mV, level 4. We then spun down the slurry in an ultracentrifuge 30 min at 24,100 rpm (67,000 g). We added the resulting lysate to chilled sephadex beads, added another 10 mL buffer A (20 ml total) and allowed it to shake on a rocker at 4ºC for 1 h. After this 1 h incubation, we spun down the beads at 4,000 g 5 min at 4ºC and resuspended and washed the beads 4 times with 5 volumes of 1x lysis buffer [50 mM HEPES, pH 7.4, 10 mM MgCl2, 100 mM NaCl, 1 mM dithiothreitol (DTT), 0.1% Triton X-100, 10% glycerol, Complete® protease inhibitors (Roche)]. Afterward, we spun down the beads at 4,000 g 5 min at 4ºC and repeated this wash. We eluted the tRNA by incubating 1 h with 2 times the bed volume of

formamide, rocking on an orbital shaker. We then spun down the resulting mixture at 4,000 g 5 min at 4ºC and saved the supernatant for analysis.

6.6.2. Chemical transformation of plasmids into DH5α

To transform our plasmids into DH5α for purposes of maxiprep or miniprep, we used the chemical transformation protocol. We removed DH5α competent cells from -80ºC and allowed them to incubate on ice 30 min. We added 1 µl of plasmid DNA, at a concentration of 10 ng/µl or greater, to the 100 µl cell aliquot. We pipetted the mixture up and down and allowed it to incubate on ice another 30 min. We next heat shocked the cells in a 42ºC water bath for 45 sec and added 400 µl of SOC media immediately afterward, pipetting up and down. We placed the newly transformed cells into a fresh culture tube and incubated them at 37ºC in a shaking incubator for 1 h. We plated 50 µl of cells on LB plates containing the appropriate antibiotics and incubated them overnight at 37ºC. We also spread the LB plates with a strain of bacteria sensitive to the antibiotics it contained, to make sure the plates were still fresh.

6.6.3. Maxiprep of plasmids

We performed maxiprep of the plasmids pCAXΔDBD, KS61, KS62 and eGFP positive control using the Qiagen Maxiprep kit, following its protocol as follows: Two starter cultures of 5 mL LB were grown for each plasmid with appropriate antibiotics overnight at 37ºC. We then used 500 µl of each starter culture to inoculate 250 mL of LB with appropriate antibiotics. We incubated the LB overnight at 37ºC shaking. The next day, we harvested the culture in 50 mL Falcon tubes and centrifuged them at 5,000 rpm at 4ºC for 30 min. We resuspended the pellet in 10 mL buffer P1 (containing RNase A and Lyse blue), combining tubes and pipetting up and down with a hand pipettor. We then added 10 mL of buffer P2, inverting to mix until the contents had turned blue. We incubated the tubes at room temperature for 5 min. Next, we added 10 mL of pre-chilled buffer P3 and inverted to mix until the blue had disappeared and turned white. We

incubated the tubes on ice 20 min. We then centrifuged the contents at 12,000 rpm 40 min at 10ºC. Afterward, we poured the contents into new tubes and centrifuged again at 12,000 rpm 30 min at 10ºC. While the mixture was centrifuging, we equilibrated a Qiagen tip by applying 10 mL buffer QBT and allowing it to flow through by gravity. We applied the supernatant from the centrifuge step to the column. We washed the column with two 30 mL (column volumes) of buffer QC. We eluted the DNA into clean 50 mL Falcon tubes with 15 mL buffer QF. We then precipitated the DNA by adding 10.5 mL (0.7 volumes) room temperature isopropanol and mixed. We centrifuged the resulting mixture at 12,000 rpm (17,870 g) for 30 min at 10ºC. We carefully decanted the supernatant away from the pellet and washed the DNA pellet with 5 mL room temperature 70% ethanol and centrifuged it at 12,000 rpm for 10 min. Afterward, we carefully decanted the supernatant again and air dried the pellet for 5-10 min, re-dissolving it in 1 mL Nanopure water. We measured the UV-Vis absorbance at 260 nm using a NanoDrop 2000c spectrophotometer and stored it at -20ºC.

6.6.4. Lipofectamine 2000 transfection of HEK293FT cells

In our initial tests, we performed transfection of HEK293FT cells with lipofectamine LTX and PLUS reagent from Invitrogen. We performed the transfection according to the Invitrogen protocol as follows: we aliquoted 150 µl of Opti-Mem reduced serum media into two Eppendorf tubes. In one tube, we added the pCAXΔDBD plasmid (1000 ng/µl) at a concentration of 2000 ng/well; thus, we used 12 µl for six wells. In the other tube, we added (2 µl/well x 6 wells) 12 µl of lipofectamine LTX reagent. We added Plus reagent (3 µl or 0.5 µl / well x 6 wells) to the tube containing plasmid. We then mixed the tubes together and incubated at room temperature for 5 min. After incubation, we aspirated the media from the cells and added 450 µl of fresh media (DMEM, 10% FBS, 1% pen-strep) and aliquoted 50 µl per well of the DNA/lipofectamine solution onto the cells. We incubated the cells at 37ºC, 5% CO_2 for 48 h.

6.6.5. PEI transfection of HEK293FT cells

Prior to transfection, all reagents were brought to room temperature. In a sterile tube, total plasmid DNA (µg) was diluted in serum-free DMEM without phenol red (volume of media is 10% of final volume in culture vessel). Transfection was performed in 6-well plates, splitting approximately one day beforehand and aliquoting 500,000 cells per well. For each well, 3 µg of total DNA was added to 200 µl of media without phenol red. Afterward, PEI (1 µg/µl) was added to the diluted DNA. The DNA and PEI were mixed gently by pipetting up and down. For a 6 well-plate, each well should have 9 µl of PEI at 1 µg/ml concentration. The volume of PEI used is based on a 3:1 ratio of PEI (µg): total DNA (µg). After mixing, the DNA and PEI was incubated 15 min at room temperature and then added dropwise to HEK293T cells. The cells were harvested 48 h post-transfection.

6.6.6. Calcium phosphate transfection of HEK293T cells

For calcium phosphate transfection, we used a calcium phosphate transfection kit from Oz Biosciences (catalog #: CP90000) and followed its protocol. We plated HEK293T cells at 300,000 cells per well in a 6-well plate and waited until they were 60-80% confluent before transfecting. We used DMEM media containing 10% FBS and 1% pen-strep, incubating at 37ºC at 5% CO_2. It is important for this transfection not to use RPMI. We replaced the cell culture media 1-2 h before transfection. It is important not to use old cell culture media or pink media. For each well that is transfected, we diluted 4 µg of each plasmid in 120 µl of 1x HBS buffer supplied in the kit. We then added 6.6 µl of $CaCl_2$ solution mixed immediately by pipetting up and down. We incubated the mixture at room temperature for 30 min. We added the complexes drop by drop to the cells growing in serum and homogenized by gently rocking the plate side-to-side to ensue uniform distribution of the mixture. We then incubated the cells at 37ºC at 5% CO_2 under standard conditions for 48 h.

6.6.7. Flow cytometry preparation

After transfection of cells, we performed the following procedure to prepare them for flow cytometry: we aspirated the media from the cells and added 300 µl of trypsin to each well and incubated at 37ºC for 5 min. We then added 700 µl of DMEM media 10% FBS to quench the trypsin, pipetted up and down to mix the cells and transferred them to Eppendorf tubes. We then centrifuged the cells at 300 rcf for 5 min, aspirated the supernatant and added 700 µl warmed 1x PBS to resuspend the pellet. We centrifuged again at 300 rcf 5 min, aspirated the supernatant and repeated the 1x PBS wash. We then aspirated off the media again, added 500 µl of 1x PBS and transported the cell suspension on ice to the flow cytometry core.

6.7. References

1. Ponchon, L.; Beauvais, G.; Nonin-Lecomte, S.; Dardel, F., A generic protocol for the expression and purification of recombinant RNA in Escherichia coli using a tRNA scaffold. *Nat Protoc* **2009,** *4* (6), 947-59.
2. Ponchon, L.; Dardel, F., Recombinant RNA technology: the tRNA scaffold. *Nat Methods* **2007,** *4* (7), 571-6.
3. Ponchon, L.; Dardel, F., Large scale expression and purification of recombinant RNA in Escherichia coli. *Methods* **2011,** *54* (2), 267-73.
4. Nelissen, F. H.; Leunissen, E. H.; van de Laar, L.; Tessari, M.; Heus, H. A.; Wijmenga, S. S., Fast production of homogeneous recombinant RNA--towards large-scale production of RNA. *Nucleic Acids Res* **2012,** *40* (13), e102.
5. Yoshida, H., Unconventional splicing of XBP-1 mRNA in the unfolded protein response. *Antioxid Redox Signal* **2007,** *9* (12), 2323-33.
6. van Schadewijk, A.; van't Wout, E. F.; Stolk, J.; Hiemstra, P. S., A quantitative method for detection of spliced X-box binding protein-1 (XBP1) mRNA as a measure of endoplasmic reticulum (ER) stress. *Cell Stress Chaperones* **2012,** *17* (2), 275-9.
7. Back, S. H.; Lee, K.; Vink, E.; Kaufman, R. J., Cytoplasmic IRE1alpha-mediated XBP1 mRNA splicing in the absence of nuclear processing and endoplasmic reticulum stress. *J Biol Chem* **2006,** *281* (27), 18691-706.
8. Iwawaki, T.; Akai, R.; Kohno, K.; Miura, M., A transgenic mouse model for monitoring endoplasmic reticulum stress. *Nat Med* **2004,** *10* (1), 98-102.
9. Peschek, J.; Acosta-Alvear, D.; Mendez, A. S.; Walter, P., A conformational RNA zipper promotes intron ejection during non-conventional XBP1 mRNA splicing. *EMBO Rep* **2015,** *16* (12), 1688-98.

10. Nasim, M. T.; Eperon, I. C., A double-reporter splicing assay for determining splicing efficiency in mammalian cells. *Nat Protoc* **2006,** *1* (2), 1022-8.

11. Walker, S. C.; Scott, F. H.; Srisawat, C.; Engelke, D. R., RNA affinity tags for the rapid purification and investigation of RNAs and RNA-protein complexes. *Methods Mol Biol* **2008,** *488*, 23-40.

Chapter 7: Perspectives and Future Work

7.1. Mechanism of DzNPs

Our lab's study of the mechanism of DNAzyme-nanoparticles (DzNPs) is primed to move forward with studying GATA-3 gene knockdown in T47D cells using the Hgd40 DNAzyme. We will produce active 3'-attached Hgd40 DzNPs and compare them to core-attached DNAzymes. As mentioned in Chapter 3, when the DNAzyme is attached via its catalytic core to the AuNP, it is ~98% inactivated. We can then compare gene knockdown with both particles, along with appropriate controls. If we observe gene knockdown in the core-attached DzNPs, we know that knockdown could only occur through the DNAzyme first coming off the particle, lending credence to the hypothesis that DzNPs dissociate in the cytosol. However, if we observe very little knockdown, it suggests that DzNPs may act as a unit, even after escaping the endosome. Controls include a Hgd40 inactive strand with a single point mutation in the catalytic core, abolishing its activity. This DNAzyme will report on what percentage of gene knockdown results from the antisense effect rather than DNAzyme cleavage. We will also use a scrambled Hgd40 DzNP, scrambling the binding arms as well as the catalytic core, to determine if these nucleotides have off-target effects, aside from their activity. Once we expose T47D cells to these particles, we will extract the RNA and perform quantitative real-time PCR on the samples to determine levels of gene expression as compared to 18S. If this work is successfully able to elucidate the mechanism of DzNP action inside cells, we may extend it to look at different types of thiol-AuNP attachment and its effect on gene knockdown. If we find that the DzNPs dissociate in the cytosol, it may be desirable in certain cases to prevent this dissociation from occurring. In that case, we could use di- and tri-thiol linkers to increase the association of the DNAzymes with the AuNP and test their stability inside cells. In future work, we are also interested in exploring how to increase endosomal escape of the DzNPs. If more DzNPs escape the endosome, it could provide a significant boost to their gene knockdown capabilities. There are many potential

strategies to modulate endosomal escape; however, this area constitutes a large sub-field of spherical nucleic acid literature and is outside the scope of this thesis.

7.2. In Vitro RNA Splicing by DzNP-Nanozymes

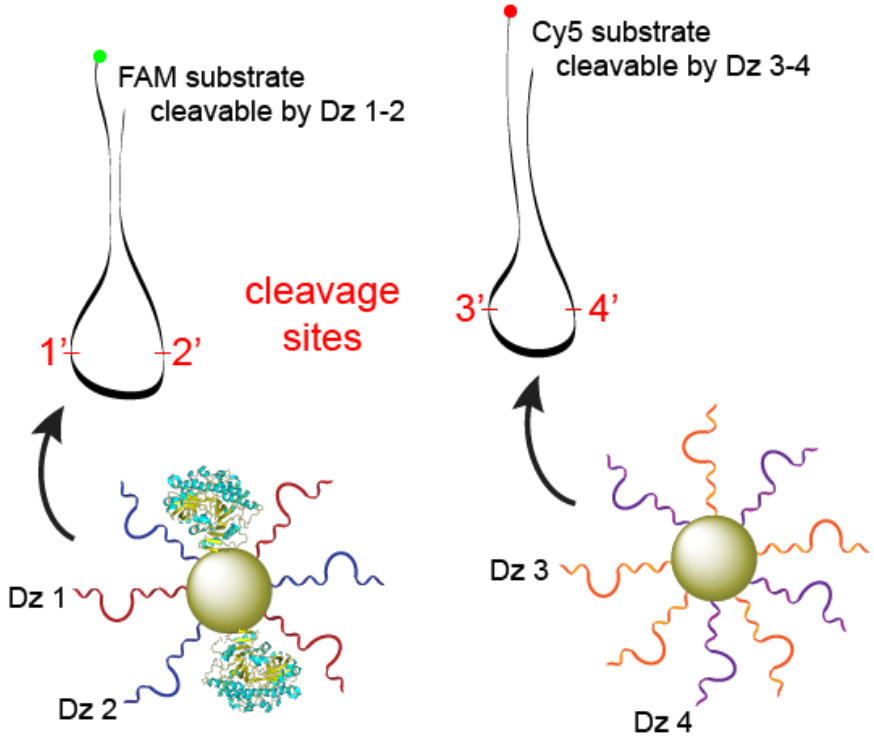

Figure 7.1. Representative schematic of the setup for a dual-splicing experiment.

In looking at building a splicing nanozyme from DzNPs and RtcB ligase, one question that we did not completely address was whether a nanozyme is more efficient as a unit than the individual DNAzyme and RtcB subunits. We hypothesize that, attached to a scaffold together, splicing would be more efficient together than the units separately. To test this hypothesis, we need two separate splicing stem-loop substrates that could be distinguished from each other, with different attached fluorophores: one with a 5'-FAM and one with a 5'-Cy5 (Fig. 7.1.). Each substrate will have affinity to two separate DNAzyme pairs: Dz(s) 1-2 and Dz(s) 3-4. One can then make a nanozyme with Dz1-2, including RtcB, and a separate nanozyme with Dz3-4 that does not include RtcB. If it is possible for RtcB to complement Dz(s) 3-4, then splicing will occur with the Cy5 substrate as well as the FAM substrate. However, if splicing of the FAM substrate is more efficient than splicing of the Cy5

substrate, this data would support our hypothesis that the DNAzymes and RtcB work more efficiently in concert on the same particle than apart. We have the materials to perform this experiment, and it would be excellent to test out this idea to confirm what is happening *in vitro*.

7.3. Cellular RNA Splicing by DzNPs

Performing cellular splicing with our nanozyme largely depends on the hypothesis that the DNAzymes remain associated with the particle in the cell. If the DNAzymes remain on the particle, it may even be possible to recruit cellular RtcB to the particle surface for specific splicing, with the help of a recruiting peptide. However, if the DNAzymes are reduced off the particle in the cytosol, stronger thiol attachment may be necessary. There are two main points of inquiry concerning splicing in cells, regardless of the means used to test these hypotheses. Namely, we want to investigate whether it is possible for DzNPs alone, without attached RtcB, to perform splicing in cells. It may not be necessary to attach RtcB to the particle, if we recruit cellular RtcB for this purpose. Recruitment may happen naturally, through diffusion to the source of cleavage of the target gene, or it may need the help of a recruiting peptide to be efficient. If neither of these approaches works, we can then ask, does attaching RtcB to the DzNP particle to make a splicing nanozyme lead to cellular splicing?

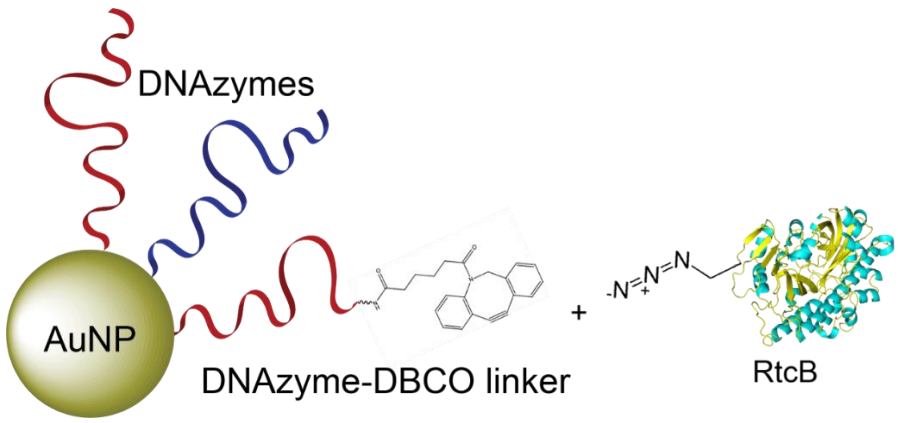

Figure 7.2. Potential means of attaching DNAzymes and RtcB via click chemistry.

In order to answer this question, we must first produce a more active splicing nanozyme, by arraying more RtcB around the particle surface through use of a linker strand. The RtcB could be attached to the DNAzymes themselves (Fig. 7.2.) or the linker could be a neutral molecule such as polyethylene glycol (PEG) (Fig. 7.3.) Once this particle had been characterized *in vitro*, we could then study the cellular splicing that resulted in cells. The other major question to address concerning cellular splicing is also the splicing reporter used in cells. Likely, the construct should be a dual reporter, with one tag to give evidence of transfection efficiency and the other to report on splicing efficiency. Additionally, it appears from our past work that three stop codons in between the intron and the splicing reporter is necessary to prevent read-through. Once we address and optimize the amount of splicing in the XBP1 system, we should be able to manually upregulate the unfolded protein response in the absence of stress, as a proof-of-concept demonstration of splicing. From there, we can look at splicing a disease-relevant gene, such as dystrophin, to modulate the RNA splicing disease Duchenne muscular dystrophy (DMD). The long-term goal would be transitioning this therapeutic to a mouse model, in preparation for evidence of efficacy that might proceed human trials. Finally, it is important to note that, in a recent mouse trial with 2251-DzNPs, we noticed some toxicity to high doses of the particles, which presumably occurs due to the gold core. It would be interesting, therefore, to attempt other means of attaching DNAzymes in a spherical arrangement to produce splicing particles, perhaps by using liposomes or lipid nanodiscs.

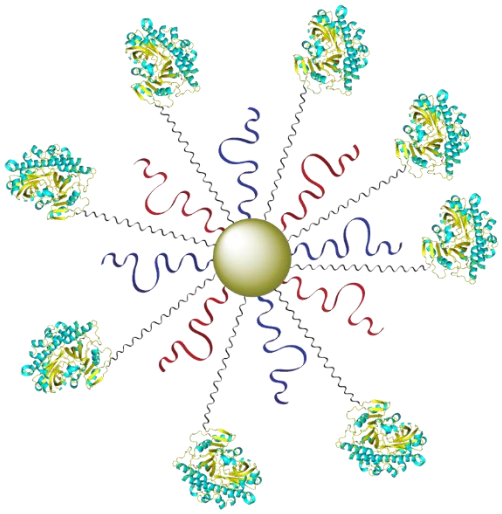

Figure 7.3. RtcB attached to DzNP through flexible PEG linker.